THE UNIVERSITY OF SHEFFIELD

DEPARTMENT OF MECHANICAL ENGINEERING

THE LEONARDO TRIBOLOGY CENTRE

Ultrasonic Reflection Technique for Measuring

Contact Conditions at the Tool Chip Interface

DLAIR OBAID RAMADAN

This thesis has been presented by the above author in partial fulfilment of the requirements for the degree of

DOCTOR OF PHILOSOPHY

July 2016

SUMMARY

The measurement of the interface conditions in a cutting tool contact is essential information for performance monitoring and control. In this work, a new method for measurement of interface conditions, based on the reflection of ultrasound, is evaluated for use in turning in both dry and wet cutting conditions. An ultrasonic wave will be partially reflected when it strikes an interface between materials with different acoustic properties. The proportion of the wave reflected depends on the nature of the interface.

A transducer was positioned on the underside of a cutting tool insert and a pulse propagated through the insert. The pulse was reflected back at the tool-chip interface and received by the same transducer. The amplitude of the reflected wave was processed in the frequency domain. Reflection coefficient measurements were then used to investigate the tool-chip interface at different machining parameters including cutting speeds, depth of cut and feeds. It was seen clearly that the reflection coefficient increases with increasing cutting speed due to either a reduction in the tool-chip contact area or a decrease in the pressure applied on the rake face cutting tool. While the reflection coefficient decreases with increasing cutting depth and feed due to either an increase in the tool-chip contact area or an increase in the pressure. The results also showed that the reflection coefficient was significantly affected by feed followed by cutting speed whereas the depth of cut had the lowest effect on reflection coefficient. These results were attributed to the affect of tool-chip contact length with the machining parameters, where the depth of cut had the least effect on contact length.

When applying the cutting fluid, more energy was reflected back from the tool-chip interface and thus a higher reflection coefficient was recorded than in dry condition and this was due to the lower pressure that was applied on the rake face cutting tool.

The use of ultrasound in the monitoring of contact condition at the tool-chip interface is shown to be a viable technique for research and condition monitoring.

DEDICATION

This thesis is dedicated:

To whom who are the cause of what I become today. My beloved parents

To my beloved brothers and sisters particularly my elder brother, Simko, who stands by me when things look bleak

To my wonderful wife

To my beloved daughters

ACKNOWLEDGEMENTS

Praises to Allah and peace be upon the beloved final Prophet Muhammad. Thanks to Allah to be always with me to give guidance and mercy along my life, for his help and blesses to give me strength and patience to complete the thesis.

I would like to express my sincerest gratitude to my supervisor Prof. Rob Dwyer-Joyce, for his support, patience and invaluable help from the preliminary to the concluding level I appreciate all his contributions of time and ideas to make my PhD experience productive and stimulating. It has been a real pleasure and I aim to continue to have a thriving working relationship with him in the future. Thank you to Matt Marshall for his guidance during my study. I would also like to thank Hassan Ghadbeigi for his help and guidance.

I would like to acknowledge the financial support of Kurdistan Regional Government-Ministry of Higher Education and Scientific Research during my PhD. I also wish to acknowledge the University of Koya for giving me the opportunity to do my PhD in one of the world renowned universities.

Sincerest thanks to Robin Mills and Tom Howard for their seemingly endless amount of knowledge, patience and willingness to go out of their way to help me and teach me some of the most valuable skills I have learned throughout my studies. I would like to acknowledge the help and support I have received from all of the members of The Leonardo Centre for Tribology. It has been a pleasure being part of such a wonderful research group and I am thankful for some of the friendships I have made.

Thanks to the research technician Dave Butcher for the day-to-day technical support and for always being so willing to help out. Thank you for also investing so much time in teaching me to use a lathe and milling machine and actually make things myself. It has been great fun, and has made me a better engineer. I would also like to acknowledge the help and support I have received from all of the technicians, especially Jamie Booth, Paul Downs, Geof Hibberd, David Webster and John Bradley, thank you to all of you.

Thanks to Phil Harper and his team at Tribosonics for all the advice and ultrasound knowledge.

Thank you to all the folks at the AMRC whom I've had the pleasure of working with in the last two years of my study. Sincerest thanks to Chris Taylor for all the advice and machining knowledge.

I would also like to gratefully and sincerely thank Dr. Cédric Courbon at Tribology and System Dynamics Laboratory's (LTDS) for his assistance and guidance. Many detailed and in-depth discussions with him have invaluably shaped the course of this research.

I am extremely grateful to Justin Davies at Sandvik Coromant UK for the good advice and cutting tool knowledge.

I also would like to thank my friends in Iraq, Kurdistan, Sheffield and around the UK, especially Radwan Addaiy, Hossen Alharbi, Karzan Ghafoor, Zrar Xalid, Kamaran Ismail for their help, motivational support and close friendship.

Beyond all, I greatly appreciate the endless support and patience of my beloved parents. Thank you for always enabling me to pursue my goals and ambitions. I hope that this achievement will complete the dream that you had for me all those many years ago when you chose to give me the best education you could. I also would like to express my wholehearted thanks to my brothers and sisters for their generous support they provided me throughout my entire life.

I owe profound gratitude to my love, Noora, who gave me the moral support all the time. Thank you for being great pillars of support, for your love and patience throughout this, I couldn't have done it without you. I would like to extend thanks to my lovely daughters Dania and Yara for the moral support which has made me feel stronger and inspired. There is no greater support and encouragement besides all of you.

Finally, I would like to thank my Mum in law and my brothers in law for their support. This thesis is only a beginning of my journey.

Dlair O'laid Ramadan
The University of Sheffield
July 10, 2016

CONTENTS

LIST OF FIGURES

LIST OF TABLES

NOMENCLATURE AND ACRONYMS

All symbols are also defined in the text.

Symbol	Description	Units
A_m	Amplitude of reflected pulse	V
A_{ref}	Amplitude of reference pulse	V
A_C	Tool-chip area contact	mm^2
L_c	Tool-chip contact length	mm
L_s	Sliding length	mm
L_{st}	Sticking length	mm
R_{ref}	Reflection coefficient of reference pulse	-
z_1	Acoustic impedance material 1	$kg/m^2 s$
z_2	Acoustic impedance material 2	$kg/m^2 s$
B	Bulk modulus	Pa
c	Speed of sound	m/s
F	Frequency	Hz
h	Chip thickness	mm
K	Interface stiffness	$GPa/\mu m$
r	Chip curls radius	mm
N	Spindle speed	RPM
p	Pressure	Pa
R	Reflection coefficient	-
T	Transmission coefficient	-
t	Cutting depth	mm
f	Feed	mm/rev
V	Cutting speed	m/min
V_C	Chip velocity	m/min
F_t	Thrust force	N
F_C	Cutting force	N
K_t	Specific thrust force	N/m^2

K_C	Specific cutting force	N/m^2
α	Side relief angle	$degree$
ρ	Material density	kg/m^3
ω	Angular frequency	rad
φ	Shear angle	$degree$
λ	wave length	m

ABBREVIATIONS AND ACRONYMS

BUE	Built up edge
BUL	Built up layer
SEM	Scanning electron microscopy
EDX	Energy-dispersive X-ray spectroscopy (EDX, EDS, or EDXA)
EDM	Electrical discharge machining
CCD	Centre composite design
NDT	Non-destructive testing
FFT	Fast Fourier Transform
BNC	Bayonet Neill-Concelman type connector
UT	Ultrasonic
UPR	Ultrasonic pulser-receiver
PZT	Lead zirconium titanate
PC	Personal computer
PCI	Peripheral component interconnect
FMS	Film measurement system
DAQ	Data acquisition
LabVIEW	Graphical array-handling program language
MATLAB	High level array-handling programming language
ANOVA	Analysis of variance

1

Introduction

Metal cutting, or simply machining, is a broad term used to describe a group of processes that are used to change the shape of a workpiece to a desired geometry by removing unwanted material from the workpiece, after it has been produced by various methods, in the form of chips (Astakhov 2006). The material layer which is removed from the workpiece, the chip, rubs and slides over the rake face of the cutting tool. During this process, high stresses and tribological conditions occur between the cutting tool and the chip interface, and when uncontrolled can lead to rapid tool wear (Totten & Hong 2004). In order to understand this phenomenon, research and studies have been carried out to predict and control the friction and wear at this interface. In the present research work, a novel technique was used to investigate and monitor the interface between the cutting tool and the chip. The statement of the problem, the aim and objectives of the study, ultrasonic application and the thesis layout are discussed in this chapter.

1.1 Statement of the Problem

Industries have to optimize their cutting processes with the aim to improve their productivity. To achieve this objective, industries use high cutting regimes by using a high cutting speed and feed rate (Ben Abdelali et al. 2012). In contrast, the use of these high cutting regimes leads to a rise in the stress and temperature in particular at the tool-chip interface as well as close to the cutting edge. Thus causes excessive tool wear or even premature tool failure (Ben Abdelali et al. 2011; Zemzemi et al. 2009).

The useful work in the cutting process, i.e. removing material from the workpiece needs only 30-50% of the energy that is expended in the cutting process while the rest of the energy is consumed in the tool-workpiece and tool-chip interfaces due to tribological conditions (Astakhov 2006). The tribological contact condition at the interface between the cutting tool and the chip has a strong influence on the metal cutting mechanics. This is because of the correlation between the deformation process on the shear plane and the contact conditions at the cutting tool-chip interface (Hwang & Chandrasekar 2011). Hence, the need to investigate the nature of contact condition at the tool-chip interface is important. Any change in the contact condition such as contact length or friction results in a substantial change in cutting temperature or energy expenditure and shear angle (Dogra et al. 2010). This change again influences tool wear or integrity of the machined surface. Thus, it is very difficult to fully understand the process of metal cutting without detailed knowledge of the contact conditions at the tool-chip interface. For this reason, numerous endeavors have been made to comprehend the nature of contact conditions at the interface between the tool and the chip in machining.

Lubricating and cooling the cutting process are the main reason for using cutting fluid in machining or metal cutting, hence reducing tool wear and increasing the tool life (Claudin et al. 2010). Using the cutting fluid during the machining process results in removing the heat from the tool-workpiece interface by convecting it away. (Sharma et al. 2009). Due to the limited guidance from theory, selecting a suitable cutting fluid for a specific application, among the large number of available commercial fluids, is considered as an issue (Trent & Wright 2000), so understanding the action of coolants and lubricants in metal cutting is still at a rather primitive level since the conditions are complex and the selection of cutting fluids still relies on practical experience.

In this study, a new method has been used to measure the tool-chip interface conditions in dry and wet cutting conditions. This method is based on the reflection of the ultrasound wave at the interface. When an ultrasound wave is travelling through a medium to another one passing through an interface, some of the waves are transmitted through the asperities and some of the wave are reflected back through the gaps.

1.2 Aim and Objectives

The aim of this study has been to develop and investigate the use of ultrasonic reflection to monitor the interface conditions in a cutting tool contact in dry and wet cutting conditions. This thesis explores the relationship between the reflection coefficient with cutting forces and cutting parameters.

The following are the specific objectives of the research work:

1. Devise an ultrasonic method which allows the cutting tool-chip interface to be monitored in situ and non-invasively.
2. Analysing ultrasonic measurements in order to extract features concerning the cutting process and built-up edge (BUE) formation.
3. Investigate the effects of machining parameters such as cutting speed, cutting depth and feed on the tool-chip interface in dry and wet cutting conditions using the ultrasonic reflection. The aluminium alloy 6082 was selected for this study as the work material.
4. Measure the contact area between the rake face cutting tool and the chip and cutting forces and then establishing a correlation between the reflection coefficient and the contact area and cutting forces.
5. Develop a model to fit the experimental data, especially the reflection coefficient, cutting forces and tool-chip contact length.

1.3 The Use of Ultrasonic Reflection in Tribology

Ultrasonic is a process of creating an inaudible sound wave and sending these waves to the interface between two media and then sensing the reflected wave. This process is called ultrasonic reflectometry. When an ultrasound wave travelling through a medium and incident at point having different acoustic properties, some of the ultrasound wave will be reflected. Detecting imperfections and cracks are the most common fields in engineering which are using this technique.

The ultrasonic reflection has been successfully used in a numerous engineering applications in different interfaces including dry interface (solid-solid) contact, lubricated interface (solid-oil-solid) contact and mixed interface.

Kendall & Tabor (1971) used the ultrasonic method to investigate dry contact for the first time. They found that the interfacial stiffness affected the transmission of ultrasound. Using ultrasound to examine dry contact has been continued, for example Marshall et al. (2004) carried out a static ultrasonic contact measurement using a scanning system to examine interference fits. In another work, Marshall et al. (2006) used the same system to investigate the static contact pressure and area between a wheel and rail. Marshall and his colleagues continued with static dry contact investigation where they examine the dry contact between the bolted plates using the scanning system (Marshall et al. 2010).

The use of lubrication in engineering application is very important to separate surfaces and cool the components. The lubricant film thickness is most important where it should be a thick enough to separate the asperities from the both surfaces but not too thick that it causes a leakage. Numerous researches have been carried out to measure the lubricant film thickness using ultrasound, see Dwyer-Joyce et al. (2003) and Reddyhoff et al. (2005). The application of ultrasonic reflection for measuring the oil film thickness has been applied to different engineering applications such as rolling element bearings (Dwyer-Joyce et al. 2004A; Dwyer-Joyce et al. 2004B), journal bearings (Reddyhoff et al. 2006) and mixed lubricant contacts (Dwyer-Joyce et al. 2011).

It is of interest to note that to date there is no research on the use of ultrasonic reflection in machining. The work presented in this thesis will develop the technique needed to investigate the contact conditions at the cutting tool-chip interface. In addition to the information about the tool-chip interface obtained from the ultrasonic reflection during dry cutting condition for different machining parameters, the ultrasonic method can be used to obtain details about the penetration of the cutting coolant into the tool-chip interface.

1.4 Thesis Layout

This thesis is divided into the following chapter headings: Literature Review, Ultrasonic Background, Cutting Tool Ultrasonic Instrumentation Method, Analysis of Machining Processes, Cutting Force and Chip Morphology Measurements, Ultrasonic Reflection from Tool-Chip Interface, Analysis and Discussion of Experimental Results and finally Conclusions and Recommendations. A brief summary of each chapter is as follows;

- Chapter Two. Literature Review. This chapter reviews the literature of the tribological conditions at tool-chip interface in a machining process.

- Chapter Three. Ultrasonic Background. In this chapter, the principles of ultrasound are introduced. The generation of ultrasound waves and typical ultrasonic transducers are also presented.

- Chapter Four. Cutting Tool Ultrasonic Instrumentation Method. This chapter introduces the initial attempt to apply the ultrasonic reflection to machining. In addition, the chapter also presents the ultrasonic apparatus and the temperature effect on the piezoelectric materials. In the last section of the chapter, the experimental procedure to obtain the reflection from the tool-chip interface was discussed.

- Chapter Five. Analysis of Machining Processes. In this chapter, the machine setup, and the experiment design are introduced. This chapter also presents all the apparatus used in this study excluding the ultrasonic apparatus which mentioned in Chapter 4.

- Chapter Six. Cutting Force and Chip Morphology Measurement. The experimental results of the cutting forces and the tool-chip contact area are presented and discussed in this chapter. Furthermore, the chapter also introduces the temperature measurements and its effect on the cutting forces and contact area.

- Chapter Seven. Ultrasonic Reflection from Tool-Chip Interface. The ultrasonic method is applied to a carbide cutting tool on a CNC machine. The ultrasonic

measurement data obtained from the orthogonal cutting are analysed and discussed in this chapter.

- Chapter Eight. Analysis and Discussion of Experimental Results. In this chapter, a correlation between the different measurements is presented.

- Chapter Nine. Conclusions and Recommendations. This chapter presents the main conclusions drawn in the thesis and some suggestions for future work.

2

Literature Review

The tribological conditions at the tool-chip interface in a machining process, such as the built-up edge (BUE), tool-chip contact length and contact area phenomena, are intimately responsible for the rising tool temperature, fluctuation of cutting forces, tool wear and thus tool life. In the literature, there are several techniques developed and used in order to measure the interfacial conditions at the tool-chip interface. A brief overview of these measurement methods is given in this chapter.

2.1 Machining Operation

Machining is defined as the process of removing unwanted materials from a workpiece to obtain the desired shape. A large piece of stock is available in various standard shapes, such as solid bars, flat sheet, shaped beam and hollow tubes, which can be used to produce the workpiece. The most widely used conventional machining processes are: turning, milling and drilling. Below is a brief description of each of these processes.

2.1.1 Turning

Turning is one of the common processes in machining, which is utilised to produce circular shapes by removing undesired material. The turning operation involves a machine called a lathe together with appropriate fixture, cutting tool and workpiece. The workpiece is secured in the lathe machine by using the fixture (chuck) which is attached itself to the machine. The lathe utilises a single-point cutting tool, more details are given in Section 2.2, and is also secured in the lathe machine. In turning process, the workpiece is rotated about its axis and the cutting tool is fed into it, cutting away unwanted material in the form of small chips and producing the desired shape. There are two different cutting methods in turning processes namely; orthogonal and oblique cutting which are described in detail in Section 2.3.

2.1.2 Milling

Milling is a process that uses a multi-point cutting tool to remove unwanted material from the workpiece to produce the desired part. The workpiece in the milling machine is secured to a fixture, which itself is attached to the platform of the machine, and moves linearly. While the cutter or the cutting tool is secured to the milling machine and is rotates about its axis. In milling process, the cutter is rotated about its axis and the workpiece is fed into it, unwanted material is cut away from the parent metal in the form of small chips and producing the desired shape.

2.1.3 Drilling

A drilling machine is specifically used to make a hole into a workpiece. The workpiece in the drilling machine is secured to a fixture, which is attached to the platform of the machine. The drilling cutting tool is also called a drill which has normally two cutting

edges. In drilling operations, the cutting tool or the drill is rotated about its axis and it feeds into the workpiece, undesired material is cut away from the workpiece in the form of small chips and obtaining the desired shape.

In addition to the above mentioned three most popular machining processes, there are many other material removal processes such as planing, shaping, broaching, sawing, grinding and boring.

2.2 Classification of Cutting Tools

A cutting tool is any tool that is used to remove metal from the workpiece by means of shear deformation. A cutting tool may be classified into two groups namely: single-point and multi-point cutting tool depending upon the number of the cutting edges. Single-point cutting edge is used in turning, boring, planing and shaping. Grinding, drilling and milling tools are multi-point cutting tool. Figure 2.1 shows examples of different types of cutting tools.

a) Single-point cutting edge   b) Multi-point cutting tool
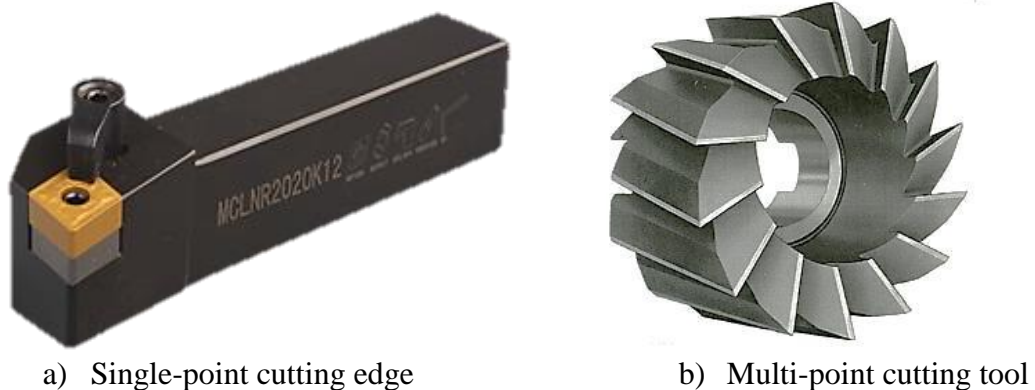
Figure 2.1 Types of cutting tools (Courtesy of Sandvik Coromant)

2.3 Methods of Metal Cutting

The turning processes can be classified into two main categories: orthogonal cutting and oblique cutting depending upon the angle between the tool cutting edge and the cutting direction. Figure 2.2 shows schematic of the both metal cutting configurations. In orthogonal cutting, the cutting edge is perpendicular to the direction of the cutting tool travel while in oblique cutting the angle between the cutting edge and the cutting direction is less than 90° (Black & Kohser 2013). Oblique cutting is considered as the most common type of cutting process, normally found in many machining processes

while the orthogonal cutting is the most common type used in research purposes. Orthogonal cutting was used in this study because it is easy to analyse since it is close to a two dimensional and therefore it is also known as two-dimensional cutting. The flow direction of chip is another reason for choosing orthogonal cutting in this study, where the chip moves perpendicular to the cutting edge while the chip makes an angle with the edge. Oblique cutting is more difficult to analyse since it is three-dimensional process.

Deleted due to copyright
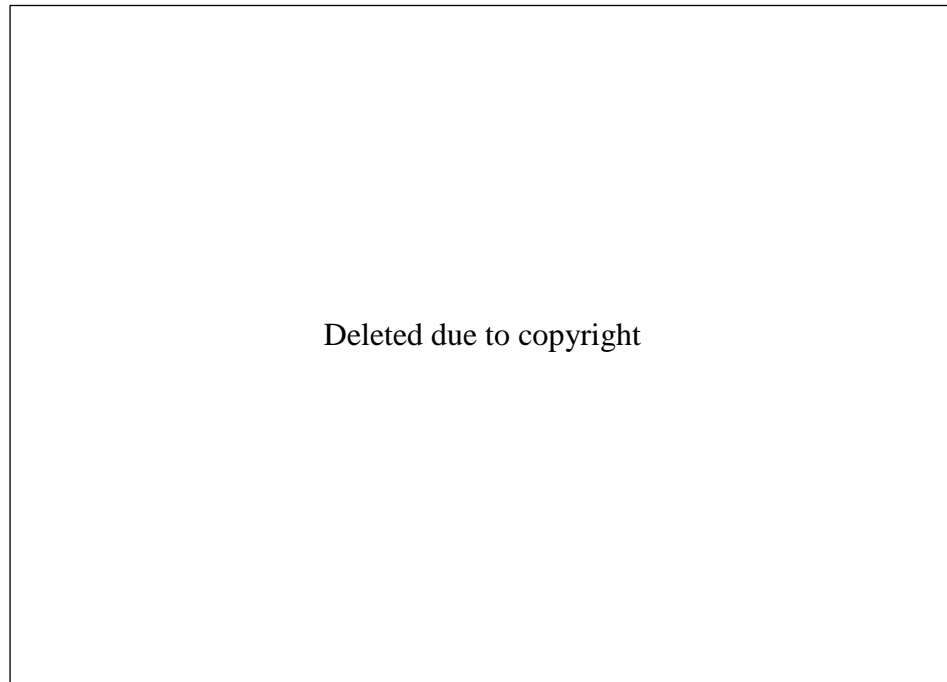
Figure 2.2 a) Orthogonal and b) oblique cutting (Trent & Wright 2000)

2.4 Types of Chips

The chip is the removed metal layer from the workpiece during the material cutting process. This layer passes through different operations before being separated from the material which are: the elastic and plastic deformations and the final form is removed by shear from the parent metal. There are different types of chips depending on the workpiece material and the cutting conditions (Figure 2.3) (Juneja et al. 2003):

a) Continuous chips,
b) Continuous chips with built up edge (BUE).
c) Discontinuous chips.
d) Serrated chips
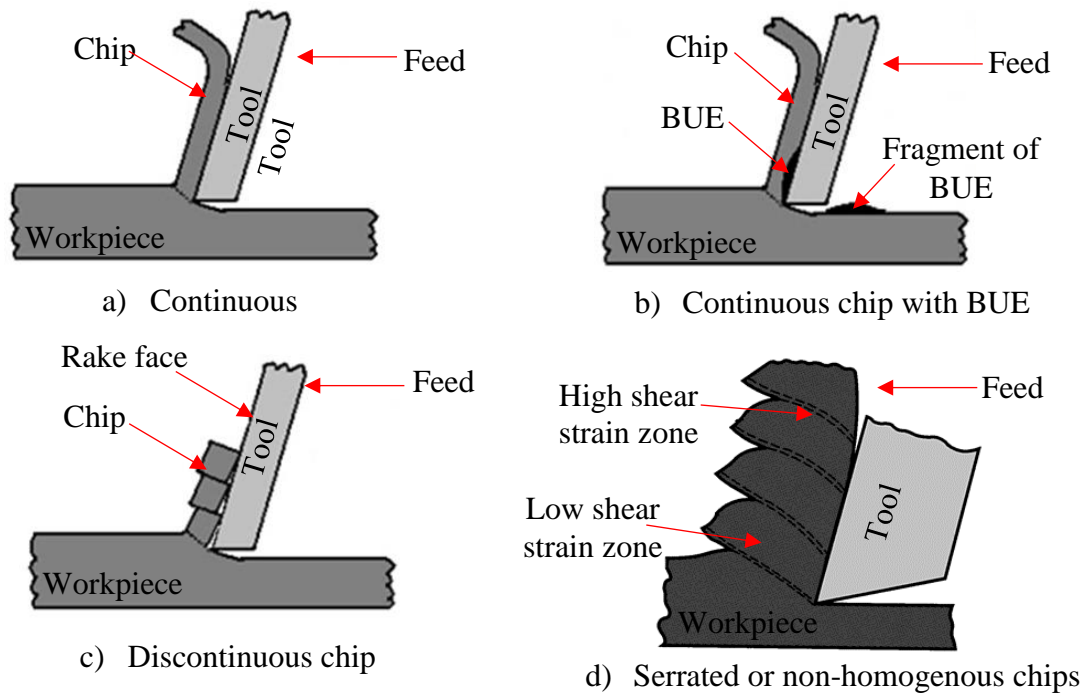
Figure 2.3 Types of chips

2.4.1 Continuous Chips

Plastic deformation of the workpiece material occurs when the tool cutting edge advances into the workpiece and the metal is separated and moves like a ribbon (Figure 2.3a). The plastic zone ahead of the cutting edge is called the primary deformation zone. The material then moves over the rake face of the cutting tool for a short distance and then curls away from the cutting tool. These types of chips are produced when cutting ductile material such as: aluminium alloys, copper, low carbon steel, etc. The deformation zone on the tool rake face is called the secondary deformation zone.

2.4.2 Continuous Chips with Built-Up Edge

The high temperature at the tool-chip interface and the high pressure of the metal on the tool rake face enable part of the chip to be welded onto the rake face of the cutting tool. This is known as the built-up edge, BUE (Figure 2.3b). The BUE is stronger than the rest of material flowing over it, becomes work hardened, because its heat has been dissipated to the tool rake face as a result of the intimate contact with the rake face. With the continuation of the machining process, some of the BUE may be combined with the chip and moves along the rake face. Part of the BUE usually remains on the tool rake face giving rise to poorer surface finish of the workpiece and reducing the

11

cutting tool life (R.Kesavan & Ramanath 2006). More details about the BUE and its effects have been detailed in Section 2.5.

The effect of the cutting conditions on the mechanism of chip formation, during machining aluminium hybrid composites, has been confirmed by the experimental work of Radhika et al. (2014), where different types of chip formation was observed during the machining of the same material but under different cutting conditions. At low cutting speed, a discontinuous chip was formed while with increasing the cutting speed the chip length was increased. The reason for changing the chip form from discontinuous to continuous is because of the increasing ductility of the workpiece material, where increasing cutting speed increases the temperature and thus increasing the ductility. They also observed that the number and the diameter of chip curls increased with increasing the feed rate. Similar results were found by Xu et al. (2014) while machining aluminium *6061-T6*.

2.4.3   Discontinuous Chips

Segmental or discontinuous chips are formed during the machining of the brittle materials such as brass, cast iron and bronze. The mechanism of chip formation is different from continuous chips, where in this case the metal is fractured instead of sheared. The power expenditure is also low. In discontinuous chips the contact length between tool rake face and chip is shorter than the continuous chips; this in turn enables the chip to carry most of the heat produced in the chip (Figure 2.3c). As a result, the tool temperature is lower than the previous one, therefore, the tool life is longer (Juneja et al. 2003).

2.4.4   Serrated Chips

They are semi-continuous chips formed due to the non-uniform strain on the material during cutting. It has a saw tooth-like appearance due to zones of low and high shear strain (Figure 2.3d). This type of chip formed in the materials which are very difficult to machine such as titanium alloy, nickel based super alloy and austenitic stainless steel. Serrated chips or non-homogenous chips are likely to be formed when materials are cut at very high speed.

2.5 Built-Up Edge (BUE)

In single point cutting of metals, a built-up edge (BUE) is an accumulation of material against the rake face that adheres to the tool tip, separating it from the chip. While if the adhered material is on the rake face of the cutting tool then it is called a built up layer (BUL). Figure 2.4 shows a cutting edge with and without the BUE.
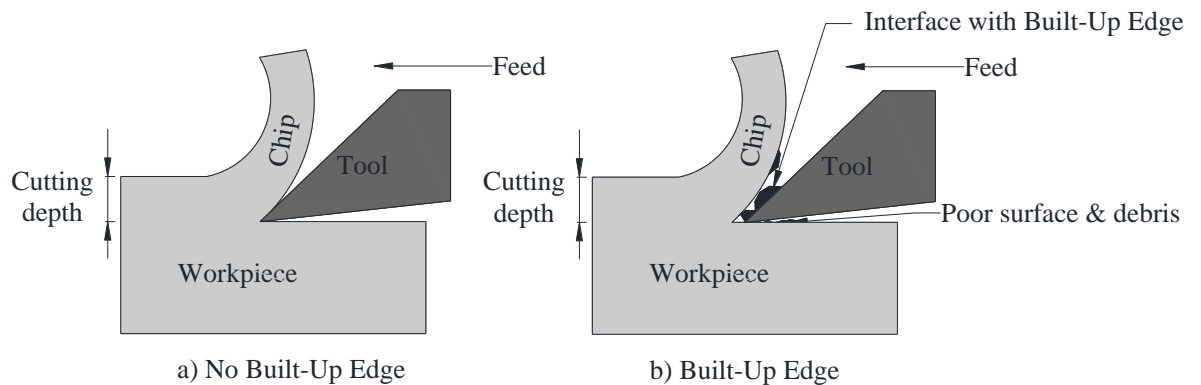
Figure 2.4 Cutting edge with and without BUE

A new method of preventing BUE formation was introduced by Bandyopadhyay (1984) by preheating the tool cutting edge above the re-crystallization temperature of the workpiece material, where the heating gives rise to softening the material, thus preventing the work hardening which is necessary for the formation of the BUE. This phenomenon (i.e. preheating the cutting tool) interprets the eliminating of the BUE as the cutting velocity increases, where the temperature increases with increasing the cutting speed.

During the cutting process the BUE dimension grows until it reaches the maximum point, at which point the BUE dimension starts to decrease until it completely disappears at a critical cutting speed. The critical cutting speed is defined as the speed at which the BUE disappears and is denoted by $V_{critical}$. The frequency of appearance and disappearance of the BUE increases as it approaches the value of the critical cutting speed, when it vanishes completely. Figure 2.5 shows the relation between the BUE dimension and the cutting speed (Algarte et al., 1995, cited in Reis et al. 2007).

Deleted due to copyright

Figure 2.5 Variation in BUE dimensions as a function of cutting speed, identifying the stable and unstable regimens and the critical cutting speed (Algarte et al., 1995, cited in Reis et al. 2007).

Carrilero et al. (2002) used a TiN cutting tool insert in machining of *AA2024-T351* to investigate the differences between a built-up edge (BUE) and a built-up layer (BUL). The BUE is accumulated close to the cutting tool edge, while the BUL is accumulated on the rake face cutting tool. The SEM images and EDS spectra recorded onto the tool rake surface show dissimilar thickness and composition between the BUL and BUE. The SEM images showed that in the nearest zones to the tool cutting edge, a much higher metal accumulation can be noticed than in the farthest zones to the edge of the cutting tool. Furthermore, the EDS spectra showed that the intensive of the Fe and Cu peaks in the BUE are much higher than in BUL for the same element. Figure 2.6 shows a schematic of the cutting tool insert showing the BUE and BUL.

Deleted due to copyright

Figure 2.6 Schematic image of cutting tool with BUE and BUL (Gokkaya & Taskesen 2008)

Predicting the length and the height of the BUE and its effect on the cutting forces and chip flow were investigated by developing a slip-line model; which at the same time predicts many other machining factors as well such as the thickness of the chip, tool-chip contact length, cutting forces and chip up-curl radius. Predicting the length and the height of the BUE is important because it is the key to estimating the fluctuation of cutting forces during machining (Fang & Dewhurst 2005).

Figure 2.7 shows a quick-stop device which was used to investigate the behaviour of the tool-chip interface, by removing the cutting tool during cutting process at a higher speed than the cutting speed. This device was employed to study the geometry of the BUE of a SAE 12L14 steel at low speeds with and without lubricant (Reis et al. 2007). The results showed that the BUE is reduced with using cutting fluid at the lowest cutting speed, but at higher cutting speed they found that the role of the cutting fluid is negligible in eliminating the BUE because at higher cutting speed the fluid has difficulty to entering into the hot chip-tool interface.

Deleted due to copyright

Figure 2.7 Diagram of the quick-stop test configuration (Reis et al. 2007).

They also found that the geometry of the BUE varied considerably along the cutting width and that, under some conditions, the largest measured area was four-fold larger than the smallest. Figure 2.8 was obtained by using the quick stop device and it shows a schematic and a micrograph of the BUE.

Deleted due to copyright

Figure 2.8 a) Schematic drawing of a BUE; b) Micrograph of the built-up edge of an Al-Si alloy (Reis et al. 2007).

The effect of the cutting conditions including cutting speeds and feed rates on the built-up edge (BUE) and built-up layer (BUL) were studied as well as on the surface roughness and cutting forces. The experiments were conducted by utilizing a CNC machine using uncoated cutting tool in machining *AA6351-T6*. The cutting process was performed in the absence of cutting fluid. The results showed that in order to avoid the formation of BUE or BUL, the cutting speed value should be between (400-500 *m/min*) or higher, whereas at lower cutting speeds an accumulation of the aluminium against the rake surface was shown (Gokkaya & Taskesen 2008). The existence of a BUE sometimes has a positive effect on the surface finish at lower cutting speed where it leads to an increase in the nose radius of the cutting tool and thus improves the surface finish (Stephenson & Agapiou 2006). They also found that at high cutting speed and low feed rate a good surface finish was obtained and the cutting forces were the lowest at the same cutting conditions. This is due to the small contact area between the tool and chip and the high temperature (Gokkaya & Taskesen 2008).

In another work, Gokkaya (2010) used the same conditions but with different material, uncoated cutting tool in machining *AA2014-T4*, to investigate the effect of the cutting conditions on the BUE, BUL, surface roughness and cutting forces. They obtained similar results to the first study.

Fang et al. (2010B) studied the effect of the BUE on vibration. They used two different tools for confirming of the existence of the BUE: microscopic and high speed camera

(HSC). The microscope was used to examine the deposit material on the rake surface of the cutting tool after cutting while the HSC was used to observe the BUE in situ. An accelerometer also was used to measure the vibration signals. The results showed that there were three distinct BUE regions which are categorised by different patterns of cutting vibration: the BUE initiation region (0.8-4 *m/min*), steady BUE region (4-20 *m/min*) and unsteady BUE region (20-100 *m/min*). They also found that kurtosis, a statistical tool, can be used to distinguish between the different regions of the BUE.

Gómez-Parra et al. (2013) investigated the effect of the BUE and BUL on the surface quality of two different alloys of the aeronautical aluminium: Al-Cu and Al-Zn. The experiments were conducted without the use of coolant. The experiments showed that the presence of the BUE and BUL adversely effect the surface condition.

The effect of coolant on the BUE formation, at different cutting speeds, were investigated by Seah & Li (1997) by utilizing a scanning electron microscope (SEM). The SEM images show the BUE as lumps or streaks of adhering material on the underside of the chip after breaking away from the cutting edge. This technique was used in this study in order to confirm the BUE existence.

2.6 Tribological Conditions at the Tool-Chip Interface

The success of machining processes demands a full understanding of the tribological conditions at the tool-chip interface, where cutting tool wear and chip formation are strongly affected by the interfacial boundary conditions at the tool-chip interface.

2.6.1   Tool-Chip Contact Length

In the orthogonal machining process, which is shown in Figure 2.9 below, the cutting tool is compelled to cut into the workpiece, a chip is generated in the shearing zone then moves on along the rake surface of the cutting tool until it bends off or breaks up. The distance of the chip, which is in contact with the cutting tool from the tip of the tool to where it leaves the tool, is called the tool-chip contact length, or simply contact length (Huang et al. 1999; Abukhshim et al. 2004; Iqbal et al. 2008; Fatima & Mativenga 2013).
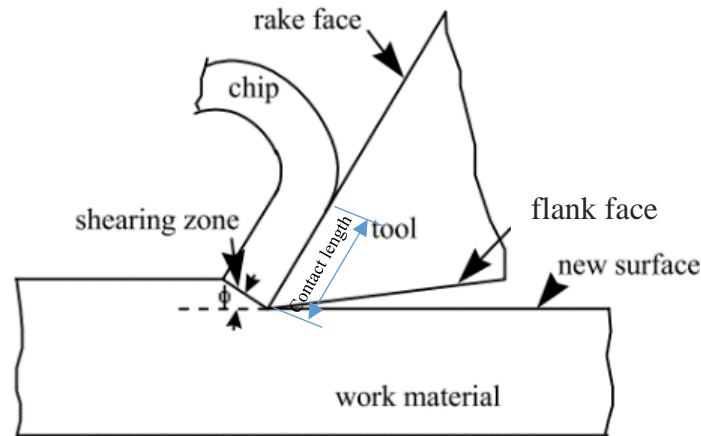
Figure 2.9 Diagram of tool action

In this process, some of the power which is supplied by cutting forces is consumed in breaking down the workpiece metal bonds in the sticking zone while some others overcome the friction in the sliding region on the rake surface. Both deformation and friction produce heat. The main heat sources thus identified in the machining process are the plastic deformation, the contact area between the tool and chip and the friction between the flank face of the cutting tool and the machined surface of the workpiece (Huang et al. 1999; Fatima & Mativenga 2013). Plastic deformation in the shear deformation zone is an example of the generation of heat. The breakage of the chemical and physiochemical bonds along the shearing region are caused by the shearing force. In addition, this particular process leads to the production of the chip which generates heat. More heat is produced as a result of the flow friction of the chip along the tool rake face. This is known as secondary sheared deformation. This generated heat is transferred to the tool through the tool-chip contact length.

The tool-chip contact length provides the path for the heat flux to the tool with larger contact lengths resulting in more heat dissipating into the tool. Therefore, and based on the result of Huang et al. (1999) study, it can be concluded that controlling the tool-chip contact length may reduce the heat and the friction force on the rake surface of the cutting tool, which results in the decrease of both cutting force and tangential (thrust) force. This can be attained by making a groove in the rake surface to restrict the contact length to a distance from the cutting edge to the groove (chip breaker). A chip breaker groove is the most simple practical method for controlling the contact length.

18

Figure 2.10 below shows the factors which are related to the contact length, where L_{st} is the sticking length, L_s is the sliding length, and L_c is the total contact length. The tool-chip contact length is affected by different parameters such as cutting parameters, tool material, workpiece material and tool geometry (Sadik & Lindström 1993; Abukhshim et al. 2004; Friedman & Lenz 1970).

Deleted due to copyright

Figure 2.10 Factors that affect the tool–chip contact length (Sadik & Lindström 1993; Sadik & Lindström 1995).

Furthermore, the contact length has a significant effect on the factors mentioned in Figure 2.11. The friction and the shear forces are the main sources of heat generation in the tool. It is obvious that the reduction of these forces lead to the decrease in temperature accumulation in the tool. By shortening the contact length, the friction force and heat along the rake face of the tool are decreased. As a result, both cutting and tangential (thrust) forces are minimized (Friedman & Lenz 1970; Sadik & Lindström 1993; Huang et al. 1999; Abukhshim et al. 2004; Iqbal et al. 2008). Predicting the contact length and the experimental evaluation will be reviewed in the next section.

Deleted due to copyright
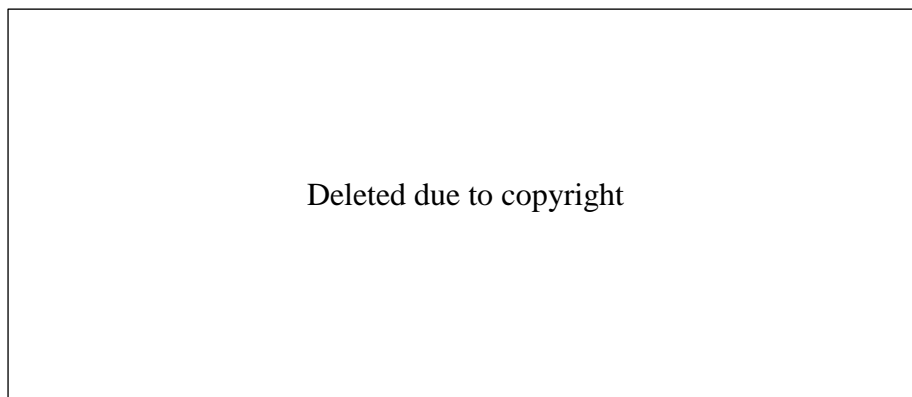
Figure 2.11 Factors affected by the tool-chip contact length (Sadik & Lindström 1993).

2.6.2 Prediction of Contact Length

In orthogonal cutting, a number of theoretical and experimental predictors have been developed to estimate the contact length (Toropov & Ko 2003; Abukhshim et al. 2004; Iqbal et al. 2008; Iqbal et al. 2009; Fatima & Mativenga 2013). Table 2.1 summarizes the contact length models in orthogonal cutting available in the literature and the workpiece materials on which these models were developed (in chronological order).

In the 1950s, the first model to predict the contact length was proposed by Lee & Shaffer (1951). This model was based on the slip line theory for mild steel (plain-carbon steel). They found that the contact length is affected by the undeformed chip thickness, shear angle and rake angle, where the largest undeformed chip thickness has the longest contact length. They also found that the contact length has an inverse relationship with the rake angle (Lee & Shaffer 1951).

During the same period, Hahn (1953) proposed another model depending on the theory of uniform stress distribution on the shear zone. Other researchers developed different models for the contact length derived on the basis of equilibrium consideration (Klushin 1960; Rubenstein 1965; Zorev 1966). In these models the shear angle had to be determined from numerous tests, therefore these models are not easily applicable to machining practice. These models also include a variable *m* factor. This factor is related to the stress distribution on the secondary shear zone, which is shown to take values between (-5 to 22) (Friedman & Lenz 1970). It has been concluded from these models that the chip thickness and the rake angle have the effect on a qualitative prediction of the contact length.

Table 2.1 Summary of contact length models

Researcher	Contact length model	Workpiece material (Cutting speed *m/min*)
Lee & Shaffer (1951)	$L_c = \dfrac{t_1\sqrt{2}}{\sin\emptyset \sin(45° + \emptyset - \alpha)}$	Mild steel
Hahn (1953)	$L_c = mt_1 \dfrac{\sin(\psi + \emptyset - \alpha)}{\sin\emptyset \cos\psi}$	-
Klushin (1960)	$L_c = m \dfrac{t_1 \cos\psi}{\sin\emptyset \sin(\psi + \emptyset - \alpha)}$	-
Abuladze (1962)	$L_c = 2t_1[\lambda(1 - \tan\alpha) + \sec\alpha]$	-
Rubenstein (1965)	$L_c = mt_1 \dfrac{\sin(\psi + \emptyset - \alpha)}{\sin\emptyset \cos\psi}$	-
Zorev (1966)	$L_c = mt_2[\tan\psi + \tan(\emptyset - \alpha)]$	Different grades of steel
Boothroyd & Bailey (1966)	$L_c = \dfrac{t_1 \cos(\emptyset - \alpha)[\cos(\psi - \alpha) + 2\sin(\psi - \alpha)]}{\sin\emptyset [2(\cos\psi \cos\alpha) + \sin(\psi - \alpha)]}$	-
Poletika (1969)	$L_c = t_1(2.05\lambda - 0.55)$	Iron, copper, bronze, steel
Kato et al. (1972) and Toropov & Ko (2003)	$L_c = 2t_2$	Aluminium, zink, copper (800), AI 6061(1000)
Tay et al. (1976)	$L_c = \dfrac{t_1 \sin\theta}{\cos(\theta + \alpha - \emptyset)\sin\emptyset}$	AISI 1016 (244)
Vinogradov (1985)	$L_c = \dfrac{t_1 \sin\frac{\pi}{4}}{\sin\emptyset \sin(\frac{\pi}{4} + \emptyset - \alpha)}$	-
Oxley (1980)	$L_c = \dfrac{t_1 \sin\theta}{\cos\alpha \sin\emptyset}\left\{1 + \dfrac{nC}{3\left[1 + 2\left(\frac{\pi}{4} - \emptyset\right) - nC\right]}\right\}$	Low carbon steel 0.16%C (6-60)
Zhang et al. (1991)	$L_c = 8.677 \times 10^{-5}t_1^{0.515}V_c^{-0.065}(90° - \alpha)^{0.733}$	AISI 1045 (30-130)
Gad et al. (1992)	$L_c = 57.5t_1^{0.671}(90° + \alpha)^{-1.69}e^{-0.0087V_c}$	S1214 steel (23.3-74.6)
Stephenson et al. (1997)	$L_c = 0.485 + 0.00280V_c$ $L_c = 2.421V_c^{-0.294}$	AISI 1018 (82) AI 2024
Marinov (1999)	$L_c = 1.61t_2 - 0.28t_1$	AISI 1018 (291)
Sutter (2005)	$L_c = 1.92t_2 - 0.09t_1$	XC 18 (3600)
Wang & Zhu (2006)	$L_c = h(1 + n\gamma) + (1 + n\gamma)\sqrt{(x + y)^2 + (x - y)^2}$	-
Woon et al. (2008)	$L_c = 1.25t_2 + 0.61t_1$ $L_c = 1.07t_2 + 0.59t_1$	Steel (100)
Iqbal et al. (2009)	$L_c = 1.56t_2 + 0.09t_1$ $L_c = 1.15t_2 + 0.70t_1$	AISI 1045 (98-880) Ti6AI4V alloy
Germain et al. (2010)	$L_c = t_2 - a\alpha + b$	Copper (140)

where:
- L_c: Contact length
- t_1: Undeformed chip thickness
- t_2: Chip thickness
- λ: Chip compression ratio
- α: Rake angle
- $\emptyset$: Shear angle
- ψ: Friction angle
- V_c: Cutting velocity
- θ: Inclination of resultant cutting force to shear plane
- h: Land length of the tool
- n: strain hardening index
- m, C: Material constants
- γ: Shear strain
- a, b: Empirical constants
- x, y: Cartesian coordinates

Other models, were developed by Abuladze (1962) and Poletika (1969) based on analytical and experimental studies, respectively. According to the results of these studies, the contact length can be estimated from the chip compression ratio and the undeformed chip thickness, this can be seen clearly from the equations in Table 2.1. Boothroyd & Bailey (1966) found that the tool-chip contact length can be predicted from the shear angle, rake angle and the undeformed chip thickness.

In the 1970s and 80s, a few works were performed on contact length prediction. Kato et al. (1972) proposed an empirical model to predict the contact length for various workpiece materials: ferrous and non-ferrous metals and the cutting speed was 50 *m/min*. The model predicted the contact length was twice the deformed chip thickness.

The estimation of the plastic contact length (sticking contact length) was conducted by Tay et al. (1976) by utilizing *AISI 1016* under orthogonal cutting conditions and the elastic contact length (sliding region) was ignored. The analysis of the secondary shear zone (tool-chip interface) was undertaken using printed grids with quick stop chip sections. The contact length was found to be affected by: undeformed chip thickness, the shear angle and the rake angle. Mathew & Oxley (1980) and Oxley (1989) developed a model to determine the contact length, when machining plain-carbon steel. This model was based on equilibrium considerations. In addition, it was based on the theory of the stress distribution on the rake face of the cutting tool. In 1985, another model was proposed by Vinogradov (1985), which is very similar to Lee & Shaffer's (1951) model. Both models are dependent on shear angle and undeformed chip thickness and are similar in their mathematical form, with the exception of the numerator component.

Zhang et al. (1991) presented another model which is completely different from its predecessors, where previous models did not take into account the effect of cutting speed on the tool-chip contact length. However, the effect of this parameter on the contact length was studied. A steel (*AISI 1045*) was used at different cutting speeds (30-130 *m/min*). The result showed that the contact length decreases with increasing cutting speed. Gad et al. (1992) also predicted the tool-chip contact length as a function of cutting speed. A statistical curve fitting technique was used to predict contact length. The contact length was found to be reduced as the cutting speed increases. This model was derived using a high-speed steel (HSS) tool with steel S1214 workpiece

material and was tested just up to a cutting velocity of 75 *m/min*. Likewise, Stephenson et al. (1997) predicted contact length as a function of speed of cutting only where this model does not show any effect of rake angle and undeformed chip thickness on contact length. It can be seen clearly from the equation (see Table 2.1) that at zero cutting speed a contact length is equal to 0.485 *mm*, which is unrealistic. The maximum cutting speed was 82 *m/min*. The contact length was found to increase as the cutting speed increases. At the end of 1990s, a model was suggested by Marinov (1999) in which a dimensional analysis was used to derive an equation for the contact length for *AISI 1018*. The researcher concluded that contact length changes with changing deformed and undeformed chip thickness.

Using the slip line theory, Toropov & Ko (2003) reached the same result of Kato et al. (1972) which is that the contact length is twice the chip thickness. Verification of these models was experimentally performed for different workpiece materials. The model proposed by Abuladze (1962) is similar to Kato et al. (1972) and Toropov & Ko (2003), for a zero rake angle tool. Therefore, three models concluded that doubling the chip thickness is a good prediction for contact length. This model has been used in this study.

Sutter (2005); Woon et al. (2008); Iqbal et al. (2009) used dimensional analysis methods similar to Marinov (1999) to predict contact length for different workpiece materials. Therefore, their contact length model is similar as well, although with different coefficients. In addition, the difference in coefficients of these models can be referred to different cutting speeds used (using different workpiece material). This obviously indicates the reliance of contact length on cutting speed and workpiece.

Wang & Zhu (2006) presented a model to estimate contact length using the slip line theory taking into account the effect of shear strain on tool-chip contact length. Recently, a model was presented by Germain et al. (2010). This model based on the empirical data. The tool-chip contact length was predicted as a function of chip thickness and rake angle (Germain et al. 2010). Such models are unsatisfactory due to unknown experimental parameters like *a*, *b* and *n*.

With regards to experimental evaluation, the most well-known method utilized for measurement of tool-chip contact length is the microscopic examination of the wear

traces left by the sliding chip on the rake face of the cutting tool (Lee & Shaffer 1951; Hahn 1953; Klushin 1960; Rubenstein 1965; Poletika 1969; Friedman & Lenz 1970; Stephenson et al. 1997; Marinov 1999; Woon et al. 2008; Iqbal et al. 2009). While, other researchers examined the wear traces of contact zone on the underside of the chip gained by a quick stop experiment for measurement of contact length (Boothroyd & Bailey 1966; Iqbal et al. 2007).

Another promising technique for measurement of contact length is painting the rake face of the cutting tool before machining. Zorev (1966) coated the tool rake face with a copper paint before cutting and then wear tracks were observed on the rake face of the cutting tool. Gad et al. (1992) used a dyeing technique, where a solution of hydrofluoric acid, hydrogen peroxide and ammonium persulfate was used to dye the rake face. This solution changes the colour of the tool rake face to black, thus measuring the contact length was conducted by measuring the rubbed contact area using a microscope. However, these techniques were appropriate at low cutting speed whereas at higher cutting speed, the coating layer was oxidized. Microphotographs is another technique for measuring contact length that was used by Zhang et al. (1991), where a device consisting of a camera and light source was used to capture the deformation situation in machining. The experiments were conducted on steel (*AISI 1045*) over a cutting speed range of 30-130 *m/min*, which is the upper limit of the conventional cutting speed for cutting steel (Fatima & Mativenga 2013). Abuladze (1962) used another technique for measuring contact length, by identifying the traces of chip's material on the tool rake face. This can be completed because of the compositional differences between tool and work material. This technique is a precursor to the energy dispersive X-ray analysis (EDX) and this method was used in this work.

The characterisation of the tool-chip contact length over the rake face of the cutting tool will be reviewed in the next section.

2.6.3   Tool-Chip Contact Phenomena

Boundary conditions of the tool-chip interface have an important role in determining the cutting tool stresses and temperature, which are important to ascertain the suitable cutting conditions and to improve the design of the cutting tool.

Presenting the precise modelling of the tool-chip interface's friction is a big challenge, although it has been studied for almost 70 years. Particularly in turning processes where the continuous contact between the tool and chip makes reaching the tool-chip interface impossible. Sliding and sticking interfaces are the boundary conditions of the tool-chip interface. The geometry of these conditions varies continually with time through the machining process.

A disagreement in terms of the characterisation of the boundary conditions of the contact length over the tool rake face have been found in the literature. The first and widely cited view is to divide the tool-chip contact length into two regions with full sticking (seizure) taking place over much of the tool-chip interface near the cutting edge where the sliding velocity is close to zero (Figure 2.12), followed by an interfacial sliding occurring near the boundary of the tool-chip contact (Zorev 1966).

Deleted due to copyright

Figure 2.12 Contact conditions at the tool-chip interface: sticking and sliding regions
(Norouzifard & Hamedi 2014)

In contrast, the second view (Madhavan et al. 2002) holds that sliding occurs over much of the tool-chip interface near the cutting edge, followed by sticking occurs near the boundary of the tool-chip contact. A third hypothesis is that the contact length is divided into four regions (Figure 2.13): a stagnation region at the cutting edge, a retardation region, a sliding region, and a sticking region near the boundary of the tool-chip contact (Ackroyd et al. 2003).

Deleted due to copyright
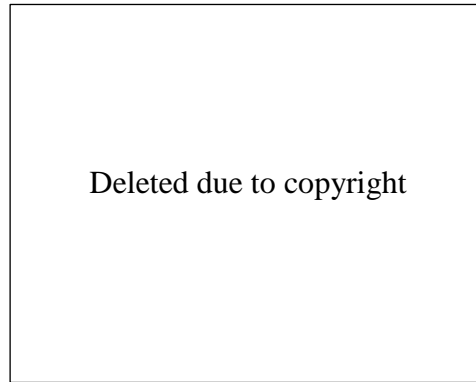
Figure 2.13 Contact conditions at the tool-chip interface: Stagnation, retardation, sliding and sticking regions (Ackroyd et al. 2003)

The distribution of the shear and normal stress at the rake face of the cutting tool has been suggested by (Zorev, 1963, cited in Kilic & Raman, 2007) to estimate a model for the frictional boundary conditions at the interface between the tool and chip. He used orthogonal cutting of steel workpiece using controlled contact length at moderate and low cutting velocities so as to measure the cutting forces for different tool-chip contact lengths. Furthermore, a different cutting depth and different rake angles were used in his experiments. Based on the results of this work, the tool-chip interface consists of sticking and sliding zones, where the sticking zone dominates the cutting edge due to the occurrence of intense plastic shearing of the weaker material. While, the sliding zone represented the remaining parts of the contact area (see Figure 2.14), the frictional boundary conditions in this area is less than the sticking zone. Distinguishing these two areas was achieved using photomicrographs through a quick-stop mechanism.

Deleted due to copyright
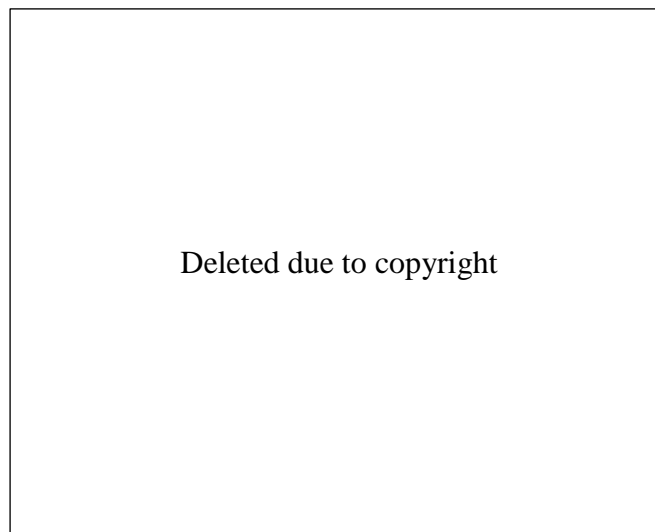
Figure 2.14 Distribution of shear and normal stress at tool-chip interface (Kilic & Raman 2007)

26

Zorev presumed that in the sticking area the shear stress was uniformed with a power law decrease in the sliding area, while the distribution of the normal stress was measured according to the power law equation of $\sigma = qx^y$, where q and y are constants and x is the distance between the cutting edge and the point where the chip leaves the rake face of the cutting tool.

Wallace & Boothroyd (1964) studied the frictional conditions at the tool-chip interface. They used different cutting tools with different rake angles to cut an aluminium alloy at different cutting velocities. A quick-stop technique was used in order to investigate the bottom side of the chip (i.e. the side which is in contact with the rake face of the cutting tool) and the variation of the friction at the tool-chip interface. The results showed that the interfacial friction relied on different factors including the coefficient of sliding friction, shear strength of the chip material and the distribution of the normal stress on the rake face of the cutting tool.

In contrast to Zorev's results, (Horne et al., 1978, cited in Wright et al., 1979) proved that the sliding conditions occur at the area behind the cutting tool edge while the sticking zone was shown at the rear part of the tool-chip contact length. They used transient sapphire cutting tools to cut soft materials like lead. Conversely, when cutting hard workpiece materials such as iron and steel by using metal cutting tools, the sticking zone will prevailed the area just behind the cutting tool edge.

Wright (1981) attributed the reason for sliding and sticking occurring to the distribution of stress on the rake face of the cutting tool and also to the surface tool conditions. He found that there were many factors affecting the interface boundary conditions including the cutting time, cutting velocity, immediate environment and workpiece-tool combination. He also mentioned that when cutting soft material with coated cutting tool for short times the sliding conditions would occur. While the sticking conditions would dominate if the duration of cut was long, there were high cutting velocities and there were low hardness values of workpiece and tool materials. In other work, Wright et al. (1979) stated that the sticking condition is "defined as a solid phase weld between totally clean metal surfaces devoid of oxide". While the sliding conditions is "defined as relative movement between last layer of atoms and the tool surface". They also proposed a model for interpreting the interaction between

sticking and sliding regions at the secondary shear zone (i.e. tool-chip interface). The model is

$$A_s = KA_r \qquad\qquad 2.1$$

where: A_s: the sticking area, A_r: the real contact area (total contact area), and K: constant.

The range of the K values is between (0-1) which depends on many factors such as the cutting speed, tool rake angle, cutting time, tool material and workpiece purity. Such models, however, have failed to determine the exact value of K.

A high-speed imaging system has been used by Madhavan et al. (2002) to study the boundary conditions at the tool-chip interface; this system consisted of an optical microscope with a charge coupled device (CCD) –based high speed camera. Using this system enabled the observation of the contact conditions in situ in orthogonal cutting of aluminium, pure lead and copper at low cutting speeds and without using a lubricant. The contact area between tool and chip was classified into three different regions of contact, as shown in Figure 2.15. A zone close to the cutting edge which was free of deposition of chip material onto the rake face of the cutting tool (zone 1) and was considered by sliding region. Followed by Zone 2a and 2b which were a deposition of the chip material on the tool rake face and were characterized by sticking zones.

Deleted due to copyright
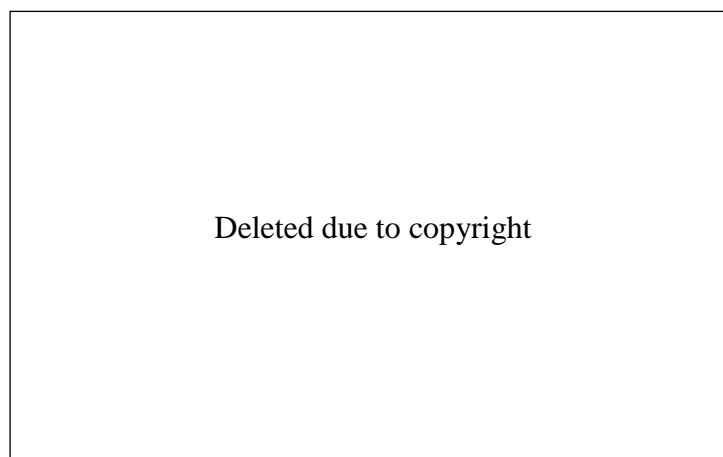
Figure 2.15 Schematic of the tool rake face showing the different zones (Madhavan et al. 2002)

The high-speed imaging system was used by other researchers to enable the details of the tool-chip interface to be determined at high spatial and temporal resolution while

cutting at velocities varying from (1-2000 *mm/sec)*. They used orthogonal cutting of pure lead workpiece using an optically transparent sapphire cutting tools. They concluded that the tool-chip contact area can be divided into four different regions, as shown in Figure 2.16, a stagnation region at the cutting edge, followed by a retardation region, a sliding region and sticking region which is placed near the boundary of the tool-chip contact. In the sticking region a thin layer of the chip material is deposited on the rake face of the cutting tool (Ackroyd et al. 2003).

Deleted due to copyright

Figure 2.16 Model of tool-chip contact conditions derived from the observation (Ackroyd et al. 2003)

New methods were used to investigate the adhesion layers on the rake face of the cutting tool after the cutting process, because of the contact area between the tool and chip is small and the difficulty of investigations in situ through cutting process. These methods are the laser mass spectrometry, scanning electron microscopy (SEM)-energy dispersive X-ray spectrometry (EDX) and 3D white light interferometry. These techniques were used by M'Saoubi & Chandrasekaran (2005) to classify the chemical composition of the deposit layer on the tool rake face after machining 316L steel at different cutting speed and different times of cut. They pointed out that the longitudinal and lateral sections of 3D maps could be utilized to determine the thickness of the adhesive layer. They observed that the thickness of the adhesive layer increases with increasing cutting speed and cutting time. They also observed through using the EDS analysis that the tool-chip interface was divided into three regions: a region with small chip material transfer adjacent to the cutting edge, a sliding region and a sticking region where a thick layer of the chip material is deposited on the rake face of the cutting tool.

Raman et al. (2002) used the scanning electron microscope (SEM) and image analysis to investigate the fractal nature of the contact regions. They found that the cutting

speed effects the fractal geometry of the sliding and sticking regions, where the fractal dimension decreases with increasing the cutting speed.

Kilic & Raman (2007) used oblique cutting of aluminium alloys using carbide cutting tool at different cutting speeds to investigate the interfacial boundary conditions at the tool-chip interface including the BUE, sticking and sliding regions. The tool rake face was investigated after tests by utilizing different techniques such as: SEM, Laser Scanning Confocal Microscopy (LSCM) and surface profilometer. They found that there were different factors effecting the BUE, sticking and sliding regions such as: the cutting conditions, cutting geometry and workpiece material; where these boundary conditions vary according to these factors. They also observed that at low cutting speeds the sticking condition was dominated by the contact area between the tool and chip, while with increasing the cutting speeds three different regions were shown: I. sticking region close to the cutting edge, followed by a sliding region and the remaining parts of the contact area were represented by II. sticking region (see Figure 2.17). The increasing of the cutting speeds lead to decreasing the I. sticking zone and vice versa. They attributed the causes of the disappearance of BUE at high cutting speeds to two factors: there was no adequate time for the chip at high cutting speeds to stick on the tool rake face and the second was with increasing the cutting speeds the compression forces were decreased.

Deleted due to copyright
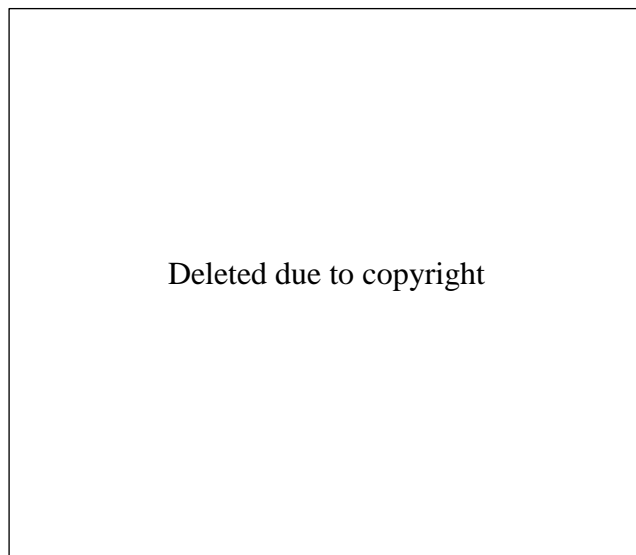
Figure 2.17 SEM image of tool-chip contact area, showing different contact conditions (Kilic & Raman 2007)

The analyses of the tool-chip contact area to distinguish between the sticking and sliding zones were performed by Courbon et al. (2013) by utilizing SEM-EDXA using

dry orthogonal cutting. They found that the tool-chip contact area decreases with increasing the cutting speed and reducing the feed rate. They concluded that the contact region consists of two regions: sticking zone which is close to the cutting edge and it is free of deposits of chip's material and the second region is sliding zone.

2.7 Measurement Techniques

2.7.1   Cutting Forces

In orthogonal cutting, there are two components of cutting forces, which are acting on the cutting tool, namely thrust force and main cutting force. The thrust force is in the feed direction (also known as feed force) and it is denoted by F_t, while the main cutting force is perpendicular to the cutting edge (known as cutting force) and denoted by F_c (Figure 2.18). These two forces are typically measured using a dynamometer.
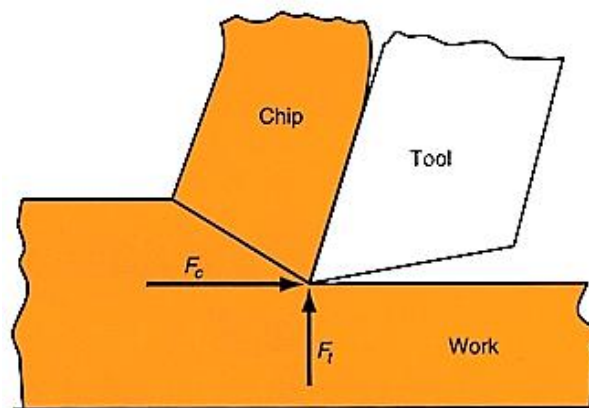
Figure 2.18 Forces in orthogonal metal cutting

Below are some works which have been conducted to investigate the influence of the cutting forces on the machining performance.

For machining aluminium, the data presented by (Trent 1977; Trent & Wright 2000) shows that the relationship between cutting speed and cutting force is inversely proportional (see Figure 2.19). It seems possible that these results are due to the softening of the workpiece material resulting from an increase in temperature at the tool-chip interface when the cutting speed increases.

Deleted due to copyright
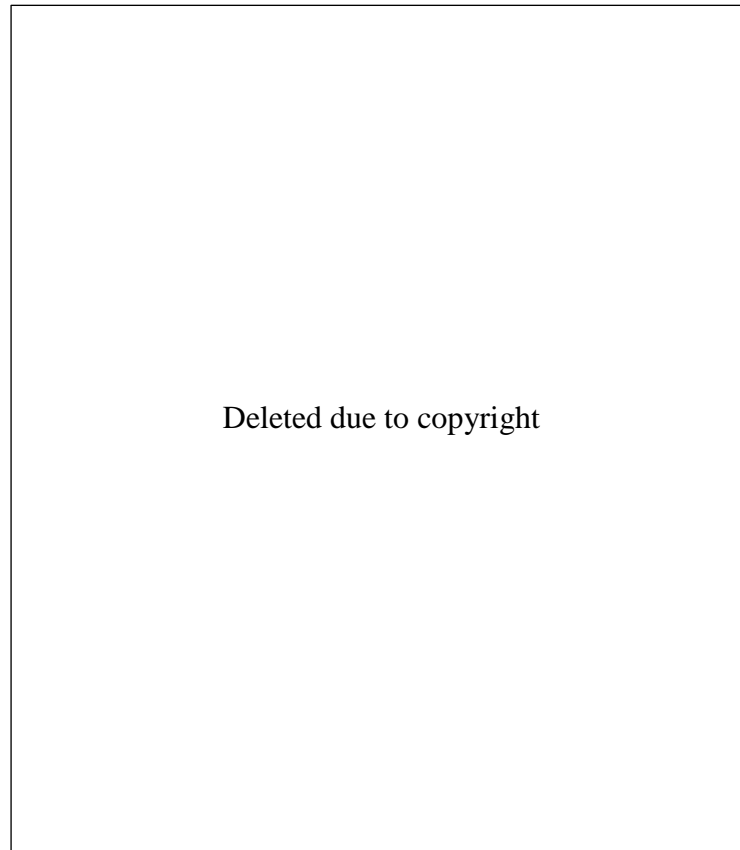
Figure 2.19 Forces vs cutting speed-aluminium and magnesium (Trent & Wright 2000)

Seah & Li, (1997) conducted an experimental investigation on *AISI 1050* steel material during turning operations using P30 uncoated cemented carbide cutting tool at a different cutting speeds (10-200 *m/min*). The experiments were performed with and without coolant, and the coolant was applied on the rake face of the cutting tool. The experimental results revealed that the role of coolant in term of cutting forces depends on the cutting speed, where at low cutting speeds the coolant caused a decrease in the cutting forces while at high cutting speeds the coolant role was negligible. The tool temperature is not too high at low cutting speeds, therefore, the cutting fluid act as a lubricant and reduces the friction at the contact areas between the tool and workpiece.

The effect of the cutting forces on the temperature of the machined surface, during machining of aluminium *Al 6082-T6*, has been confirmed by the experimental work of O'Sullivan & Cotterell, (2001). The experiment was performed in the absence of fluid. The cutting forces and the machined surface temperature were found to decrease as the cutting speed increases and increase with tool wear.

The influence of coolant on the cutting forces was investigated during cutting of aluminium *Al* 6061 at different cutting speeds (up to 400 *m/min*). The trials were conducted by utilizing a diamond-coated carbide cutting tool, and all the experiments were carried out both with and without cutting fluid. The author used two different methods for the coolant conditions, namely minimum quantity lubrication (*MQL*) and flood coolant. It has been concluded that the cutting forces affected by the machining environments, where at the unlubricated conditions the cutting force was the highest whereas at the flood coolant the cutting force was found to be the lowest. For the *MQL*, the researcher clarified that needs more investigation (Sreejith 2008).

Gokkaya (2010) used cutting speed and feed rate as cutting variables to investigate their effect on the cutting force. The experiments were conducted on aluminium *A2014* using uncoated carbide cutting tool in dry conditions. Gokkaya found that the main cutting force increased with increasing the feed and decreased with increasing cutting speed. Jr et al. (2011) used different materials for the same purpose, *6262-T6* and *7075-T6* aluminium alloys, and the same results of Gokkaya (2010) were observed.

The influence of the BUE on the fluctuation of cutting forces has been studied by Fang et al. (2010A). They observed that the cutting forces fluctuated significantly within cutting speed up to 100 *m/min* and they attribute this fluctuation to the BUE existence. Whereas, during cutting beyond 100 *m/min*, no significant fluctuation of the forces observed due to the vanishing of the BUE.

In another work, and in order to investigate further about how the cutting forces affected by the machining parameters; Ojolo & Ohunakin, (2011) used high-speed steel (HSS) cutting tool to cut aluminium alloy rods in dry and wet conditions. The experiments were conducted at different cutting parameters: cutting speed (1.7, 2.33, 3.08 and 4.15 *m/s*), cutting depth (0.5, 1, 1.5, 1.8 and 2 *mm*) and feed rate (1, 1.5, 1.8 and 2 *mm/rev*). They reported that the cutting force increased with increasing cutting depth and feed, but decreased with increasing cutting speed.

More recently, Popov & Dugin, (2014) attributed the increasing of cutting forces with using coolant to the built-up edge (BUE), because cutting with a cutting fluid prevents the BUE on the rake face and therefore, the cutting is conducted with the nose radius

at a negative rake angle. Where cutting without cutting fluid, a built-up edge is formed, which changes the cutting edge geometry.

Eliminating or reducing the cutting fluid during the cutting process was a scope of one of the researchers to get a healthy environment. Where Davoodi & Tazehkandi, (2014) conducted an experimental investigation on Aluminium *5083-O* during turning cutting using coated carbide cutting tool in dry and wet conditions in order to remove coolant. It has been concluded that the cutting force mainly affected by feed or the uncut chip thickness. They also concluded that the possibility of machining *Al 5083-O* at high cutting speeds and low feeds without using cutting fluid.

Davoodi et al. (2012) found that at wet conditions the cutting force decreased with increasing feed within a specific range (up to 0.282 *mm/rev*) but behind this range the cutting force was found to increase.

2.7.2   Acoustic Emissions (AE)

Acoustic emissions are defined as transient elastic stress waves generated due to the rapid release of energy in a material as a result of a rearrangement of its internal structure (Lauro et al. 2014). To detect these waves, microphones or sensors are used and coupled to the surface of the sample. Acoustic emissions are used in numerous applications like pressure vessels, pipeline leak detection, aircraft, solidification, and machining.

The acoustic emissions are typically measured using AE sensor. There are many sources of acoustic emissions in machining process including deformation at the shear cutting zone, sliding friction at tool-chip interface, chip breakage and the waves which occurs as a result of chips impact on the cutting tool and workpiece.

In orthogonal cutting, a number of experiments have been carried out to measure the machining performance by utilizing acoustic emission. The first analysis of the emitting sound from the cutting process was conducted by Grabec & Leskovar (1977). The experiments were carried out orthogonally on aluminium at the cutting speeds range of (100-1000 *m/min*), cutting depth range of (0.5-3.5 *mm*) and feed range of (0.027-0.132 *mm/rev*). It was found that the cutting process is a severe generator of continuous acoustic emission in both ranges: audible and ultrasonic. In the audible

range, the spectrum is discrete, while the spectrum is continuous in the ultrasonic range, which is known later as AE. The effect of the machining parameters on the distribution of the spectrum was studied, and a qualitative explanation of the corresponding effects was given. They proposed that the AE could possibly be used to evaluate the sharpness of a cutting tool.

Kannatey-Asibu & Dornfeld (1981) presented a theoretical relationship between the root mean square of the acoustic emission (AErms) and cutting parameters. Verification of this model was experimentally conducted during orthogonal cutting of two different workpiece materials, namely *6061-T6* tubular aluminium and *SAE 1018* tubular steel. The trials performed for different cutting speeds from 0.128 to 1.9 *m/s* and different rake angles from 10° to 40°with a constant feed of 0.089 *mm/rev*. The RMS of the acoustic emission was found to be increased with increasing the rake angle and cutting speed.

Hu & Qin (2008) investigated the generation of acoustic emission signals during machining of two different aluminium alloys; *A390* and *A359/SiC/20p*. The investigation was conducted by using a cutting tool coated with a nano-diamond. They used different cutting parameters for each material, for A 390 alloy, the cutting speeds (3.3 *m/s* and 10 *m/s*) and the feed (0.2 *mm/rev*, 0.8 *mm/rev*) with a constant cutting depth (2 *mm*) were selected. For A359/SiC/20p the two cutting speeds were (4 *m/s* and 8 *m/s*), feeds (0.15 *mm/rev* and 0.3 *mm/rev*) and the depth of cut of (1 *mm*). They analysed the data in the time domain in respect of the amplitude of the raw signals and the root mean square of the acoustic emission (AErms), they also analysed the signals in frequency domain using Fast Fourier Transform (FFT). They concluded that the amplitude of the acoustic emission signals increases considerably with increasing the cutting speeds while there was a minor effect of the feed on the signals. They also found that the prevailing effect for generation the acoustic emission signals refers to the chip formation and segmentation.

The effect of the cutting parameters including cutting speed, feed or (undeformed chip thickness) and the tool-chip contact length on the AE signal energy was studied by Rangwala & Dornfeld (1991) by utilizing *6061-T6* aluminium using the orthogonal cutting. They found that the RMS of the AE signal increases with increasing cutting speed.

2.7.3 Machining Vibration

In a cutting process, there are three major categories of vibration: free, forced and self-excited vibration. Forced vibration is induced as a result of the unbalance influence of the machine tool assemblies such as bearings, spindles and gears and free vibration is caused by shock. Self-excited vibration or chatter are induced when the cutting tool is cutting a workpiece that had a wavy surface from the previous tool revolution (Siddhpura & Paurobally 2012). Chatter has a bad effect on the surface finish, productivity and tool life (Stephenson & Agapiou 2006). Therefore, many researchers tried to avoid chatter either by detecting it as soon as occurs or by predicting its occurrence earlier.

As described in Section 2.5 of this chapter, the BUE has a profound effect on the machining surface, vibration and cutting forces. Therefore, a study has been carried out by Fang et al. (2010A) to predict the BUE formation. The study was performed during orthogonal tube cutting of *2024-T351* aluminium alloy using two different cutting tools: sharp and round edge tools. the experiments were conducted at different cutting speeds (0.8-250 *m/min*) and different feeds (0.01-0.3 *mm/rev*), while the cutting depth was constant which is equal to the tube wall thickness. A dynamometer and an accelerometer were used to measure the cutting forces and vibration, respectively. The results of the cutting forces have been reviewed in Section 2.7.1 of this chapter. Regarding to the vibration results, they concluded that the vibration amplitude depends on the cutting speeds where they divided the cutting speeds into three ranges according to the variation of the vibration amplitude. At the speeds below 20 *m/min*, the amplitude of the vibration increased rapidly as the cutting speeds increased. For the speeds (20-100 *m/min*), the vibration amplitude found to be slightly varied as the speeds increased. For the speeds higher than 100 *m/min*, they reported that the amplitude drops as the cutting speeds increased. They observed that this variation of the vibration amplitude with the cutting speeds is related to the BUE formation. They also found that the vibration produced from the sharp edge tool were different from the round edge tool, where the round edge tools produced a higher amplitude than the sharp edge tools.

In another study, and as mentioned in Section 2.5, Fang et al. (2010B) established a relationship between the cutting vibration and the BUE formation. Establishing this

relationship was experimentally performed at different cutting speeds (0.80-100 *m/min*) during orthogonal cutting of *2024-T351* aluminium tube using cemented carbide cutting tool. They analysed the vibration signals in time and frequency domains. The results indicated that kurtosis, a statistical tool, can be used to confirm the existence of the BUE and to distinguish between the different regions of the BUE. Where the results showed that there were three distinct BUE regions which are categorised by different patterns of cutting vibration: the BUE initiation region (0.8-4 *m/min*), steady BUE region (4-20 *m/min*) and unsteady BUE region (20-100 *m/min*).

2.7.4   Temperature Increase and Its Effects on Machining

In metal cutting, there are three main sources of heat (Figure 2.20): primary deformation zone, secondary deformation zone (tool-chip interface) and tertiary deformation zone (tool-workpiece interface) according to Kus et al. (2015).
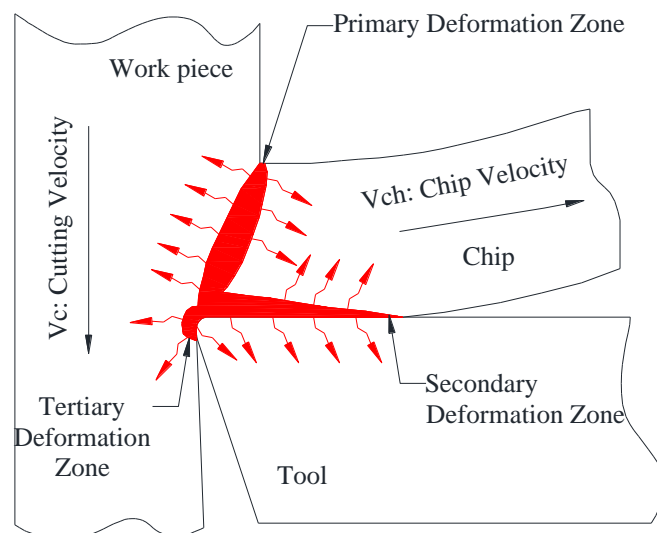
Figure 2.20 Heat sources and propagation in metal cutting

The heat generated in cutting process is shared by the cutting tool, workpiece and the chip. The maximum amount of the generated heat is carried away by the flowing chip, while the amount of heat which shared by the cutting tool is about 10-20 % of the total heat and some of heat is goes to the workpiece. With increasing cutting speeds, the amount of the generated heat that shared by the cutting tool are decreased (see Figure 2.21).

Deleted due to copyright

Figure 2.21 Distribution of heat amongst chip, tool and workpiece (Abhang & Hameedullah 2010B)

There are different methods for measuring the temperature in the cutting processes including tool-workpiece thermocouple, embedded thermocouple, Infrared cameras and infrared thermometers.

2.8 Design of Experiments

The experimental design technique is a powerful tool that allows the modelling and analysis of the influence of design factors on dependent factors. The process factors can be defined as a design factor which determines the dependent factors, also known as response factors. Although many variables are used as machining parameters in a cutting process, the cutting speed, cutting depth and feed are the most common parameters considered by researchers (Barman & Sahoo 2009; Devi et al. 2015). In this study, the other machining parameters have been set to be constant over the design of experiment while the selected process factors are taken in consideration.

There are many methods of experimental design such as full factorial design, partial factorial design, Box-Behnken design and centre composite design (CCD). The full factorial design is not feasible, in cases involving many factors, because of time restrictions and the cost involved in performing these experiments. In metal cutting modelling, studies show that a centre composite design (CCD) developed by Box and Wilson, is the most recommended method of experimentation, where experiments are conducted for all variable combinations (Oraby 1989), and therefore, it was used in this study to design the experiments.

For modelling a quadratic (second-order) response surface, the most widely used experimental method is a rotatable central composite design (Myers et al. 2002). This was used for conducting these trials. To fulfil a rotatability for a given number of process factors, α is required and is calculated as

$$\alpha = (2^k)^{1/4} \qquad\qquad 2.2$$

where k is the number of the process factors.

Rotatability refers to the uniformity of prediction error. In rotatable designs, all points at the same radial distance (r) from the centre point have the same magnitude of prediction error. The total number of experiments for a rotatable second-order CCD is calculated as

$$N = n_a + n_o + n_c \qquad\qquad 2.3$$

where:

N: Total number of experiments

n_a: Axial point, $n_a = 2k$

n_o: Centre point

n_c: Corner point, $n_a = 2^k$

The axial points $n_a = 2k$ are positioned on the coordinate axes of factorial space [($\pm$ α,0,…0),(0,$\pm$ α,…0), (0,0, …$\pm$ α)] and n_o is centre points (0, 0, 0, 0…, 0). The number of centre points can be calculated from the equation below

$$n_o = \frac{(n_a + n_c)(\lambda(k+2) - k)}{k} \qquad\qquad 2.4$$

where; λ is constant and it depends on the number of the design parameters, for instance at $k = 3, \lambda = 0.86$ (Box & Hunter 1957). The corner points(n_c) are known as factorial points and usually coded as ± 1.

In this experimentation, there are three design factors (k): cutting speed, cutting depth and feed. For $k = 3$; $n_c = 8$ (corner points), $n_a = 6$ (axial point) and $n_o = 6$ (centre points), a total of 20 experimental runs have been considered (Figure 2.22). From

equation **2.2**, $\alpha = 1.6817$, A randomized experimental run was conducted to minimize the error as a result of machining set-up.
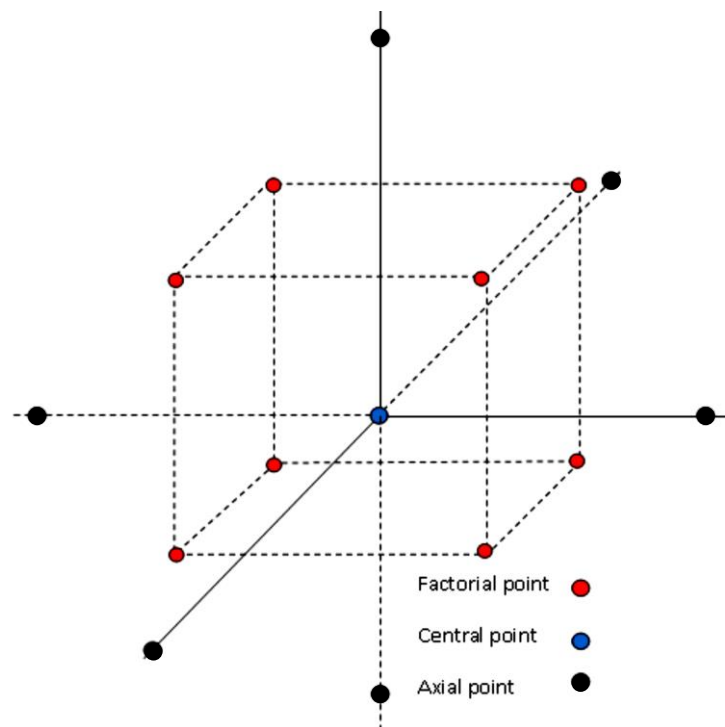
Figure 2.22 Generation of a central composite design for three factors

2.9 Conclusions

The terminology of the machining operations has been presented in this chapter. The difference between the metal cutting methods and the reason for choosing the orthogonal cutting were also stated. The chip types and the mechanism of formation of the BUE and BUL and them effect on the machining performance were presented. The significance of the tribological conditions at the tool-chip interface in machining process were discussed in detail. In the last part of this chapter, the instrumentations of the cutting tools have been defined and reviewed including the techniques for measuring the cutting forces, acoustic emissions, vibration and temperature. The effect of increase temperature on machining performance were also presented in this chapter.

3

Ultrasonic Background

There are many advantages of the ultrasound technique which make it widely used in non-destructive testing and many other applications such as industrial control and medical imaging. Among these advantages, the use of ultrasound is a safe method, non-destructive and it is a portable technique. In addition, because of increasing capabilities of pulsing and digitizing equipment as well as the reducing cost, the use of ultrasonic method is becoming increasingly extensive. This chapter presents the fundamental principles of ultrasound which will be useful in the following investigation of the tool-chip interface.

3.1 An Introduction to Ultrasound

The humans have a limited ability to sense sounds, where the humans are unable to hear sound with a frequency below 20 *Hz* and above 20 *kHz*. Ultrasound is acoustic energy in the form of mechanical waves having a frequency higher than the upper limit of human hearing range, i.e. greater than 20 *kHz* (see Figure 3.1). Today, ultrasound is used in many fields, from a basic car parking sensor to an advanced medical sonography to visualize internal organs and foetuses in the human womb. It is also widely used in manufacturing industry as a non-destructive tool for the inspection of imperfections in a solid body.

| Infrasound | Audible Sound | Ultrasound |

Frequency Range (*Hz*)   20   20000
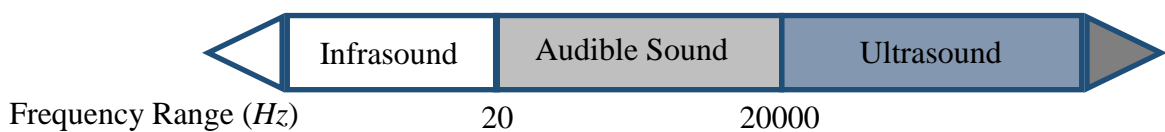
Figure 3.1 The frequency ranges of sound

3.2 Fundamental Principles of Ultrasound

3.2.1   Ultrasonic Wave Propagation

Sound wave move through a host medium as a result of the particles oscillation within the medium. This motion can be modelled as a collection of particles held in position by springs which represent the elastic forces. Figure 3.2 shows a model of the elastic body. The model behaves like a spring where the particles can perform elastic oscillations. If the material particles on the left side of the model are excited with sinusoidal oscillations, the particles on the first plane are then forced to oscillate with the same amplitude. The elastic forces transmit the oscillations to the particles in the second plane. This process will repeat itself for following planes of particles in the medium and, therefore, the vibratory movement of the particles will propagate through the medium.
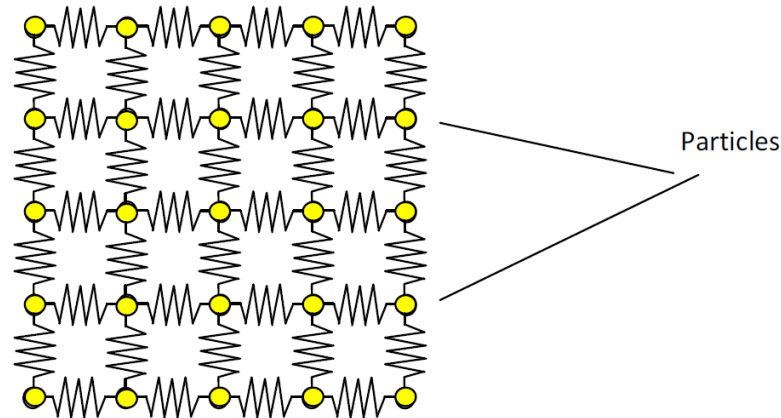
Figure 3.2 Model of an elastic body

Sound waves can propagate in solids in four principle modes that depend on the way the particles oscillate; shear waves, longitudinal waves, surface (Rayleigh) waves, and in thin materials as plate (Lamb) waves (NDT Resource Centre, 2012).

3.2.1.1 Longitudinal Waves

If the particle motion and the wave propagation are in the same direction, then it creates what is known as a longitudinal wave. The wave shown in Figure 3.3 shows an example of a longitudinal wave. This sort of longitudinal wave is also called as pressure or compression waves. This mode (i.e. longitudinal waves) considered the most common modes of propagation used in ultrasonic test and will be the subject of this study.
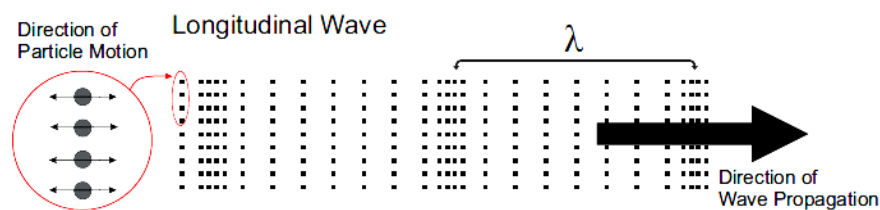
Figure 3.3 Representation of longitudinal wave

3.2.1.2 Shear, Surface and Lamb Waves

The other form of propagation is that of transverse waves depicted in Figure 3.4. In this type of propagation, the motion of particles is perpendicular to the motion of the wave. This wave is also known as a shear wave. The shear wave can only propagate in the medium which support shear forces and because a liquid has not the ability to

support the shear force, so the shear wave cannot propagate through the liquid. The speed of sound of a longitudinal wave, c_L through a medium is approximately double of the shear speed of sound, c_S.
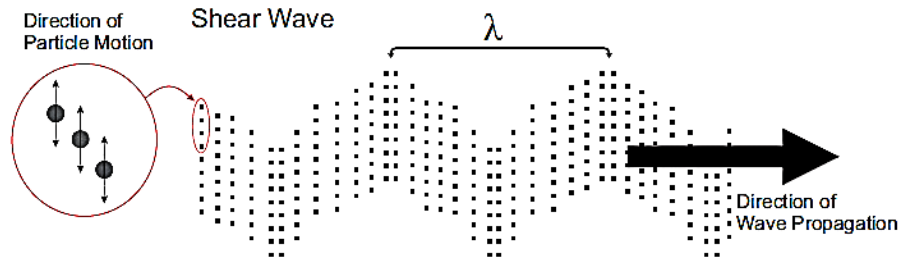
Figure 3.4 Representation of shear wave

Surface waves are a combination of shear and longitudinal waves interacting. These waves are also known as Rayleigh waves. Rayleigh waves only exist on the surface of a material.

Plate waves (also known as Lamb waves) are like the Rayleigh waves, they are a combination of longitudinal and shear waves, but plate waves only occur in thin plates.

Transverse (shear), surface (Rayleigh) and plate (Lamb) waves were not used in this study, to monitor the tool-chip interface, because of their unsuitableness in respect of either ability of detection or application (transverse waves cannot propagate in a liquid, plate waves only occur in thin plates and surface waves cannot propagate through the material where only propagate on the surface of the material).

This study is primarily concerned with longitudinal waves which were sent through the tool–chip interface to measure the interface conditions.

3.2.2   Acoustic Properties of Materials

As mentioned in Section 3.2.1, ultrasonic waves propagate by oscillating particles within a medium. Therefore, the ultrasonic wave properties are affected by the properties of the medium through which the wave is travelling. In this section, factors correlated with ultrasonic waves are presented with their relevance to the host medium.

3.2.2.1   Speed of Sound

As already stated, the vibrating particles within a material transmit the sound or the ultrasonic wave. The time it takes the particles to travel through the medium depends

on the intensity of the elastic forces between these particles (Marshall, 2005 cited in Reddyhoff, 2006). Different materials transmit an ultrasound wave at different rates because different materials have different elastic forces. For a given material, the speed of sound is constant at any frequency and wavelength. Equation 2.1 shows the relation between the speed of sound with the frequency and wavelength.

$$c = f\lambda \qquad\qquad 3.1$$

where c is the speed of sound (*m/s*), f is the frequency (*Hz*) and λ (*m*) is the wave length. See Table 3.1 for some typical values of speed of sound for different materials.

The host material does not affect the frequency of the ultrasound wave while the wave speed is specific to the host material. Ultrasonic waves are produced from a source with a given frequency, and they are sent through a material with a known thickness. From the time of flight equation (equation 3.2), the speed of sound in a medium can be obtained.

$$c = \frac{2h}{t} \qquad\qquad 3.2$$

where h is the thickness of the sample and t is the time.

3.2.2.2   Acoustic Impedance of Material

Acoustic impedance is considered as one of the most important properties of the host material in this study, which significantly determines the behaviour of the reflected signal from an interface. The acoustic impedance is defined as a product of the density ρ times the speed of sound c and it is denoted by z (Krautkramer & Krautkramer 1977).

$$z = \rho c \qquad\qquad 3.3$$

The units of the acoustic impedance are $kg/m^2 s$, also known as Rayls. Typical values of acoustic impedance for various materials are shown in Table 3.1. Sonically hard is the name given to the materials that have a high acoustic impedance, while the materials that have a low acoustic impedance are called sonically soft.

Table 3.1 Acoustic properties for various materials.

Materials	Speed of Sound, m/s	Density, kg/m^3	Acoustic Impedance, $kg/m^2 s$
Aluminium	6320	2700	17.1×10^6
Tungsten	5180	19250	101.0×10^6
Steel	5900	7700	45.4×10^6
Water	1480	1000	1.48×10^6
Air	343	1.2041	413.3×10^0

3.2.2.3 Attenuation of a Sound Wave

Absorption and scattering are the causes of attenuation, which causes a reduction of the signal amplitude as it travels through a medium. The attenuation level relies on the frequency of the ultrasound signal which is transmitted through the medium and the material itself. If the attenuation is too high then distinguishing the interest signal, from the background noise will be much difficult.

The natural inhomogeneity of materials causes acoustic scattering. This inhomogeneity in material nature leads to a difference in acoustic impedance within the same material which causes the signal to reflect when it meets a boundary in a material. Grain boundaries, inclusions and voids can be reasons for these boundaries.

Absorption occurs when the ultrasound signal travels through the host material as a part of the energy contained in the ultrasound wave is converted to another form of energy. Several processes can be responsible for this (Mason & Thurston 1979). The absorption is increased with increasing the wave frequency because at higher frequencies the particles within the material vibrate faster, hence, more energy is converted to heat (Marshall 2005).

 The attenuation coefficient, α of ultrasound in a material can be defined by:

$$A_h = A_o e^{-\alpha h}$$
<div align="right">3.4</div>

where A_o is the initial amplitude of a wave and A_h is the amplitude after it has transmitted through a thickness of material h. By taking the natural logarithm for equation 3.4 gives

$$\alpha h = \ln \frac{A_o}{A_h} \qquad\qquad 3.5$$

The attenuation coefficient in equation 3.5 is expressed regarding a dimensionless number of nepers per unit length, (i.e. *Np/m*). Nepers per unit length can be converted to decibels per unit length using equation 3.6.

$$\frac{\alpha}{m} = 0.1151 \; \frac{dB}{m} \qquad\qquad 3.6$$

To overcome the attenuation effect, the transmitter voltage and the gain can be amplified.

3.3 Generating Ultrasound

The ultrasound transducers are used to generate and receive the ultrasound waves. These transducers convert one energy form to acoustical energy and vice versa. There are several types of ultrasonic transducers that use different methods for generating the ultrasound. These include optical methods and laser, electro-magnetic and heat shock by suddenly heating the body surface (White 1963). The crystal oscillators which are based on the piezoelectric effect are used to generate the ultrasound wave, and considered as the most popular method for generating ultrasound. The other generating methods are beyond the scope of this investigation and will not be detailed here, but more information about these methods can be found in references (J. Blitz 1963; Krautkramer & Krautkramer 1977)

In 1880, the piezoelectric effect was presented by the Pierre Curie brothers. They noted that a plate cut from crystal in a certain direction, an electrical charges are generated across the plate as it is deformed as a result of the external mechanical pressure. In 1881, Lippman predicted the reverse effect and concluded that, in consonance with the electrical signals applied, such crystals could be used either to generate mechanical vibration or to generate electrical signals.

Because of the behaviour of the piezoelectric materials when applied to mechanical pressure, which produce an electric charge, they are utilised in many applications. These effects establish the base of ultrasound transmitters and receivers for the non-destructive testing, e.g. ultrasonic transducers.

Today, different piezo materials are used for generating and receiving ultrasound signals. Piezoelectric ceramics such as lead zirconate titanate (PZT), lead metaniobate, barium sodium niobate and lead titanete are largely in use for material testing. Lithium niobate, piezoelectric monocrystals which are quartz, lithium tantalite, lithium sulphate, ionic acid and zinc oxide are rarely used.

3.4 Ultrasonic Transducers

Figure 3.5 a) shows a typical pulse from an ultrasonic transducer. The amplitude spectrum illustrated in Figure 3.5 b), was created by taking a Fast Fourier Transform (FFT) of the waveform. It can be seen clearly from the amplitude spectrum that the pulse has energy over a range of frequencies with a roughly Gaussian distribution about the frequency of the high amplitude which is known as the centre frequency. In general, the transducer centre frequencies in non-destructive testing (NDT) varies from ~0.5 *MHz* to 50 *MHz* relying on the application. Therefore, the bandwidth range is used to extract the useful information from a signal, where the energy outside of this range is so little and has a very little effect on the analysis. As shown in Figure 3.5 b), the bandwidth is defined as the range of the useful frequency which has an amplitude greater than half of the peak/maximum amplitude. This corresponds to a 6 *dB* below the peak amplitude.

a) Time domain   b) Frequency domain (Amplitude
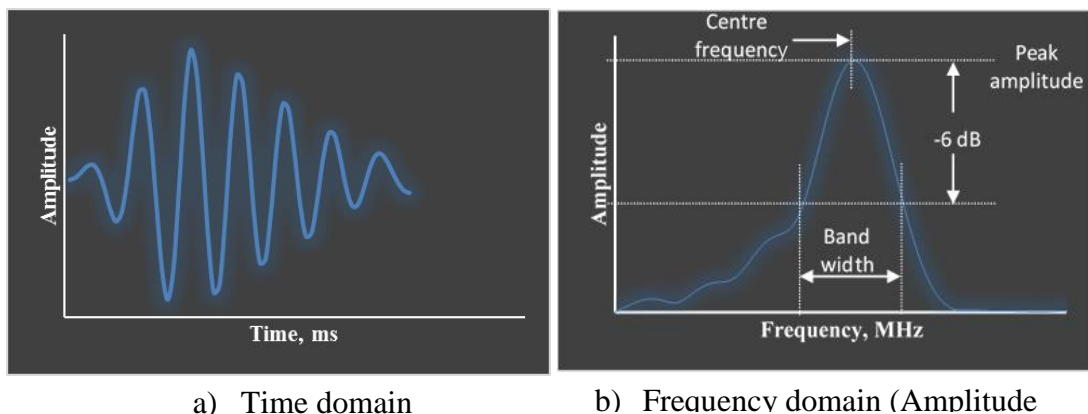
Figure 3.5 Example of a pulse produced by an ultrasonic transducer

Ultrasonic transducers can be classified into different groups according to the wave propagation whether they produce longitudinal or shear waves, and whether the pulse is focused or not. Figure 3.6 shows the classification of the ultrasonic transducers.

The need for permanent bonding of the sensor to the substrate gives rise to the using of bare piezo elements in this study. This was driven by the risk of damage to expensive NDT transducers and the low cost of bare piezo elements. The possibility of cutting the bare piezo element to small size according to the tool-chip contact was another reason for choosing the bare piezo element in this study, more details are presented in Chapter 5.
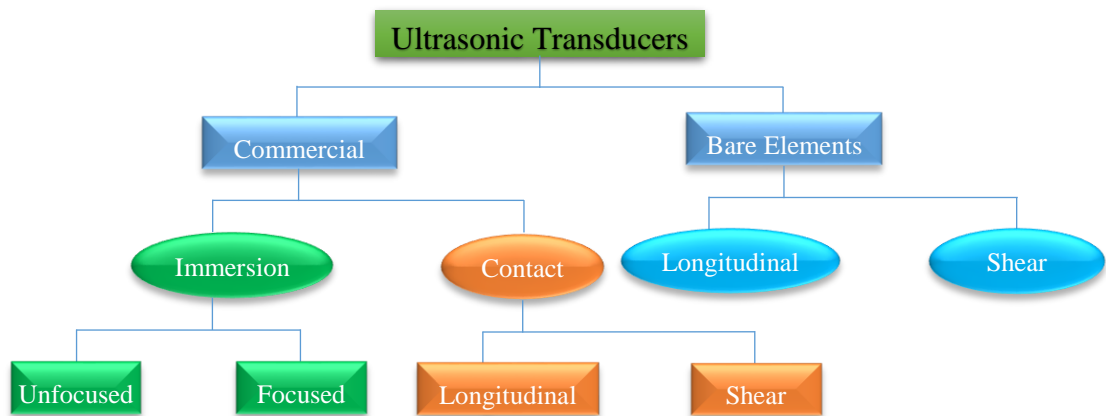
Figure 3.6 Tree diagram showing types of ultrasonic transducers

3.5 Ultrasonic Reflection from an Interface

When an ultrasonic wave is normally incident on a complete boundary between two media, some proportion of the sound wave will be transmitted and some will be reflected. This is shown in Figure 3.7, where the proportion of the wave reflected, is known as the reflection coefficient, R. While the proportion of the wave that is transmitted through the interface is known as the transmission coefficient, T, (Tattersall 1973).

$$R = \frac{z_1 - z_2}{z_1 + z_2} \qquad\qquad 3.7$$

$$T = \frac{2z_2}{z_1 + z_2} \qquad\qquad 3.8$$

where z is the acoustic impedance of a material (which is equal to the product of its density and the speed of sound through it), and the subscripts *1* and *2* refer to the materials on either side of the interface. Equation 3.7 shows that the reflection coefficient, *R*, depends on the acoustic impedance mismatch between the two materials.
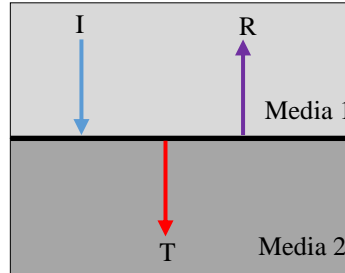
Figure 3.7 Ultrasonic reflection and transmission at a perfectly bonded interface (I: incident wave, T: transmitted wave and R: reflected wave)

If the materials on either side of the interface have the same acoustic impedance, then the reflection coefficient is equal to zero, and the entire wave is transmitted. While if the wave is travelling through acoustically very different materials, then the reflection coefficient will be close to unity and nearly all the signal will be reflected back. This is the case of a wave travelling through a metal then strikes at an air interface. This is because the acoustic impedance of the air is much lower than that of the metal (see Table 3.1).

3.6 Ultrasonic Reflection and Spring Model for an Interface

In real engineering surfaces, surfaces are always rough to some extent and pressing them together lead to contact at the asperities. The interface so consists of regimes of contact separated by air gaps. Therefore, an ultrasonic wave incident at rough surface contact will be partially reflected as shown in Figure 3.8a). If the wavelength of the incident ultrasound is large compared with the size of the air gaps then the spring model can be used to determine the response of the interface (Lewis et al. 2005). It is then the interface stiffness, *K*, determines the relation between reflection coefficient and interfacial layer thickness (Dwyer-Joyce, et al. 2004B).

$$R = \frac{(z_1 - z_2) + i(\frac{\omega}{K})z_1 z_2}{(z_1 + z_2) + i(\frac{\omega}{K})z_1 z_2}$$ \hfill 3.9

where ω is the angular frequency of the ultrasonic wave ($2\pi f$), and z_1 and z_2 are the acoustic impedance of the materials one and two, respectively and it is equal to (the product of the density, ρ and the speed of sound c). Because of the expression for reflection coefficient (equation 3.9) is a complex number it cannot be measured directly. Therefore, in order to get an expression for reflection coefficient, a Pythagoras's theorem was applied to equation 3.9.

$$\text{if} \qquad R = \frac{a + bi}{c + di} \qquad\qquad 3.10$$

$$\text{so} \qquad R^2 = \frac{a^2 + b^2}{c^2 + d^2} \qquad\qquad 3.11$$

By applying this theory to equation 3.9

$$\text{Then,} \qquad R^2 = \frac{(z_1 - z_2)^2 + \dfrac{w^2 z_1{}^2 z_2{}^2}{K^2}}{(z_1 + z_2)^2 + \dfrac{w^2 z_1{}^2 z_2{}^2}{K^2}} \qquad\qquad 3.12$$

Rearranging equation 3.12

$$|R| = \sqrt{\frac{(wz_1 z_2)^2 + K^2(z_1 - z_2)^2}{(wz_1 z_2)^2 + K^2(z_1 + z_2)^2}} \qquad\qquad 3.13$$

For the case of identical materials either side of the interface $z_1 = z_2 = z$ this reduces to:

$$R = \frac{1}{\sqrt{1 + \left(\dfrac{2K}{\omega z}\right)^2}} \qquad\qquad 3.14$$

To measure stiffness, equation 3.13 can be arranged at follow:

$$K = wz_1 z_2 \sqrt{\frac{1 - |R|^2}{|R|^2(z_1 + z_2)^2 - (z_1 - z_2)^2}} \qquad\qquad 3.15$$

Equation 3.15 used to calculate layer stiffness from a reflection coefficient for a wave reflected from a layer.
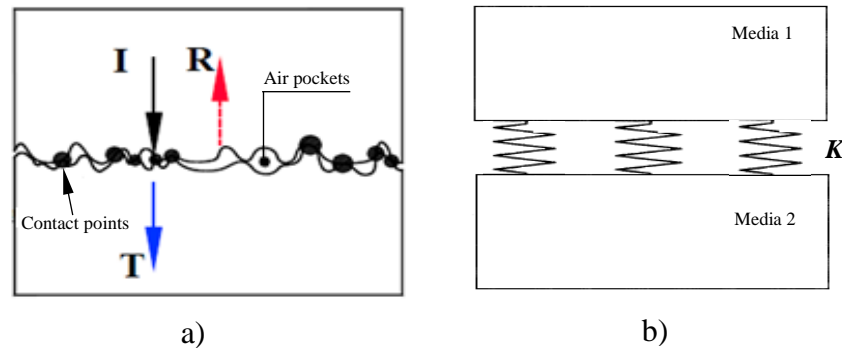
Figure 3.8 Reflection of ultrasound, from a) not perfectly bonded interface and b) spring model of the interface.

3.6.1 Layer Stiffness

The stiffness of an interfacial layer, *K*, expressed per unit area, is given by the rate of pressure change, *p* with approach of the surface, *h* (Wan Ibrahim et al. 2012).

$$K = -\frac{dp}{dh}$$

3.16

The spring model approach provides a method for interrogating tribological contacts. Figure 3.9 shows the prediction from the spring model for a series of interfaces of varying stiffness plotted from equation 3.14. The stiffer the interface (because the contact area is greater or the surfaces are separated for a thinner oil film), the more ultrasound wave can transmit through the interface and therefore the lower the reflection coefficient (Drinkwater et al. 1996; Dwyer-Joyce & Drinkwater 2003). For contacts made up of surfaces machined with standard engineering finishes (grinding, polishing, turning etc.) the stiffness of the interface is such that it can be measured using conventional ultrasonic frequencies. The spring model describes the ultrasonic response well (Dwyer-Joyce 2005).
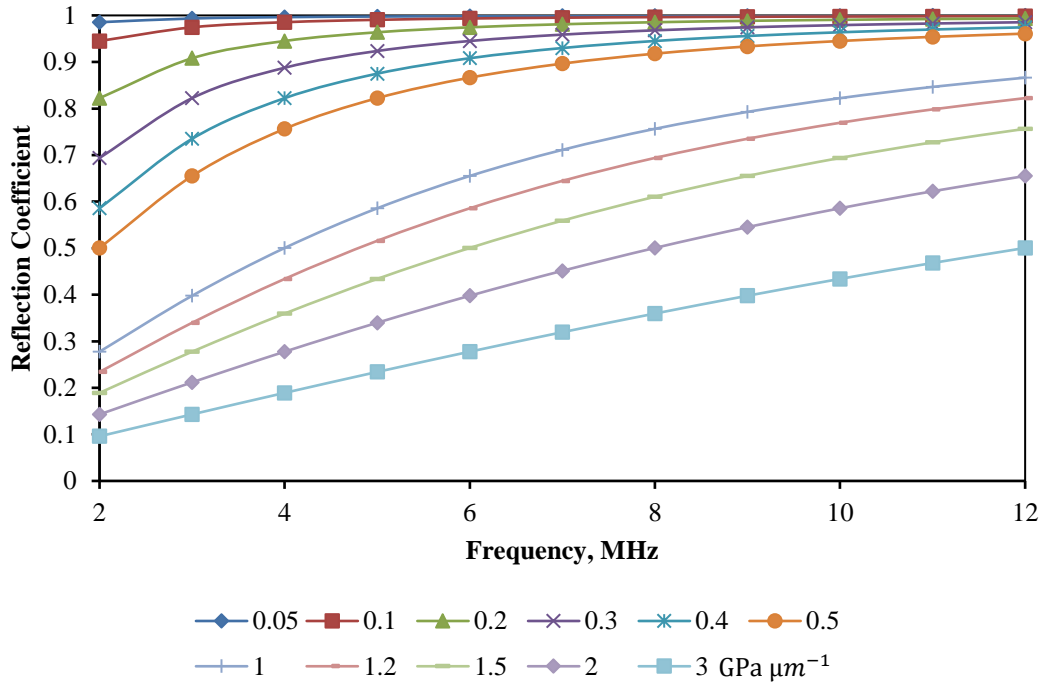
Figure 3.9 The spring model of reflection coefficient for various stiffnesses

3.7 Ultrasonic Reflection from an Oil Film

The spring model also can be used if there is a thin film of oil or any other liquid between two surfaces (Figure 3.10). Where, the spring model applies when the wavelength of the ultrasound is large compared the layer thickness (Dwyer-Joyce et al. 2003).
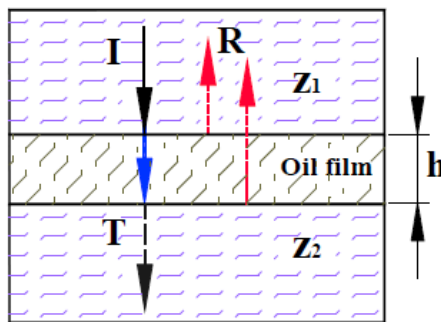
Figure 3.10 Reflection of ultrasound from an oil film between two surfaces

If the interface is a liquid then the stiffness is determined by the thickness, *h*, and bulk modulus, *B*, of the layer.

$$K = \frac{B}{h} \qquad\qquad 3.17$$

53

The speed of sound through a liquid, c , is related to the bulk modulus, B , and density, ρ , by (Harper et al., 2005).

$$c = \sqrt{\frac{B}{\rho}}$$

3.18

Combining equations (3.17) and (3.18) gives the stiffness of the layer in terms of its acoustic properties:

$$K = \frac{\rho c^2}{h}$$

3.19

where h is the film thickness of the layer.

Finally, by substitute equation (3.19) in equation (3.15) and rearranging gives the film thickness in terms of the reflection coefficient.

$$h = \frac{\rho c^2}{\omega z_1 z_2} \sqrt{\frac{R^2(z_1 + z_2)^2 - (z_1 - z_2)^2}{1 - R^2}}$$

3.20

If the materials either side of the interface are identical (i.e. $z_1 = z_2$), then equation 3.20 simplified to

$$h = \frac{2\rho c^2}{\omega z} \sqrt{\frac{R^2}{1 - R^2}}$$

3.21

Figure 3.11 shows the expected reflection coefficient variation against frequency for a series of oil films between two steel bodies (according to equation 3.21). It can be seen that as the film thickness increases, the reflection coefficient increases as more of the wave is reflected.
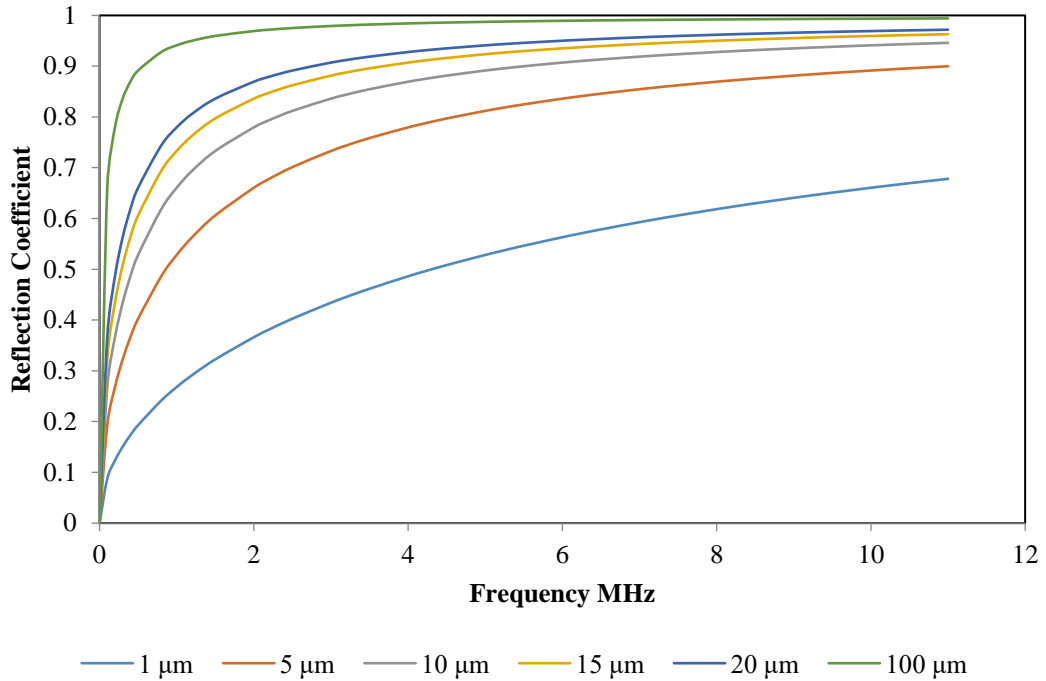
Figure 3.11 Response of a layer to an ultrasonic wave, for steel-oil-steel system, according to equation 3.21, for various oil film thicknesses.

3.8 Ultrasonic Reflection from Mixed Contact

If the interface is contained solid and liquid as shown in Figure 3.12a), then the stiffness of the interface can be modelled by two springs in series, one of them representing the stiffness of the liquid and the other the stiffness of the solid contact as shown in Figure 3.12b).
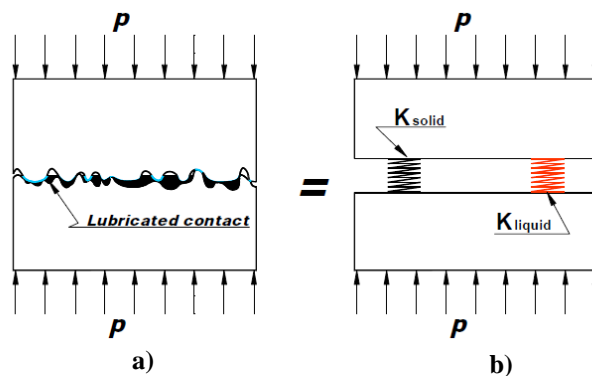
Figure 3.12 Modelling of a mixed contact by means of two springs

The ultrasonic reflection will rely on the total of these stiffnesses in parallel (Gonzalez-Valadez et al. 2005):

$$K_{total} = K_{liquid} + K_{solid} \qquad 3.22$$

55

where, K_{solid} is the stiffness of the dry interface and K_{liquid} is the stiffness of the liquid interface.

3.9 Conclusions

The ultrasound principles and the acoustic properties of the materials, namely speed of sound, impedance and attenuation, have been presented in this chapter. The piezoelectric effect and the generation of the ultrasound wave have been detailed. Typical transducer waveform and its FFT spectrum showing centre frequency and bandwidth, have been introduced.

The ultrasonic wave reflection can be acquired and processed to achieve information about the contact nature at the interface. Therefore, in this work, the ultrasonic reflection was used to investigate the contact conditions at the tool-chip interface in dry and wet cutting process during machining of aluminium *Al 6082*.

4

Cutting Tool Ultrasonic Instrumentation Method

This chapter presents the practicalities of how the tool-chip interface was monitored ultrasonically. Ultrasonic equipment for the interface monitoring, such as the ultrasonic pulser-receiver (UPR), transducer, coupling and cable are introduced. The instrumentation of the cutting tool is explained in detail. The size and location of the piezoelectric element are described and explained. This chapter also describes how the temperature effect on the ultrasonic measurement and the way to overcome this issue is presented.

4.1 Ultrasonic Measurement Apparatus

The ultrasonic apparatus consisted of a pulser, receiver and digitiser. In this work, a combined system was used that contained all these components as PCI (peripheral component interconnect) cards, and they were installed into an industrial computer, more details are in the following subsections. Several factors have made the PCI based system more popular in the present day including lower cost than individual components, reducing the mismatch between the components, compact units, the ease of use and portability and the capability to fit these cards into an existing computing hardware.

4.1.1   Ultrasonic Apparatus

In this study, the ultrasonic measurement was taken by using an ultrasonic pulsing hardware unit. The unit called a "Film Measurement System" (FMS-100 PC) from Tribosonics Ltd, which was used to generate, capture, display and record the ultrasonic signals. This unit is illustrated in Figure 4.1, and it consists of an ultrasonic pulsing and receiving card (UPR) and digitiser. The UPR is the core unit of the ultrasonic apparatus which consisted of two components, namely the ultrasonic pulser and ultrasonic receiver. Generating high-frequency voltage pulses, which are used to excite the transducer causing it to resonate, is the responsibility of the pulser component. This component comprises a peripheral component interconnect (PCI) card, built by Tribosonics Ltd, with eight channels. These channels can be configured separately, allowing different sensors to be excited as needed. A maximum achievable pulse rate of the pulser component is 80000 *pulse/second*, split between active channels, which were active during the process.

The receiver component also contains a PCI card which is from Tribosonics Ltd as well. This component received the reflected pulses from the ultrasonic sensor (i.e. the piezoelectric element). It has also eight channels which can equally be configured separately to improve the performance of the ultrasonic system.
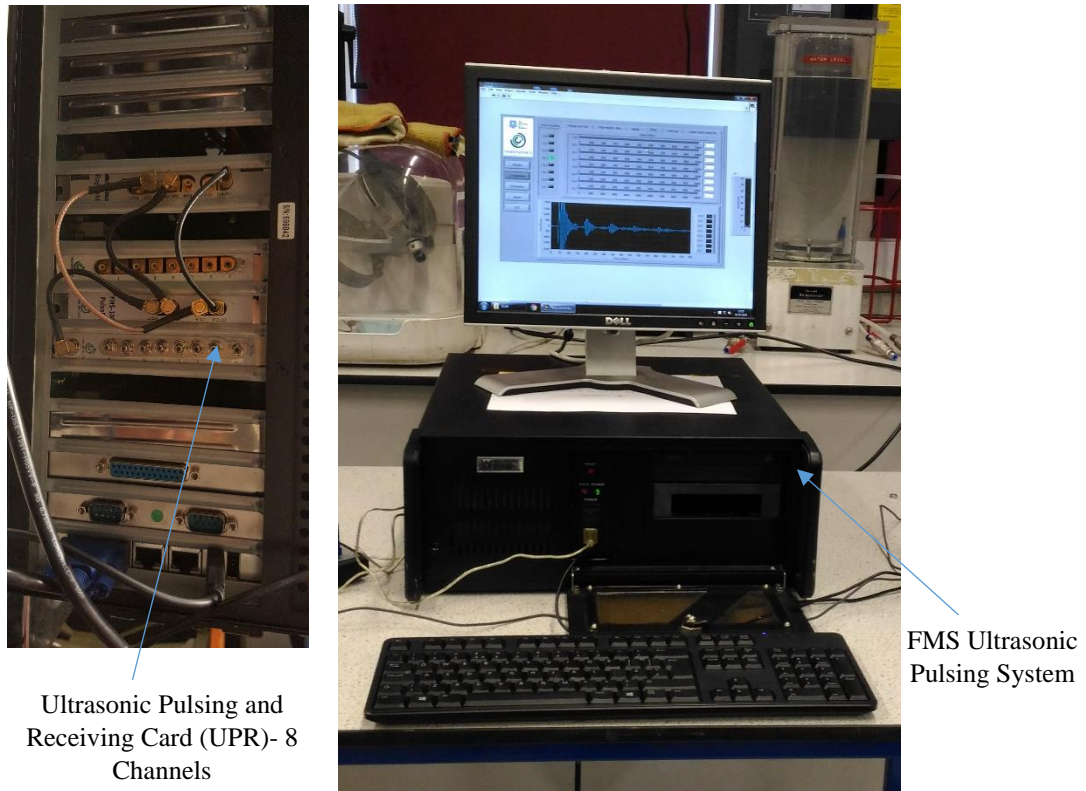
Figure 4.1 A photo showing a FMS-100 pulsing system

The UPR control software was written using LabVIEW (National Instruments). The ultrasonic sensor was connected to the pulsing unit, with a pulse rate of 1 *kHz*. As mentioned above, the UPR is used to produce a high-frequency voltage pulse. These pulses are used to excite the transducer causing it to resonate. The transducer then emits a wide band pulse, sending it through the cutting tool and the reflected pulses, from the tool-chip interface, are received by the same transducer where, the transducer acts as both an emitter and receiver. The reflected pulses are amplified by the digitiser, fitted in the PC, at 100 *MHz* with a 12 *bits* resolution. The PC carries out the signal processing and shown results with software written in LabVIEW. Figure 4.2 shows a schematic diagram of the apparatus used for generation and measurement of ultrasonic signals in monitoring the tool-chip interface during the cutting process.
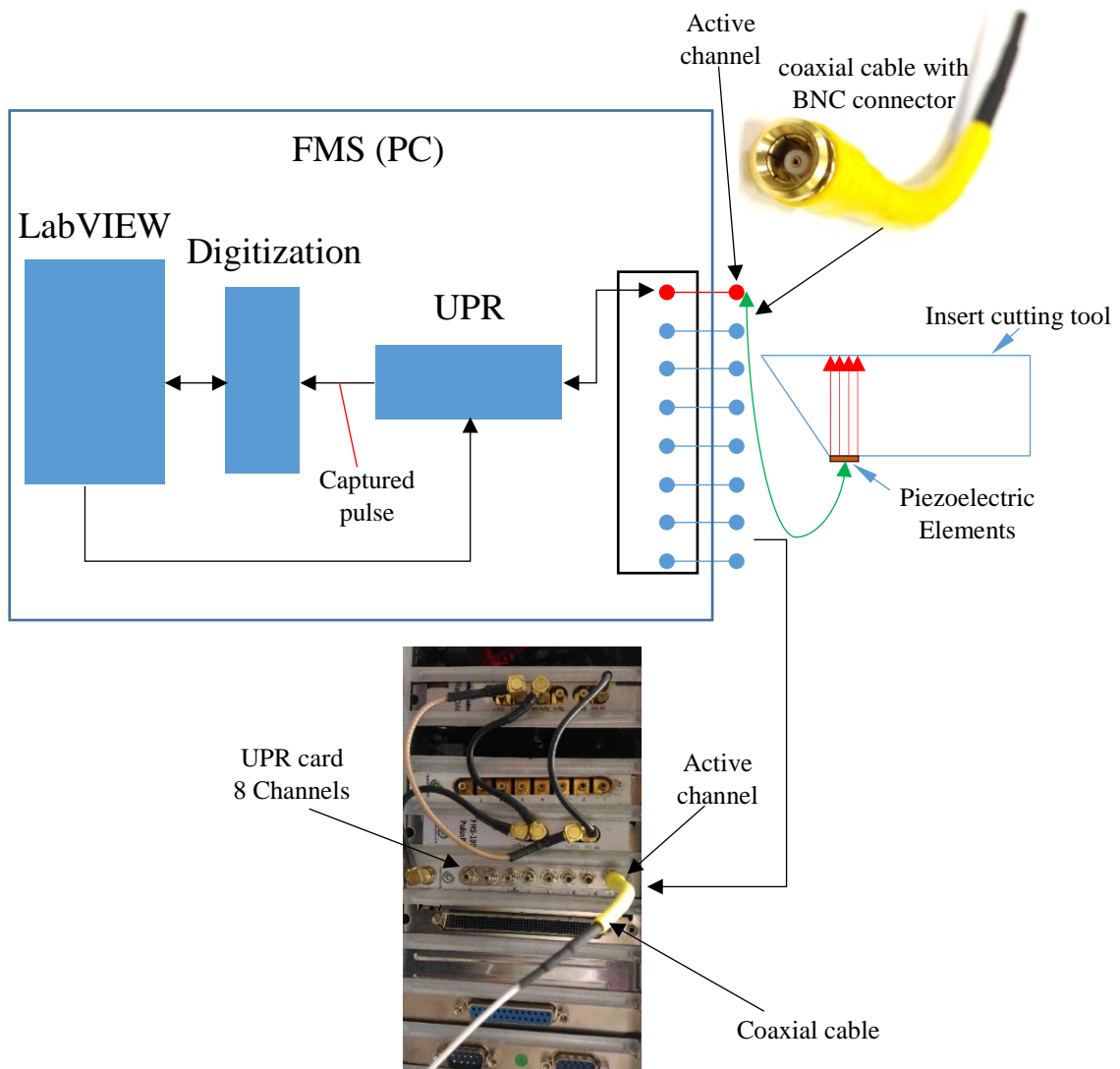
Figure 4.2 Schematic diagram of the measurement apparatus

4.1.2   Transducers

There are different types of ultrasonic transducers as mentioned in Chapter 3, among these types, a piezoelectric transducer was selected in this study. The need, in this study, for permanent bonding of the sensor (i.e. the piezoelectric element) to the substrate (cutting tool insert) led to the use of the piezoelectric element. This attributed to the risk of damage to expensive transducers and the low cost of the bare piezoelectric elements. In addition, the possibility to cut the bare piezoelectric element into smaller sizes in order to cover a smaller area was another reason for choosing this kind of sensors. If the ultrasonic wavelength is larger than the size of the air gaps, then the proportions of the ultrasonic energy reflected and transmitted are dependent on the stiffness of the interface and to a small extent on the effective damping and mass of

the interface where no longer dependent on the exact size and shape of each air gap (Drinkwater et al. 1997). If the sizes of the air gaps in the plane of the interface are in the range 5-50 *μm* then a wavelength of above 500 *μm* is required. The speed of the longitudinal ultrasonic wave in carbide tungsten carbide is around 5180 *m/s* (see Table 3.1). This corresponds to a centre frequency of below 11 *MHz* in tungsten carbide. In this study, a piezoelectric sensor of 10 *MHz* centre frequency was used which is within the right range to study the tool-chip interface.

The transducer used is formed from lead zirconate titanate (PZT) and has a disc shape with 10 *MHz* in centre frequency, 0.2 *mm* in thickness and 7.1 *mm* in diameter. Figure 4.3 shows the comparative size of a 10 *MHz* transducer element, used in this study.

Figure 4.3 Photograph of 10 MHz piezoelectric element

4.1.3   Coupling

A layer of coupling medium is usually required between a transducer and the test piece, so as to transmit the ultrasonic wave into the test piece. Without this coupling layer, the ultrasonic signal can not transmit through the test piece where a layer of air exists, which has a low impedance and very high attenuation, thus preventing the wave transmission. There are different types of couplant such as water, treacle, water based gel and adhesive. The bare piezo element can be very small, require attachment of connecting wires, contain negligible internal damping and have a low unit cost. Due

to these factors, adhesive bonding is the most satisfactory method of coupling. In this study, M-Bond 610 high-temperature adhesive (up to 230°C), from Vishay Measurement Group UK Ltd, was used as a couplant and for sticking the element to the cutting tool, which will be explained later in this chapter.

4.1.4 Cables

Cables are used to connect transducer to the pulsing equipment. Cables which are employed in this study are made of three main components: the conductor, the dielectric, and shield. An outer protective jacket surrounds these components. Figure 4.4 shows a cross-sectional view of a typical cable. The conductor acts as the positive connection of the cable while the shield acts as the negative. The dielectric isolates the conductor from the shield (Olympus NDT 2010).
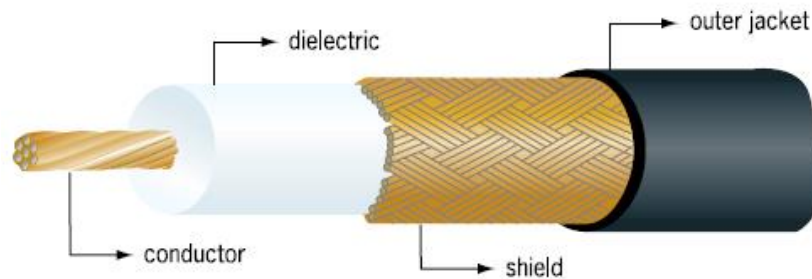
Figure 4.4 Cross-sectional view of a typical cable (Olympus NDT 2010)

4.1.5 Temperature Effect

The piezoelectric transducers have a specific response to temperature because these transducers consist of a multi-layer construction and each of these layer has a different thermal expansion coefficient. This limits their maximum operating temperature as a result of the stresses that can occur in the layers. Exceeding the maximum operating temperature can lead to disbonding of one or more of the layers.

Temperature rise can influence the transducer along with other variables such as couplant contact area, sound speed of couplant and couplant thickness. Therefore, it is extremely difficult to quantify the response of an NDT transducer.

In addition, in a cutting process and because of the tests being run at different cutting speeds, temperatures on the cutting edge is increased, this raises several issues.

Changes in temperature effect the output from the ultrasonic transducers (Reddyhoff et al. 2008). This is due to the temperature dependence of both the element itself and the properties of the adhesive layer between the element and the cutting tool insert.

Due to these changes with temperature, and in order to use these sensors in machining process a method of temperature compensation is required, which is discussed in more detail in Chapter 5.

4.2 Instrumentation of a Cutting Tool

Before discussing the instrumentation of the cutting tool, the area of investigation in this study must first be addressed. In this section, the area of interest is highlighted and then selecting the cutting tool insert is discussed. The steps of bonding the piezoelectric element to the cutting tool are described in detail.

4.2.1   The Studied Area

Figure 4.5a) shows the setup of the cutting test which was performed in this study. The workpiece consisted of a hollow cylinder with an outer diameter of 100 *mm* and a different wall thickness, more details are presented in Chapter 5. As soon as the tool cutting edge engaged with the workpiece and due to the stress concentration, an elastoplastic region was formed in front of the cutting edge. The stress concentration, ahead of the tool cutting edge, occurs as a result of the pure compression of the removal layer to be removed from the workpiece. Thus, the elastoplastic zone which is created ahead of the cutting tool allows the cutting edge to penetrate further into the workpiece. Thus, a part of the material layer being removed, from the workpiece, comes in close contact with the rake face of the cutting tool. This layer slides over the rake face by the moving chip which was formed due to the severe tribological conditions in the secondary deformation region. The contact area between this chip and the rake face of the cutting tool insert was the main area of interest for the investigation in this research (see Figure 4.5b), and it can be examined using an ultrasonic transducer underneath the cutting tool insert (i.e. the opposite side of the tool-chip contact area), Figure 4.5c) shows the location of the ultrasonic sensor. More detail about the piezoelectric element location is given in the next section.
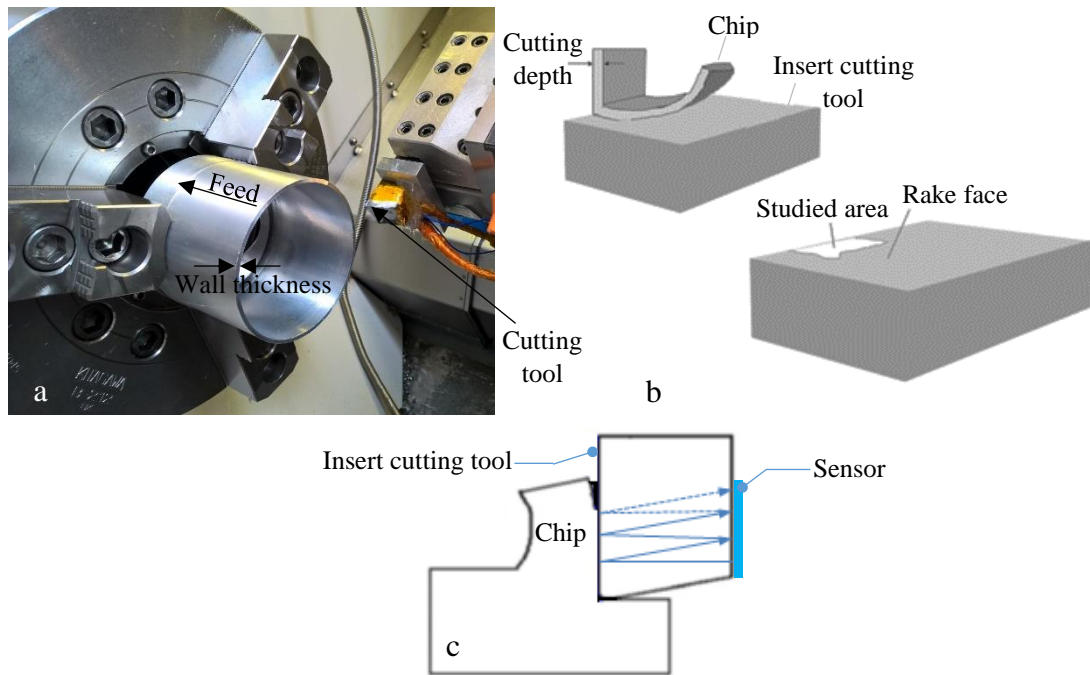
Figure 4.5 Setup of the turning test (a) and schematic pictures of the cutting insert (b), showing the location of investigated area, (c) showing the location of the ultrasonic sensor

4.2.2 Size and Location of the Sensor

A series of orthogonal cuts were conducted using aluminium *6082-T6* to determine the size and location of the piezoelectric element. The experiments were carried out under the same cutting conditions used in this study. An SEM was used to measure the tracks length on the rake face cutting tool. It has been found that the smallest tool-chip contact length was 0.804 *μm* and was gained when machining at a cutting speed of 120 *m/min*, cutting depth of 1.5 *mm* and feed of 0.12 *mm/rev* (see Figure 4.6). The experiments are presented in detail in Chapter 6. It was necessary to make the contact area larger in length than the sensor size so that all the waves from the sensor are incident on the tool-chip interface. A set of tests was carried out to investigate the smallest applicable size of the sensor; it was found to be 0.7 *mm* for the positive side. The negative side measures 1.3 *mm*, making the overall size of the sensor 2 *mm* in length. Therefore, with the expected contact length identified, the size of the sensor which was used in this work was about 1 *mm* by 2 *mm.*
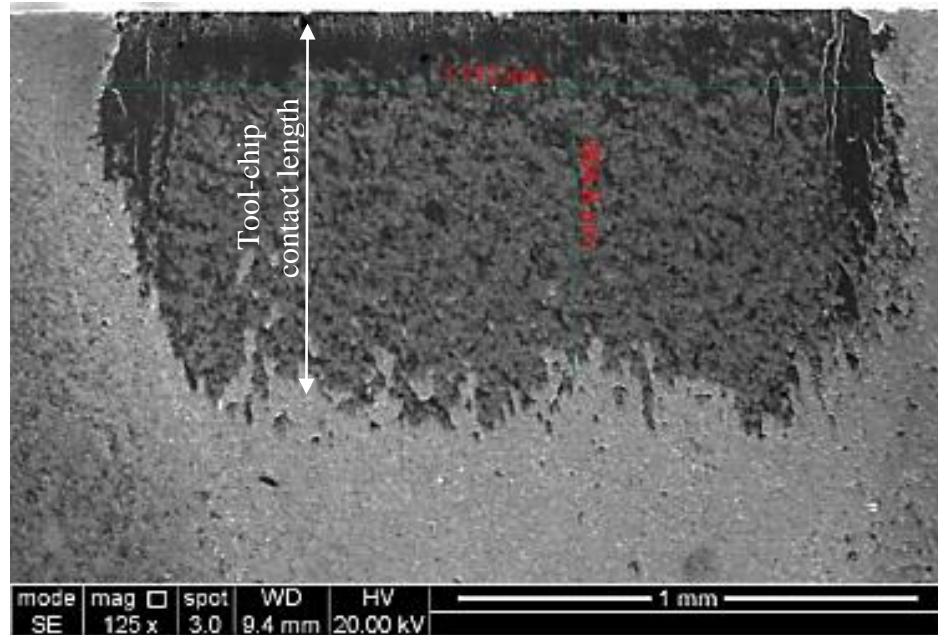
Figure 4.6 SEM photograph of the rake face cutting tool during dry cutting conditions of *Al 6082* at a cutting speed 120 *m/min*, cutting depth 1.5 *mm* and feed of 0.12 *mm/rev*.

As for the sensor location, it has been chosen the opposite side of the tool-chip contact area. Figure 4.7 shows a schematic diagram of the location of the piezoelectric element on the bottom of the cutting tool insert.
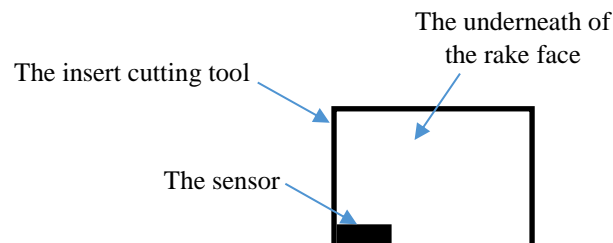
Figure 4.7 An explanatory figure for the position of the sensor on the cutting tool insert

4.2.3 Selecting the Cutting Tool

In the turning process, selecting a certain cutting tool insert is dependent on many factors including the workpiece material and the types of turning process (longitudinal turning, facing, parting, grooving and boring). Among the various types of cutting tool insert, a rhombic 80º insert of a flat rake face has been chosen. The flat rake face geometry of the cutting tool insert was chosen so as not to restrict the tool-chip contact length and thus affecting the ultrasonic reflection. The tool inserts selected were commercially available uncoated with geometry [CCMW 12 04 04] from KYOCERA (see Figure 4.8a). This insert has a positive rake angle, with 0.4 *mm* nose radius, the

thickness of the insert is 4.76 *mm,* and the insert clearance angle (side relief angle) is 7°. This cutting tool insert is recommended by the manufacturer to cut aluminium based alloy. These inserts were mounted on CERATIZIT [SCACR 2020 K12] tool holder and all the dimensions are shown in Figure 4.8b).

	f_1 mm	b mm	l_1 mm	l_3 mm
(b)	20	20	125	17

(a)
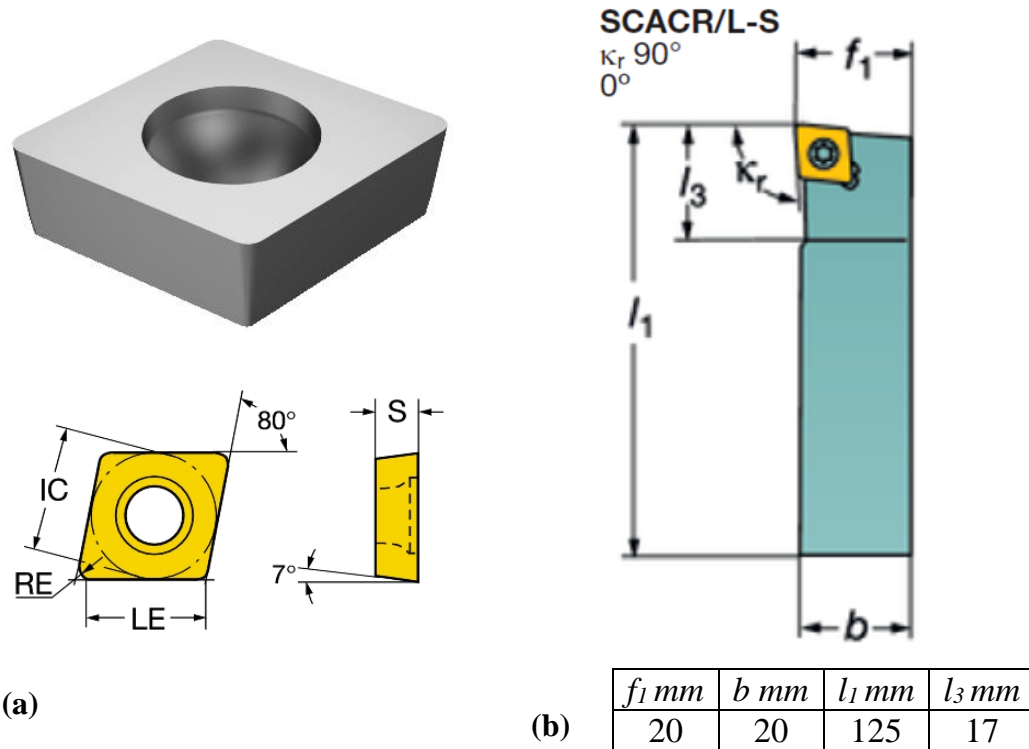
Figure 4.8 (a) shown the cutting tool insert and (b) shown the tool holder used in this study with the specification

Figure 4.9 shows an explanatory figure for the tool cutting edge used in this study, where α refers to a side relief angle of the cutting tool, it measures 7˚. The height of the cutting tool insert is 4.76 *mm* therefore $x \cong 0.6$ *mm*, where x is the contact length between the tool-chip interfaces which cannot be detected by the sensor. In order to investigate the tool-chip interface by the sensor, the contact length must be bigger than 0.6 *mm*.
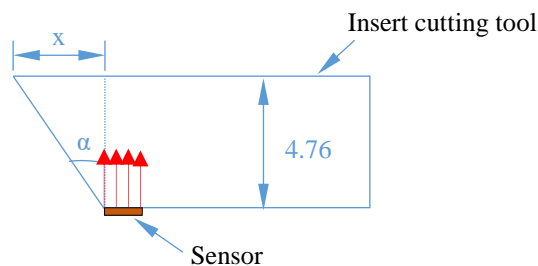
Figure 4.9 An explanatory figure for the cutting edge

4.2.4   Cutting Tool Modification

The tool holder, cutting tool insert and the shim require some significant modification in order to position the ultrasonic transducer and thermocouple wire. A hole was made on the underneath of the cutting tool insert, close to the location of the ultrasonic element, using Electrical Discharge machining (EDM) in order to accommodate the thermocouple wire. The hole diameter is 0.8 *mm* and depth of 2 *mm,* where the thermocouple tip is 0.5 *mm*. Further to this, modifications were made to the shim to make a space for the ultrasonic element and soldered junction. In order to limit vibration and tool deflections, the space was as small as possible, and it consisted of a groove with 2.5 *mm* wide from each side and 1 *mm* in deep. A hole also has been made on the shim to guide the coaxial cable of the ultrasonic sensor and thermocouple wires to the tool holder. A drilling machine was used to drill a hole in the tool holder to pass the wires through. Finally, a groove was made on the underneath of the tool holder to protect the wires against shearing off during the cutting process. Figure 4.10 shows a diagram of the modified cutting tool while Figure 4.11 shows the photographs of the cutting tool used in this study.
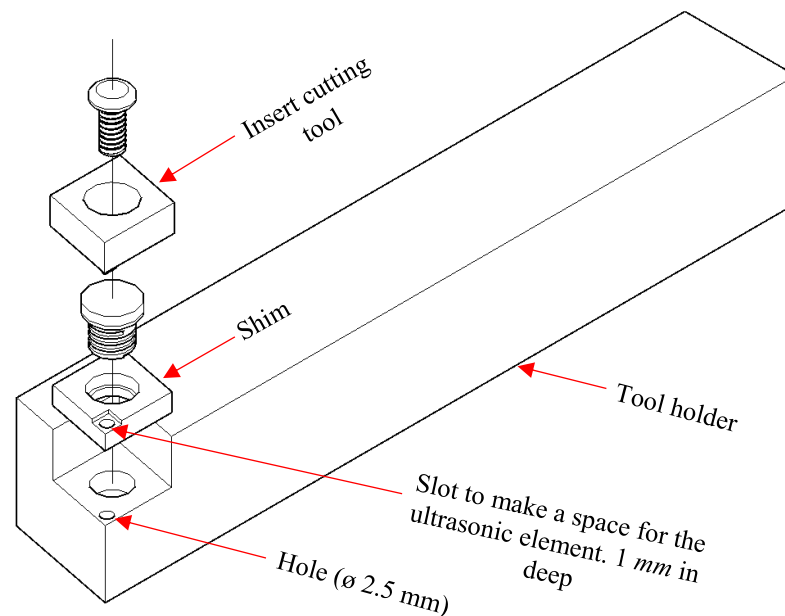
Figure 4.10 A diagram of the modified cutting tool used in this study

Hole (ø 2.5 *mm*) in the shim for the coaxial
cable and thermocouple wire

Hole (ø 2.5 *mm*) in the tool holder for the
coaxial cable and thermocouple wire

Slot in the shim to make a space
for the ultrasonic element.
1*mm* in deep

Groove on the underneath of tool
holder, to put the wires.
1.3 *mm* wide and 1.5 *mm* deep

Insert cutting
tool

Shim

Shim

Rake face

Hole (ø 0.8 *mm*
x 2 *mm* deep)

Figure 4.11 Photographs of the modified cutting tool used in this study

4.2.5   Ultrasonic Sensor Development

In this study, as stated in Section 4.2.2, the 10 *MHz* piezoelectric sensor was cut into a shape of 2 *mm* in length and 1 *mm* in width as illustrated in Figure 4.12. By following an installation procedure, the piezoelectric element was installed on the cutting tool insert.
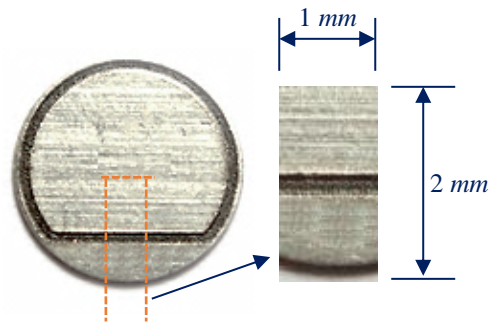
Figure 4.12 Dimension of the piezoelectric element

The bare piezoelectric element was coupled to the underneath of the cutting tool insert (i.e. the opposite side of the tool-chip contact area). To insure a perfect bonding, the coupling surface must be free from grease, oil, dust and dirt to the naked eye and or extraneous materials. For this purpose, an ultrasonic cleaning tank, filling with Acetone, was used to clean the cutting tool insert. Then the bare element was bonded to the cutting tool using M-Bond 610 high-temperature adhesive. A heat resistant tape was used to cover the cutting tool with the bare element in order to protect the sensor from the high temperature of the oven, and then pressure was applied to the sensor using a G-clamp with a silicon rubber, to protect the sensor from cracking and applying a distributed force, and putting them into a temperature controlled oven. A Carbolite oven was used for curing the sample in this study. The curing process was performed in three steps, namely ramping, dwelling and ramping. Where in the first step the temperature increased with a rate 1*degree/min* starting from the room temperature to 200°*C* then to hold at this temperature for one hour (i.e. dwelling for 60 minutes) then the oven starting cooling down. Figure 4.13 shows the curing cycle and the post-curing which will discuss later in this section. Figure 4.14 shows a schematic and a photograph of the cutting tool with the sensor bonded to the back face of the cutting tool insert after removal from the oven.
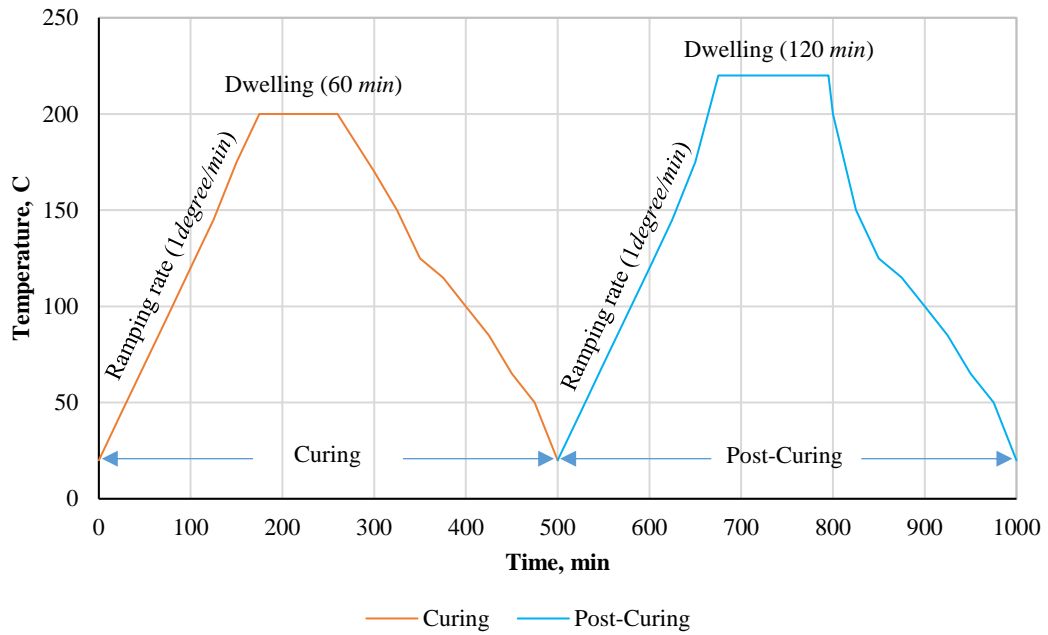
Figure 4.13 A diagram showing the curing and post-curing process
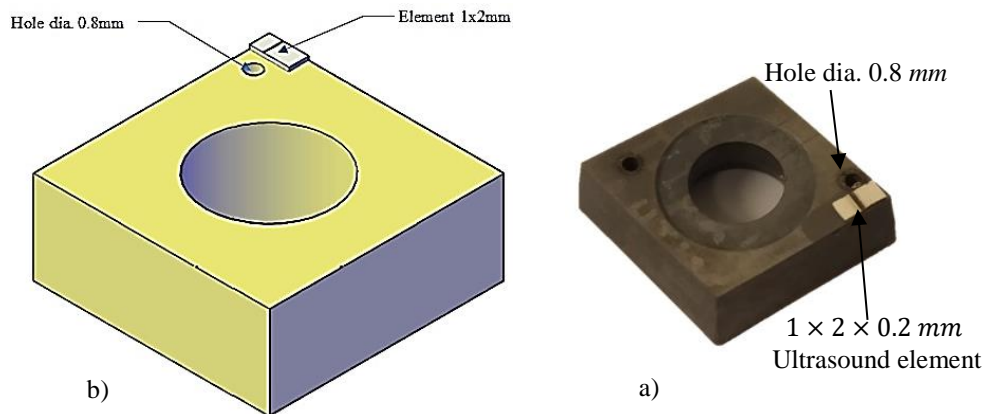
Figure 4.14 A schematic and a photograph of the sensor bonded to the back of the cutting tool insert

Once the piezoelectric element was bonded to the cutting tool, a coaxial cable with a diameter of 0.4 *mm* was then wired to the sensor as shown in Figure 4.15. A photograph of the instrumented end fitting can be seen in Figure 4.16. It is worth noting that a heat transfer compound, with operating temperature up to $200°C$, was used to fill the gaps around the thermocouple tip inside the hole.
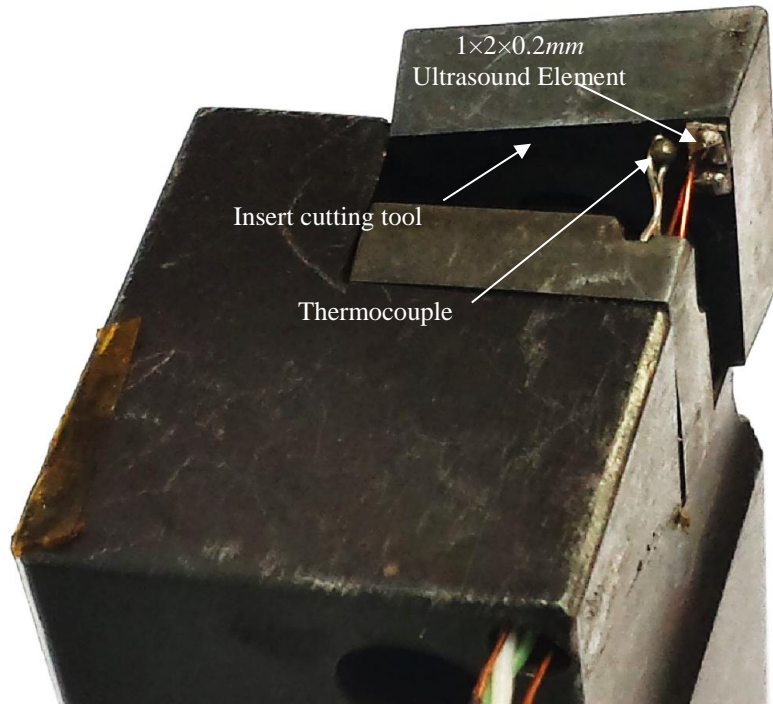
Figure 4.15 Cutting tool instrumented with an ultrasonic element and thermocouple
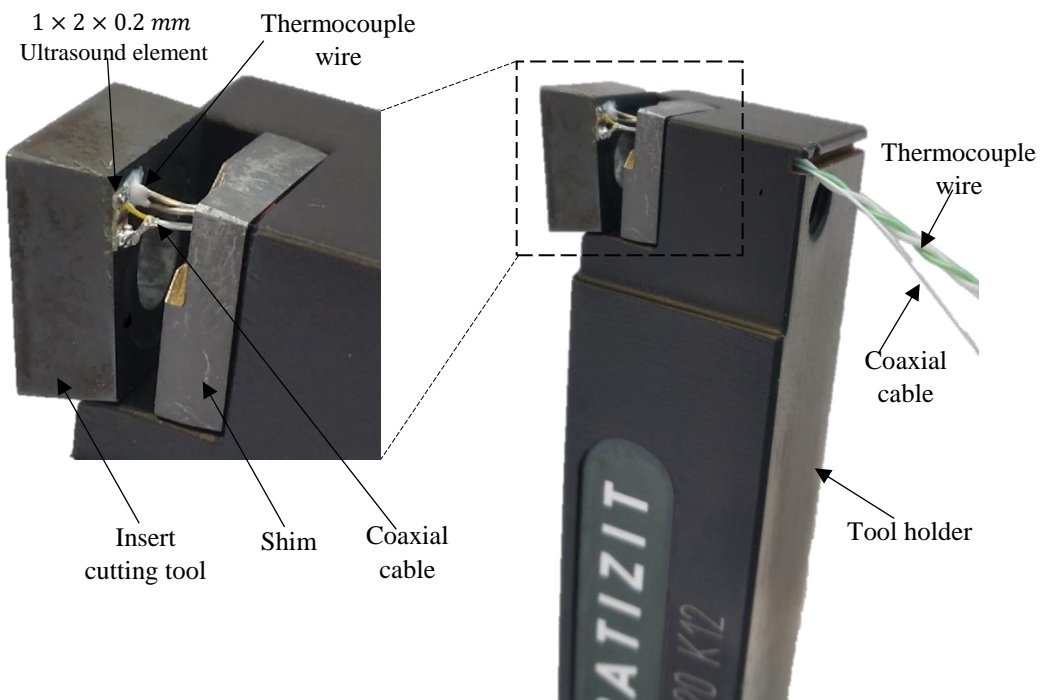
Figure 4.16 The complete end fitting assembly with the ultrasonic element and thermocouple wires

To prevent the wires from breaking during the machining process and to protect the sensor from damage during the cutting process and handling, the soldered wires with the bonded sensors, at the points where they were soldered, were then covered with a high-temperature epoxy resin. This epoxy cover also helps to damp the oscillations of

the piezoelectric transducer. Figure 4.17 shows the tool holder with the cutting tool in their final form. Finally, as recommended by the Tribosonics Ltd and Vishay Measurement Group UK Ltd, a post-curing was carried out for the assembly at a $20°C$ higher than the curing temperature. The post-curing cycle is shown in Figure 4.13.
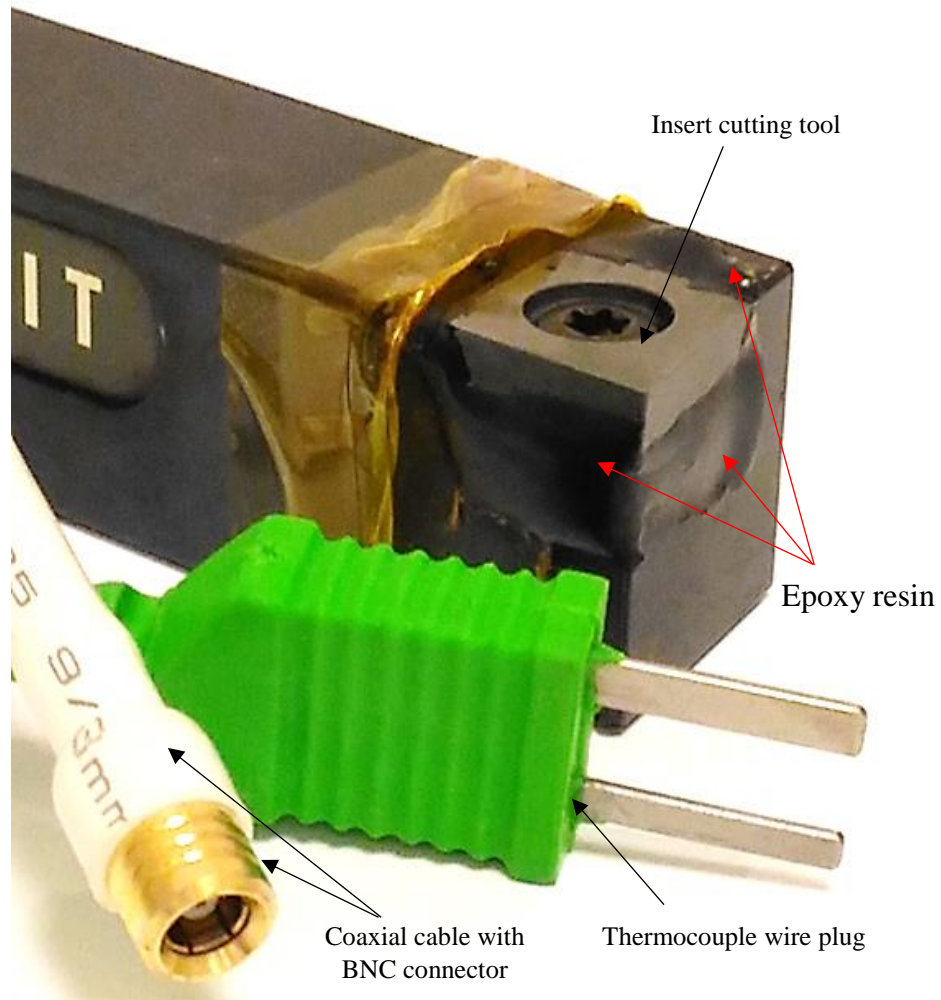
Figure 4.17 Showing the cutting tool with the cable which is covered by the epoxy

Finally, the transducer is connected to the UPR which is connected to the digitiser in the PC.

4.3 Cutting Parameters

As mentioned in Sections 4.1.5, that the ultrasonic transducer and the couplant (M-bond 610) both are affected by the temperature. Therefore, care must be taken when selecting the cutting conditions where the temperature should not exceed $230°C$, which is equal to the operating temperature of the adhesive (M-bond 610). As a result, a set of experiments were carried out separately to measure the temperature and thus

selecting the cutting conditions that do not excede the temperature of the allowable limit. Therefore, with the expected temperature identified, it was found to be the cutting speed range from 40-140 *m/min*, cutting depth range from 1.2-2.8 *mm* and feed range from 0.09-0.23 *mm/rev*. More detail is presented in Chapter 5.

4.4 Conclusions

This chapter has described the ultrasound instrumentation of the cutting tool. The ultrasonic apparatus, transducer, coupling and cutting tool used during testing has been described. The temperature effect on the ultrasonic sensor significant modification in cutting tool and significant development in ultrasonic element are explained and described. Finally, the criteria for selecting the cutting conditions is explained.

5

Analysis of Machining Processes

Chapter five detailed instrumentation of the cutting tool and implementation of the ultrasonic measurement. This chapter deals with some of the machining performance measurements. The machine setup and the design of the experiment are described in detail. The significance of selecting orthogonal cutting rather than oblique cutting is also explained in this chapter.

5.1 Experimental Setup

5.1.1   Machine Tool

A series of orthogonal cutting tests were conducted on a CNC lathe machine (MAG HAWK 300) to monitor the tribological conditions of the tool-chip interface in dry and wet conditions using different sensors. The data were acquired simultaneously from the sensors. Figure 5.1 shows the experimental setup, while Figure 5.2 shows the cutting tool with the locations of the different sensors.
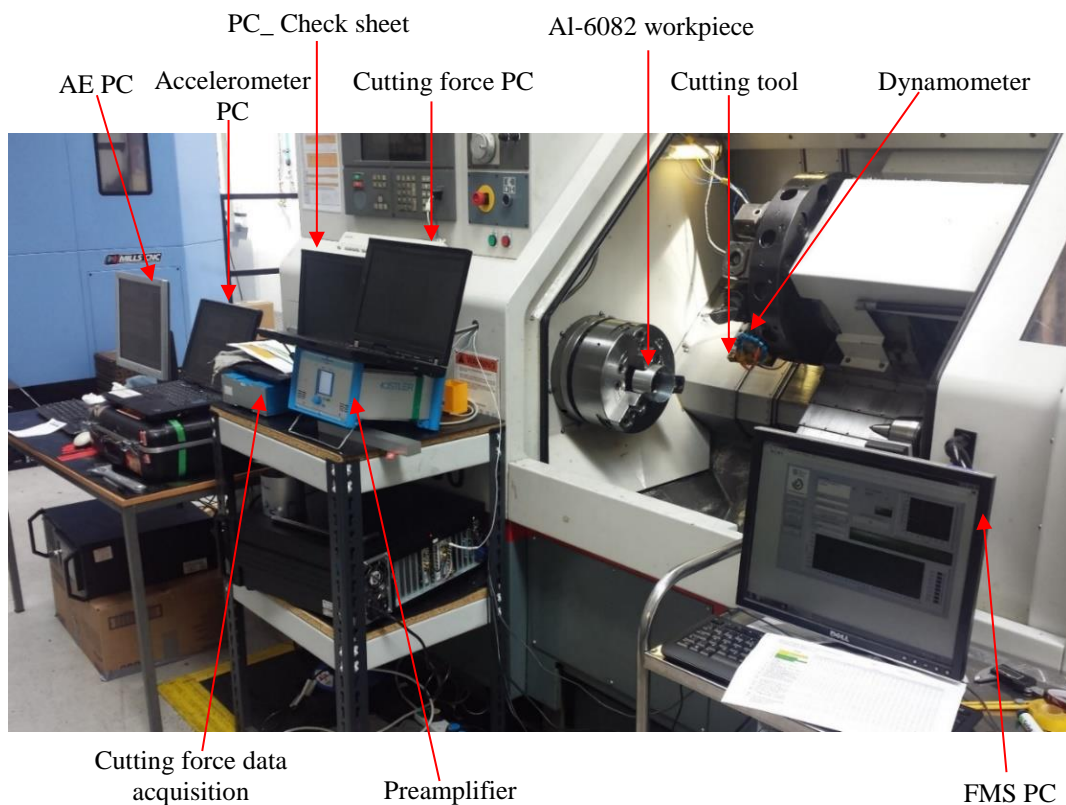
Figure 5.1 Experimental Setup

It is worth noting that in these experiments different sensors have been used including the ultrasonic sensor, dynamometer, acoustic emissions (AE) and accelerometer sensors. The AE measurements and the vibration measurements will not described in this study as they are not within the scope of this research.
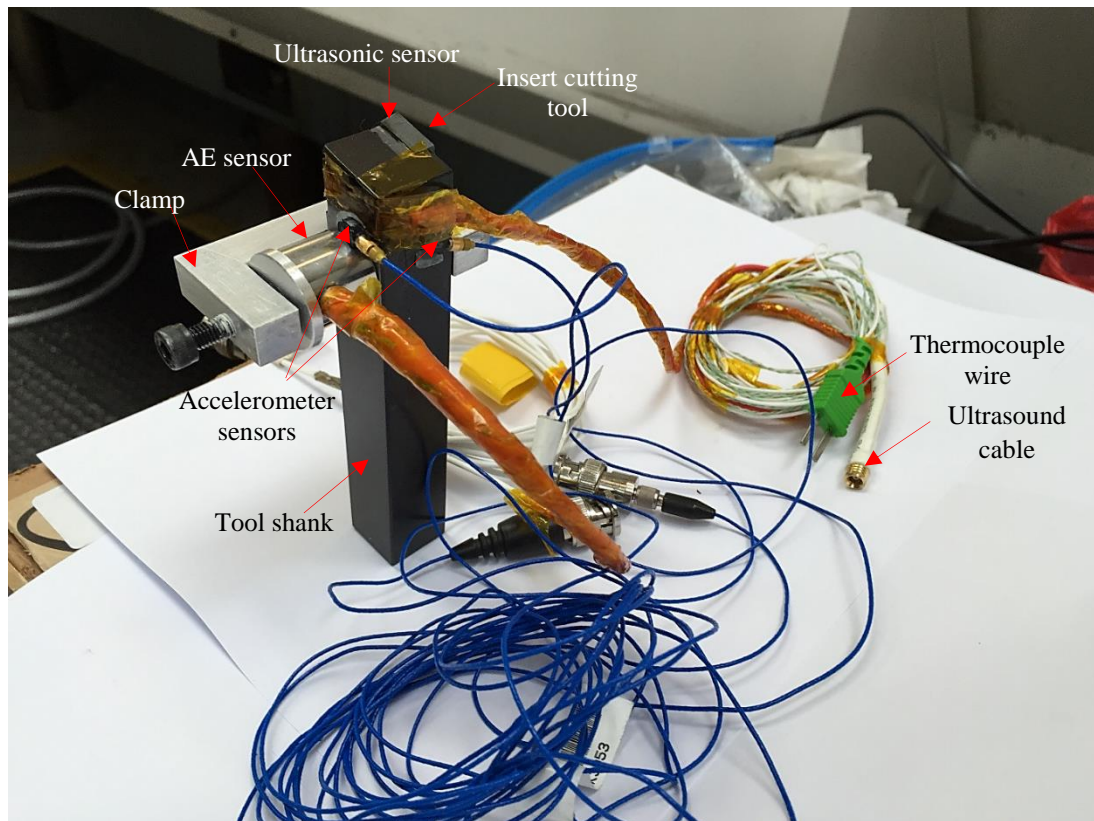
Figure 5.2 Cutting tool with sensors combination set-up

5.1.2 Work Material

The experiments were performed on a *6082-T6* aluminium tube. Aluminium was chosen because it is widely used in many applications such as automotive parts, aerospace applications and many other applications, in addition, aluminium is easy to machine. Another advantage of using aluminium was ignoring the tool wear without seriously distorting the understanding of the tool-chip contact condition, more details are given in Section 5.1.4.

Table 5.1 and Table 5.2 show the detailed chemical composition and the physical properties of *Al 6082-T6*, respectively.

Table 5.1 Chemical composition of *Al 6082-T6*, wt%

Mn	Fe	Mg	Si	Cu	Zn	Ti	Cr	Al
0.4-1.0	0.0-0.5	0.6-1.2	0.7-1.3	0.0-0.1	0.0-0.2	0.0-0.1	0.0-0.2	Balance

Table 5.2 Physical properties of *Al 6082-T6*

Physical Property	Value
Density	$2.70 \ g/cm^3$
Melting Point	$555 \ ^\circ C$
Thermal Expansion	$24 * 10^{-6}/K$
Modulus of Elasticity	$70 \ GPa$
Thermal Conductivity	$180 \ W/m.K$
Electrical Resistivity	$0.038 * 10^{-6}\Omega.m$

5.1.3 Workpiece

To remove any possible surface irregularities and ensure similar surface properties for all the specimens, aluminium tubes (*Al 6082-T6*) were pre-machined with a 1.5 *mm* cut. Then, to get orthogonal cutting, the tubes were pre-machined, using a separate cutting tool insert, to a different wall thickness tube (1.2, 1.5, 2, 2.5 and 2.8 *mm*) having an outer diameter of 100 *mm*. The large workpiece diameter was used in the machining experiments to get high cutting speeds.
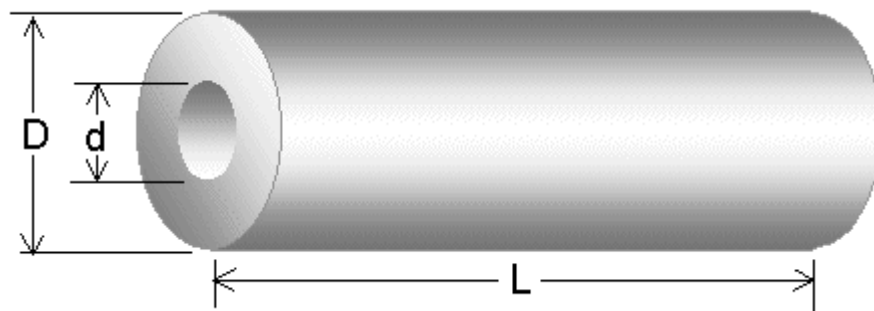
Figure 5.3 Geometry of the specimen

In order, that the sample be more stable and safely mounted in the chuck of a lathe and to reduce vibration, a particular length of the workpiece was chose that was 100 *mm*, where 75 *mm* of the workpiece length extended out of the chuck. With a projecting length of 75 *mm*, the specimen was found to be more stable, and not subjected to static deflection or vibration for all the cutting conditions in this work. The tubes were

deflected as a result of the pressure of the chuck, especially with 1.2 *mm* thickness, even with low chuck pressure. Therefore, to overcome this issue, a support was made from steel that fit over the end of the tube as shown in the Figure 5.4.
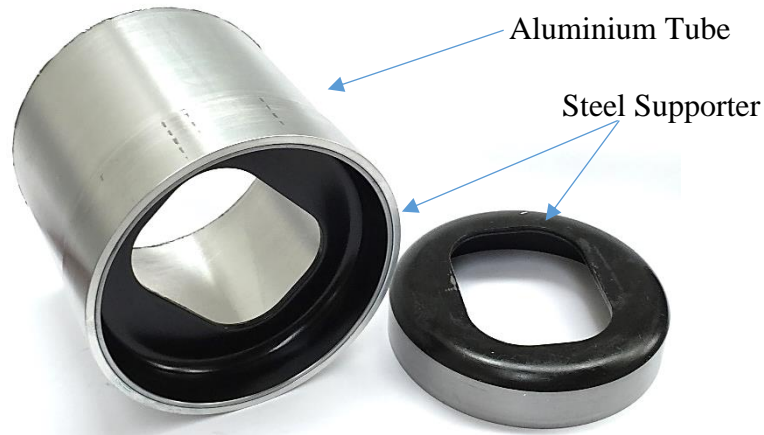
Figure 5.4 Workpiece with Steel Supporter

5.1.4   Cutting Tool

As explained in Section 4.2.3, the tool inserts selected were commercially available uncoated with geometry [CCMW 12 04 04] from KYOCERA. This insert has a positive rake angle, with 0.4 *mm* nose radius and the insert clearance angle is 7°. The rake face geometry of the inserts cutting tool was chosen so as not to restrict the tool-chip contact length. These inserts were mounted on CERATIZIT [SCACR 2020 K12] tool holder. Figure 5.5 a) shows the tool-workpiece setup and b) shows the cutting tool with the dynamometer.

a)   b)
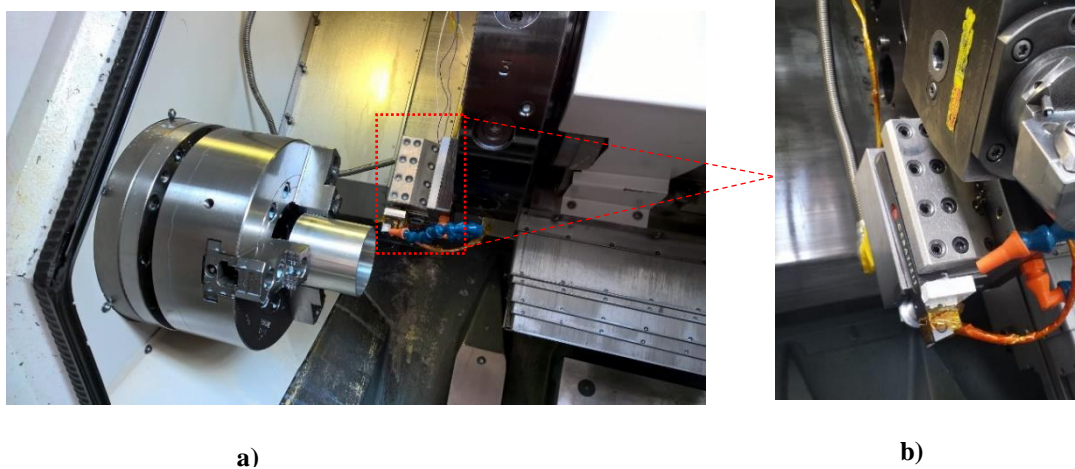
Figure 5.5 a) Tool-workpiece setup, b) Cutting tool with Dynamometer

All the orthogonal cutting experiments were conducted in dry and wet cutting conditions. In the wet cutting condition, the cutting fluid (Houghton Hocut 795B – 5.2% concentration) was applied using the standard pumping system of the machine-tool with a flow rate of 17 litres/min. The fluid concentration was frequently checked with a refractometer. Figure 5.6 shows the experiment set-up, which produces orthogonal cutting with the tool feed being equivalent to the uncut chip thickness and the thickness of the tube wall is equal to the width of the chip. To ensure repeatability of the experimental results, each cutting experiment was repeated three times and an average was taken.
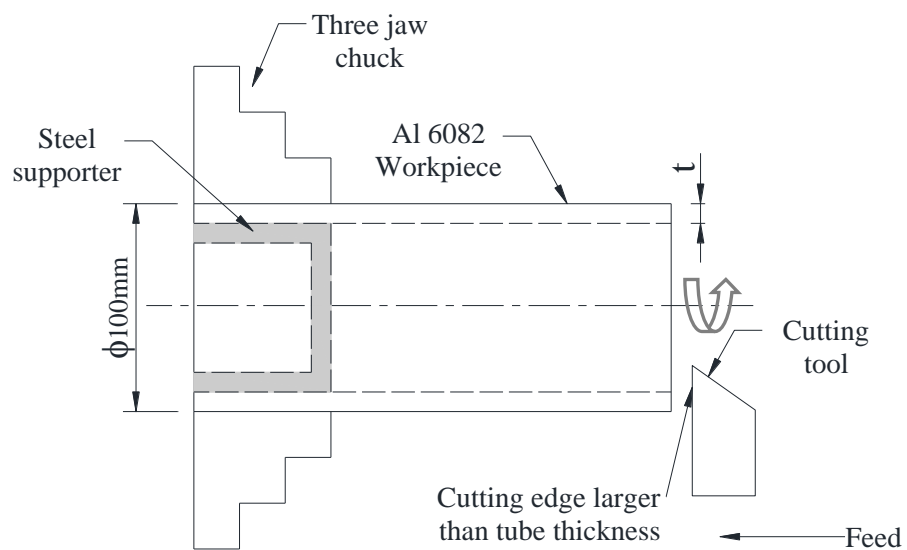
Figure 5.6 Orthogonal metal cutting

As mentioned in Section 5.1.2, aluminium was chosen in this study because it is easy to machine and do not wear the rake face of the cutting tool much (i.e. ignoring the cutting tool wear), where Stephenson & Agapiou (2006) stated that the tool wear rate is very low in machining aluminium alloy. In this study, this was confirmed by examining the cutting tool surface topography using a ContourGT optical microscope, after carrying out all the experiments. Figure 5.7 shows the surface topography of the rake face of the cutting tool, that was used in this study, after machining *Al 6082-T6*. It can be seen clearly from the figure that the rake face not affected and it is in a good condition.
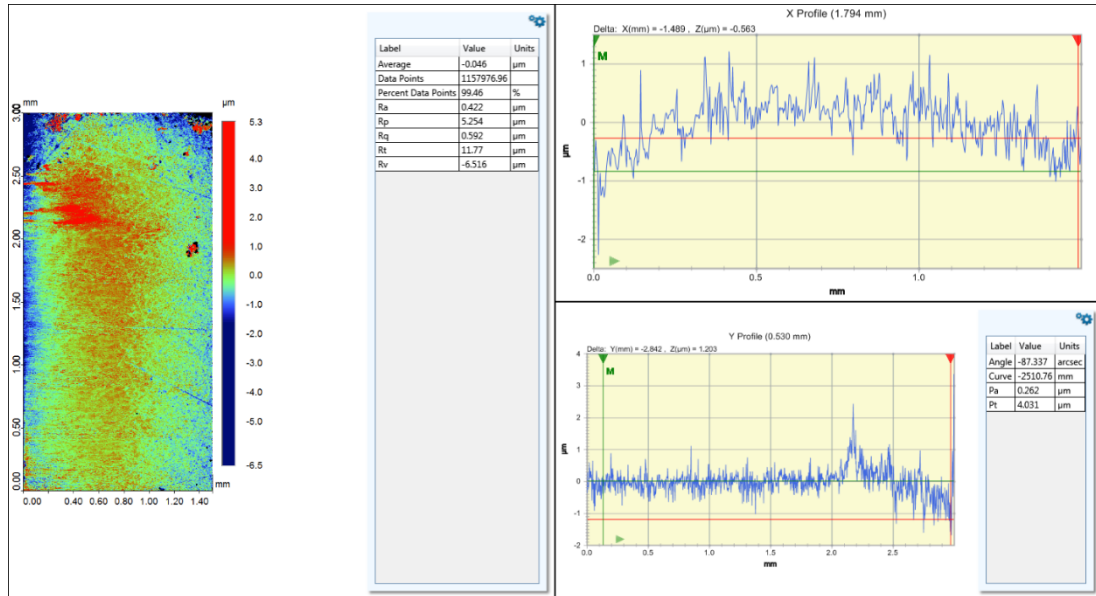
Figure 5.7 A ContourGT optical microscope image of the rake face of the cutting tool after conducting all the experiments of this study

5.1.5 Cutting Conditions

Designed experiments were conducted for a selected combination of five different cutting speeds, cutting depths and feeds as shown in Table 5.3. It is worth noting that the values for these cutting conditions were selected with respect to the maximum temperature, as discussed in Section 4.3, because these experiments have been used in monitoring the tool-chip interface as well as using the ultrasonic reflection. Where a series of orthogonal cutting experiments were carried out to monitor the temperature for different cutting parameters.

Table 5.3 Cutting conditions

Parameters	Levels				
	1	2	3	4	5
Cutting speed (m/min)	40	60	90	120	140
Depth of cut (mm)	1.2	1.5	2	2.5	2.8
Feed (mm/rev)	0.09	0.12	0.16	0.2	0.23

The tool-chip contact length, tool-chip contact area and the three components of forces, radial force in X direction; F_x, thrust force in Y direction; F_y and the cutting force in Z direction; F_z were measured. The third component of force is negligible because it is orthogonal cutting. The constants for the correlation between input parameters (cutting speed, feed and depth of cut) and measured output parameters

(contact length, contact area and cutting forces) were established for different lubrication conditions by applying nonlinear regression analysis to the quantitative data obtained from the experiments. This is explained in detail in a later section.

5.2 Experimental Procedure

5.2.1 Experiment Design

As presented in Chapter 2, a centre composite design (CCD) method was utilised in this study to carry out the orthogonal experiments. A total of 20 experimental runs have been considered. The sequence of the 20 trials were randomized using a random number table to minimize the error as a result of machining set-up.

As mentioned in Section 5.1.4, each cutting trial was repeated three times to ensure the repeatability of the measurement data, and an average was taken. It is worth noting that the number of experiments involving dry and wet turning conducted in this study was more than 125 experiments.

Table 5.4 lists the cutting parameters levels including feed, cutting depth and cutting speed for the experiments. Depending on the experimental plan which based on the second order of central composite rotatable design the trials have been conducted. The matrix of the whole experimental design involving the coded and physical values of the design parameters and the run order are shown Table 5.5.

In this work, a commercially available statistical software package (Minitab 17) was used for the computation of the regression constants and exponents.

Table 5.4 Physical and coded values of cutting parameters for experiment design

Symbol	Parameters/Levels	Lowest	Low	Centre	High	Highest
	Coding-classical experimental design	-1.6817	-1	0	+1	+1.6817
A	Cutting speed (*m/min*)	40	60	90	120	140
B	Depth of Cut (*mm*)	1.2	1.5	2	2.5	2.8
C	Feed (*mm/rev*)	0.09	0.12	0.16	0.2	0.23

Table 5.5 Central Composite Design (CCD) used in this work

Test Number	Coded Values			Uncoded/Physical Value		
	A	**B**	**C**	**Cutting Speed** (*m/min*)	**Depth of Cut** (*mm*)	**Feed** (*mm/rev*)
1	0	0	0	90	2	0.16
2	0	0	0	90	2	0.16
3	0	0	0	90	2	0.16
4	-1.6817	0	0	40	2	0.16
5	-1	1	-1	60	2.5	0.12
6	-1	1	1	60	2.5	0.2
7	1	-1	-1	120	1.5	0.12
8	1.6817	0	0	140	2	0.16
9	0	-1.6817	0	90	1.2	0.16
10	1	-1	1	120	1.5	0.2
11	0	1.6817	0	90	2.8	0.16
12	1	1	1	120	2.5	0.2
13	-1	-1	1	60	1.5	0.2
14	0	0	0	90	2	0.16
15	0	0	0	90	2	0.16
16	0	0	1.6817	90	2	0.23
17	0	0	0	90	2	0.16
18	-1	-1	-1	60	1.5	0.12
19	1	1	-1	120	2.5	0.12
20	0	0	-1.6817	90	2	0.09

5.2.2   Analysis of Variance (ANOVA)

The statistical method of analysis of variance (ANOVA) was carried out on the experimental data for identifying the parameters significantly affecting the chip characteristics, cutting forces and reflection coefficient during machining aluminium *Al 6082*. The analysis was conducted by using the P-value. If P-values are less than 0.05 (or 95% confidence) then the obtained models are considered as statistically significant (Song 2006). The highest influence for the corresponding output parameters has the lowest the P-value. The stepwise technique, is an automated tool used in statistics to add the most significant variable during each step or removes the least significant variable, was used to remove the non-significant variables from the model. It indicates that the chosen parameters in the model have a significant effect

on the output factors. Minitab 17, a statistical software, was employed to carry out the ANOVA.

5.2.3   Cutting Force Measurement

A three component piezoelectric quartz crystal Kistler 9121 type dynamometer was used for measuring the three orthogonal components of the cutting forces: F_r, F_t and F_c. The force data were acquired for 30 *s* at a sample rate of 10 *kHz*. The time process (30 seconds) was divided into three stages according to the cutting tool position with respect to the workpiece. In the first 10 *s*, no forces were recorded as the cutting tool was not in contact with the workpiece, in the second 10 *s* the cutting tool engages the workpiece and the cutting forces were acquired. In the last 10 *s*, the cutting tool reaches the workpiece end and same as the first stage no forces were recorded, more details are presented in Chapter 6.

The piezoelectric dynamometer is connected to a multi-channel charge amplifier (type 5070A) using a high insulation cable. The multi-channel charge amplifier converts the charge produced by the piezoelectric sensor to a voltage, which is used as an input variable for monitoring and control processes. The amplifier is connected to a data acquisition system (type 5697A) which is connected to the PC. Kistler provides a software for the data acquisition and analysis known as Dynoware software. This software has been used to analyze the cutting force data and present the results in both time and frequency domain. The average mean values for the cutting forces are reported. A schematic diagram of the cutting force data acquisition system is shown in Figure 5.8, while a photograph of the apparatus and the dynamometer setup are shown in Figure 5.9.

Further signal processing using Fast Fourier Transform (FFT) analysis of the cutting data was implemented in MATLAB software, where a MATLAB code was written to convert the time domain cutting data into frequency domain cutting data. Furthermore, the time domain cutting data were subjected to post processing to calculate some statistics features by utilizing MATLAB.
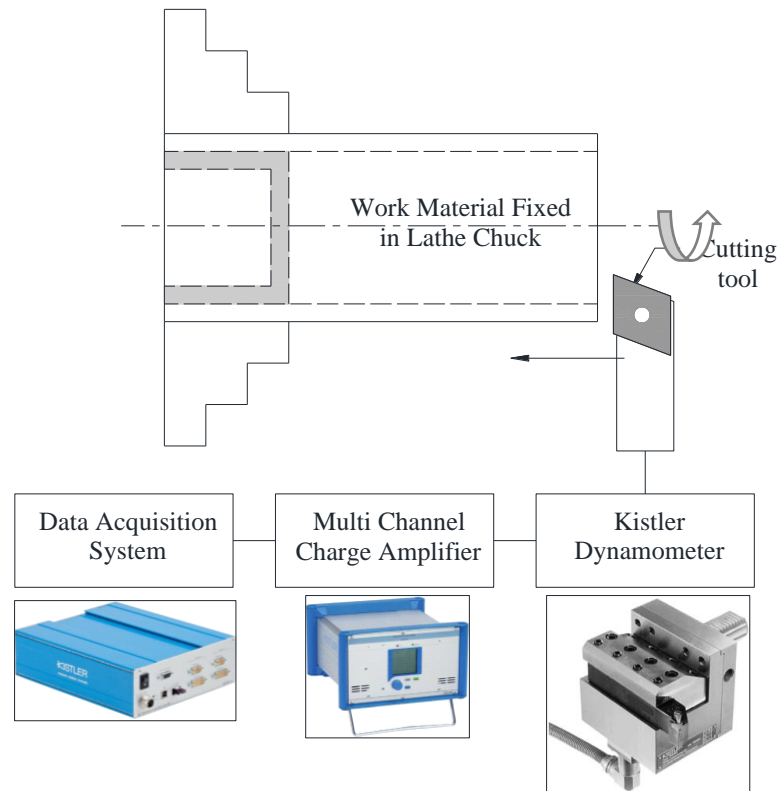
Figure 5.8 Schematic diagram of force data acquisition system

a)   b)
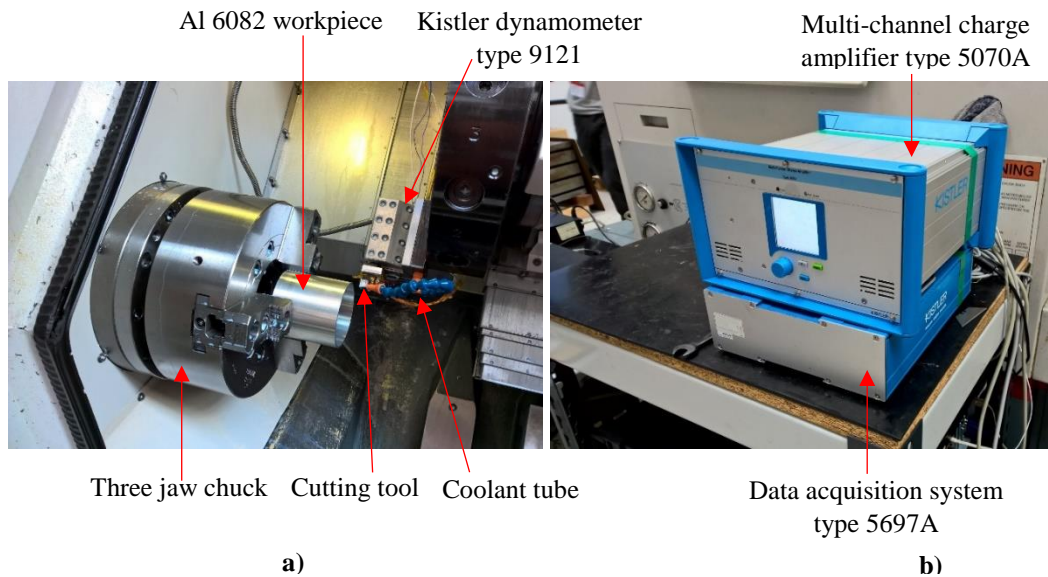
Figure 5.9 a) Workpiece and dynamometer setup inside the CNC machine, b) Kistler data acquisition and amplifier

5.2.4   Chip Morphology Measurement

Chips from each experiment were collected accurately, a container was used to avoid the side spread of the small amount of the chip. The thickness and width of the chips

were measured at six different locations along their length, and the average was calculated. The chip thickness measurements were made using a ball type micrometre gauge while for measuring the chip width a digital Vernier calliper was used. Because of the small size of the chips in the thickness direction, a difficulty was found to measure the chip width by using a micrometre. That is why a digital Vernier calliper was used instead of micrometre. Furthermore, a digital scale type Mettler PJ3000 was used to measure the chip weight. Figure 5.10 shows the scale that was used in this study. The shear band angle and the chip velocity were measured using equations 5.1 and 5.3, respectively.

$$\tan \varphi = \frac{\frac{f}{h} \cos \alpha}{1 - \frac{f}{h} \sin \alpha} \qquad \qquad 5.1$$

where: φ is shear angle, f is feed, h is chip thickness and α is rake angle.

Due to the cutting tool used in this study has a zero rake angle, so the equation 5.1 will simplify to

$$\tan \varphi = r \qquad \qquad 5.2$$

where r is the chip ratio and is equal to feed divide by chip thickness ($\frac{f}{h}$).

The chip velocity was calculated using the equation

$$V_C = \frac{V \sin \varphi}{\cos(\varphi - \alpha)} \qquad \qquad 5.3$$

where V_C is the chip velocity (*m/min*), V is the cutting speed (*m/min*), φ is shear angle and α is rake angle.
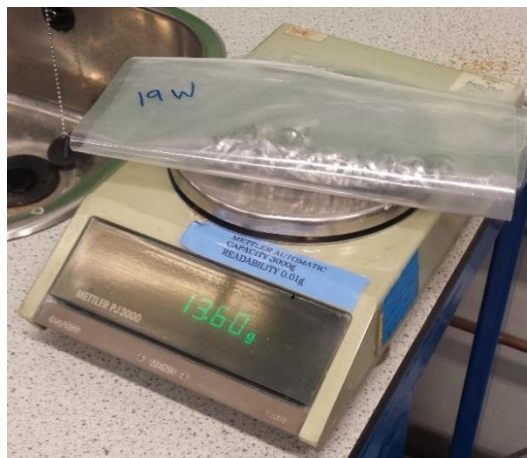
Figure 5.10 Digital scale used in this study

5.2.5   Tool-Chip Contact Length Measurement

In the orthogonal cutting process, the chip contacts the cutting tool from the tip to where it leaves the cutting tool. This distance is defined as the tool-chip contact length, or simply the contact length (Iqbal et al. 2008; Huang et al. 1999). In this study, the contact length was measured experimentally and determined theoretically. Because only one cutting tool was used in all the experiments, measurement of the contact length was impossible. Therefore, additional orthogonal experiments were conducted using low to high cutting speeds, using a fresh tip for each experiment, to measure the contact length. The experiments were carried out by using two different cutting tools and the same workpiece was used on a Triumph 2500 lathe machine. A scanning electron microscope SEM was used after machining to measure the contact length by measuring the contact track on the rake face cutting tool. The contact length was further checked by using the energy dispersive X-ray analysis (EDXA) as explained in Chapter 2, where the transfer of aluminium from the chip to the rake face was quantified. There is no aluminium concentration beyond the area of the tool–chip contact. Figure 5.11 shows the SEM that was employed in this study. Furthermore, the contact length was also calculated using Kato's and Toropov's model (see Section 2.6.2 for further details about the model), which is the contact length is twice the chip thickness (Kato et al. 1972; Toropov & Ko 2003), and compared with the experimental results.
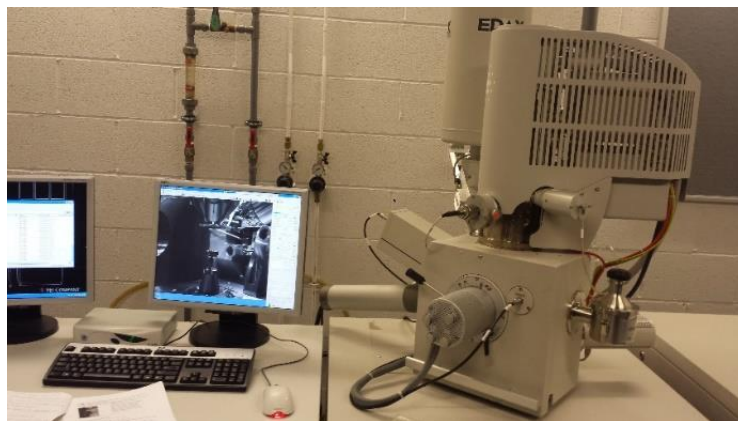
Figure 5.11 SEM

5.2.6   Existence Confirmation of Built-Up Edge (BUE)

As mentioned in Chapter 2, a built-up edge (BUE) is an accumulation of material against the rake face that adheres to the tool tip, separating it from the chip. In this

study, the observation of the formation of BUE is made from the underside of the chips obtained when cutting *Al 6082* at different cutting speeds, with and without cutting fluid. From scanning electron microscopy (SEM), the existence of BUE is confirmed through the presence of streaks or lumps of adhering material on the underside of the chips. This technique also was used by Seah & Li (1997). More details of the BUE confirmation are given in Chapter 6.

5.2.7   Temperature Measurement

To measure the temperature during the machining process, a small hole 0.8 *mm* in diameter and 2 *mm* in depth was made (see Figure 5.12), using Electro Discharge Machining (EDM), on the opposite side of the rake face of the cutting tool and close to the position of the ultrasonic transducer as described in Section 4.2.4. A thermocouple type K was fitted to the hole to ensure that thermocouple will be located at the same position in all machining tests. The thermocouple tips diameter was 0.5 *mm,* a high temperature thermal conductivity paste with operating temperature up to 200°C, was used to ensure perfect thermal contact between thermocouple and hole.

Hole dia. 0.8 mm
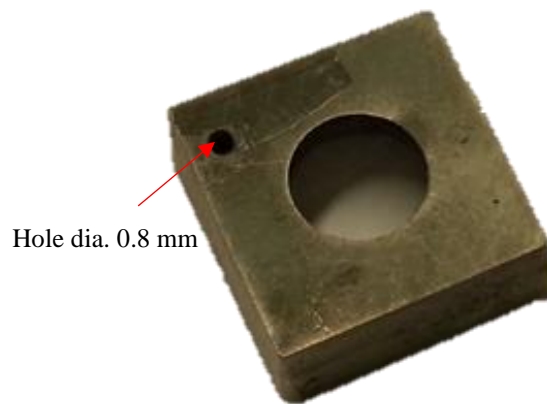
Figure 5.12 Cutting tool insert showing the thermocouple location

The temperature data was collected using Pico-TC 08 data logger that has 8 channels, as shown in Figure 5.13, and each channel can record temperature data with a sampling time of 100*ms*.

Figure 5.13 Channels Thermocouple Data Logger

The thermocouple wire was positioned to measure the temperature of the cutting edge of the cutting tool insert close to the location of the ultrasonic transducer. More details of the temperature measurement are given in Chapter 6.

5.3 Conclusions

This chapter has described the machining processes analysis. The experimental setup of the orthogonal cutting has been explained. Measuring the machining performance including cutting forces, chip morphology, contact length and temperature have been described and explained. The results will be presented in the next chapter.

6

Chip Morphology and Cutting Force Measurements

This chapter presents the experimental results of the cutting force components which have been carried out to correlate with the ultrasonic reflection results in order to investigate how much the tool-chip contact area is related to the cutting forces and ultrasonic reflection. The analysis of variance (ANOVA) of the experimental results is explained in detail. This chapter also introduces the comparison between the experimental results of the cutting forces and the predicted results obtained from the mathematical model. The tool-chip contact and the BUE are also explained in detail in this chapter.

6.1 Experiment Procedure

As described in Chapter 5, different techniques have been used for investigating the tool-chip interface in dry and wet cutting conditions in situ in orthogonal cutting of aluminium. These techniques were ultrasonic reflection, cutting force, thermocouple, AE and accelerometer sensors. A centre composite design (CCD) technique was used in this study, as explained in Chapter 5, to carry out these experiments and different data were recorded simultaneously. As presented in Table 5.5 and according to the CCD methodology, 20 trials were conducted including the centre point which was repeated six times (cutting speed 90 *m/min*, cutting depth 2 *mm* and feed 0.16 *mm/rev*). Each of the augmented tests was repeated three times, to confirm the repeatability of the trials, and an average with a standard deviation were taken. The results of these experiments are presented in the following sections of this chapter while the ultrasonic reflection results will be presented in the next chapter. The AE and vibration measurements will not be presented in this study as they are not within the scope of this work.

6.2 Analysis of Variance (ANOVA)

As presented in Chapter 5, the ANOVA was conducted on the experimental data to identify the main significant parameters on the chip characteristics and cutting forces during machining aluminium *Al 6082*, and also to develop the empirical relationships by using the regression analysis. The same procedures have been taken as described in Chapter 5, where the analysis was conducted by using the P-value; if the P-values are less than 0.05 then the obtained models are considered as a statistically significant. The highest influence for the corresponding output parameters has the lowest the P-value. Only the significant parameters are presented in this chapter while the complete ANOVA results are presented in Appendix A.

6.3 Temperature Measurements

As described in Chapter 4, a thermocouple was attached to the cutting tool insert at a depth of 2 *mm* from the underneath surface of the cutting tool. This temperature value is not exactly at the tool-chip interface, but, still it gives a good indication of the cutting tool temperature. The main reason for measuring the temperature, in this study, was to calibrate the ultrasonic transducer output not the temperature itself. Figure 6.1 shows the profile of the temperature data recorded during orthogonal tube cutting of

aluminium *Al 6082* at dry and wet conditions. The figure demonstrates that the experimental process is divided into three regions according to the position of the tool cutting edge with reference to the tube workpiece. In the first 10 *s* of the experiment, the tool cutting edge is not in contact with the workpiece. Therefore, the temperature recorded was around the room temperature. As soon as the tool cutting edge engaged the workpiece, a sharp increase in the temperature starts to accumulate and continuing increases until the tool cutting edge reaches the end of the cutting length of the tube workpiece. In the last 10 *s*, the temperature starts to decrease sharply indicating the end of the cutting process. The average temperature value of the cutting region is reported in this study.
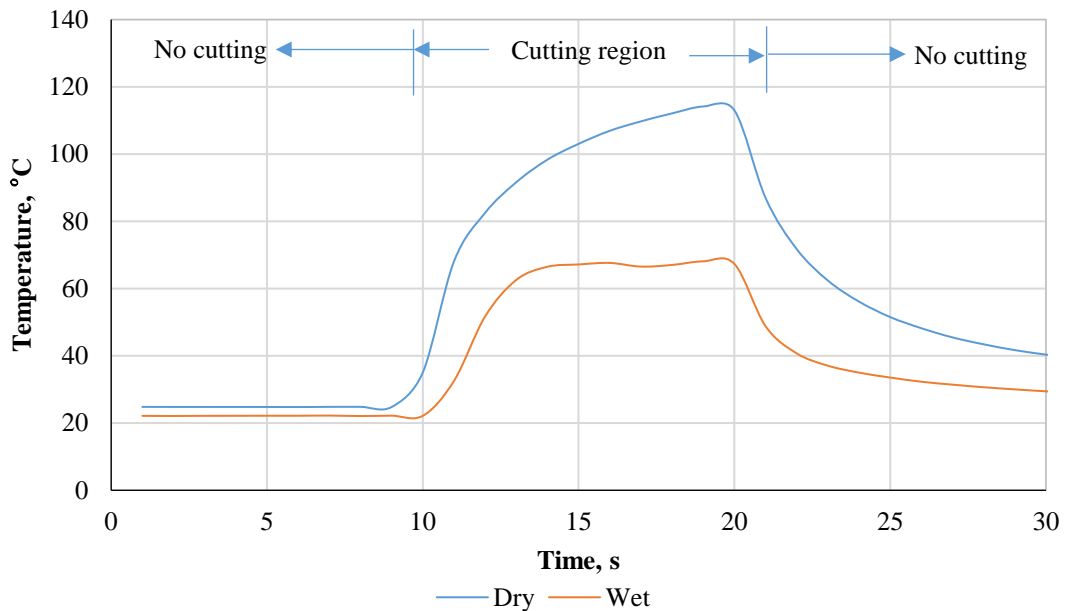
Figure 6.1 Temperature profile during *Al 6082* cutting at *V*=90 *m/min*, *t*=2 *mm*, and *f*= 0.09 *mm/rev*

The design of experiments (mentioned in Chapter 5) was carried out and the different data were recorded simultaneously (as discussed earlier in this section). In this part, the experimental results of the temperature at dry and wet machining conditions are presented. Figure 6.2 shows a comparison of the temperature between dry and wet machining conditions during orthogonal cutting. The error bars in the figure represent the maximum and minimum values. The results are also given, in detail, in Appendix A (Table A.1).
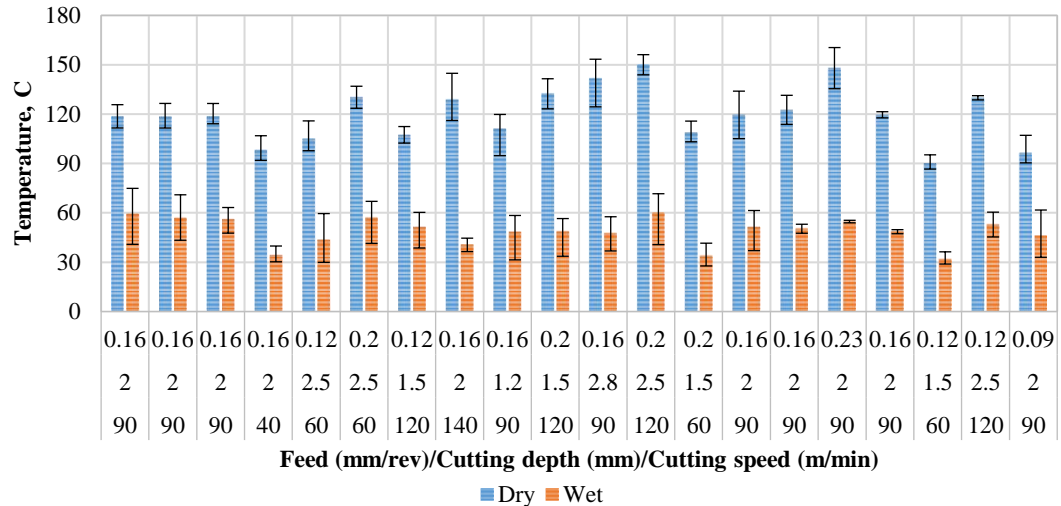
Figure 6.2 Comparison of the temperature for dry and wet cutting conditions

In dry machining (see Figure 6.2), the results show that the temperature increased with increasing cutting speed, cutting depth and feed. The lowest temperature was gained when machining at low cutting speed (*V*=60 *m/min*), low feed (*f*=0.12 *mm/rev*) and low cutting depth (*t*=1.5 *mm*). While the highest was obtained at *V*=120 *m/min*, *f*=0.2 *mm/rev* and *t*=2.5 *mm*. To study the influence of the cutting speed, cutting depth and feed individually on the temperature, some results from Figure 6.2 have been extracted and presented below.

Figure 6.3 demonstrates the influence of cutting speed on temperature where the temperature increased with increasing cutting speeds (*V*=40, 90, 140 *m/min*) with constant cutting depth (*t*=2 *mm*) and feed (*f*=0.16 *mm/rev*) and this due to the insufficient time to dissipate the heat generated when the cutting speed increases where increasing cutting speed lead to increase the strain rates in secondary and primary cutting zones which results generating heat flux (Carvalho et al. 2006). The results are supported by literature references in many articles (Vieira et al. 2001; Gekonde & Subramanian 2002; Nouari et al. 2003; Carvalho et al. 2006; Sreejith 2008; Radhika et al. 2014). It was observed that the influence of cutting speed on temperature is higher at low speeds than high speeds, since the temperature roughly increased 20% from increasing cutting speed 40 m/min to 90 m/min while the increasing is less than half of this value from 90 m/min to 140 m/min and it is about 8%.
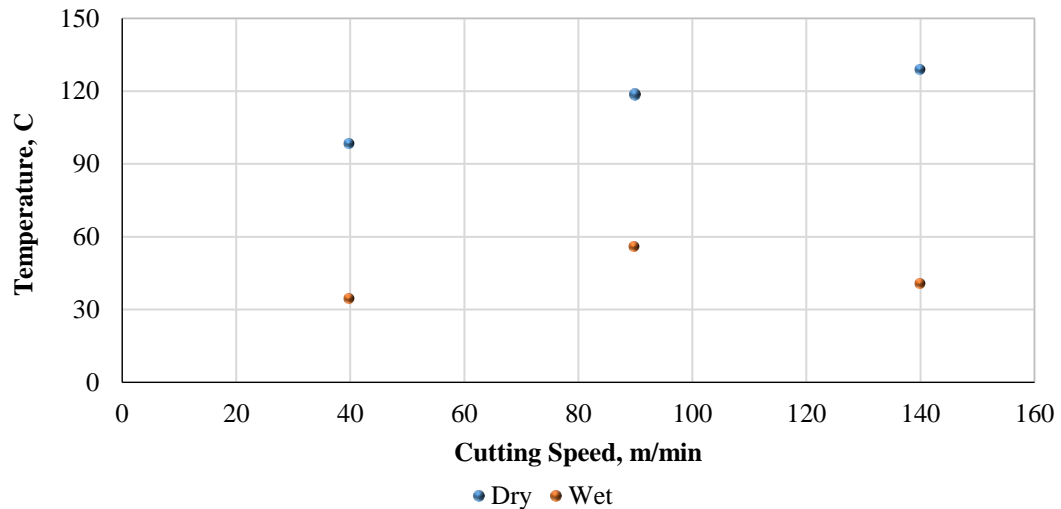
Figure 6.3 Comparison of the temperature under dry and wet machining of *Al 6082-T6* at different cutting speeds with a constant cutting depth and feed (*t=2 mm*, *f=0.16 mm/rev*).

With applying coolant, one unanticipated finding was that the temperature increased with increasing cutting speed up to 90 *m/min* and then decreased (see Figure 6.3 and Figure 6.4). In addition to the lubricant effect, there are, however, other possible explanations. One reason why temperature has declined, at cutting speeds > 90 *m/min*, is that and as mentioned earlier in this section that this temperature is not exactly at the tool-chip interface where the interface temperature is still higher than this. Another reason is, as mentioned in the literature review (see Figure 2.21), that with increasing cutting speeds the amount of heat that shared by the cutting tool decreased (Abhang & Hameedullah 2010B).

To investigate more about the influence of the cutting speed on the temperature, further experiments were carried out. Figure 6.4 shows the results of these experiments where it can be seen clearly that the temperature in dry conditions increased with increasing cutting speed. In wet conditions, the graphs show that the influence of cutting speed is divided into two parts according to its range. At cutting speeds (*V<90 m/min*) the results show that as in Figure 6.3 the temperature increased with increasing cutting speed, while at cutting speeds (*V>90 m/min*) the temperature decreased with increasing cutting speeds.
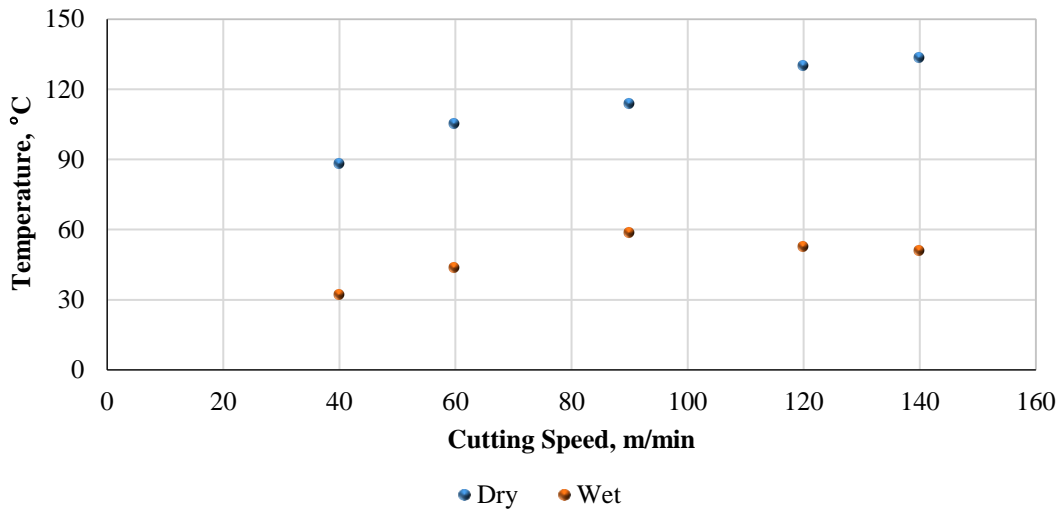
Figure 6.4 Comparison of the temperature under dry and wet machining of *Al 6082-T6* at different cutting speeds with a constant cutting depth and feed (*t*=2.5 *mm*, *f*=0.12 *mm/rev*).

Figure 6.5 shows that cutting aluminium *Al 6082* at different depth of cut (*t*= 1.2, 2 and 2.8 *mm*) with a constant cutting speed (*V*=90 *m/min*) and feed (*f*=0.16 *mm/rev*) results in increasing temperature because of the large volume of workpiece material being removed. This result agrees with previous researchers (Abhang & Hameedullah 2010a). Where the increase in the temperature was smaller from (*t*=1.2 to *t*= 2 *mm*) (6%) than from (*t*=2 to *t*=2.8 *mm*) (20%).
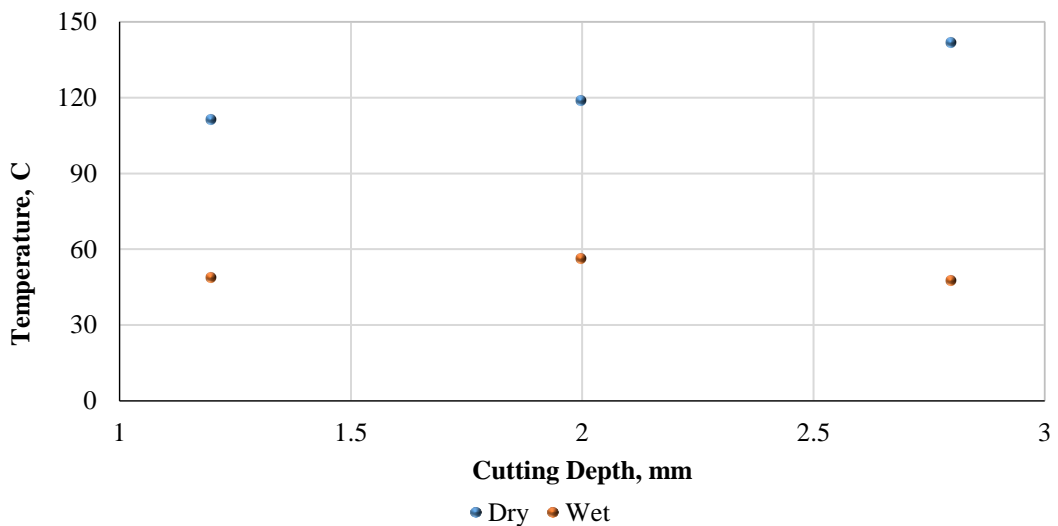
Figure 6.5 Comparison of the temperature under dry and wet machining of *Al 6082-T6* at different cutting depth with a constant cutting speed and feed (*V*=90 *m/min*, *f*=0.16 *mm/rev*).

The effect of feed on the temperature can be seen clearly from the Figure 6.6, where the relation between them is a direct relationship since the temperature increased with increasing the feed. The results are supported by (Gómez-Parra et al. 2013; Carvalho

et al. 2006; Nouari et al. 2003) where increasing the feed rate leads to increasing in the temperature. Increasing feed result in thicker chips, so there is less opportunity for the generated heat to be dissipated with a large thickness to the surface area of the chip, therefore, temperature increases, more detail are presented in Section 6.4.1.
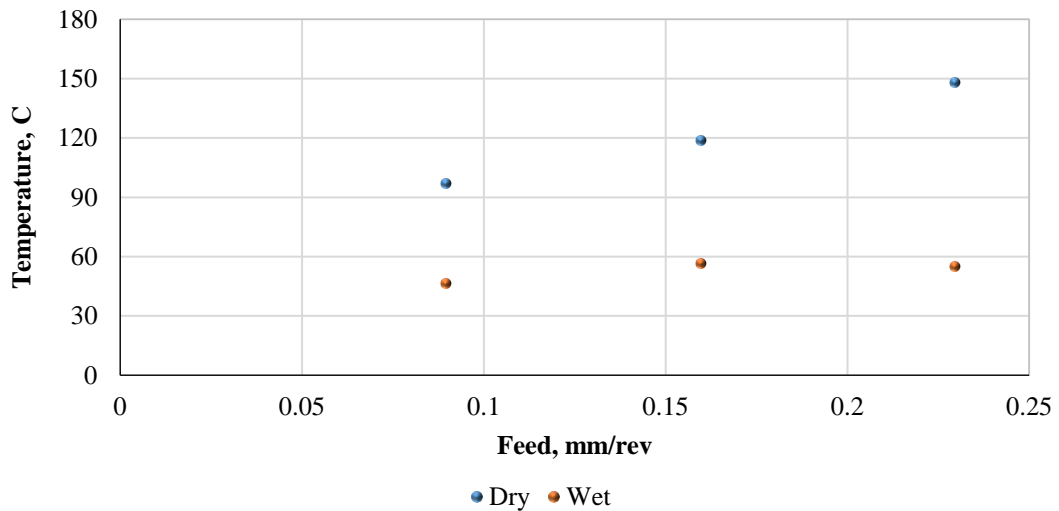
Figure 6.6 Comparison of the temperature under dry and wet machining of *Al 6082-T6* at different feed with a constant cutting speed and cutting depth (*V=90 m/min*, *t=2 mm*).

Contour plots of the temperature versus the machining parameters including feed, cutting speed and depth of cut in dry and wet cutting conditions are shown in Figure 6.7. The contour plots can be used for monitoring temperature at different machining parameters.

Dry   **Wet**
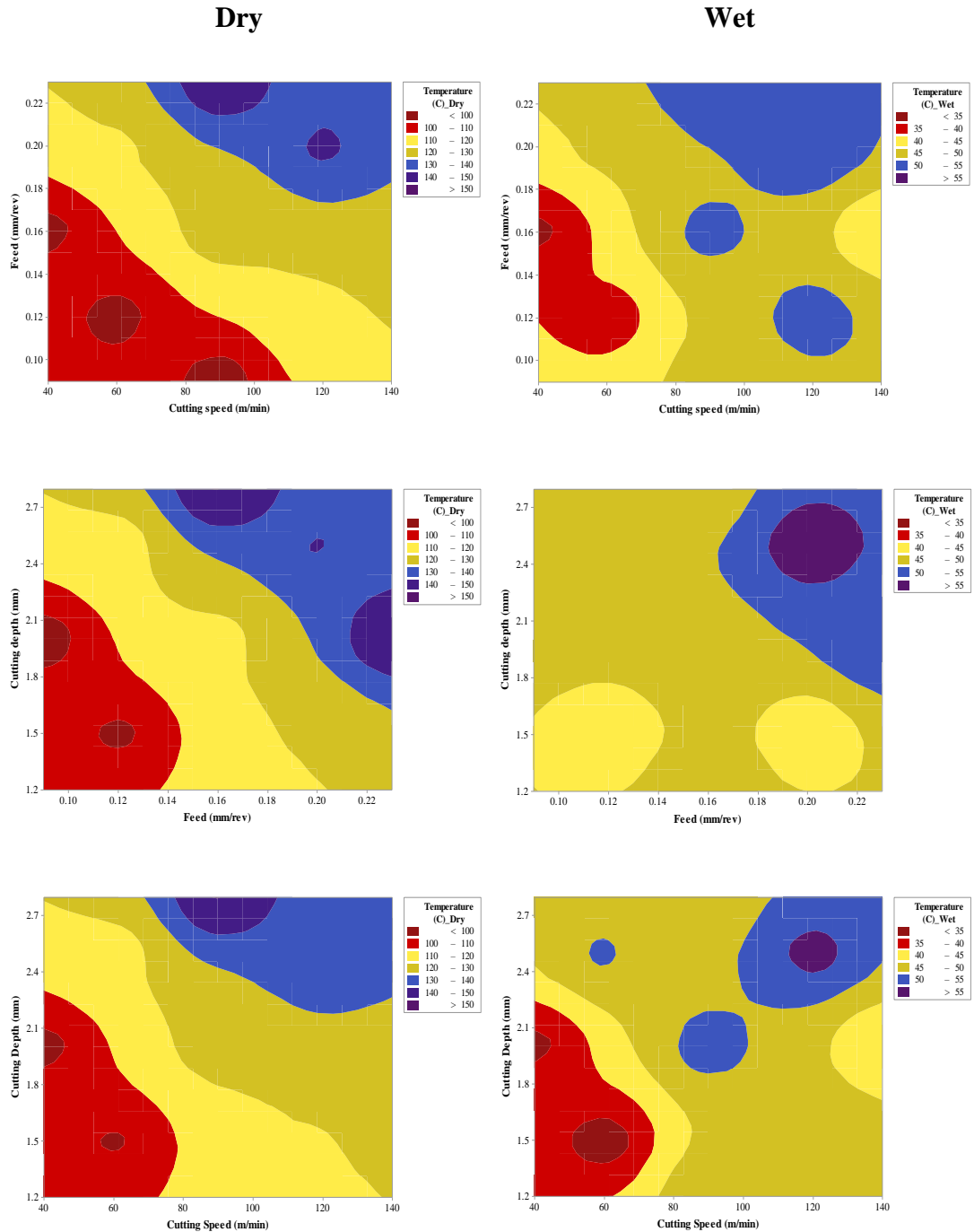
Figure 6.7 Contour plot of temperature versus cutting parameters at dry and wet cutting conditions

6.4 Chip Morphology and Characteristics

In order to investigate the tool-chip interface at different cutting parameters, a number of physical parameters were investigated during post-experiment study, including the chip thickness, shear band angle, chip velocity, tool-chip contact length, tool-chip

96

contact area and built-up edge (BUE). The influence of the cutting speed, feed and cutting depth on these parameters are given in the following sections.

6.4.1 Chip Thickness

As explained in Section 5.2.4, the chip thickness was measured using a ball type micrometre gauge. The results obtained from these experiments are shown in the graphical format in Figure 6.8 and the error bars represent the standard deviation. The results are also given, in more detail, in Appendix A (Table A.2).

In dry conditions, the results show that the chip thickness decreases with increasing cutting speed and cutting depth and increased with increasing feed (see Figure 6.8).
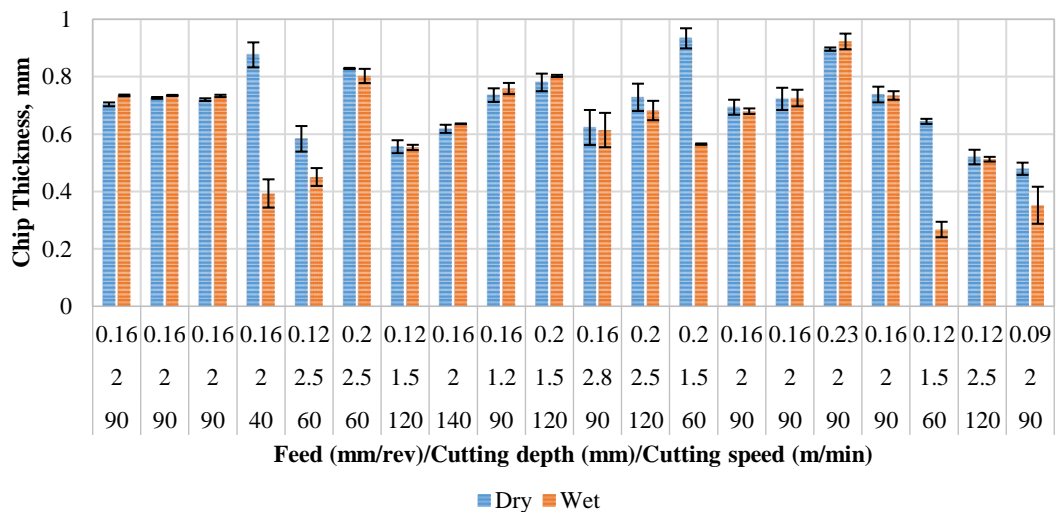
Figure 6.8 Comparison of the chip thickness for dry and wet cutting conditions

To study the influence of each cutting conditions individually on the chip thickness, some results of Figure 6.8 have been re-presented in linear graphs. The influence of cutting speed on chip thickness in the dry and wet cutting condition can be seen from the Figure 6.9, where the dry results show that there has been a steady decrease in the chip thickness with increasing cutting speed while the cutting depth and feed were kept constant at *t*=2 *mm*, *f*=0.16 *mm/rev*, respectively.
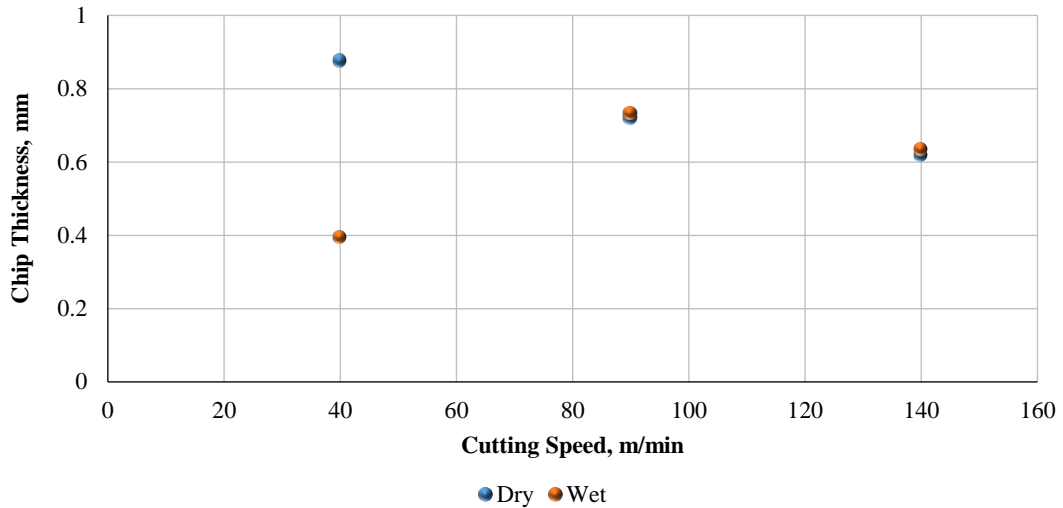
Figure 6.9 Comparison of the chip thickness under dry and wet machining of *Al 6082-T6* at different cutting speeds with a constant cutting depth and feed (*t=2 mm*, *f=0.16 mm/rev*).

These results may be explained by the temperature effect, with increasing cutting speed the temperature of the tool-chip interface increased and this leads to softening the workpiece and hence the friction at the tool-chip interface reduces. These result in increasing shear angle and thus reducing chip thickness. More detail about the temperature effect were given in Section 6.3. This result is in agreement with (Davoodi & Tazehkandi 2014; Xu et al. 2014; Kouam et al. 2013; Dhananchezian & Kumar 2010; Seah & Li 1997).

When applying coolant, the chip thickness shows a different trend. Here, the chip thickness initially increases and then decreases with the cutting speed. Where at low levels, *V<90 m/min*, the chip thickness found to increase with increasing cutting speed (see Figure 6.9 and Figure 6.10); whereas at high levels, *V>90 m/min,* the results found that the influence of the machining parameters on the chip thickness is same as the dry conditions, which is decreased with increasing cutting speed (see Figure 6.9 and Figure 6.10). The results also found that at wet conditions, the chip thickness was found smaller than in dry conditions and at low cutting speed (below 90 *m/min*). At cutting speeds higher than 90 *m/min*, there were no significant differences between the chip thickness in dry and wet cutting conditions (see Figure 6.9 and Figure 6.10). This result matches the previous finding by Seah & Li (1997). It seems possible that these results, are due to the temperature effect; where using cutting fluid reduce the effect of friction at the tool-chip interface and hence increasing the shear angle, which led to thinner chips. More detail about the shear angle are presented in the next section.

Further experiments were carried out to investigate the influence of the cutting speed on the chip thickness, by examining different machining parameters. The results of these experiments are graphically depicted in Figure 6.10 where the same trend was observed at a constant cutting depth (*t*=2.5 *mm*) and feed (*f*=0.12 *mm/rev*) with different cutting speeds.
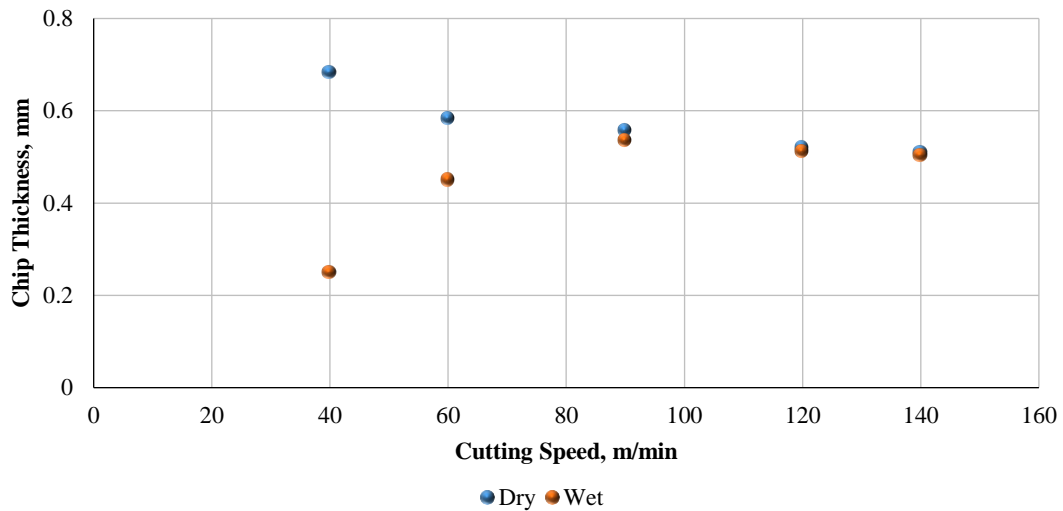
Figure 6.10 Comparison of the chip thickness under dry and wet machining of *Al 6082-T6* at different cutting speeds with a constant cutting depth and feed (*t*=2.5 *mm*, *f*=0.12 *mm/rev*).

The results show that the feed has a significant effect on the chip thickness than the cutting speed and cutting depth. The data reveals that there has been a gradual increase in the chip thickness with increasing feed while the cutting depth and cutting speed were kept constant at *t*=2 *mm*, *V*=90 *m/min*. Figure 6.11 show the effect of feed on the chip thickness. These results are likely to be related to the size of the primary shear zone, where with the increase in feed, the thickness of the primary shear zone increases and the strain rate at the zone decreases as reported by (Adibi-Sedeh et al. 2003). These results are in agreement with those obtained by (Adibi-Sedeh et al. 2003; Kouam et al. 2013; Dhananchezian & Kumar 2010).
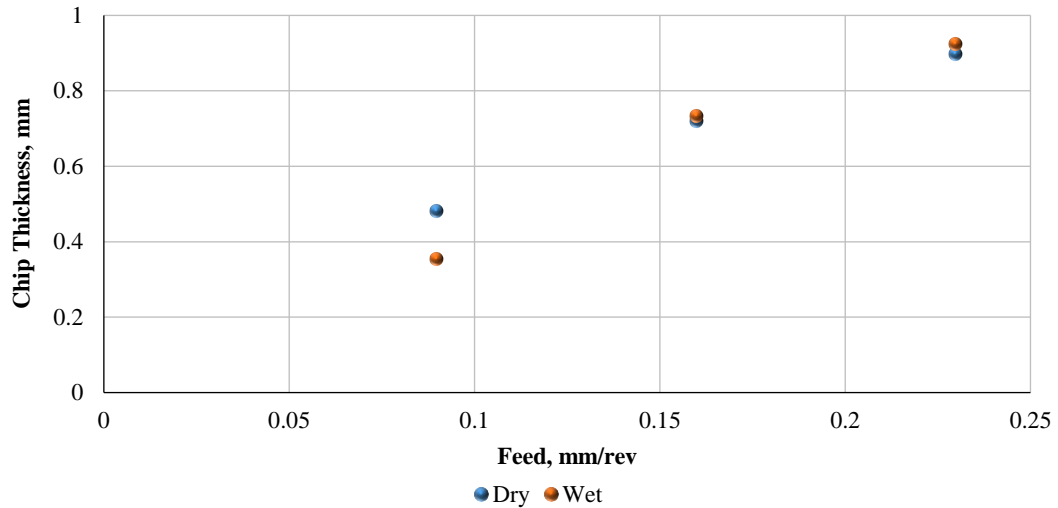
Figure 6.11 Comparison of the chip thickness under dry and wet machining of *Al 6082-T6* at different feed with a constant cutting speed and cutting depth (*V=90 m/min, t=2 mm*).

The data reveals that there has been a slight decrease in the chip thickness with increasing cutting depth while the cutting speed and feed were kept constant (Figure 6.12). These results are in agreement with those obtained by Bermingham et al. (2011).
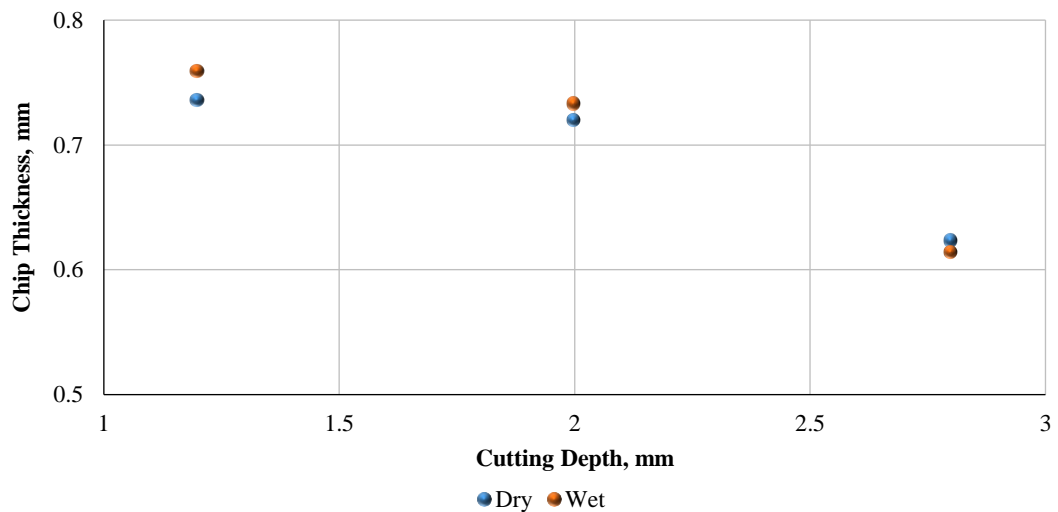
Figure 6.12 Comparison of the chip thickness under dry and wet machining of *Al 6082-T6* at different cutting depth with a constant cutting speed and feed (*V=90 m/min, f=0.16 mm/rev*).

With wet cutting conditions, it was found that the chip thickness trend remained constant with changing cutting depth and feed from low to high levels, as happened with the cutting speed, where in all the levels the relationship between chip thickness and cutting depth and feed is directly proportional, which increased with increasing feed and decreased with increasing cutting depth, (see Figure 6.11 and Figure 6.12). The ANOVA results of the chip thickness are presented in Appendix A.

6.4.2 Shear Angle and Chip Velocity

As explained in Section 5.2.4, the shear angle and the chip velocity were calculated using equations 5.2 and 5.3, respectively. Figure 6.13 shows a comparison of the shear angle between dry and wet machining conditions during orthogonal cutting while Figure 6.14 presents the effect of cutting speed on shear angle in the dry and wet cutting condition, where the dry results show that there has been a steady increase in the shear angle with increasing cutting speed while the cutting depth and feed were kept constant at *t=2 mm, f=0.16 mm/rev*, respectively.
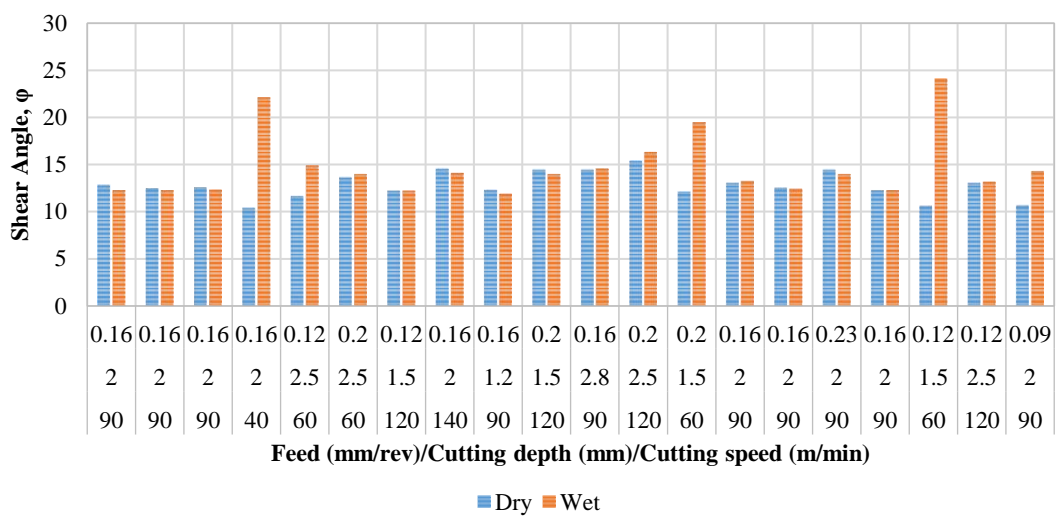
Figure 6.13 Comparison of the shear angle for dry and wet cutting conditions

At wet cutting conditions, the shear angle shows a different trend. Here, the shear angle initially decreases and then increases with the cutting speed. Where at low levels, *V<90 m/min*, the shear angle found to decrease with increasing cutting speed (see Figure 6.14); whereas at high levels, *V>90 m/min,* the results found that the influence of the machining parameters on the shear angle are same as the dry conditions, which is increased with increasing cutting speed.
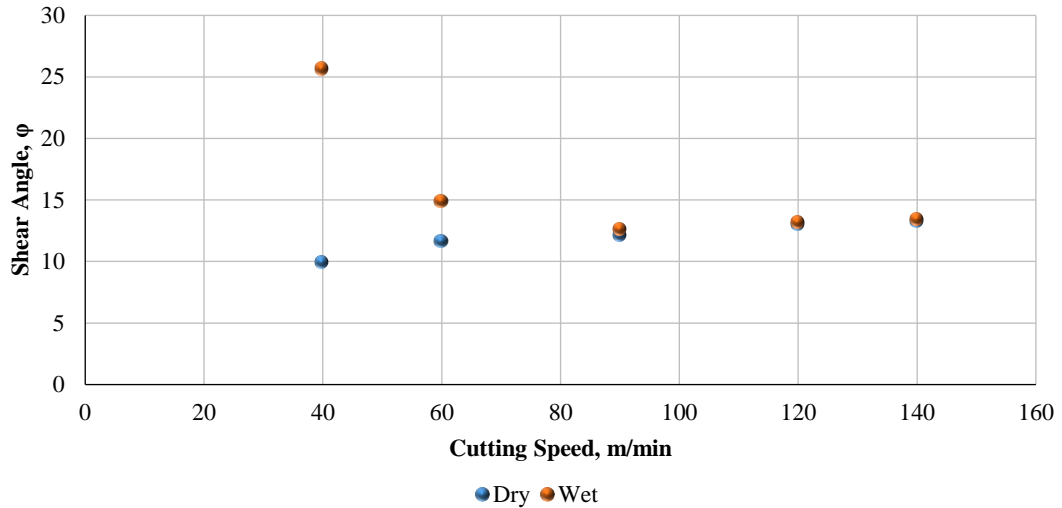
Figure 6.14 Comparison of the shear angle under dry and wet machining of *Al 6082-T6* at different cutting speeds with a constant cutting depth and feed (*t=2.5 mm*, *f=0.12 mm/rev*).

The comparison of the chip velocity between dry and wet machining conditions during orthogonal cutting are presented in Figure 6.15. The data reveals that in the absence of cutting fluid there has been a gradual increase in the chip velocity with increasing cutting speed while the cutting depth and feed were kept constant (see Figure 6.16).
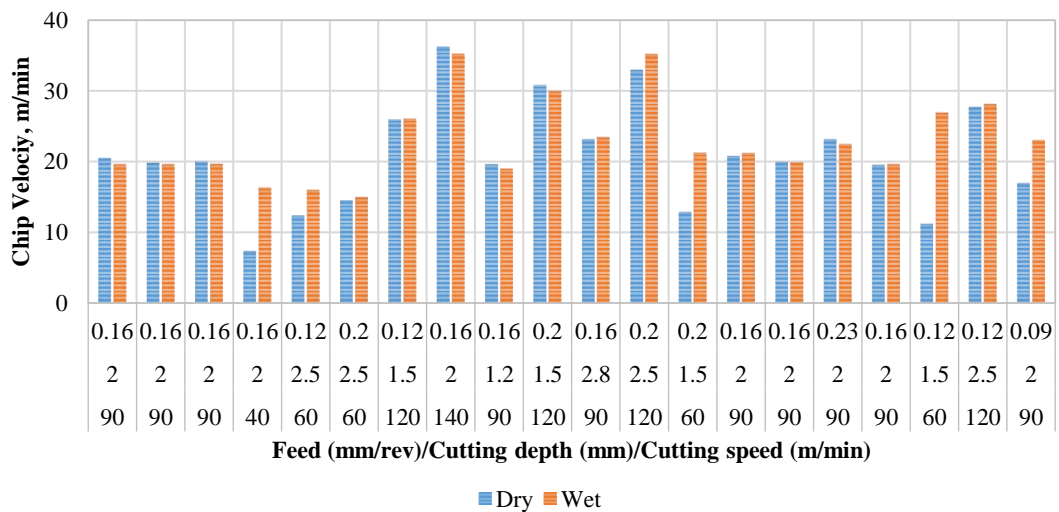
Figure 6.15 Comparison of the chip velocity for dry and wet cutting conditions

With using cutting fluid, the chip velocity shows a different trend. Here, the chip velocity initially decreases and then increases with the cutting speed. Where at low levels, *V<90 m/min*, the chip velocity found to decrease with increasing cutting speed; whereas at high levels, *V>90 m/min,* the results found that the influence of the machining parameters on the chip velocity is same as the dry conditions, which is increased with increasing cutting speed (see Figure 6.16).

102

Figure 6.16 Comparison of the chip velocity under dry and wet machining of *Al 6082-T6* at different cutting speeds with a constant cutting depth and feed (*t*=2.5 *mm*, *f*=0.12 *mm/rev*).

The ANOVA results of the chip morphology analysis including the chip thickness, shear angle and chip velocity are presented in Appendix A.

6.4.3 Tool-Chip Contact Length

6.4.3.1 Contact Length-Pilot Studies

The tool-chip contact length or simply contact length L_C was calculated theoretically, in this study, according to the model concluded by Kato et al. (1972) and Toropov & Ko (2003), as discussed in Chapter 2. The model predicts that the contact length is twice the deformed chip thickness ($L_C = 2 * chip\ thickness\ (h)$). This model has been used due to the difficulty of measuring the contact length practically, as stated in Chapter 5 (Section 5.2.5), because one cutting tool insert was used for conducting all the experiments in this study, therefore, to verify the possibility of using the aforementioned model (Kato et al. 1972 and Toropov & Ko 2003 model), two pilot studies were carried out in this work using fresh cutting tool inserts in each study. In these two pilot studies, the tool-chip contact length was measured experimentally using an SEM and compared to the aforementioned model (more detail are presented in Appendix A). The first pilot study was conducted to verify the model at low to high cutting speeds (45, 65, 95, 145, 215, and 305 *m/min*) with a constant cutting depth *t*=2.5 *mm* and feed *f*=0.16 m*m/rev* for both dry and wet cutting conditions. While the second pilot study was carried out at different cutting speed, cutting depth and feed. The machining parameters used in these two studies are presented in Appendix A (see

Table A.15 and Table A.16). The first pilot was carried out by using cutting tool (SCMW 12 04 08 from Sandvick) and without employing the experiments design while the other study was conducted using the same cutting tool as the main study and using the design of experiments (CCD). The both pilot studies were conducted on a Triumph 2500 lathe machine using orthogonal cutting of *6082-T6* aluminium tube as a workpiece.

The results of these two studies are presented in Appendix A. The same results were obtained from both pilot experiments, and this confirms the validity of Kato et al. (1972) and Toropov & Ko (2003) model. Therefore, this model was used in calculating the tool-chip contact length for the rest of experiments. Thus, from now on all the results presented here were obtained based on the use of this model. The tool-chip contact area was measured by multiplying the contact length by the chip width. More detail about measuring the contact area are presented in Appendix A (Section A.2.2.1.2).

6.4.3.2 Contact Length-Main Study

According to the design of experiments mentioned in Chapter 5, a set of orthogonal cutting experiments were conducted in order to investigate the influence of the machining parameters including feed, cutting speed and cutting depth on the tool-chip contact length and thus the tool-chip contact area during cutting *Al 6082* workpiece tube in dry and wet conditions. In this section, the experimental results of the contact length at dry and wet machining conditions are presented. As explained in Section 6.4.3.1, the contact length was measured using Kato et al. (1972) and Toropov & Ko (2003) model and the contact area was measured by multiplying the contact length by the chip width. Figure 6.17 shows a comparison of the contact length between dry and wet machining conditions during orthogonal cutting. For more details, the results obtained from the aforementioned model are also set out in Table A.17 in Appendix A.
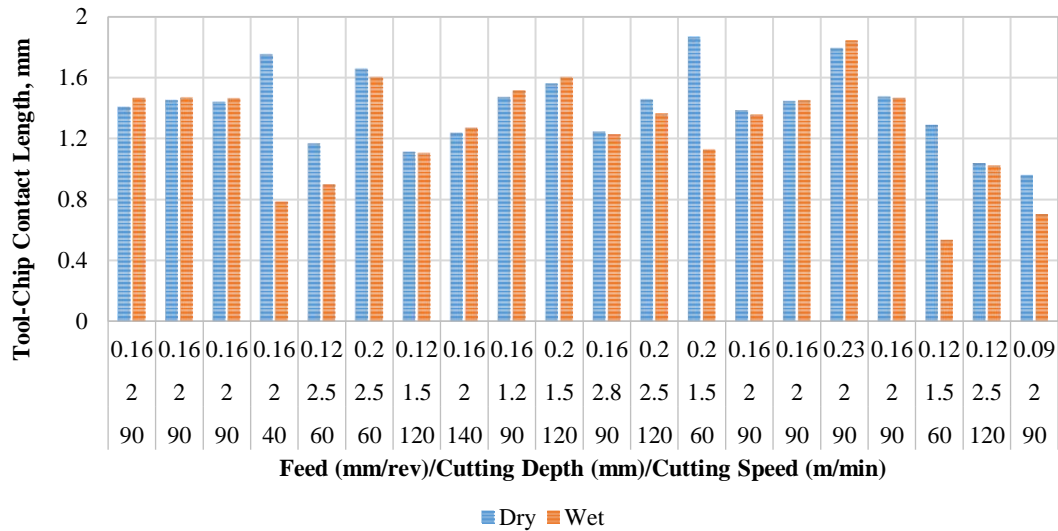
Figure 6.17 Comparison of the tool-chip contact length for dry and wet cutting conditions

In dry conditions, the results show that the contact length decreases with increasing cutting speed and cutting depth and increased with increasing feed (see Figure 6.17). Some results of Figure 6.17 have been re-presented in graphs to study the influence of the cutting speed, cutting depth and feed individually on the contact length and are presented below.

The influence of cutting speed on contact length in the dry and wet machining condition can be seen from the Figure 6.18, where the contact length was decreased at with increasing cutting speed in dry condition while the cutting depth and feed were kept constant at *t*=2 *mm*, *f*=0.16 *mm/rev*, respectively.

These relationships may be explained by the effect of temperature, as discussed in Section 6.3, with increasing cutting speed the temperature of the tool-chip interface increased and this leads to softening the workpiece and hence the friction at the tool-chip interface reduces. These result in increasing shear angle and thus reducing chip thickness and contact length (see Figure 6.9, Figure 6.10 and Figure 6.14). This result is in agreement with (Abukhshim et al. 2004; Ojolo & Awe 2011).
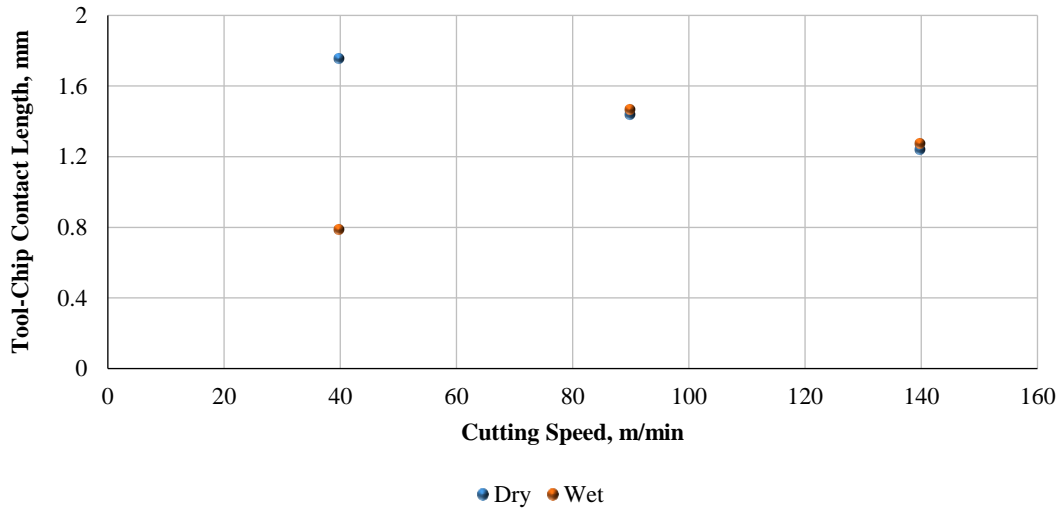
Figure 6.18 Comparison of the contact length under dry and wet machining of *Al 6082-T6* at different cutting speeds with a constant cutting depth and feed (*t=2 mm*, *f=0.16 mm/rev*).

At wet cutting conditions, the tool-chip contact length shows a different trend. Here, the contact length initially increases and then decreases with the cutting speed. Where at low levels, *V<90 m/min*, the contact length found to increase with increasing cutting speed; whereas at high levels, *V>90 m/min,* the results found that the influence of the machining parameters on the tool-chip contact length are same as the dry conditions, which is decreased with increasing cutting speed and cutting depth and increased with increasing feed. The results also found that, with applying the cutting fluid, the contact length was found smaller than in dry conditions and at low cutting speed (below 90 m/min). At cutting speeds higher than 90 m/min, there were no significant differences between the contact length in dry and wet cutting conditions (see Figure 6.17 and Figure 6.19). It seems possible that these results, as explained in Section 6.4.1, are due to the temperature effect.

Further experiments were carried out to investigate more about the influence of the cutting speed on the contact length, by examining different machining parameters. The results of these experiments are presented in Figure 6.19 where the same trend was observed at a constant cutting depth (*t=2.5 mm*) and feed (*f=0.12 mm/rev*) with different cutting speeds.
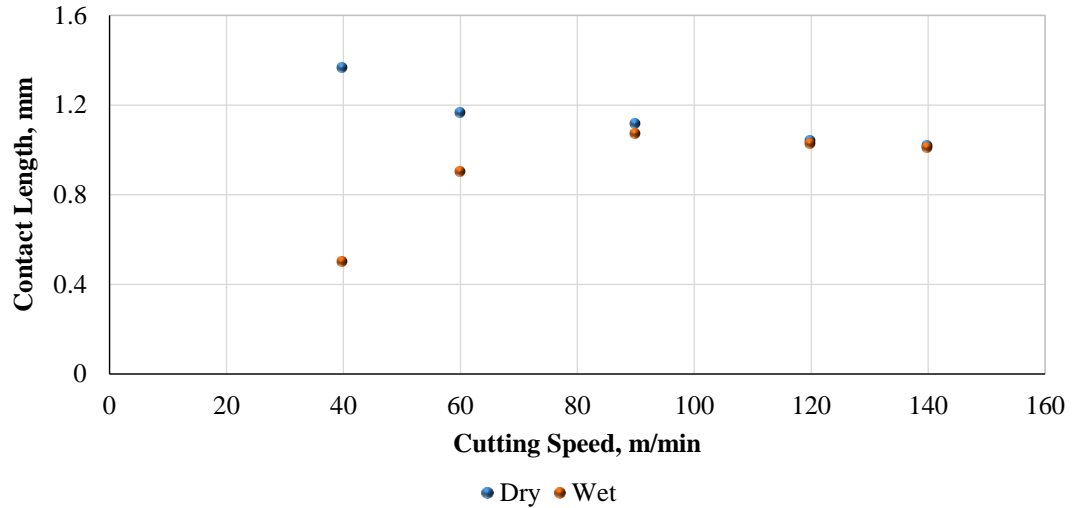
Figure 6.19 Comparison of the contact length under dry and wet machining of *Al 6082-T6* at different cutting speeds with a constant cutting depth and feed (*t=2.5 mm*, *f=0.12 mm/rev*).

Figure 6.20 shows that the feed has a more significant effect on the contact length than the other machining parameters. Where the data reveals that there has been a gradual increase in the contact length with increasing feed while the cutting depth and cutting speed were kept constant at *t=2 mm*, *V=90 m/min,* respectively. These results are in agreement with those obtained by (Ojolo & Awe 2011; Bermingham et al. 2011).
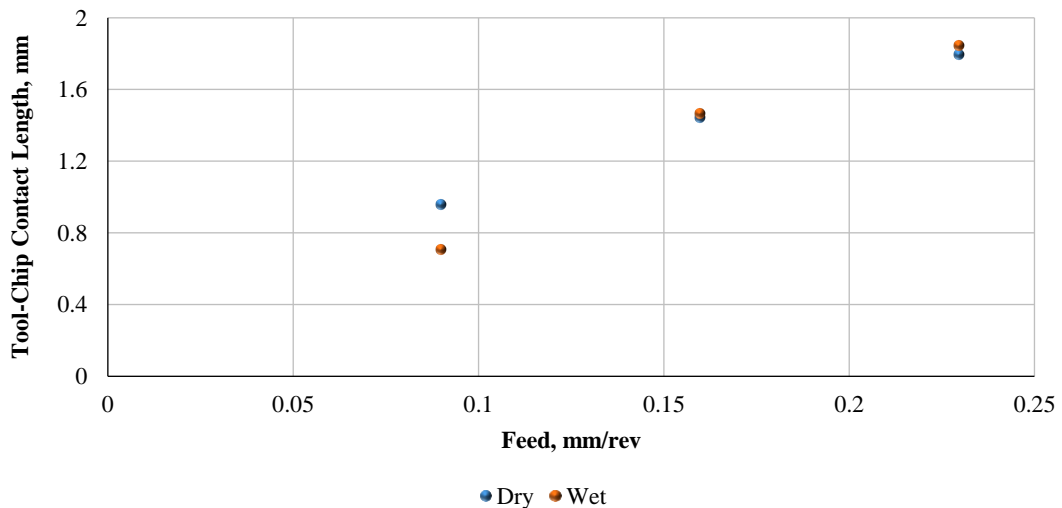
Figure 6.20 Comparison of the contact length under dry and wet machining of *Al 6082-T6* at different feed with a constant cutting speed and cutting depth (*V=90 m/min*, *t=2 mm*).

The effect of cutting depth on the contact length was very small where it is almost negligible (Figure 6.21). The figure shows that there has been a slight decrease in the contact length with increasing the cutting depth while the cutting speed and feed were

kept constant. These results are in agreement with those obtained by Bermingham et al.(2011).
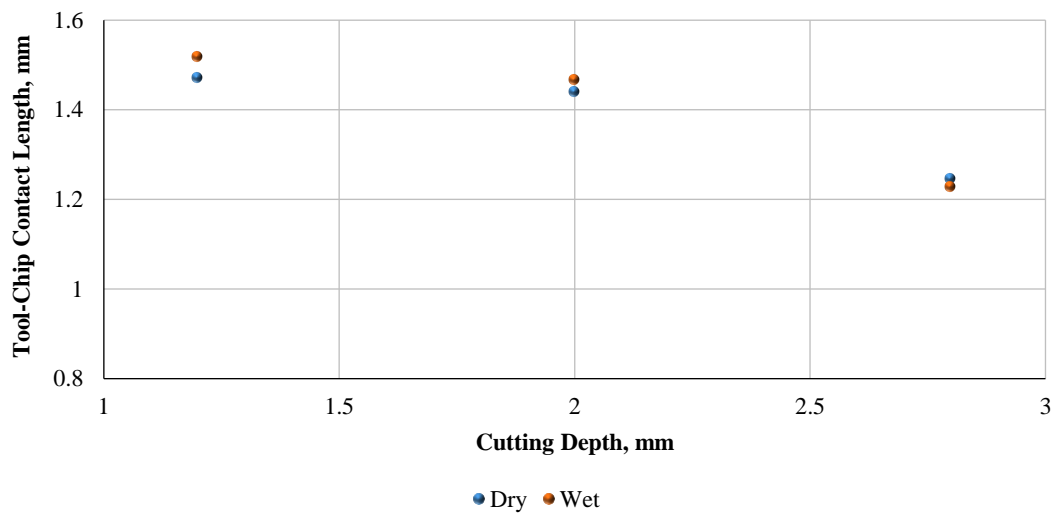
Figure 6.21 Comparison of the contact length under dry and wet machining of *Al 6082-T6* at different cutting depth with a constant cutting speed and feed (*V=90 m/min*, *f=0.16 mm/rev*).

As can be seen from the Figure 6.20 and Figure 6.21, that with applying cutting fluid the contact length trend does not change with changing cutting depth and feed, as it is with the cutting speed, from low to high levels where in all the levels the relationship between contact length and cutting depth and feed is proportional.

As mentioned in Chapter 5, the chip width was measured at six different locations along their length using a Vernier calliper, and the average were calculated. Multiplying the chip width by the contact length giving the tool-chip contact area. Figure 6.22 and Figure 6.23 show the contact area results, where Figure 6.22 show the comparison of the tool-chip contact area between dry and wet conditions at different cutting conditions. While Figure 6.23 show the comparison at different cutting speeds and the cutting depth and feed are constant.
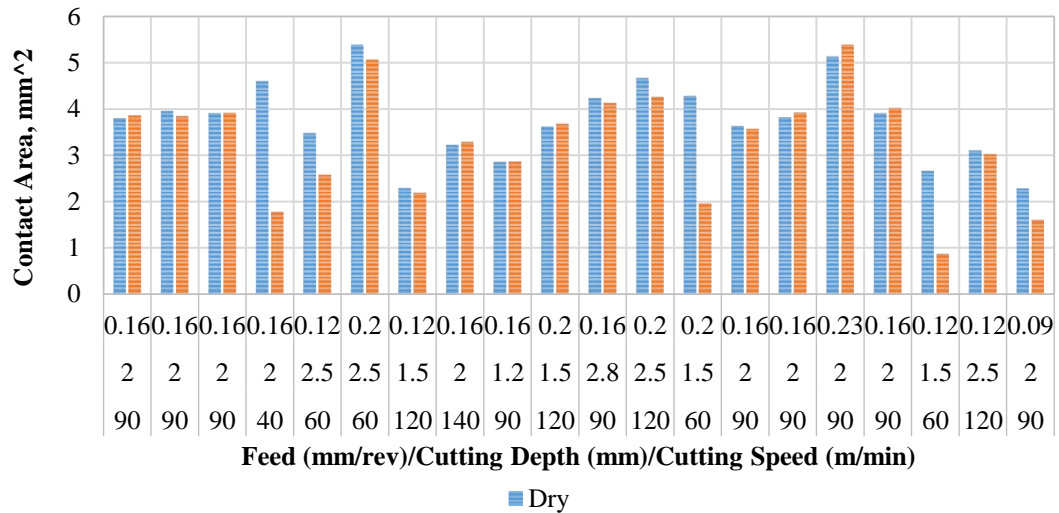
Figure 6.22 Comparison of the tool-chip contact area for dry and wet cutting conditions
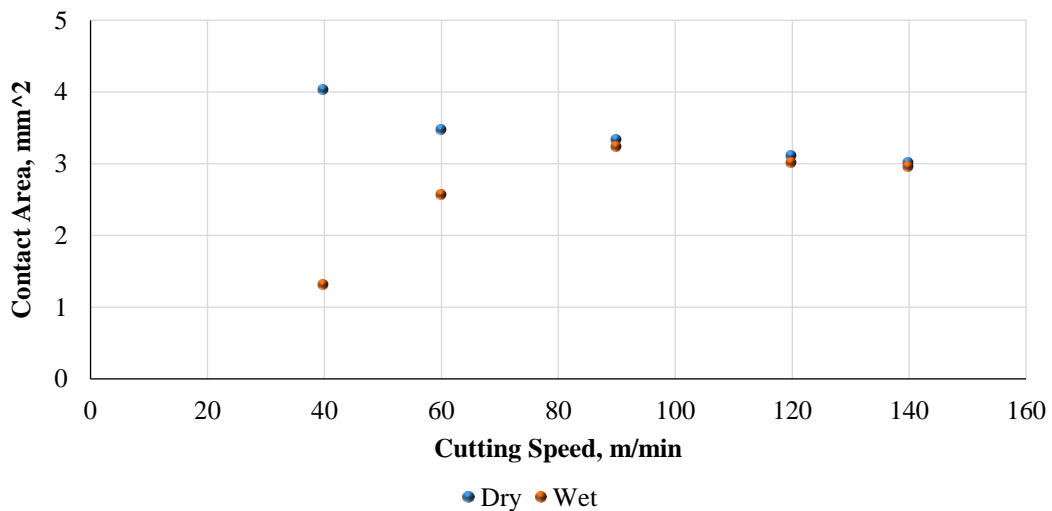
Figure 6.23 Comparison of the tool-chip contact area under dry and wet machining of *Al 6082-T6* at different cutting speeds with a constant cutting depth and feed (*t=2.5 mm*, *f=0.12 mm/rev*)

The analysis of variance (ANOVA) of the tool-chip contact length and contact area are given in Appendix A.

6.4.4   The Built-Up Edge (BUE)

After collecting the chips from each experiment, as mentioned in Chapter 5, they were analysed for the BUE existence as previously reported by (Seah & Li 1997). The existence of BUE is confirmed through the presence of streaks or lumps of adhering material on the underside of the chips. The observation of the BUE was made, using an SEM, from the underside of the chips gained when cutting *Al 6082* with different machining parameters, with and without cutting fluid.

109

Figure 6.24 presents some SEM images of the side of the chip which is in contact with the rake face of the cutting tool in dry and wet cutting conditions at different cutting speeds while the cutting depth and feed are constant, t=2.5 *mm* and f=0.12 *mm/rev*, respectively. It can be seen from Figure 6.24 that the BUE amount decreased with increasing in cutting speed. In dry cutting, at low cutting speeds, (*V*=40 *m/min*, 60 *m/min*), the BUE were observed while at cutting speed higher than 90 *m/min* no observed BUE was found on the chip. A possible explanation for this might be that as the cutting speed increased the chip flow rate increased as well which leads to a reduced likelihood of the breakaway material adhering to the chip (see Figure 6.16). Another possible explanation is that, as mentioned in Section 6.1, the temperature increased with increasing cutting speed. This increasing in temperature gives rise to BUE recrystallisation which would result in weakening of its structure and eventually breakdown. These results are in agreement with those obtained by (Takeyama & Ono 1968; Seah & Li 1997; Fang et al. 2010A; Jomaa et al. 2014; Gokkaya & Taskesen 2008; Carrilero et al. 2002; Yazman et al. 2013).
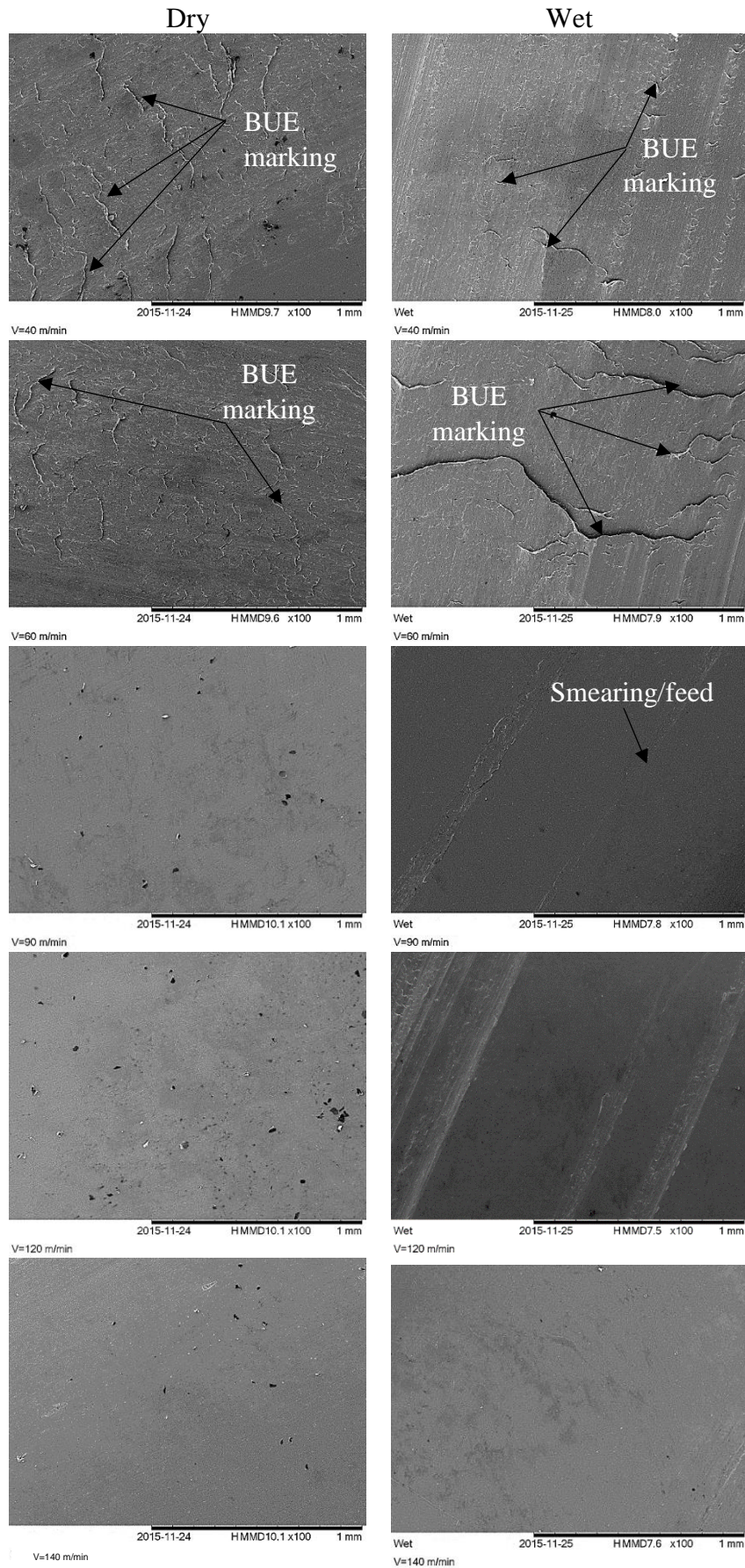
Figure 6.24 SEM photograph of chip underside during dry and wet cutting conditions of *Al 6082* at different cutting speeds and constant cutting depth and feed, *t*=2.5 *mm*, *f*= 0.12 *mm/rev*.

111

In wet conditions, it can be seen clearly from the Figure 6.24 that the BUE decreased with increasing cutting speeds, just as in dry conditions. The BUE material can still be observed on the chip at cutting speeds of 90 *m/min* and 120 *m/min*. while no BUE can be observed on the chip at cutting speed of 140 *m/min*. This shows that the stability of the BUE on the cutting edge is prolonged with the application of cutting fluid. This result may be explained by the fact that the temperature at the tool-chip interface decreased with cutting fluid which impedes the breakdown of the BUE structure.

Figure 6.25 shows the SEM images of the chip underside in dry and wet conditions at different cutting speeds and a constant feed of *f*=0.16 *mm/rev*. The results show that the BUE affected by the feed as well where the BUE on the chip seems to increase with increasing feed. For example, at a cutting speed of 90 *m/min* and feed of 0.12 *mm/rev*, no BUE was observed in dry condition (see Figure 6.24) while at the same cutting speed and with a higher feed (0.16 *mm/rev*) a small amount of BUE was observed. These results are in agreement with those obtained by (Gokkaya 2010; Fang et al. 2010B). In dry condition and at a cutting speed of 140 m/min and feed of 0.16 *mm/rev*, no BUE was observed. When cutting fluid is applied, and at higher feed (*f*=0.16 *mm/rev*), the BUE was observed even at high cutting speed (*V*=140 *m/min*).
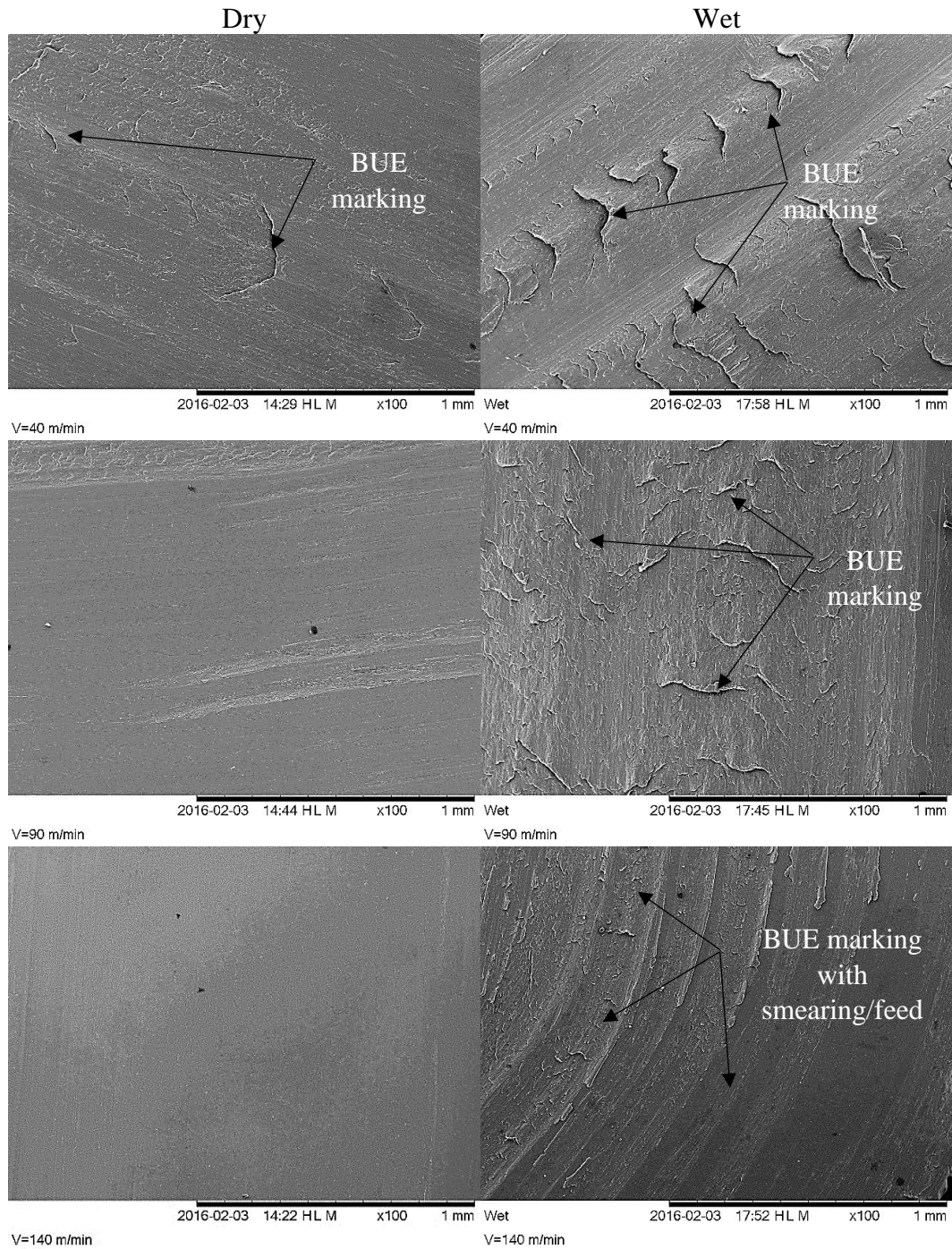
Figure 6.25 SEM photograph of chip underside during dry and wet cutting conditions of *Al 6082* at different cutting speeds and constant cutting depth and feed, *t*=2 *mm*, *f*= 0.16 *mm/rev*, respectively

6.5 Measurement of Cutting Forces

6.5.1 Typical Raw Force Measurements

Figure 6.26 shows a typical cutting force versus time curve which was recorded during orthogonal tube cutting of aluminium *Al 6082* at a cutting speed (*V=60 m/min*), cutting depth (*t= 2.5 mm*) and feed (*f=0.2 mm/rev*). As mentioned in Chapter 5, according to the position of the cutting edge with reference to the workpiece the cutting process can be clearly divided into three stages, initially the cutting edge is not engaged with the workpiece and the background noise in the data signal is due to machine tool vibration. As soon as the cutting edge engaged the workpiece, a sharp increase in the cutting forces occurs followed by a plateau where the cutting forces oscillate around an average value. This oscillation is most likely due to the brief periods of cutting force relaxation as the swarf breaks and chips are formed (Andreasen & Chiffre 1993; Ward 2010). Cutting force profile remains almost constant at which maximum cutting forces are observed. Once the cutting tool reaches the end of the workpiece, the cutting forces drop down sharply indicating the end of the cutting process.
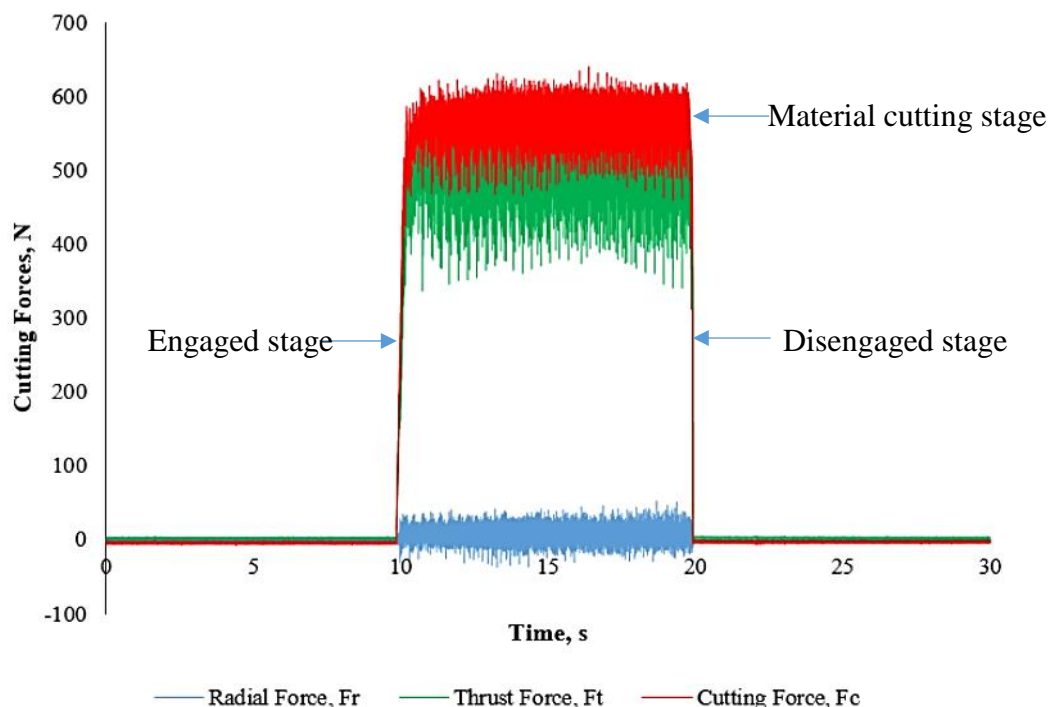
Figure 6.26 Cutting forces profile during *Al 6082* cutting at *V=60 m/min*, *t=2.5 mm*, *f=0.2 mm/rev*

The cutting process was conducted orthogonally. Therefore, the radial force *Fr* is very small and has been neglected. The cutting forces data can be adjusted to remove the effect of long-term thermal drift and offset using the DynoWare software. Figure 6.27 shows the profile of the rest cutting forces after removing the radial force and applying a smooth and drift compensation on the data. The average values of the cutting force components are reported in this study (see Figure 6.27).
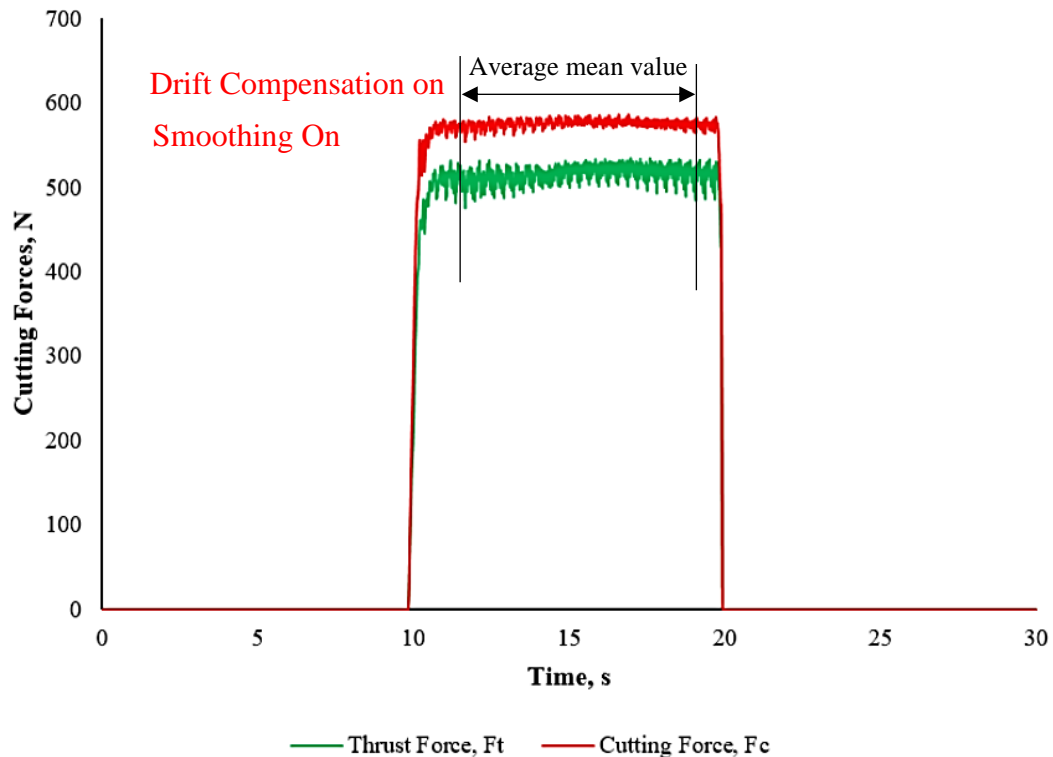
Figure 6.27 Cutting forces profile after data processing during *Al 6082* cutting at *V=60 m/min*, *t=2.5 mm*, *f=0.2 mm/rev*

6.5.2   Influence of Cutting Parameters on Cutting Forces

Figure 6.28 and Figure 6.29 compare the experimental data, that obtained from the orthogonal cutting experiments, on the thrust and cutting forces, respectively in dry and wet cutting conditions. The error bars represent the maximum and minimum values. The results are also given, in more detail, in Appendix A (Table A.26).

The results show that cutting forces in the absence of cutting fluid decreased with cutting speed and increased with cutting depth and feed. The lowest thrust and cutting forces were obtained when machining at high cutting speed (*V=120 m/min*), low feed (*f=0.12 mm/rev*) and low cutting depth (*t=1.5 mm*). While the highest were obtained at *V=60 m/min*, *f=0.2 mm/rev* and *t=2.5 mm* (see Figure 6.28 and Figure 6.29). With

applying cutting fluid, the lowest thrust *Ft* and cutting forces *Fc* (132.03, 196.73 *N* respectively) were obtained when machining at the cutting speed (*V=60 m/min*), low feed (*f=0.12 mm/rev*) and low cutting depth (*t=1.5 mm*). While the highest thrust *Ft* and cutting forces *Fc* (493.53, 579.13 *N* respectively) were obtained at *V=60 m/min*, *f=0.2 mm/rev* and *t=2.5 mm* which is the same as in the dry conditions.
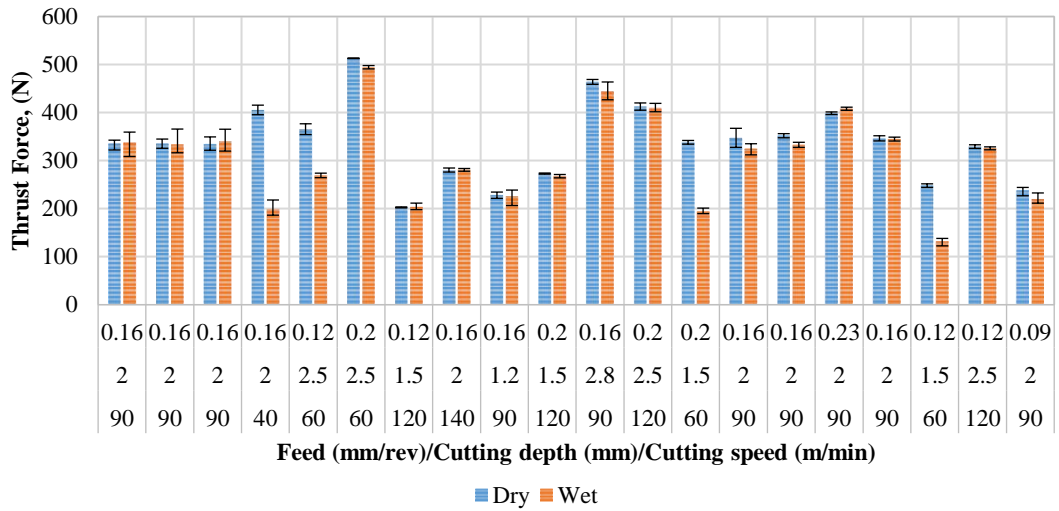
Figure 6.28 Comparison of the average maximum thrust force for dry and wet cutting conditions
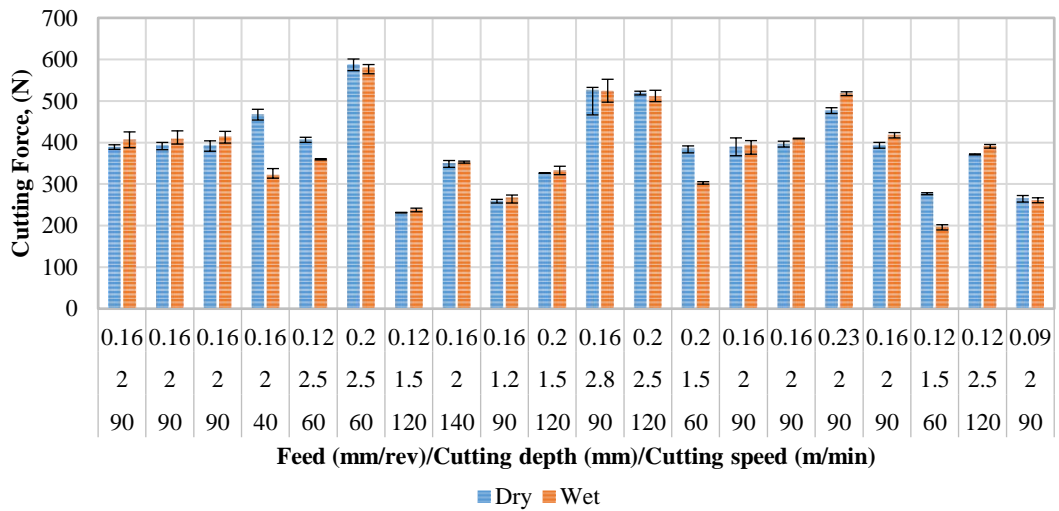
Figure 6.29 Comparison of the average maximum cutting force for dry and wet cutting conditions

Some data in Figure 6.28 and Figure 6.29 have been re-plotted in order to examine the influence of each machining parameters and are presented below. The influence of cutting speed on the thrust and cutting forces in the dry and wet cutting condition can be seen from the Figure 6.30 and Figure 6.31, respectively. Where the dry results show

that there has been a steady decrease in both components of cutting force with increasing cutting speed while the cutting depth and feed were kept constant at *t*=2 *mm*, *f*=0.16 *mm/rev*. It seems possible that these results are due to the softening of the workpiece material resulting from an increase in temperature at the tool-chip interface when the cutting speed increases (Gokkaya 2010; Sun et al. 2009; Gokkaya & Taskesen 2008). The low frictional forces on the rake face of the cutting tool at high cutting speeds is another reason for decreasing the cutting forces with increasing cutting speed (Gokkaya & Taskesen 2008). The results are supported by literature references in many articles (Fatima & Mativenga 2013; Pang 2012; Gokkaya & Taskesen 2008; Saglam et al. 2007; O'Sullivan & Cotterell 2001).
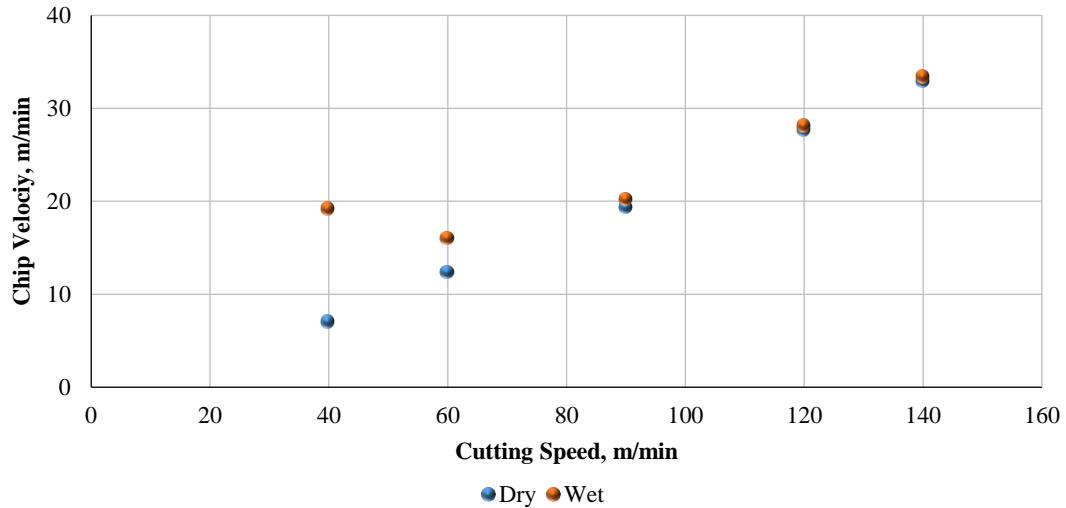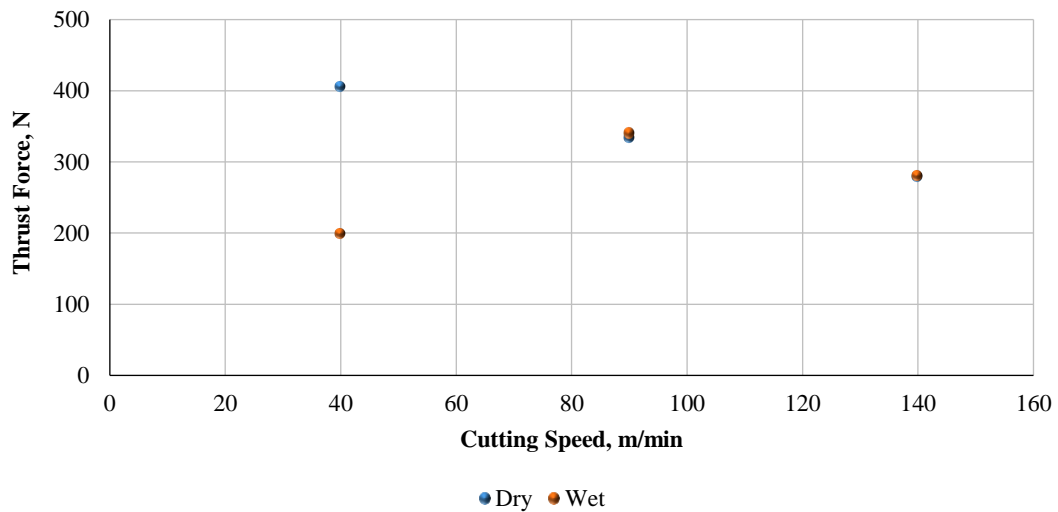

Figure 6.30 Comparison of the thrust force under dry and wet machining of *Al 6082-T6* at different cutting speeds with a constant cutting depth and feed (*t*=2 *mm*, *f*=0.16 *mm/rev*).
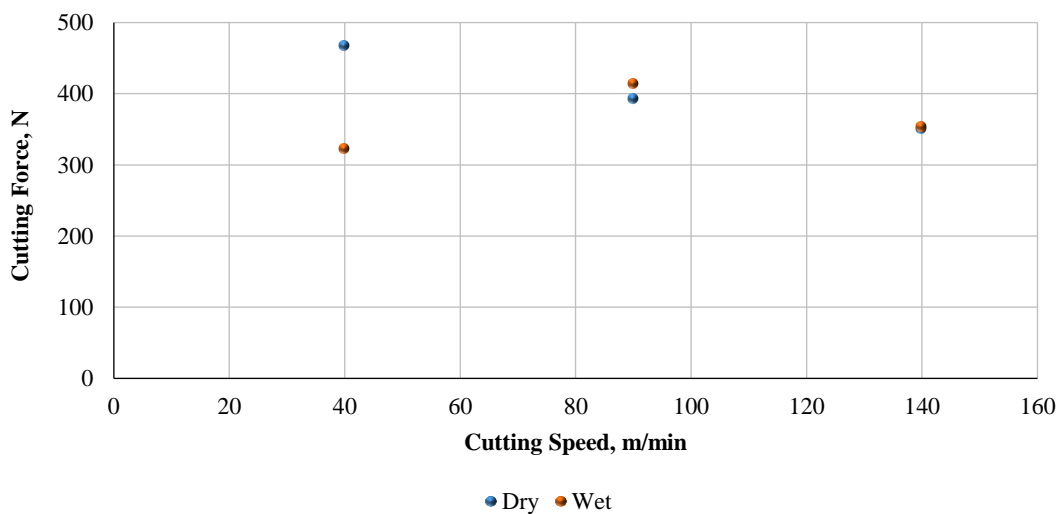
Figure 6.31 Comparison of the cutting force under dry and wet machining of *Al 6082-T6* at different cutting speeds with a constant cutting depth and feed (*t*=2 *mm*, *f*=0.16 *mm/rev*).

117

With applying the cutting fluid, the thrust *Ft* and cutting forces *Fc* show a different trend where they are smaller at low cutting speeds when coolant is applied than when dry. Here, the thrust and cutting forces initially increase and then decrease with cutting speed. Where at low cutting speed, *V<90 m/min*, the thrust and cutting forces were found to increase with increasing cutting speed; whereas at high levels, *V>90 m/min,* the results found that the influence of the machining parameters on the thrust and cutting forces are same as the dry conditions, which is decreased with increasing cutting speed. This is because at low cutting speeds, when the tool temperature is not too high, the coolant act as a lubricant and reduces the friction at the contact areas between the tool and workpiece (Seah & Li 1997). It can also be noticed from the results that the thrust force is more affected by the coolant than the cutting force. The results also show that the role of cutting fluid are considered negligible at high machining parameters (see Figure 6.30 and Figure 6.31). These results are in agreement with (Childs 2006).

Williams & Tabor (1977) stated that cutting fluid is drawn into the asperity contact between the cutting tool and chip through capillary action. The cutting fluid is acting as a lubricant at a low cutting speed where the cutting fluid has a longer time to penetrate more of the tool-chip interface and will thus be effective in reducing friction, therefore, it acting as a lubricant. While at higher cutting speeds, the cutting fluid has a less time to penetrate the asperities contact between the tool-chip; therefore, the cutting fluid will be less effective.

To investigate more about the influence of the cutting speed on the cutting forces, further experiments were carried out by examining a wider range of machining parameters. Five cutting speeds (*V*=40, 60, 90, 120 and 140 *m/min*), a constant cutting depth of *t*=2.5 *mm* and a constant feed of *f*=0.12 *mm/rev* were selected. Figure 6.32 and Figure 6.33 show the results of these experiments where it can be seen clearly that similar results to (Figure 6.30 and Figure 6.31) were obtained.
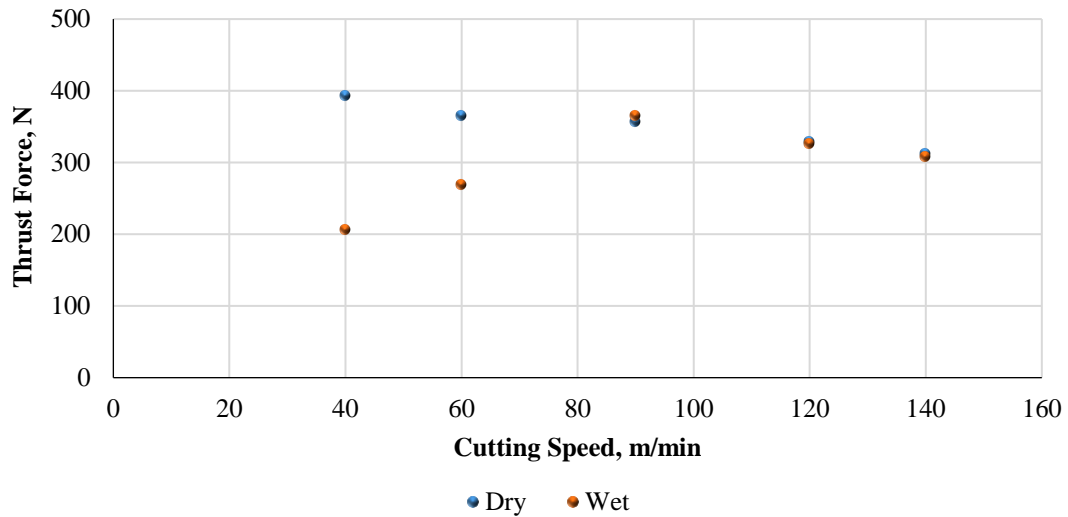
Figure 6.32 Comparison of thrust force under dry and wet machining of *Al 6082-T6* at different cutting speeds with a constant cutting depth and feed (*t=2.5 mm*, *f=0.12 mm/rev*).
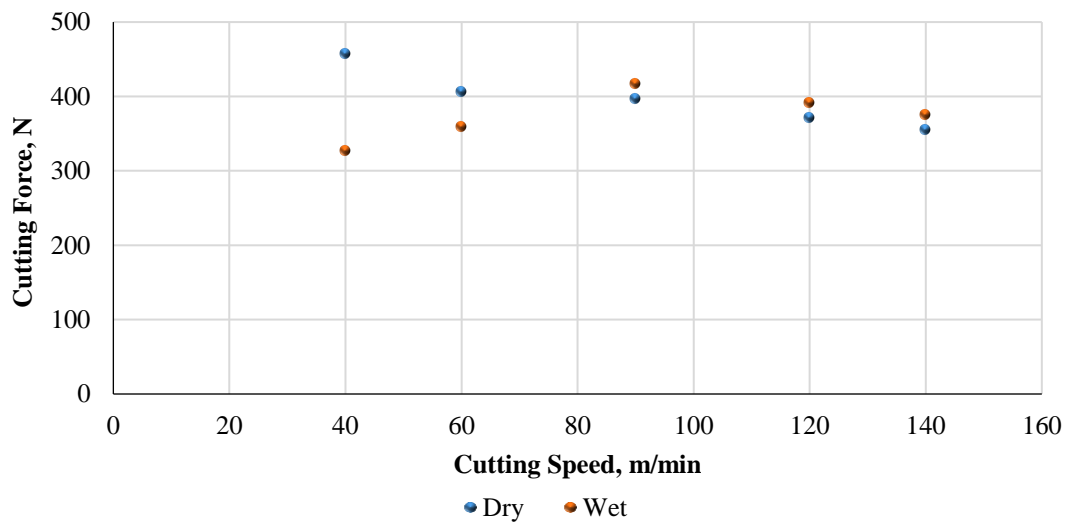
Figure 6.33 Comparison of cutting force under dry and wet machining of *Al 6082-T6* at different cutting speeds with a constant cutting depth and feed (*t=2.5 mm*, *f=0.12 mm/rev*).

Figure 6.34 and Figure 6.35 show the effect of cutting depth on the thrust *Ft* and cutting forces *Fc*. Where the data reveals that cutting aluminium *Al 6082* at different depth of cut (*t*= 1.2, 2 and 2.8 *mm*) with a constant cutting speed (*V*=90 *m/min*) and feed (*f*=0.16 *mm/rev*) results in a gradually increasing in thrust *Ft* and cutting forces *Fc* because of the large volume of workpiece material being removed. This agreed with the conclusion of (Huang et al. 1999; Sun et al. 2009).
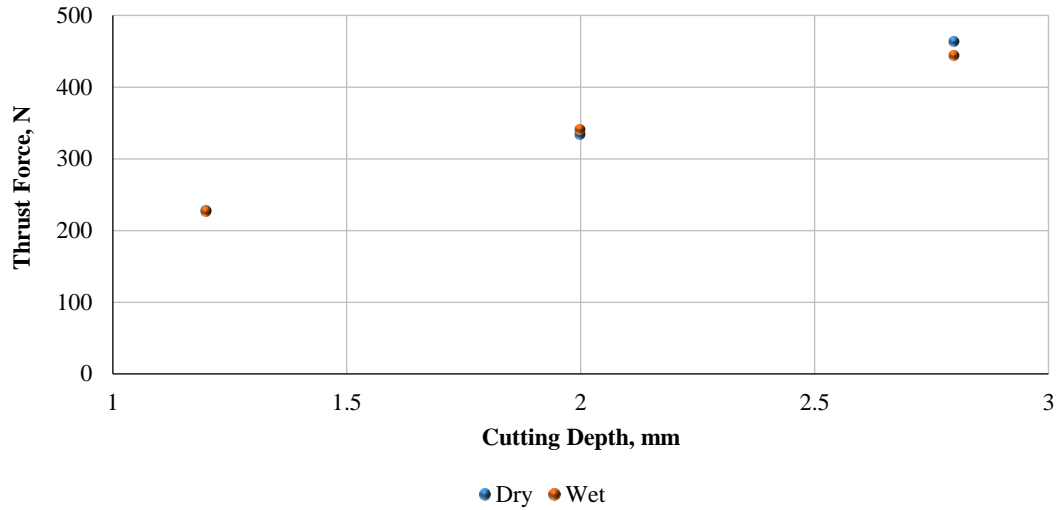
Figure 6.34 Comparison of the thrust force under dry and wet machining of *Al 6082-T6* at different cutting depth with a constant cutting speed and feed (*V*=90 *m/min*, *f*=0.16 *mm/rev*).
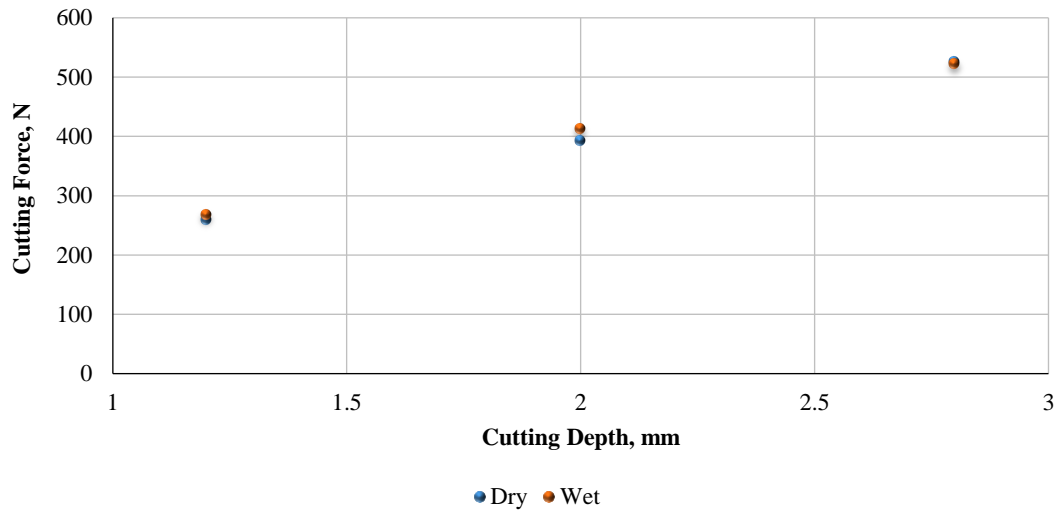
Figure 6.35 Comparison of the cutting force under dry and wet machining of *Al 6082-T6* at different cutting depth with a constant cutting speed and feed (*V*=90 *m/min*, *f*=0.16 *mm/rev*).

It can also be seen clearly from the Figure 6.36 and Figure 6.37 that the feed affects the cutting forces where the relation between them is a direct relationship since the cutting forces increased with increasing the feed. The results are supported by Asad et al. (2008) where increasing the feed rate leads to increasing in the cutting forces. Removing a large volume of the workpiece material at high cutting depth and feed are the reason for the increasing cutting forces with cutting depth and feed rate (Sun et al. 2009).
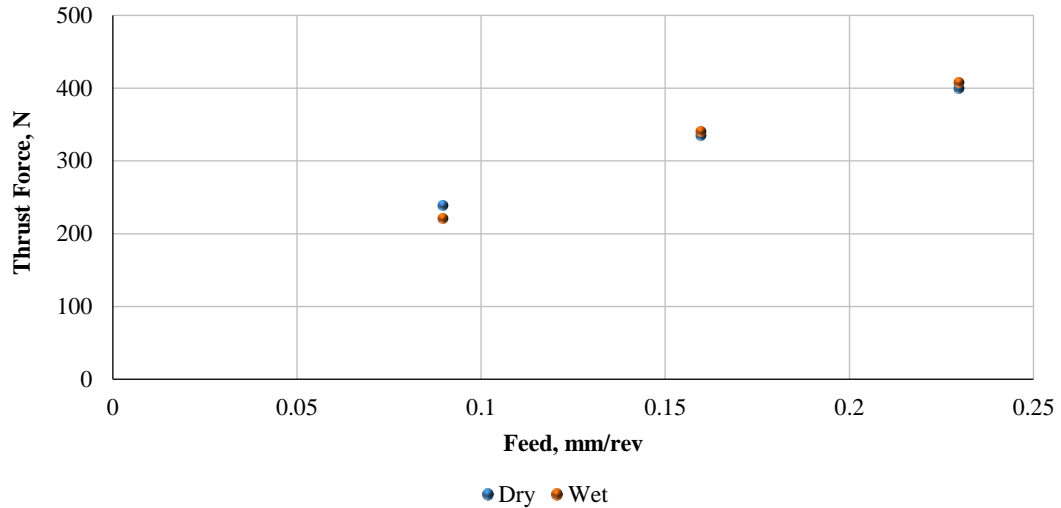
Figure 6.36 Comparison of the thrust force under dry and wet machining of *Al 6082-T6* at different feed with a constant cutting speed and cutting depth (*V=90 m/min, t=2 mm*).
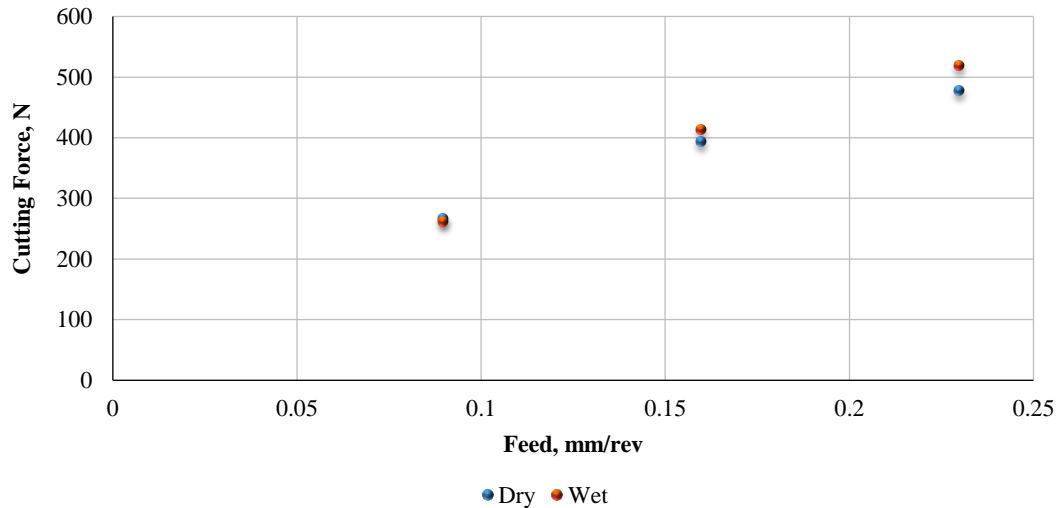
Figure 6.37 Comparison of the cutting force under dry and wet machining of *Al 6082-T6* at different feed with a constant cutting speed and cutting depth (*V=90 m/min, t=2 mm*).

It is worth noting that the relationship between the depth of cut and feed and the cutting forces are not affected by the cutting fluid where the both forces: thrust and cutting forces are increasing with increasing the cutting depth and feed with a constant cutting speed within the range of cutting depth (*t=1.2-2.8 mm*) and feed (*f=0.09-0.23 mm/rev*).

Figure 6.38 and Figure 6.39 show a contour plot of the thrust *Ft* and cutting forces *Fc* versus the cutting parameters in dry and wet cutting conditions. The contour plots were presented to examine the influence of cutting parameters as well as their interactions and thus to visually display the area of optimal factor settings.

Dry **Wet**
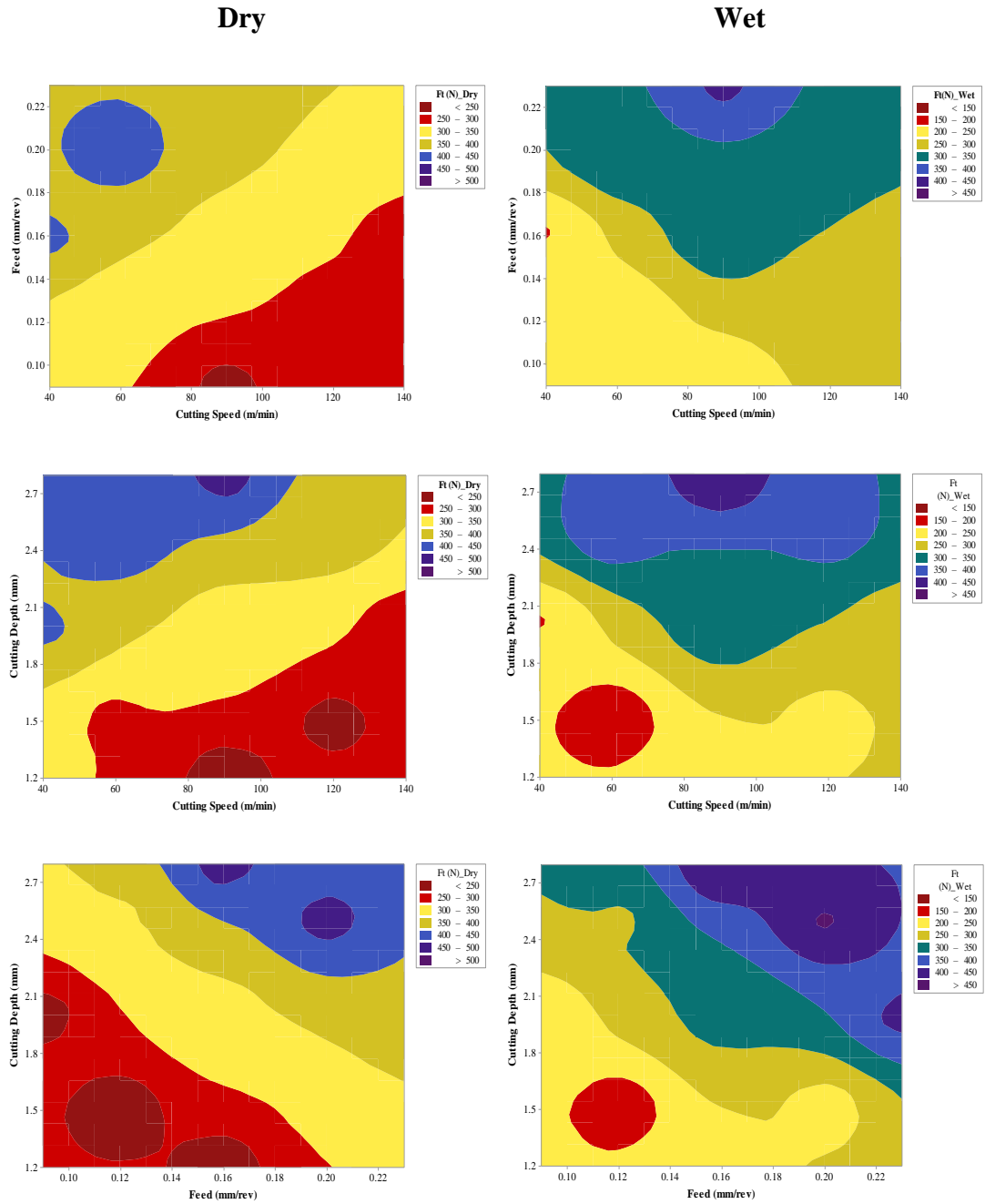
Figure 6.38 Contour plot of thrust force versus cutting parameters at dry and wet cutting conditions

Dry   **Wet**
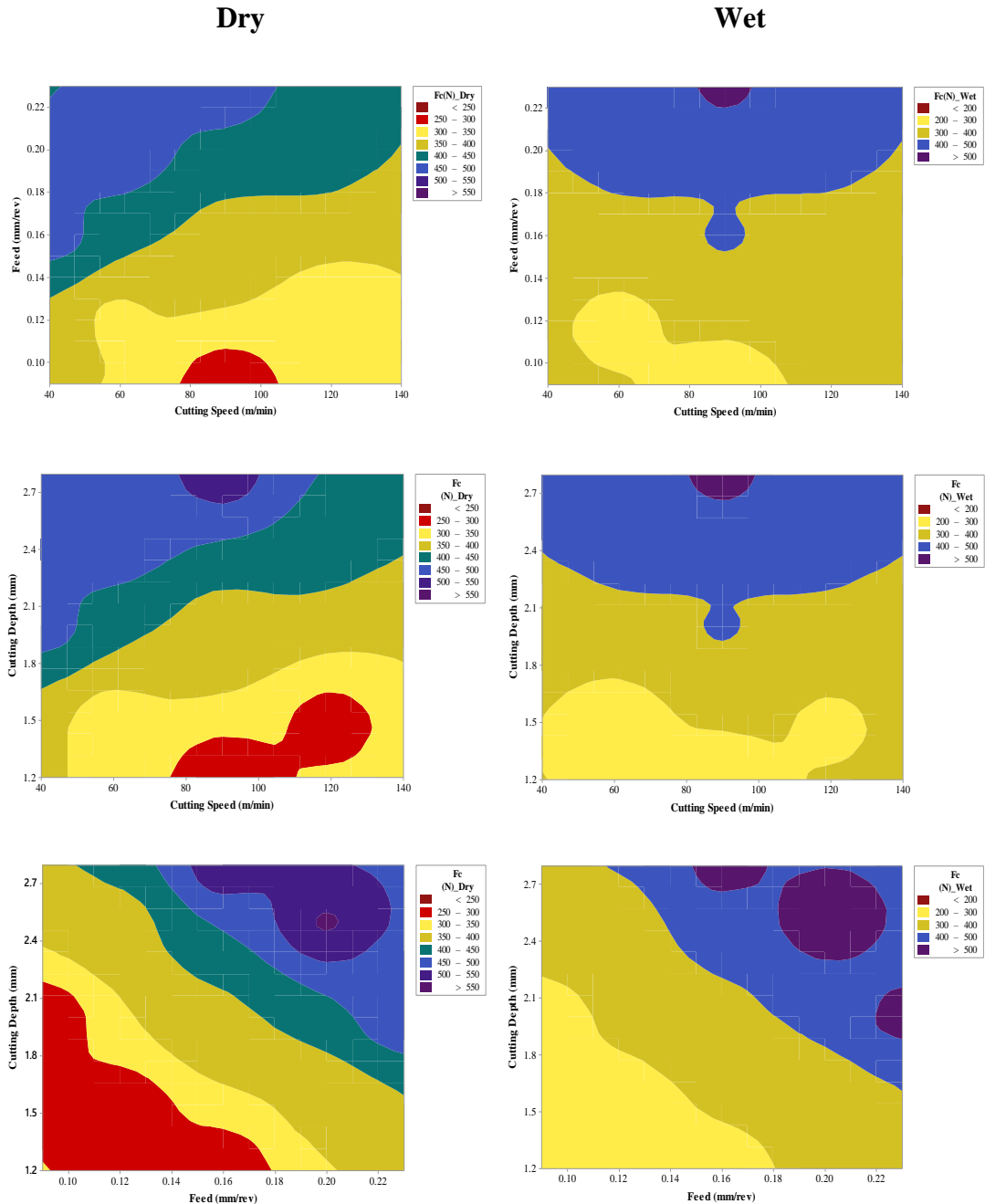
Figure 6.39 Contour plot of cutting forces versus cutting parameters at dry and wet cutting conditions

6.5.3   ANOVA of the Cutting Forces

This section presents the ANOVA results of the cutting forces. Furthermore, variations of the thrust and cutting forces with the machining parameters including cutting speed, depth of cut and feed are studied in dry and wet conditions separately. Only the significant parameters are presented in following sections while the complete ANOVA results are presented in Appendix A.

6.5.3.1   Thrust Forces *Ft*

The results of the ANOVA of thrust forces during dry and wet turning are presented in Table 6.1 and Table 6.2, respectively. These tables only show the significant effect of the machining parameters on the thrust forces (more detail are presented in Appendix A (Section A.3.1.1).

Table 6.1 presents only the significant effects (P-value<0.05) of the ANOVA outputs. It can be seen from Table 6.1 that cutting speed (*A*), cutting depth (*B*) and feed (*C*), the quadratic value of feed (*C*C*), and the interaction between cutting speed and feed (*A*C*) and the interaction between cutting depth and feed (*B*C*) all have the most significant effect on the thrust force F_t during dry turning. Table 6.1 also shows the value of the determination coefficient (R^2) 99.30%, which indicates the goodness of data fit for the model, and the values of adjusted determination coefficient (adj. R^2) and predicted determination coefficient (predR^2) are also shown in Table 6.1. The (adj.R^2) is 98.98%, which denotes a high significant of the model and the (predR^2), 97.8%, indicates the agreement with the (adj.R^2). This model can be employed to navigate the design space.

Table 6.1 ANOVA output of thrust force F_t in dry conditions (Significant)

Source	DF	Adj SS	Adj MS	F-Value	P-Value	Note
Model	6	116793	19465.5	309.31	0.000	Significant <0.05
Linear	3	114263	38087.5	605.21	0.000	
A	1	15497	15496.8	246.25	0.000	
B	1	66766	66766.3	1060.92	0.000	
C	1	31999	31999.4	508.47	0.000	
Square	1	1032	1031.6	16.39	0.001	
C*C	1	1032	1031.6	16.39	0.001	
2-Way Interaction	2	1499	749.4	11.91	0.001	
A*C	1	876	876.2	13.92	0.003	
B*C	1	623	622.6	9.89	0.008	
Error	13	818	62.9			
Lack-of-Fit	8	519	64.8	1.08	0.488	Not Significant >0.05
Pure Error	5	300	59.9			
Total	19	117611				
R-Squared	0.993					
R-Squared (adj)	0.9898					
R-Squared (pred)	0.9798					

DF: Degree of freedom Adj SS: Adjusted sum of square Adj MS: Adjusted mean square

The final equation in terms of significant factors for the thrust force model (F_t) in dry turning is given by Equation 6.1. It is worth to note that the regression equation is in

uncoded values (see Table 5.5). These models take only the influential factors into account:

$$F_{t_{Dry}} = -147.8 + 0.273A + 69.3B + 2790C - 5240C^2 - 8.72AC \\ + 441BC$$

6.1

where *A* is the cutting speed (*m/min*), *B* is the cutting depth (*mm*) and *C* is the feed (*mm/rev*).

Table 6.2 presents the significant effects of the machining parameters on the thrust forces during wet conditions. It can be seen from the table that the linear model of the machining parameters cutting depth (*B*) and feed (*C*) have a stronger effect on the thrust force F_t, while the cutting speed (*A*) has less effect on the output. The ANOVA results also show that the thrust force F_t is strongly affected by the quadratic model of cutting speed (*A*A*). Regarding to the interaction between the cutting parameters during wet turning, the results show that the thrust force is significantly influenced by (*A*B*) and (*B*C*) more than (*A*C*).

The determination coefficient (R^2), adjusted R^2 and predicted R^2 are also shown in Table 6.2 which are 96.22%, 94.02% and 77.78%, respectively.

Table 6.2 ANOVA output of thrust force F_t in wet conditions (Significant)

Source	DF	Adj SS	Adj MS	F-Value	P-Value	Note
Model	7	156825	22403.6	43.66	0.000	Significant <0.05
Linear	3	129262	43087.5	83.96	0.000	
A	1	4784	4783.9	9.32	0.010	
B	1	83133	83133.2	162.00	0.000	
C	1	41345	41345.4	80.57	0.000	
Square	1	17322	17322.5	33.76	0.000	
A*A	1	17322	17322.5	33.76	0.000	
2-Way Interaction	3	10240	3413.4	6.65	0.007	
A*B	1	3756	3756.3	7.32	0.019	
A*C	1	2368	2368.4	4.62	0.053	
B*C	1	4116	4115.5	8.02	0.015	
Error	12	6158	513.2			
Lack-of-Fit	7	5927	846.7	18.33	0.003	
Pure Error	5	231	46.2			
Total	19	162983				
R-Squared	0.9622					
R-Squared (adj)	0.9402					
R-Squared (pred)	0.7778					

DF: Degree of freedom Adj SS: Adjusted sum of square Adj MS: Adjusted mean square

The final equation in terms of significant factors for the thrust force model (F_t) in wet turning is given by Equation 6.2. These models take only the influential factors into account: Regression equation is in uncoded values (see Table 5.5)

$$F_{t_{Wet}} = -673 + 12.68A + 104.6B + 398C - 0.03818A^2 - 1.445AB$$
$$- 14.34AC + 1134BC$$

6.2

where *A* is the cutting speed (*m/min*), *B* is the cutting depth (*mm*) and *C* is the feed (*mm/rev*).

6.5.3.2   Cutting Forces *Fc*

The results of the ANOVA of cutting forces during dry and wet turning are presented in Table 6.3 and Table 6.4, respectively. These tables only show the significant effect of the machining parameters on the cutting forces F_C (more detail are presented in Appendix A (Section A.3.1.2). It can be seen from Table 6.3 that the linear model of the machining parameters cutting speed (*A*), cutting depth (*B*) and feed (*C*) have a stronger effect on the cutting force F_C. In addition, the quadratic values of cutting speed (*A*A*) and feed (*C*C*) are also significant but the effect of (*C*C*) is stronger than the cutting speed during dry turning. Regarding the interaction influence, it can be seen from the ANOVA outputs that the interaction between cutting speed and feed (*A*C*) and the interaction between cutting depth and feed (*B*C*) have a significant effect on the cutting force F_C. The determination coefficient (R^2) of the model is 99.72% which is indicating the high data fit (see Table 6.3), the values of adjusted determination coefficient (adj. R^2) and predicted determination coefficient (predR^2) are also shown in Table 6.3 (99.56% and 98.68%, respectively). It is noticed that the only influential variables take into account in this model.

Table 6.3 ANOVA output of cutting force F_C in dry conditions (Significant)

Source	DF	Adj SS	Adj MS	F-Value	P-Value	Note
Model	7	163971	23424.4	610.19	0.000	Significant <0.05
Linear	3	160274	53424.8	1391.68	0.000	
A	1	12005	12004.9	312.72	0.000	
B	1	90647	90647.3	2361.30	0.000	
C	1	57622	57622.0	1501.01	0.000	
Square	2	1488	744.0	19.38	0.000	
A*A	1	410	410.2	10.69	0.007	
C*C	1	953	952.8	24.82	0.000	
2-Way Interaction	2	2208	1104.2	28.76	0.000	
A*C	1	270	270.0	7.03	0.021	
B*C	1	1938	1938.3	50.49	0.000	
Error	12	461	38.4			
Lack-of-Fit	7	423	60.5	8.07	0.018	
Pure Error	5	37	7.5			
Total	19	164431				
R-Squared	0.9972					
R-Squared (adj)	0.9956					
R-Squared (pred)	0.9868					

DF: Degree of freedom Adj SS: Adjusted sum of square Adj MS: Adjusted mean square

The final equation in terms of significant factors for the cutting force model (F_C) in dry turning is given by Equation 6.3: Regression equation is in coded values (see Table 5.5).

$$F_{C\,Dry} = -7 - 1.275A + 38.4B + 21.21C + 0.00590A^2 - 5057C^2 \qquad 6.3$$
$$- 4.84AC + 778BC$$

where *A* is the cutting speed (*m/min*), *B* is the cutting depth (*mm*) and *C* is the feed (*mm/rev*).

The results of the ANOVA of cutting forces F_C during wet turning are presented in Table 6.4. It can be seen from the ANOVA that the linear model of the machining parameters cutting depth (*B*) and feed (*C*) have a stronger effect on the cutting force F_C. In addition, the quadratic value of cutting speed (*A*A*) are also significant. The two-way interaction shows that the interaction between (*B*C*) was the only significant affect on the cutting force F_C than the other interactions. The determination coefficient (R^2) of the model is 97.61%, the values of adjusted determination coefficient and predicted determination coefficient are also shown in Table 6.4 (96.22% and 88.02%, respectively).

Table 6.4 ANOVA output of thrust force F_C in wet conditions (Significant)

Source	DF	Adj SS	Adj MS	F-Value	P-Value	Note
Model	7	189771	27110	70.14	0.000	Significant <0.05
Linear	3	174971	58324	150.91	0.000	
A	1	534	534	1.38	0.263	
B	1	105303	105303	272.46	0.000	
C	1	69134	69134	178.88	0.000	
Square	1	9375	9375	24.26	0.000	
A*A	1	9375	9375	24.26	0.000	
2-Way Interaction	3	5425	1808	4.68	0.022	
A*B	1	1475	1475	3.82	0.074	
A*C	1	1558	1558	4.03	0.068	
B*C	1	2392	2392	6.19	0.029	
Error	12	4638	386			
Lack-of-Fit	7	4294	613	8.93	0.014	
Pure Error	5	344	69			
Total	19	194409				
R-Squared	0.9761					
R-Squared (adj)	0.9622					
R-Squared (pred)	0.8802					

DF: Degree of freedom Adj SS: Adjusted sum of square Adj MS: Adjusted mean square

Equation 6.4 presents the mathematical model of the most influential variables on the cutting force in wet machining, while the interaction between cutting speed and depth of cut and the interaction between the cutting speed and feed have to be presented in the modelling process since they were involved in two-way interactions that were significant. The regression equation is in coded values (see Table 5.5).

$$F_{C_{Wet}} = -538 + 8.93A + 118.8B + 1096C - 0.02808A^2 - 0.905AB \qquad 6.4$$
$$- 11.63AC + 865BC$$

where *A* is the cutting speed (*m/min*), *B* is the cutting depth (*mm*) and *C* is the feed (*mm/rev*).

6.5.3.3 Comparison between the Experimental and Model Results of the Cutting Forces

In this section, a comparison has been introduced between the experimental (actual) results, shown in Figure 6.28 and Figure 6.29, and the results obtained from the derived equations (6.1-6.4). The comparisons between these two values, actual and predicted values, for the two orthogonal cutting forces (F_t and F_C) at dry and wet

cutting conditions are shown in (Figure 6.40-Figure 6.43). Very good agreement between the predicted and actual cutting forces are shown.
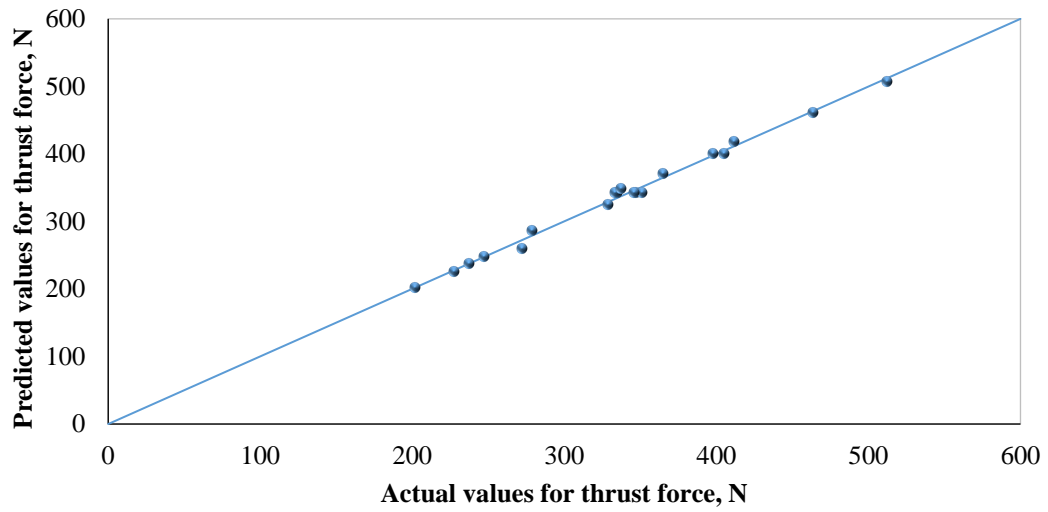
Figure 6.40 Experimental versus predicted values for thrust force F_t in dry condition, solid line indicates exact agreement
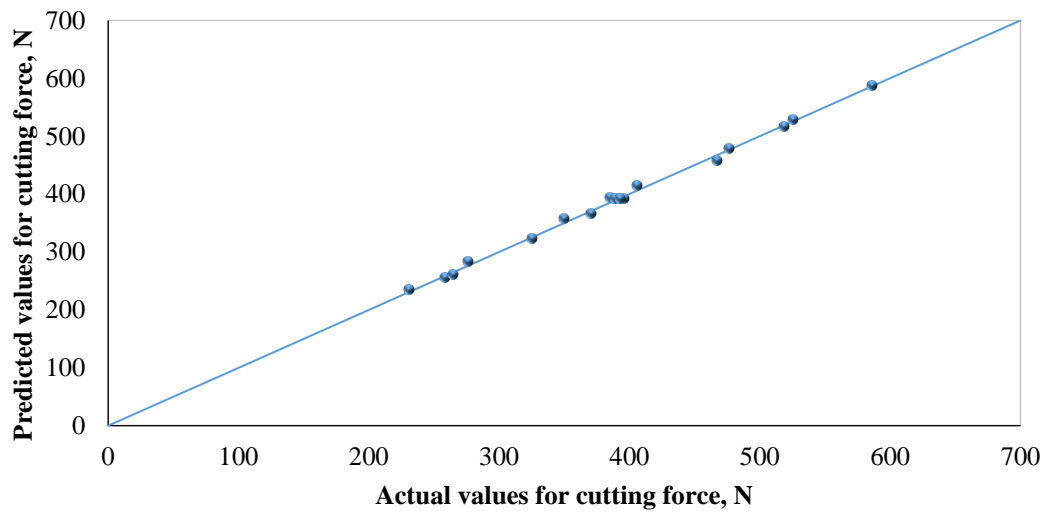
Figure 6.41 Experimental versus predicted values for cutting force F_C in dry condition, solid line indicates exact agreement
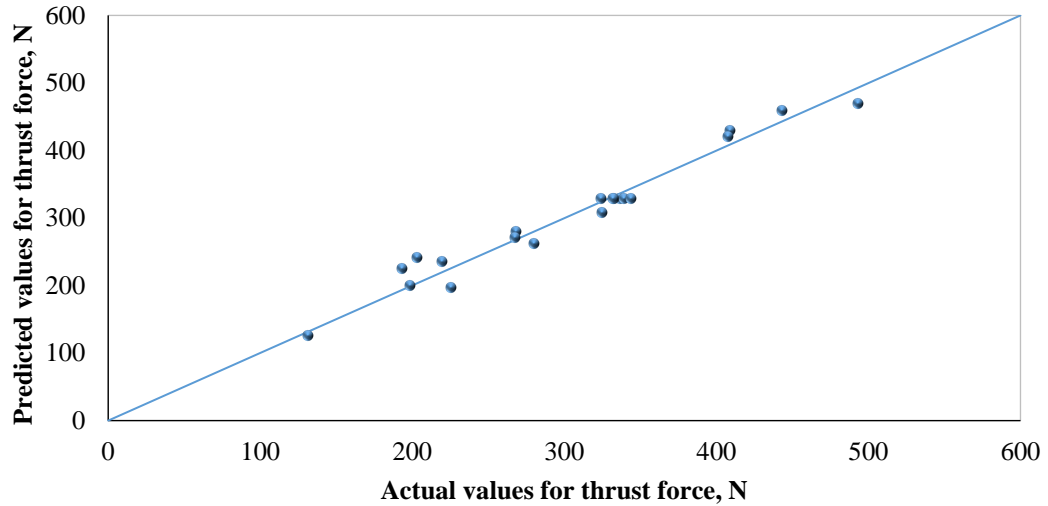
Figure 6.42 Experimental versus predicted values for thrust force F_t in wet condition, solid line indicates exact agreement
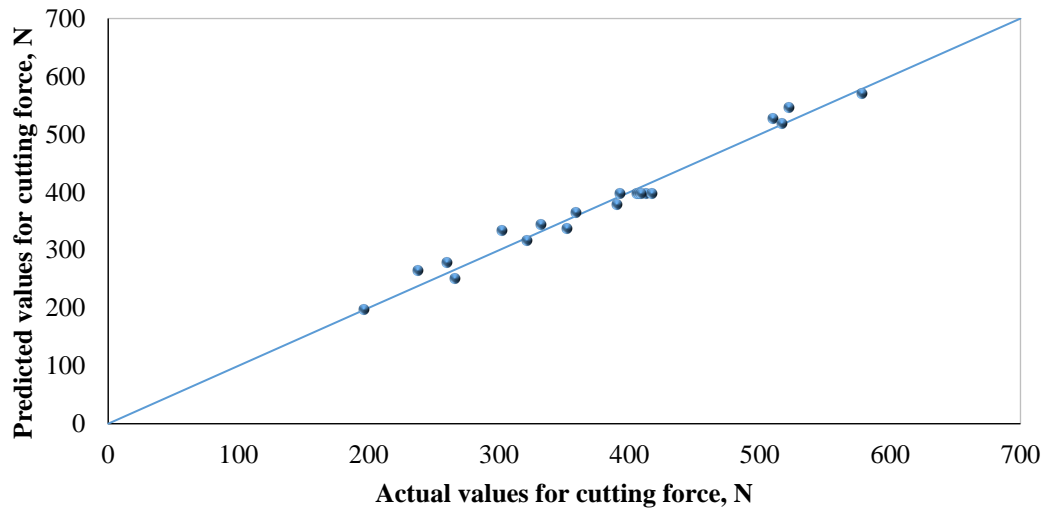
Figure 6.43 Experimental versus predicted values for cutting force F_C in wet condition, solid line indicates exact agreement

A comparison of the experimental results of machining force components, during dry and wet machining of *Al 6082-T6* at different cutting speeds with a constant cutting depth and feed (*t=2.5 mm, f=0.12 mm/rev*), respectively, and the analytically predicted values using Equations (6.1-6.4) are shown by scatter plots with smooth lines in (Figure 6.44-Figure 6.47). It can be seen clearly from the figures that the predicted machining force magnitudes agree well with the corresponding experimental results.
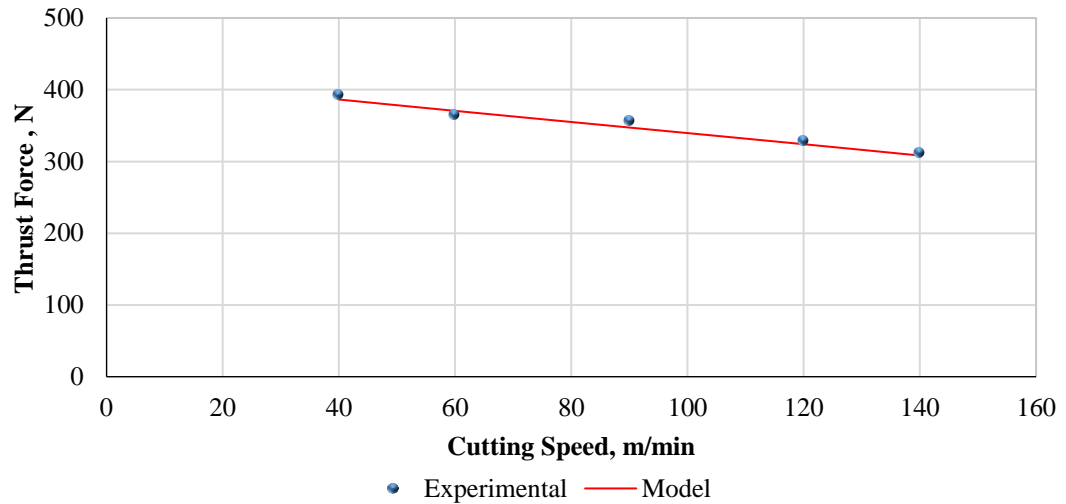
Figure 6.44 Comparison of experimental and predicted thrust forces during dry machining of *Al 6082-T6* **at different cutting speeds with a constant cutting depth and feed (***t=2.5 mm***,** *f=0.12 mm/rev***)**
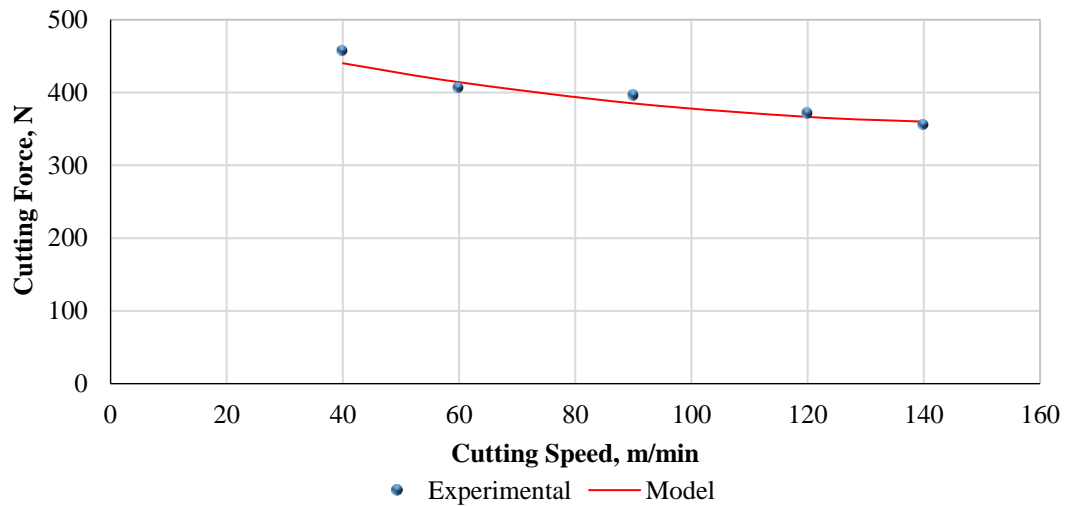
Figure 6.45 Comparison of experimental and predicted cutting forces during dry machining of *Al 6082-T6* **at different cutting speeds with a constant cutting depth and feed (***t=2.5 mm***,** *f=0.12 mm/rev***)**
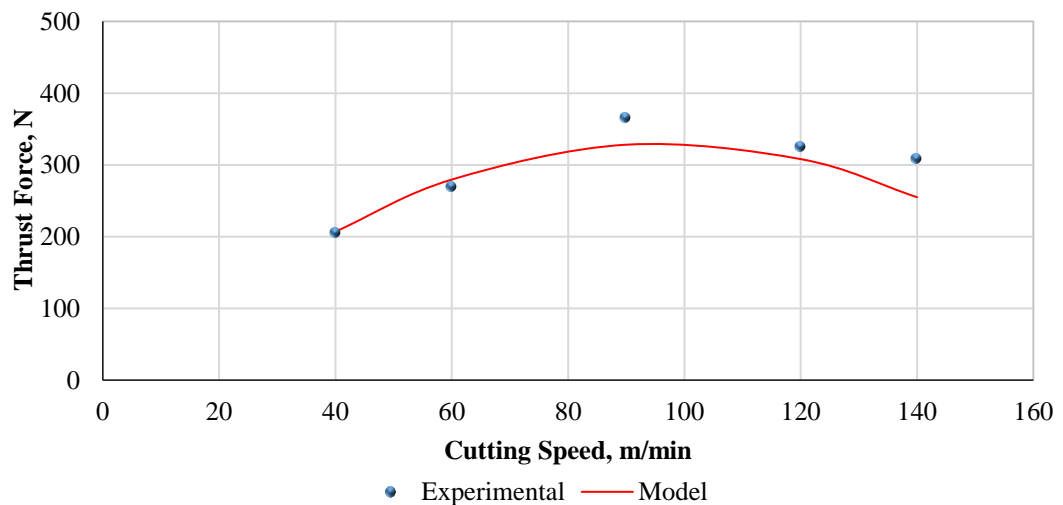
Figure 6.46 Comparison of experimental and predicted thrust forces during wet machining of *Al 6082-T6* **at different cutting speeds with a constant cutting depth and feed (***t=2.5 mm***,** *f=0.12 mm/rev***)**

131
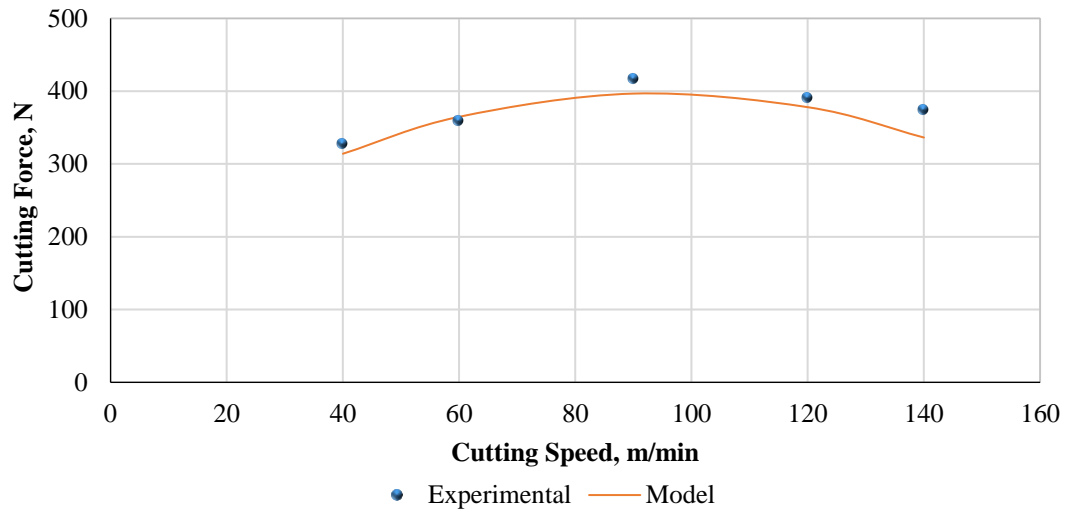
Figure 6.47 Comparison of experimental and predicted cutting forces during wet machining of
Al 6082-T6 **at different cutting speeds with a constant cutting depth and feed (***t=2.5 mm***,** *f=0.12*
mm/rev)

6.5.3.4   Model Validation Experiments

Further to the experiments runs mentioned in Table 5.5, another set of orthogonal
experiments, validation trials, have been carried out to validate and confirm the
mathematical models, (Equations 6.1-6.4). The machining parameters for the
validation experiments were chosen by default within the range of the cutting
parameters mentioned in the experimental design matrix (see Table 5.5). The
experiments were conducted during machining of *Al 6082* at dry and wet conditions
using the same cutting tool and the same CNC machine, described in Chapter 5. The
machining parameters for the validation trials are shown in Table 6.5. The results of
these experiments are graphically depicted in Figure 6.48 and Figure 6.49. The results
are also given in Appendix A (Table A.31).

Table 6.5 Machining parameters of the validation trials

Trials No.	Cutting parameters		
	Cutting Speed (m/min)	**Cutting depth (mm)**	**Feed (mm/rev)**
1	40	2.8	0.16
2	40	2.5	0.12
3	90	1.2	0.09
4	140	2.8	0.09
5	140	1.2	0.12
6	90	2.5	0.12
7	140	2.5	0.12

Figure 6.48 and Figure 6.49 show the comparison of the validation experiments results of the thrust and cutting forces, respectively, during dry and wet machining. This results confirm the significant effect of coolant, on the machining force components, at low machining parameters. The results also showed that the cutting force F_C is affected by the coolant at low machining parameters, but by less than it is in the thrust force.
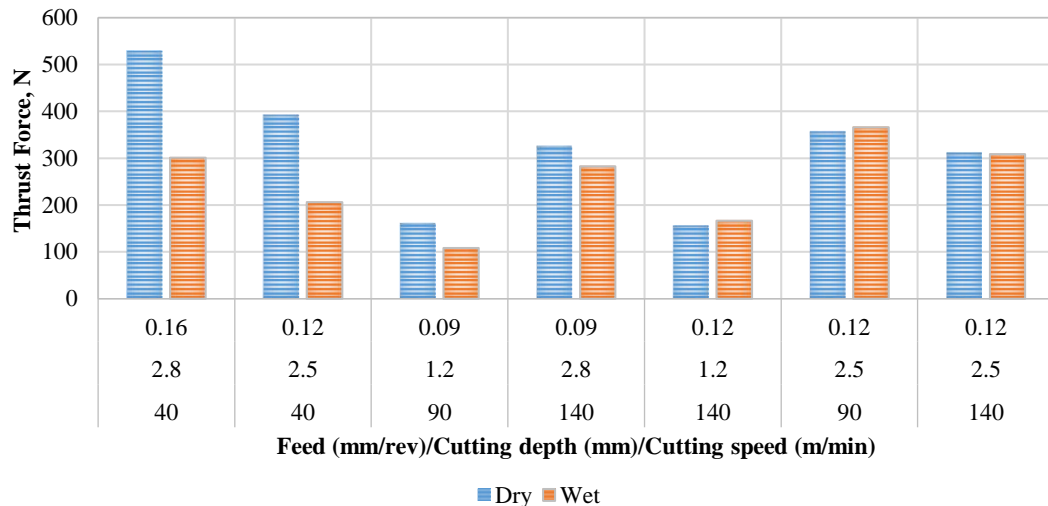
Figure 6.48 Comparison of the validation experiments results of thrust force for dry and wet conditions
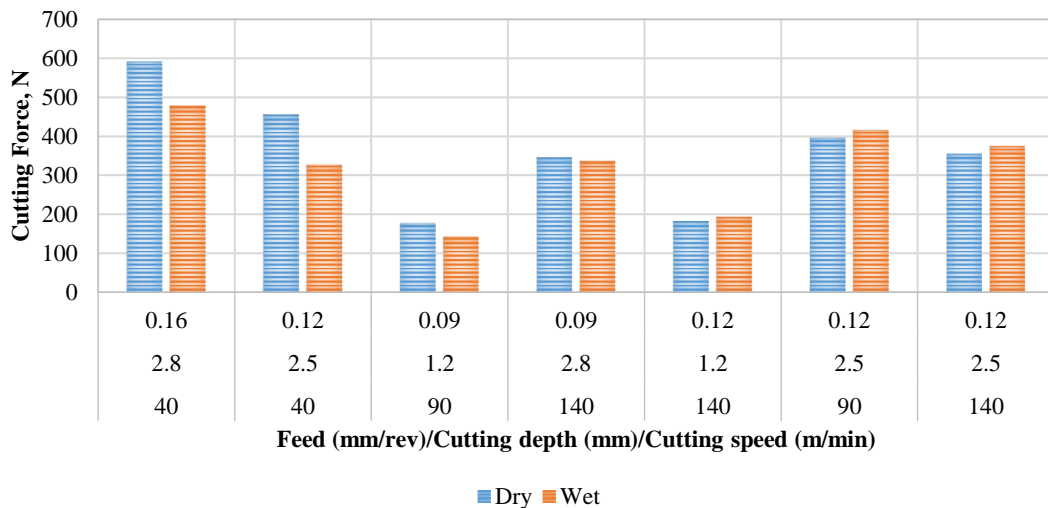
Figure 6.49 Comparison of the validation experiments results of cutting force for dry and wet conditions

The validation experiment results of the machining force components were compared with the corresponding predicted results, obtained from the empirical Equations (6.1-6.4), in order to validate and confirm the mathematical models. The comparative results are shown in (Figure 6.50-Figure 6.53). The comparisons between the

validation experiments and the corresponding analytical predicted results of the thrust force and cutting force, at dry conditions, are shown in Figure 6.50 and Figure 6.51, respectively. It can be seen from the results that analytical predicted cutting forces values agreed well with the corresponding experimental results and within an error percentage of 1.3-11.29%. While Figure 6.52 and Figure 6.53 show the comparison results at wet conditions. It can be seen from the results that the experimental results agreed well with their calculated results.
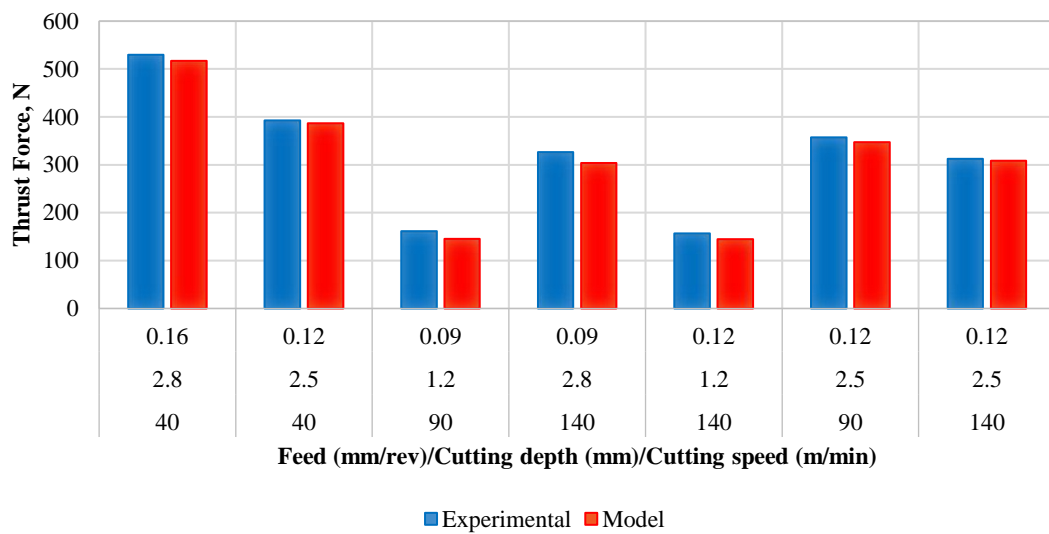
Figure 6.50 Comparison of the validation experiments and predicted results of thrust force for dry conditions.
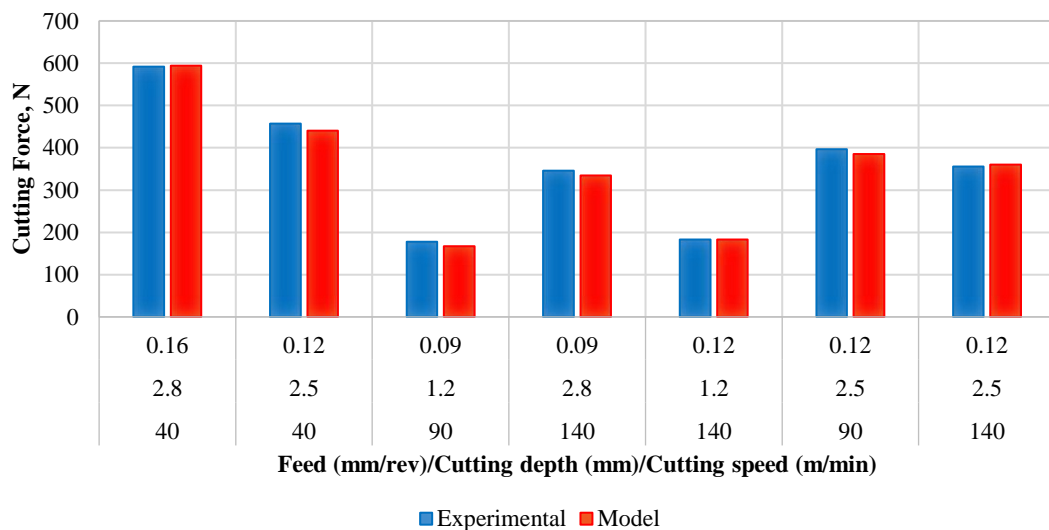
Figure 6.51 Comparison of the validation experiments and predicted results of cutting force for dry conditions.

134
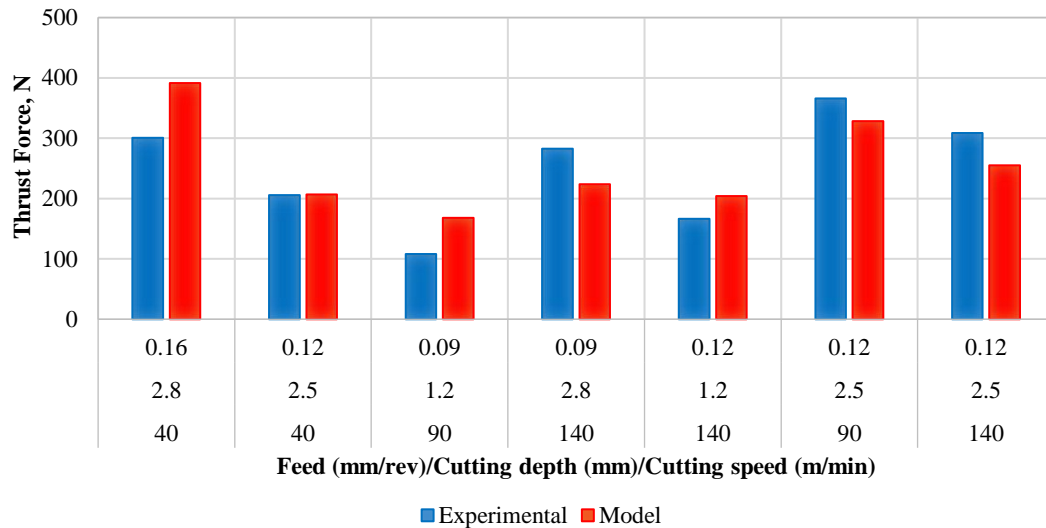
Figure 6.52 Comparison of the validation experiments and predicted results of thrust force for wet conditions.
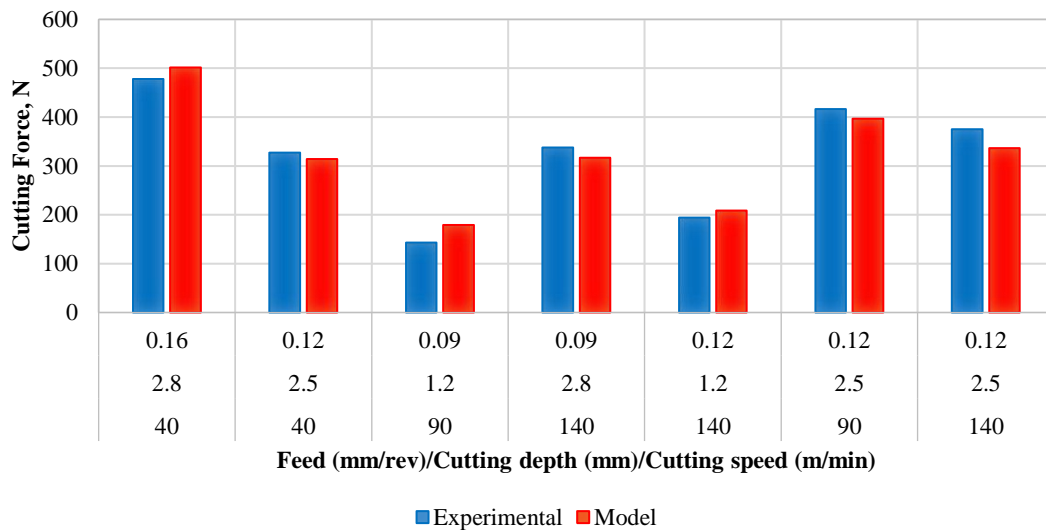
Figure 6.53 Comparison of the validation experiments and predicted results of cutting force for wet conditions.

6.6 Conclusions

An experimental investigation of turning of aluminium *Al 6082-T6* have been carried out, to evaluate the effect of the cutting speed, cutting depth and feed on the chip thickness, tool-chip contact length, BUE and the two orthogonal components of the cutting forces: thrust *Ft* and cutting forces *Fc*. The following conclusions can be drawn:

- In the absence of cutting fluid, chip thickness and tool-chip contact length were found to decrease with increasing cutting speed and cutting depth and to

135

increase with increasing feed. While with cutting fluid, the chip thickness and contact length increase with increasing cutting speed within the range less than 90 *m/min*, beyond this range the cutting fluid has a negligible effect on chip thickness and contact length.

- The reason for decreasing chip thickness with increasing cutting speed is because of the temperature effect. Where the tool-chip interface temperature increases with increasing cutting speed and thus lead to softening the workpiece and hence a reduction in the tool-chip interface friction. Both these two factors increase the shear angle and thus decrease the chip thickness.

- The influence of feed was more dominant than that of cutting speed on chip thickness whereas cutting depth has the lowest effect.

- The tool-chip contact length model of Kato et al. (1972) and Toropov & Ko (2003) ($L_c = 2h$), has been confirmed and used in this study.

- The present work confirms previous findings and contributes additional evidence that suggests the capability of confirming the existence of the BUE on the underside of the chips.

- The experimental findings in this study show that the BUE vanishes with increasing the cutting speed. This result may be explained by the fact that increasing cutting speed results in increasing temperature. This increasing in temperature leads to the recrystallisation of the BUE which would result in weakening of its structure and eventually the breakdown of the BUE, therefore, there is less BUE noticed on the chip.

- BUE occurs both with and without cutting fluid during machining of aluminium (*Al 6082*). However, the application of cutting fluid increases the threshold at which BUE occurs.

- Due to increasing temperature with increasing cutting speed, the thrust force (F_t) and cutting force (F_c) are seen to decrease with increasing cutting speed at a constant cutting depth and feed at dry cutting. Where increasing temperature leads to softening of the workpiece.

- The thrust force (F_t) and cutting force (F_c) are found to increase with increasing cutting depth and feed because of removing a large volume of the workpiece at high cutting depth and feed.

- The influence of feed on the thrust force (F_t) and cutting force (F_c) was found to be higher at low feed since the thrust and cutting forces increased roughly about 41% from increasing feed 0.09 *mm/rev* to 0.16 *mm/rev* while the increasing is half of this value from 0.16 *mm/rev* to 0.23 *mm/rev* and it is about 19%.

- At a cutting speed <90 m/min, F_t and F_c are smaller when coolant is applied than when dry condition is performed. This is because at low cutting speeds, when the tool temperature is not too high, the coolant acts as a lubricant and reduces the friction at the contact areas between the tool and workpiece.

- The research has also shown that the thrust/feed force is more affected by the cutting fluid than the cutting force.

- The chip thickness is much smaller in wet conditions, in the same cases where a force difference was seen.

7

Ultrasonic Reflection from Tool-Chip Interface

This chapter presents the results of experiments which have been carried out to understand the influence of machining parameters on the ultrasonic reflection. Various analyses are conducted in an attempt to provide further explanation of certain features that are often observed when applying the ultrasound technique to machining, but which are not well understood. Following this, the ANOVA results are presented in detail, and a comparison based upon some of the earlier findings within the chapter and the predicted results obtained from the mathematical model are presented.

7.1 Implementing Ultrasonic Measurement

This section presents the procedure for the ultrasonic measurements

7.1.1   Reflection from the Rake Face Cutting Tool

As explained in Chapter 3, the ultrasonic sensor generated waves which propagate through the cutting tool, when the sensor was excited by the voltage signals. Figure 7.1a) shows a complete recorded waveform from the cutting tool insert. The first pulse which is labelled as "sensor initial impulse" is a combination of reflection from the rear face of the cutting tool insert and sensor initiation. This pulse is stable as it is not affected by tool-chip contact. The first peak marked with (*A*) is the reflection from the rake face of the cutting tool insert and is changing as the chip contact the rake face. The rest were the echoes of this pulse occurred at the tool-chip interface. These are shown schematically in Figure 7.1b). Thus, in order to measure the interface condition in the cutting tool, the first peak (*A*) was isolated and used. In this study, this peak is known as the pulse of interest.
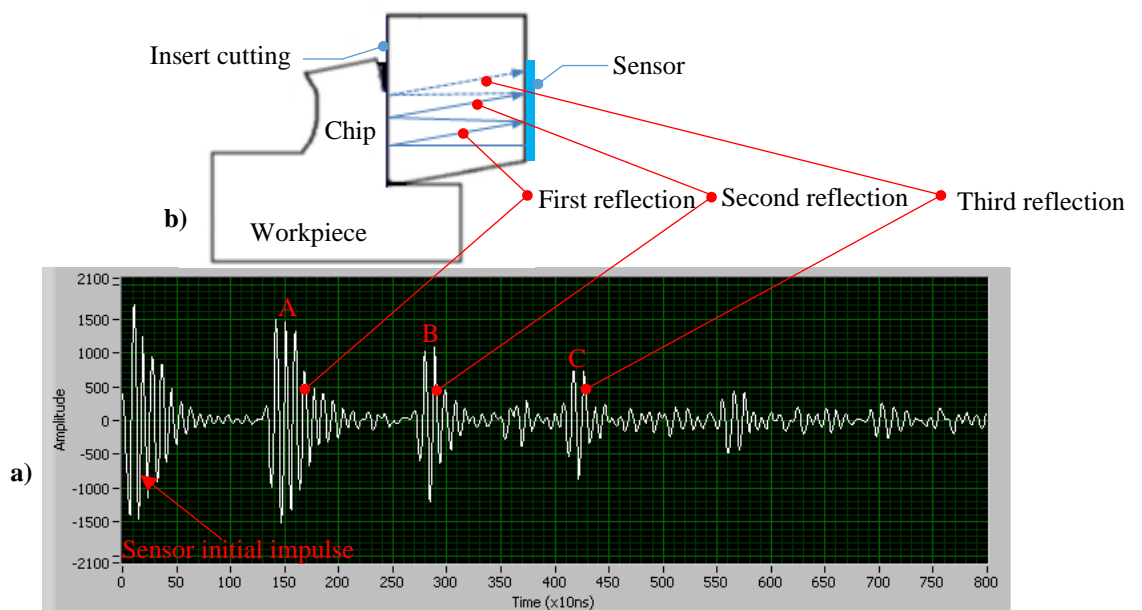
Figure 7.1 Reflection from rake surface; a) in schematic view b) in time domain

7.1.2   Reference Signal

Initially, a signal is reflected back from the rake face of the cutting tool insert when there is no chip (i.e. before the machining). This received pulse is reflected from the

cutting tool insert-air contact, and it is used as a reference signal. Due to the low acoustic impedance of the air compared to the other materials, see Table 3.1 in Chapter 3, therefore, if the matching material is air, then most of the incident waves are reflected back. This means that the wave reflected from the rake face cutting tool-air interface almost equivalent to the incident pulse/signal.

Experimentally, an incident signal is hard to measure directly, for this reason, the measurement proceeds by comparing the signal from the interface of interest to that from a known reference interface. Hence,

$$R(f) = \frac{A_m(f)}{A_{ref}(f)} R_{ref} \qquad\qquad 7.1$$

where $A_m(f)$ is the signal amplitude which is reflected from the interface (tool-chip interface), $A_{ref}(f)$ is the wave amplitude of the reference signal (tool-air interface) and R_{ref} is the reflection coefficient of the reference interface (Zhang et al. 2005). Hence, during machining a pulse is reflected which is from the interface between the cutting tool insert and the chip. Figure 7.2 and Figure 7.3 show the difference between the reflected signal from the cutting tool-air and cutting tool-chip interfaces in time and frequency domain, could be thought of as a comparison between incident and reflected signals. It can be seen clearly from the figures that there is a drop in amplitude. This is purely attributed to the partial transmission of ultrasound signal through the tool-chip contact. In this study, the signal reflected from the cutting tool-air interface is called as a reference signal.
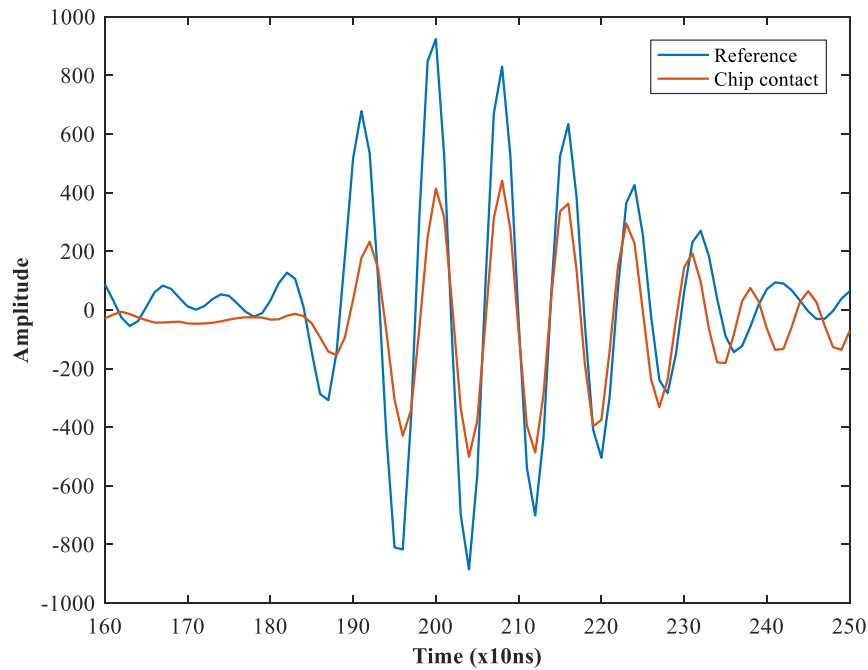
Figure 7.2 Comparison of the reflected amplitude from cutting tool-air and cutting tool-chip in time domain
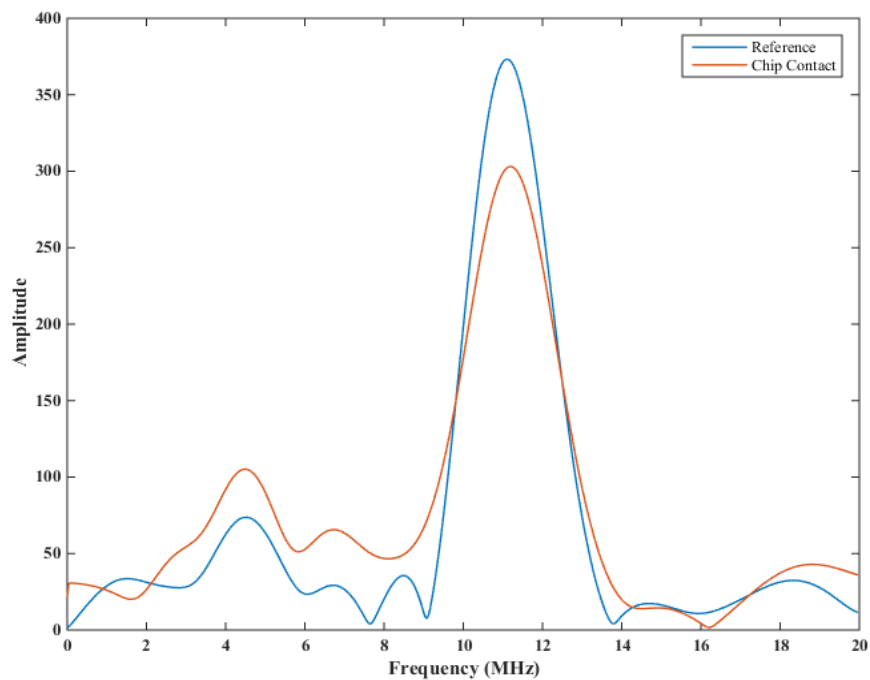
Figure 7.3 Comparison of the reflected amplitude from cutting tool-air and cutting tool-chip in frequency domain

7.1.3 Generic Signal Processing

The commercial software package LabVIEW was used, in this work, for all online and offline signal processing of the ultrasonic signals. Once the reference and measurement ultrasonic signals were captured and digitized, several steps were taken

141

to obtain the reflection coefficient value. These steps are described schematically in Figure 7.4.
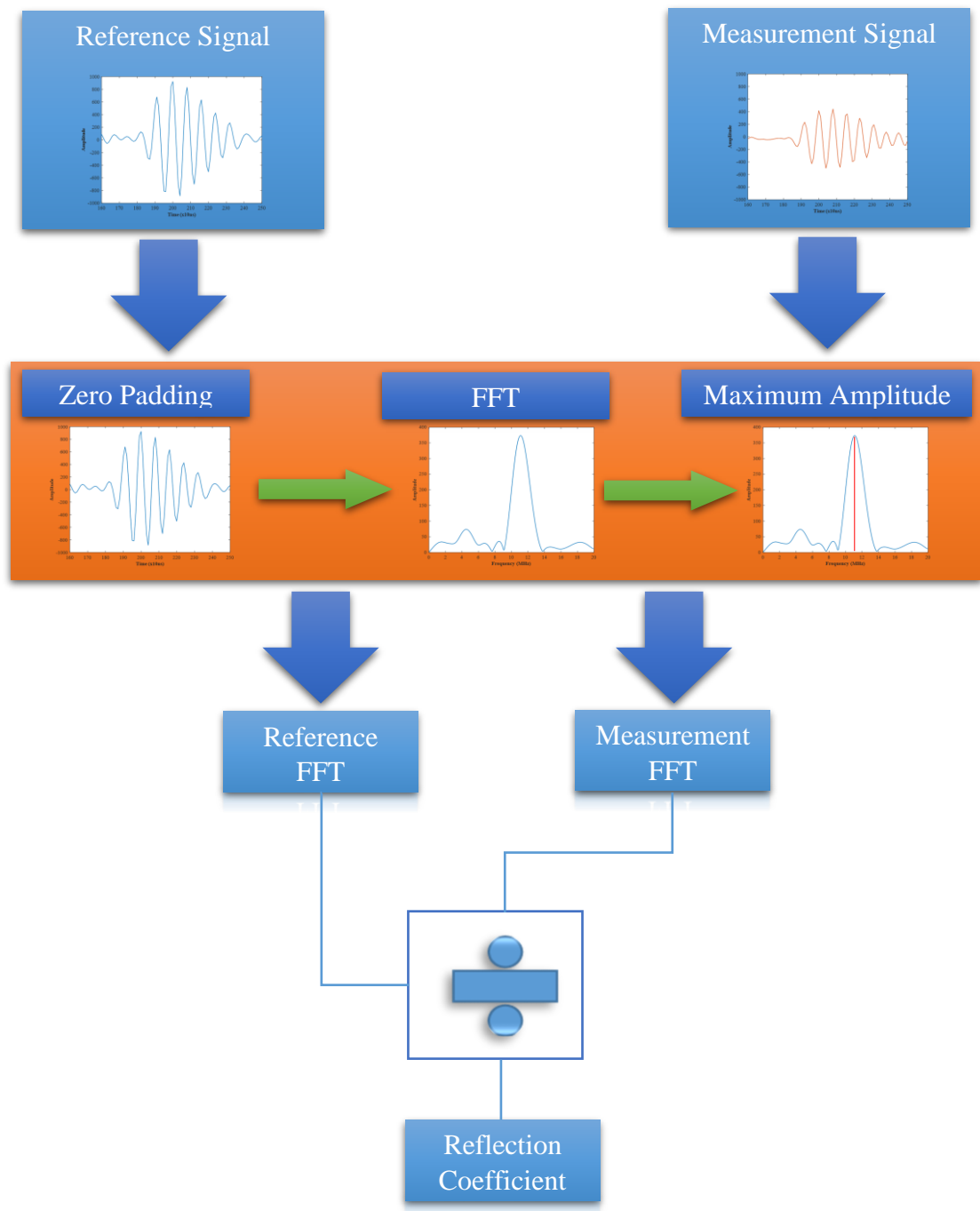
Figure 7.4 Schematic diagram of generic signal processing

To improve the accuracy and obtain further information about the reflected signal, a Fast Fourier Transform (FFT) is performed to analyse every frequency of the ultrasonic reflected signal (i.e. the reference and measurement ultrasonic signals). The FFT produces a spectrum showing signal amplitude versus frequency.

142

Before an FFT can be taken, a string of zeros can be added to the end of the input signal (both signals). This process is called a zero padding which is required to give a sufficient resolution in the resulting spectra produced by a Fourier Transform (Avan 2013). An FFT of the reference and measurement signals can now be taken as shown in Figure 7.4.

As explained in the previous section (Section 7.1.2), the reflection coefficient, which was the proportion of the amplitude of pulse by that of a reference, was obtained by dividing the FFT of measurement signal (reflected from the rake face cutting tool-chip interface) by the FFT of the reference signal (reflected from the rake face cutting tool-air interface).

The graphical outputs from a typical LabVIEW software during the signal processing is shown in Figure 7.5.
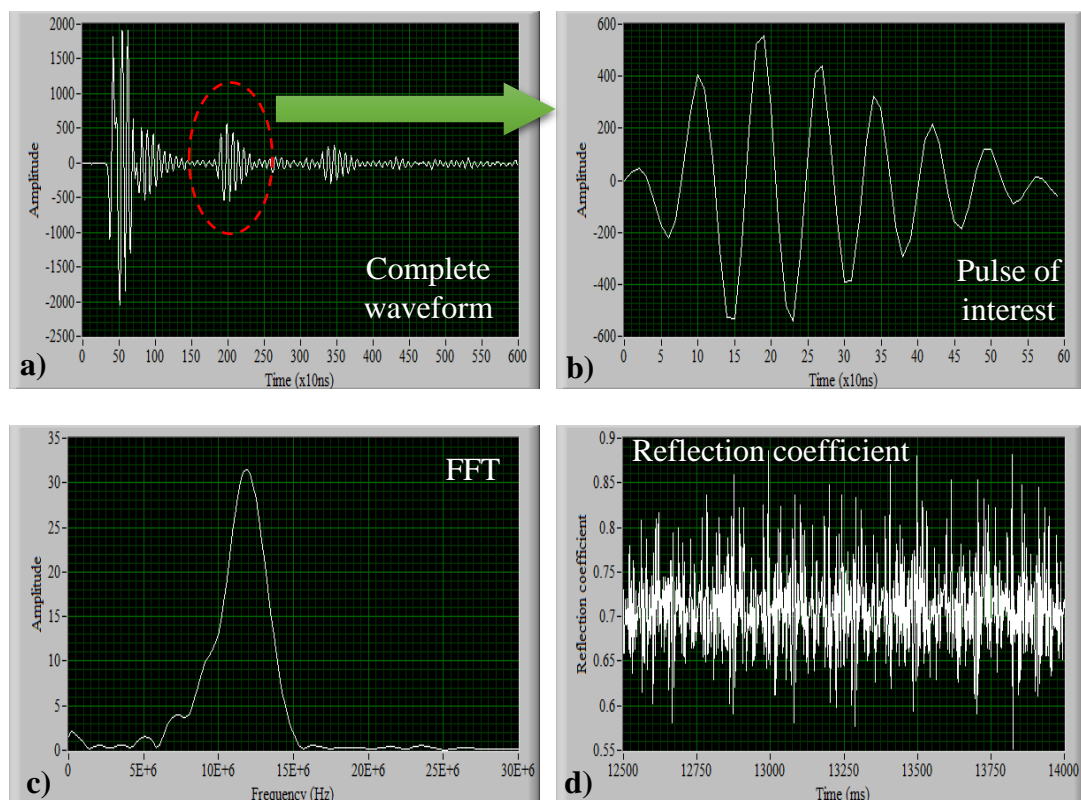
Figure 7.5 A typical graphical outputs obtained from the LabVIEW software during the signal processing; a) complete waveform, b) selected pulse, c) FFT and d) reflection coefficient with time

143

7.2 Temperature Compensation

As explained in Chapter 4, during the tests being run at different machining parameters temperatures of the cutting edge ranged up to 175˚C this raises several issues. Both the ultrasonic piezoelectric and the couplant are affected by temperature, as explained in Section 4.1.5, and thus affects the outputs from the ultrasonic element (Reddyhoff et al., 2008).

These temperature effects are detrimental to the operation of the monitoring system, as an increase in temperature would signal an erroneous increase in reflection coefficient. In order to overcome this problem, a thermocouple was attached to the cutting tool insert to monitor the temperature and its locations was shown in Figure 4.14. The thermocouple was positioned to measure the temperature of the cutting edge of the cutting tool insert close to the position of the ultrasonic transducer.

The cutting tool insert was placed into temperature controlled oven and the reference signals were recorded in a temperature range from 15˚C to 200˚C, the data was processed using LabVIEW. The reference signal has been recorded for each 5˚C increment in tool temperature during. The reference was taken during heating up and cooling down in order to check the behaviour of the element. In order to check the behaviour of the sensor over extended periods and to ensure the repeatability of the test, the reference signals were recorded 16 times, and an average taken. The average resulting plots of amplitude versus temperature at different frequencies are shown in Figure 7.6 and Figure 7.7. Figure 7.6 shows the influence of temperature on the amplitude at a frequency of 10 *MHz*, it can be seen clearly from the figure that the amplitude increases with increasing temperature. While at a frequency of 12.5 *MHz*, the data shows that the amplitude has a different trend, where the amplitude is almost constant until 120˚C approximately; then the amplitude starts to decrease until it reaches the highest temperature which was 195˚C (see Figure 7.7).

The result was checked by performing another test with using a new sensor, the test was repeated 4 times and an average was taken. The result of this test is shown in Figure 7.6 and Figure 7.7. It is worth noting that almost the same results were obtained from both sensors, and this confirms the validity of the result. The difference in amplitude of both sensors was attributed to different factors including the couplant layer, sensor size and soldering.
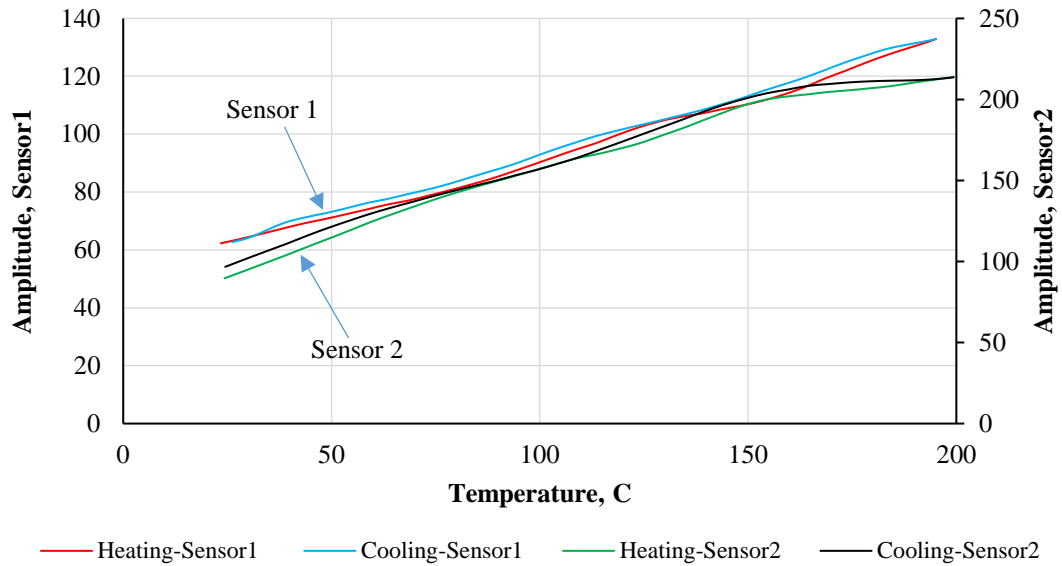
Figure 7.6 Plot of amplitude versus temperature for pulses from the rake surface at 10 MHz
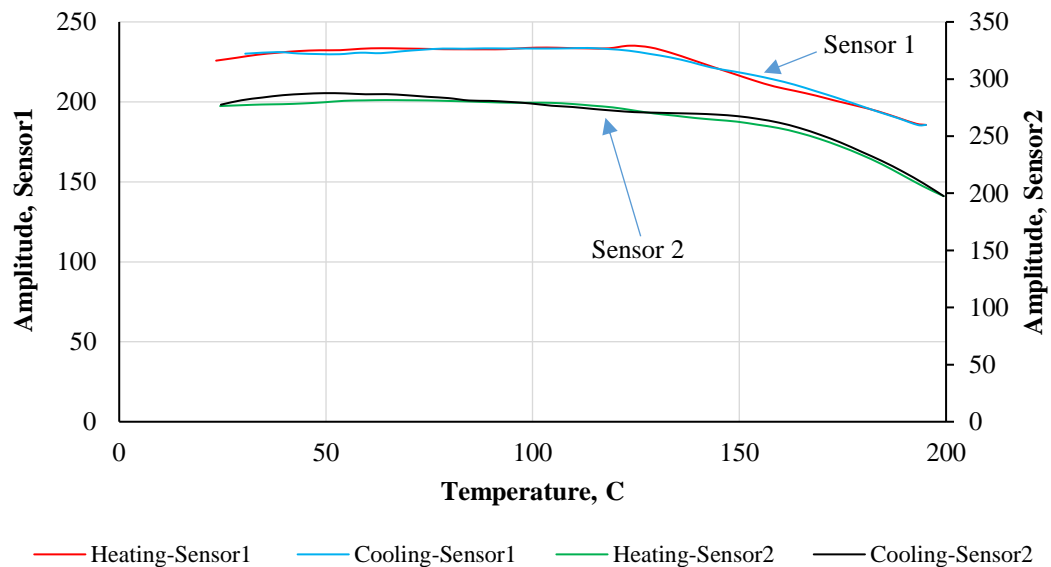
Figure 7.7 Plot of amplitude versus temperature for pulses from the rake surface at 12.5 MHz

Figure 7.8 shows the effect of temperature on the centre frequency of the element, where the centre frequency was shifted backward with increasing temperature. This shifting in the frequency affects the outputs from the element. Therefore, in order to take into account the shifting in the frequency, the maximum amplitude of the FFT was chosen regardless to the frequency. Where the reflection coefficient was calculated by dividing the maximum amplitude of the measurement signals by the maximum amplitude of the reference signal (see Figure 7.4).
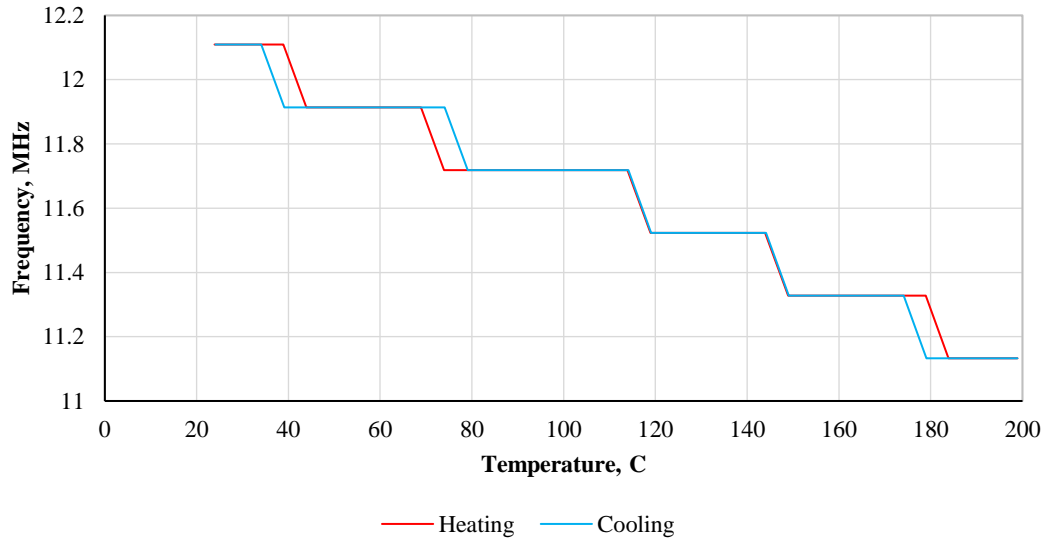
Figure 7.8 Shows how the centre frequency shifted with increasing and decreasing temperature

Another LabVIEW program was made for recording the measurement signals and temperature during machining. Finally, a LabVIEW program has been created to obtain the reflection coefficient by dividing the measurement signal by the appropriate reference signal for a given temperature. The data has been interpolated to allow the reflection coefficient to be obtained for any specific temperature. Figure 7.9 shows the effect of temperature compensation on the reflection coefficient. The compensated reflection coefficient is smaller than non-compensated because as explained before, the amplitude increases with increasing the temperature, as illustrated in Figure 7.9.
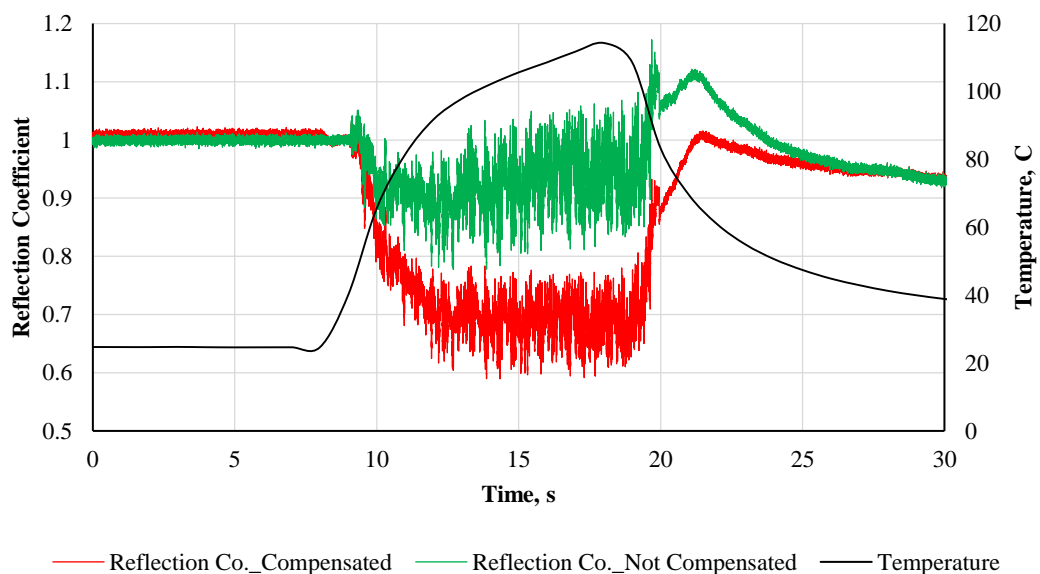
Figure 7.9 Effect of temperature compensation on the reflection coefficient during *Al 6082* cutting

146

7.3 Ultrasonic Measurements

7.3.1   General Analysis of a Reflection Coefficient Profile

Cutting experiments would typically be initiated by identifying the machining parameters such as the cutting speed, depth of cut (which equals the workpiece tube wall thickness) and feed. In this study, a set of orthogonal cutting experiments were conducted, and it was therefore possible to obtain ultrasonic measurement across a range of cutting parameters during such instances. This enabled various features of the ultrasonic measurements to be characterised as dependant on – or independent of – cutting speed, cutting depth and feed as well as the influence of the BUE and the tool-chip contact phenomenon on the ultrasonic measurements.

As described in Chapter 5, according to the centre composite design (CCD) methodology, a set of orthogonal cutting experiments were conducted (as shown in Table 5.5) in order to investigate the effect of the machining parameters on the tool-chip interface using the ultrasonic reflection when machining an aluminium *Al 6082* workpiece tube with and without a cutting fluid. The results show that the overall profile of the reflection coefficient curves is almost similar for all the trials. The results also show that the reflection coefficient profile during wet cutting conditions is different from the dry conditions, therefore, the both profile are studied separately. To study the reflection coefficient curves, three trials have been chosen and presented below while the rest of results are presented in Section 7.3.3.

7.3.1.1 Reflection Coefficient Variation in Dry Cutting

Figure 7.10 shows reflection coefficient curves obtained from orthogonal cutting of *Al 6082*, during dry machining, at a cutting speed of 90 *m/min* and depth of cut of 2 *mm* for feeds in the range of 0.09-0.23 *mm/rev* at 0.07 *mm/rev* increments. Each data set was recorded at a 1 *kHz* pulse rate, and reflection coefficient has been measured, as mentioned earlier in this chapter, at the maximum amplitude of the frequency of the ultrasonic source element (see Figure 7.4). The reference signal was obtained prior to the cutting process for temperatures in the range of 25-200 *°C* at 5 *°C* increments as described in Section 7.2.

In the figure, the contact between the rake face of the cutting tool and chip is clearly observed by way of a general reduction in reflection coefficient at 9000≤*time*≤19000 *ms*, (±500 *ms*). All the curves have been smoothed using a DIAdem software, DIAdem calculates the moving average for each value from the reflection coefficient value and from the specified number of neighbour values which is by default 15. A clear relationship can be observed between reflection coefficient and feed, where reflection coefficient is increasingly minimised as feed is increased while the cutting speed and cutting depth are constant (see Figure 7.10).
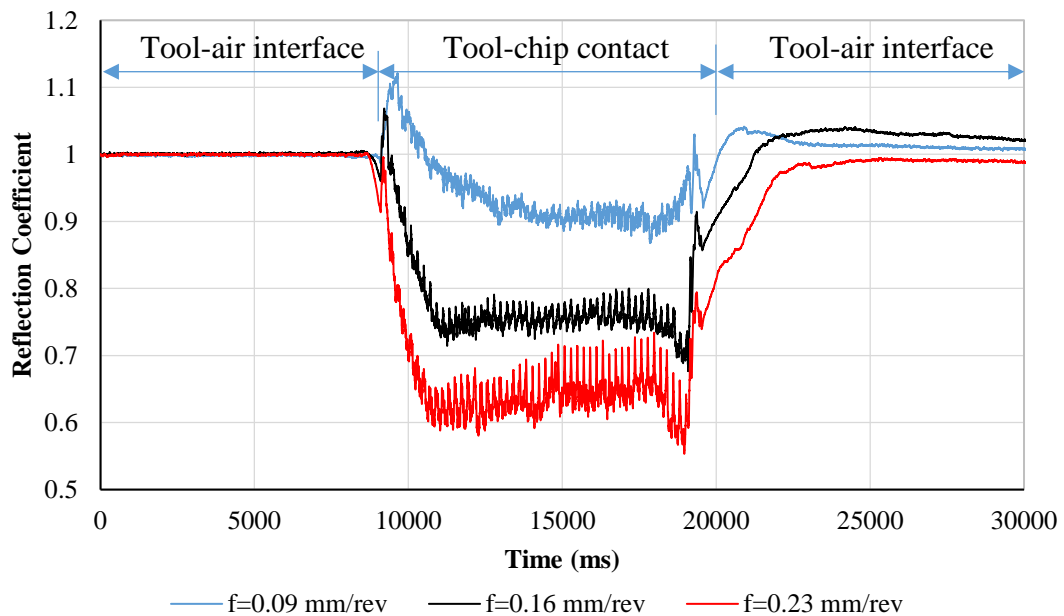
Figure 7.10 Reflection coefficient curves during dry cutting of *Al 6082* at different feeds with a constant cutting speed and depth of cut (*V=90 m/min*, *t=2 mm*).

The data also showed a number of additional features, as highlighted in Figure 7.11(a) and introduced within the following paragraphs.

Firstly, when the cutting tool edge is not engaged with the workpiece, i.e. there is no contact between the cutting tool and chip, the reflection coefficient is close to 1 (Figure 7.11(b)). As the chip forms and contacts the cutting tool the reflection coefficient starts to reduce preceded by a slight increase as shown in the last part of Figure 7.11(b). A possible explanation for this might be due to a collision of the cutting tool to the workpiece tube which is not exactly square, and thus, the cutting tool is not entirely in contact with the workpiece. This feature was observed in the experiments that have been using a new tube; therefore, this is a cutting parameter independent phenomenon. As soon as the cutting edge entirely contacts the workpiece the reflection coefficient

reduces. In some cases, reflection coefficient exceeded one at brief instances. This suggests reflected energy to be higher at brief instances than that of the cutting tool-air reference condition. This was noticed only when the BUE exists [see Figure 7.16 a), b) and c)]. A possible explanation for this might be that the measurement window (window covered by the ultrasonic waves) contains partial contact, the result is often an increase in the reflected amplitude, leading to a reflection coefficient greater than one (see last part of the Figure 7.11(b)).

As the cutting edge entirely engaged the workpiece, the chips formed and moved over the tool rake face caused a sharp reduction in the reflection coefficient, depending on the feed until the chip entirely formed then the reflection signals are almost periodic, as will be discussed in more detail in the next section, (see Figure 7.11(d)). The reason for this reduction in the reflection coefficient is the increase in tool-chip contact area that increases with increasing the feed. As the contact area increases more transmission of waves through the interface, therefore, the lower reflection coefficient is recorded. Another reason for the reduction in the reflection coefficient is due to the increase in pressure applied on the rake face cutting tool that increases with increasing the feed. As the pressure on the rake face increased, more waves are transmitted to the chip through the interface and low reflection coefficient recorded. More detail about the influence of machining parameters on reflection coefficient will be given later in Section 7.3.3.

Finally, as the cutting edge exits the cut, a similar feature to the entry stage has been observed (see Figure 7.11(c)). The reflection coefficient does not return to one. This result may be explained by the fact that the ultrasonic element properties are different from what it was before cutting where the sensor temperature is still higher than what it was before cutting and caused shifting the centre frequency of the element as discussed in Section 7.2. Another possible explanation for this might be due to the presence of aluminium deposits on the tool rake face. This feature appears to be similar for all the experiments, which can, therefore, be said to be cutting parameters independent.
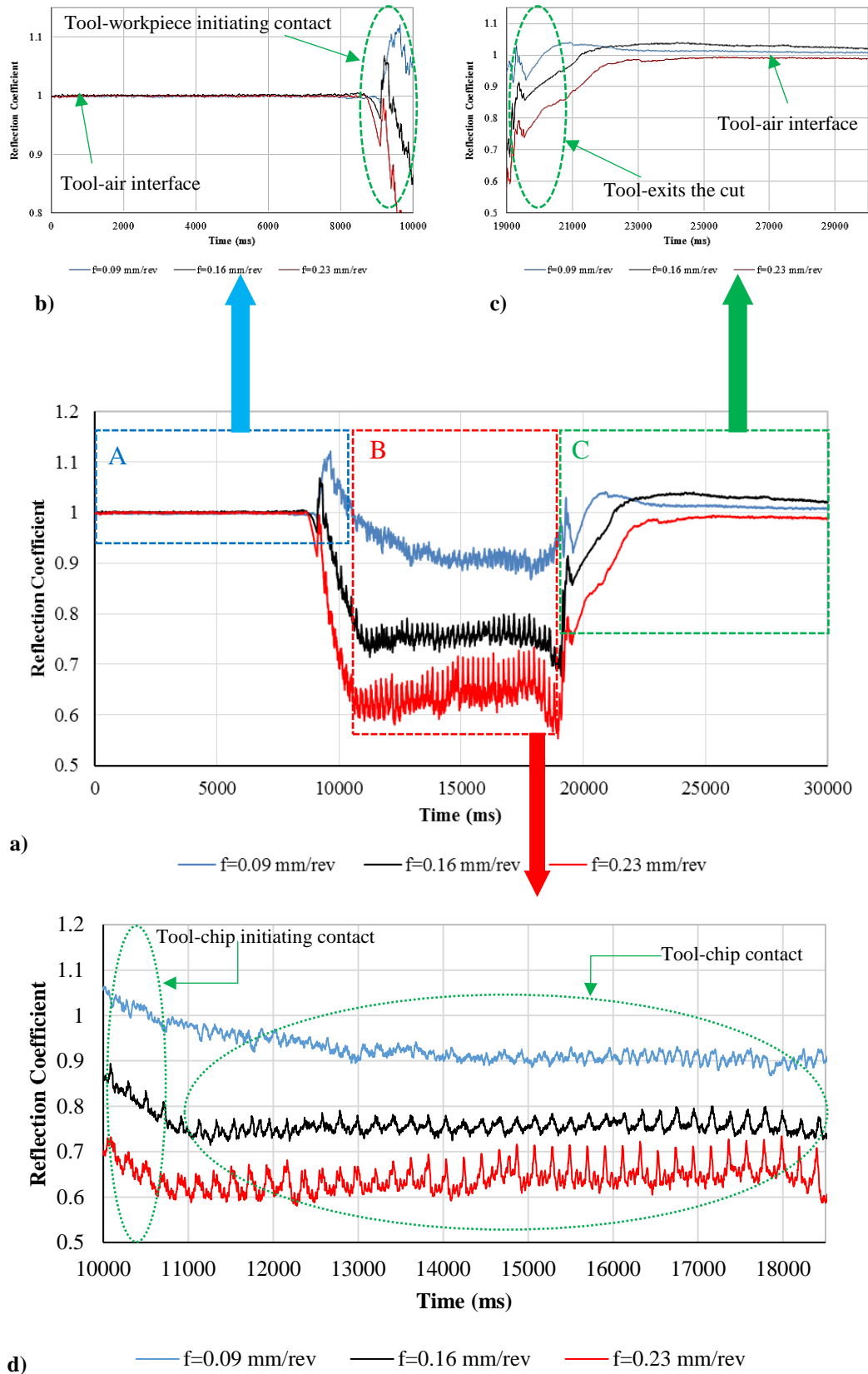
Figure 7.11 Features of interest in reflection coefficient curves, at dry conditions, of Figure 7.10

150

7.3.1.2 Reflection Coefficient Variation in Wet Cutting

With the presence of cutting fluid, reflection coefficient variation is different from the dry condition especially at high cutting speed and small cutting depth. Figure 7.12 shows reflection coefficient curves obtained from orthogonal cutting of *Al 6082*, during wet cutting, at a cutting speed of 90 *m/min* and feeds 0.16 *mm/rev* for cutting depths in the range of 1.2-2.8 *mm* at 0.8 *mm* increments. While Figure 7.13 shows reflection coefficient curves at different cutting speeds (*V*=40, 90 and 140 *m/min*) with a constant cutting depth and feed (*t*=2 *mm*, *f*=0.16 *mm/rev*), respectively.

The reflection coefficient is around 0.85 (not 1) when the cutting tool is not engaged the aluminium tube (see Figure 7.12 and Figure 7.13). This is attributed to existing a layer of oil on the rake face cutting tool before starting cutting. As shown by equation 3.7, the reflection coefficient is a function of the acoustic impedance of both materials, which in this case is cutting tool and oil. Based on Equation 3.7, presented in Chapter 3, the reflection coefficient was calculated and found to be equal to 0.885, where some of the energy is transmitted through the rake face-oil interface. The result also showed a number of additional features, as highlighted in Figure 7.14(a) and introduced within the following paragraphs.
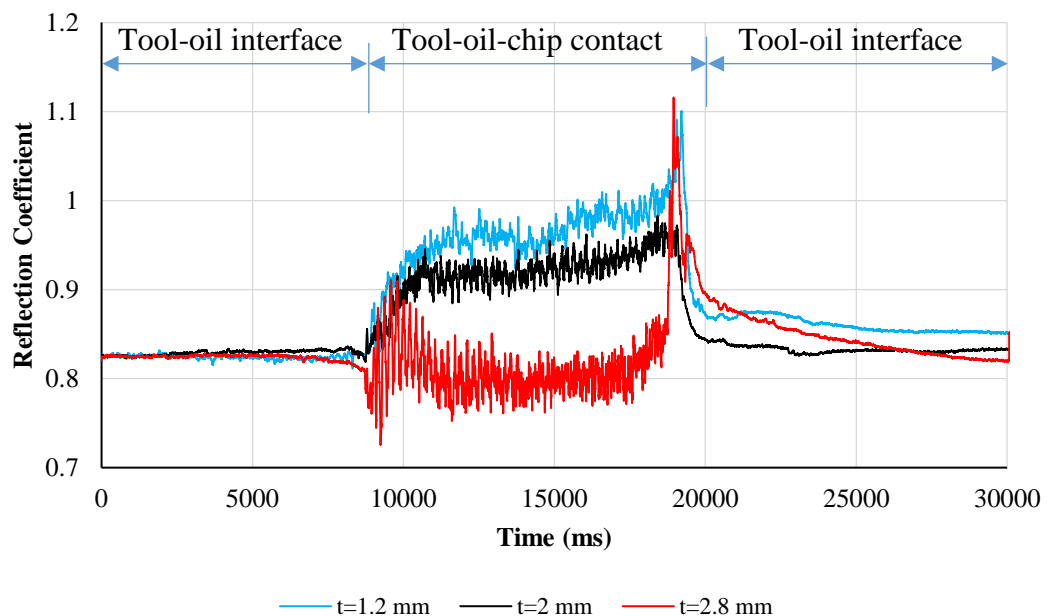
Figure 7.12 Reflection coefficient curves during wet cutting of *Al 6082* at different depth of cut with a constant cutting speed and feed (*V*=90 *m/min*, *f*=0.16 *mm/rev*), respectively.
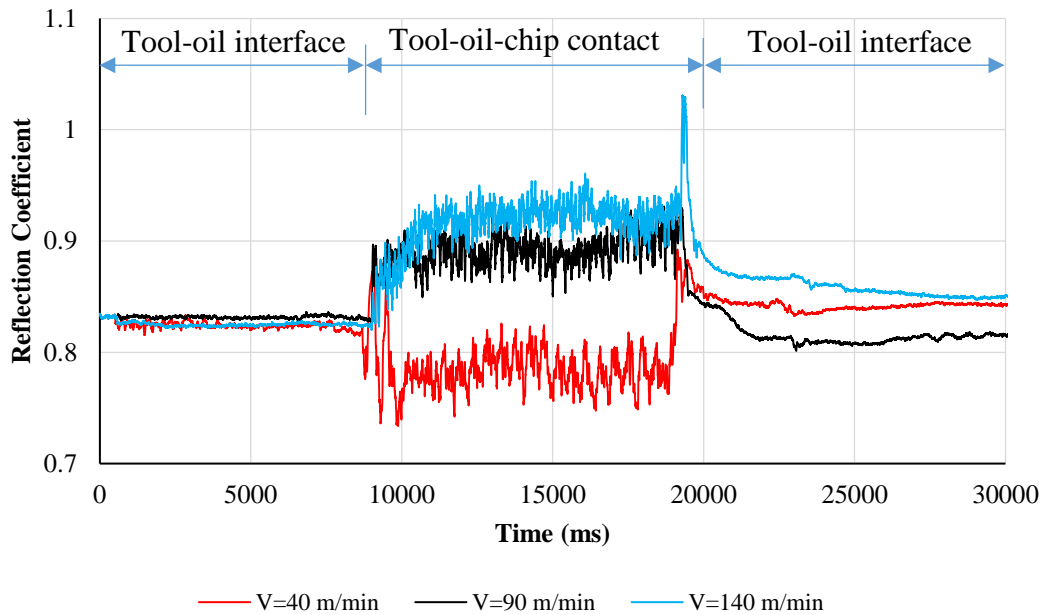
Figure 7.13 Reflection coefficient curves during wet cutting of *Al 6082* at different cutting speed with a constant cutting depth and feed (*t=2 mm*, *f=0.16 mm/rev*).

As the cutting edge engaged the workpiece, the chips formed and moved over the tool oily rake face and thus the interface consists of solid and liquid contact (mixed interface), as discussed in Chapter 3 (Section 3.8). In a mixed contact, the surface in some regions is fully separated by the fluid while in some other the surfaces are directly in contact (solid-solid contact).

As discussed in the previous section that low reflection coefficient means high pressure is applied to the rake face cutting tool, chips push the oil out from the rake face, (i.e. a small amount of cutting fluid penetrates to the tool-chip interface). As explained in Chapter 6, pressure on the rake face increases with increasing feed and cutting depth while it decreases with increasing cutting speed. This can be seen clearly from the both figures (Figure 7.12 and Figure 7.13) and (see also Figure 7.14d)), where at low cutting depth the pressure is low and thus the cutting liquid penetrate more to the interface results in a high reflection coefficient (wets well). At high cutting depth the cutting fluid has a less chance to penetrate to the interface due to the high pressure on the tool caused by the thicker chip and thus a low reflection coefficient is recorded (poor wetting) (see Figure 7.12). Furthermore, a cutting fluid in a higher cutting speed is penetrated more to the interface than in lower cutting speeds because of the pressure that is low in higher cutting speed, therefore, a high reflection coefficient is recorded (wet well). The other features are the same as in the dry condition.
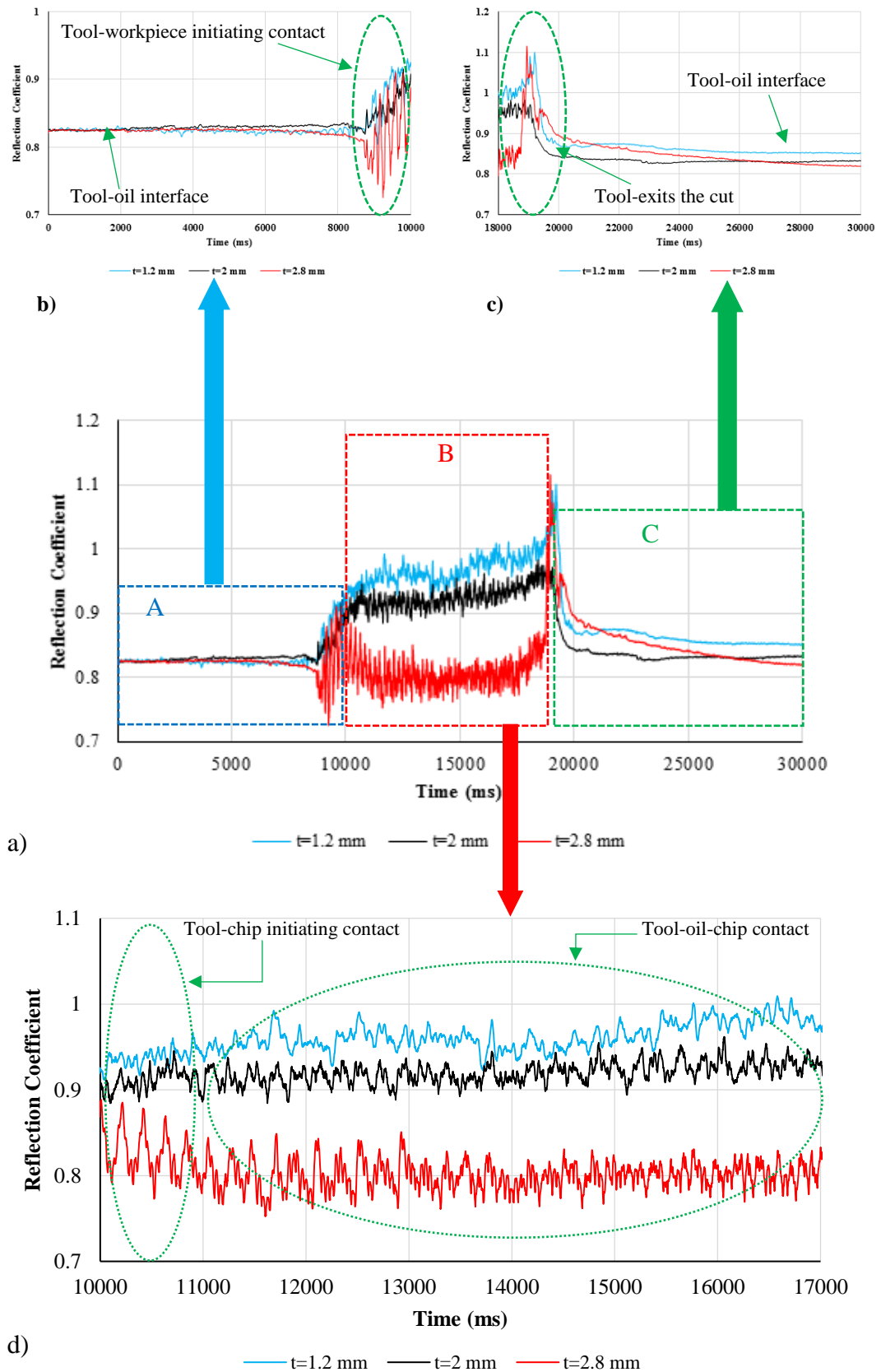
Figure 7.14 Features of interest in reflection coefficient curves, at wet condition, of Figure 7.12

153

7.3.2 Fringe Effects at Tool-Chip Contact

This section will explain the causes of the oscillation in reflection coefficient that is observed at the tool-chip contact, as highlighted in Figure 7.11(d) and Figure 7.14(d). This oscillation may be due to the chip segmentation. When the cutting edge engaged the workpiece, a crack initiation appears easily in front of the cutting edge. This crack will produce the slip of the matter where the formation of a slice (segment). This phenomenon will repeated again by giving a new segment where the process is cyclic (Childs et al. 2000). Figure 7.15 shows a schematic of the chip segmentation for an orthogonal cutting process. This process caused the variations in reflection coefficient signals. It was previously reported that the segment band increased with increasing feed and cutting speed (Barry & Byrne 2002; Atlati et al. 2011; Salem & Bayraktar 2012; Ozel & Ulutan 2013; Atlati et al. 2013).

b: Undeformed chip width
h: Undeformed chip thickness
hc: Deformed chip thickness
c: Segment band
r: Chip curls radius
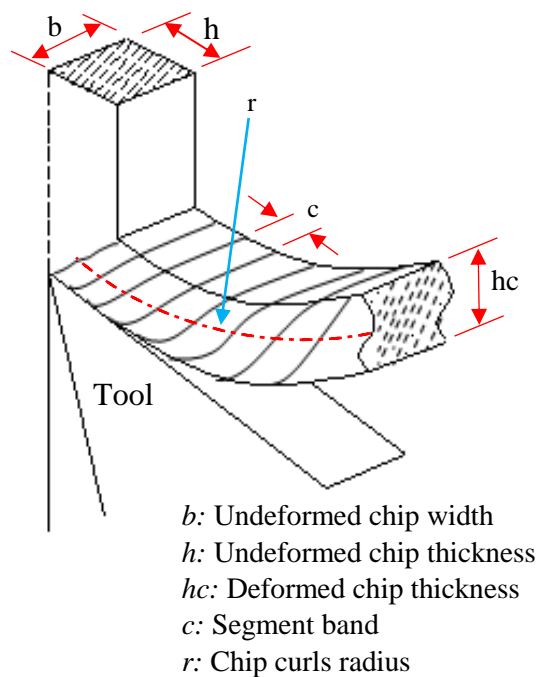
Figure 7.15 Orthogonal cutting (uncut chip cross-section)

Another possible explanation for the variations in reflection coefficient signals is that the chip curls increased with increasing feed; where at higher feed, the number of chip curls is higher than at lower feed (Dabade & Joshi 2009; Radhika et al. 2014). The chip long contact with the rake face has a larger radius than chips with shorter contact length. Therefore, due to increasing the segment band and chip curls radii with increasing feed, the reflection coefficient profiles are different (see Figure 7.16). For

instance, the reflection coefficient profile across the tool-chip interface (Figure 7.16(d)) at feed of *f*=0.09 *mm/rev* is a slightly different from what it is at feed of *f*=0.16 *mm/rev* and is very different from what it is at feed of *f*=0.23 *mm/rev*, despite all the other machining parameters, including cutting speed, spindle speed and cutting depth, are the same in these three experiments. The reason for these differences, in the reflection coefficient profiles, is because of chip segmentaion.
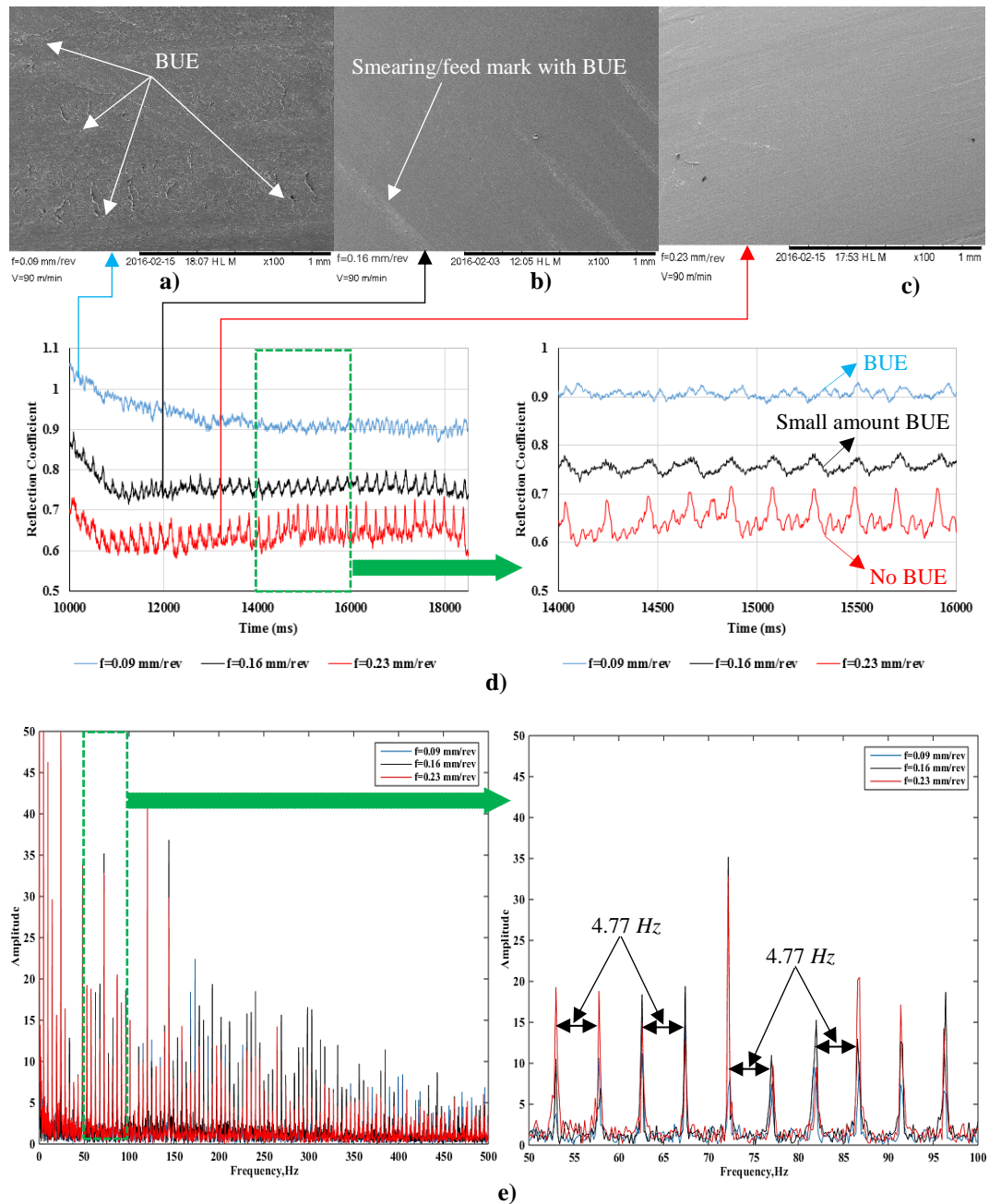
Figure 7.16: (a), (b) and (c) SEM photographs of chip underside during dry cutting of *Al 6082* at different feeds (0.09, 0.16 and 0.23 *mm/rev*), respectively and constant cutting speed and cutting depth, *V*=90 *m/min*, and *t*=2 *mm*, respectively; (d) Feature of interest in Reflection Coefficient curves of Figure 7.11 (Feature B); (e) Spectral reflection coefficient of the interest feature (d).

155

Figure 7.17 shows a chip root from *Al 6082* showing the formation of the chip under an optical microscope. It can be seen from the figure that a hill can be distinguished at the root and this was repeated along the chip length and the distance between these hills are almost equal. The existence of these hills affects the reflected signals from the rake surface of the cutting tool, which lead to the fluctuation of reflection coefficient with time. This could be another possible explanation for the variations in reflection coefficient signals.
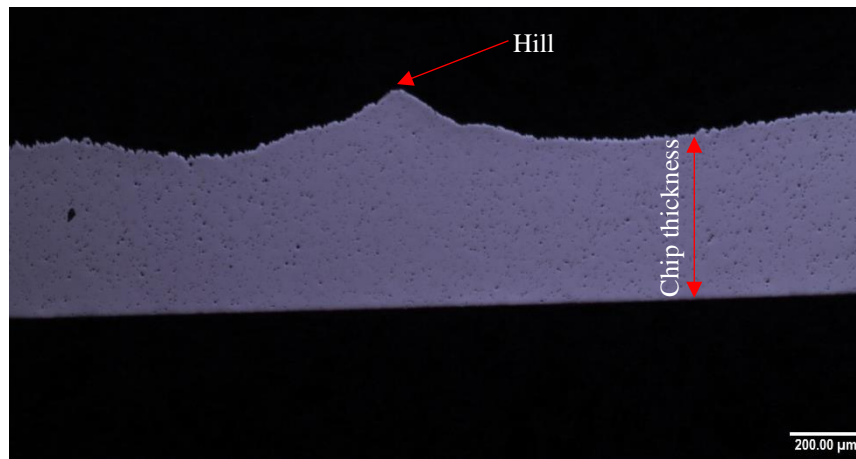
Figure 7.17 Optical image of the chip roots

It is clear from the Figure 7.16 d) that fluctuation of reflection coefficient with time at a feed of 0.09 mm/rev is varies less than the other two reflection coefficient curves (i.e. at *f*=0.16 and *f*=0.23 *mm/rev*). These results are likely to be related to the chip movement over the rake face cutting tool, where as explained earlier that at higher feed the chip contact the rake face longer than at lower feed because the chip has a larger curls radius and thus the chip does not detach the rake face early and a stable reflection coefficient is recorded.

With applying cutting fluid the variations in reflection coefficient signals are different from the dry conditions, where fluctuation of reflection coefficient, in wet condition, with time is more stable. The reason for this is due to the increasing in chip curl radius where Childs et al. (2000) stated that the chip curled increased with using cutting fluid (see Figure 7.11 and Figure 7.14).

Further analysis was conducted by converting the time domain of the reflection coefficient signals, of dry cutting, to frequency domain using Fast Fourier Transform (FFT), the frequency spectrum is shown in Figure 7.16 (e). From the data in Figure

7.16 (e), it is apparent that the distance between any two amplitudes is around 4.77 *Hz*, which is associated with the frequency of the spindle speed (i.e., number of revolution per minutes); the spindle speed of these experiments was constant (286 *RPM*) which is equal to 4.77 *Hz*, so the length between any two amplitudes are constant and it is equal to 4.77 *Hz* as shown in Figure 7.16 (e). The frequency spectrum in Figure 7.16 (e) shows that the amplitude of the same frequency at different feed is different. This result may be explained by the fact that the thickness of the aluminium tube used in this study varies (±0.05 *mm*) where aluminium tube never completely aligned. The results of the FFT analysis proves that the difference in the profile of the reflection coefficient is a cutting parameter independent phenomenon. Therefore, this clearly suggests that different between the observed feature of the Figure 7.16 (d) can be said to be a chip segmentation dependant effect.

The relation between the mean values of the ultrasonic coefficient curves versus the machining parameters are presented in the next paragraph.

7.3.3   Influence of Cutting Parameters on Reflection Coefficient

The influence of machining parameters on reflection coefficient, in dry and wet machining, is presented in Figure 7.18. The error bars in the figure represent the standard deviation; the results are also given in Appendix B (Table B.1).

In both dry and wet cutting conditions, the results show that the reflection coefficient increases with increasing cutting speed and decreased with increasing feed and cutting depth (see Figure 7.18). Increasing cutting speed results in more of the ultrasonic energy/amplitude are reflected back from the rake face of the cutting tool (i.e. tool-chip interface); while with increasing cutting depth and feed more of the ultrasonic energy are transmitted through the interface into the chip. From the data in Figure 7.18, it is apparent that with applying cutting fluid more of ultrasonic energy is reflected back from the tool than when dry machining is performed. High reflection coefficient means low tool-chip contact area, low pressure/stress or both are applied on the rake face of the cutting tool and vice versa. The results show that the lowest value of reflection coefficient (*R*=0.6755) was obtained when machining performed in dry cutting at a cutting speed of (*V*=90 *m/min*), cutting depth of (*t*=2 *mm*) and higher feed (*f*=0.23 *mm/rev*); by keeping constant the cutting speed and cutting depth at *V*=90

m/min and *t=2 mm*, respectively and decreasing the feed to the lowest value (*f=0.09 mm/rev*) the highest value of reflection coefficient was obtained (*R= 0.8951*).
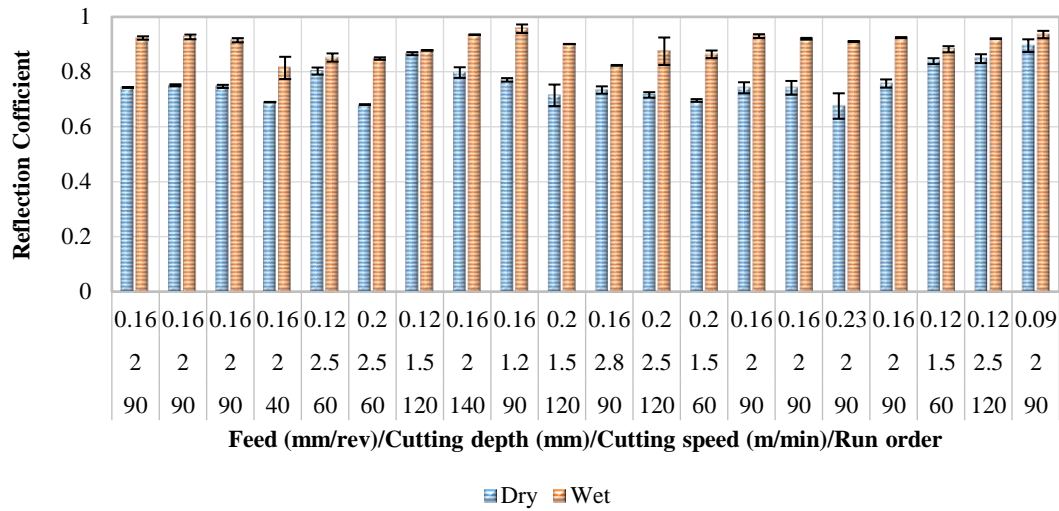
Figure 7.18 Comparison of the average reflection coefficient for dry and wet cutting conditions

The results also show that the feed has the most significant effect on the reflection coefficient during the dry condition followed by the cutting speed which has a lower significance than feed while the effect of cutting depth is very small compared to the other machining parameters. While operating with cutting fluid, cutting speed and depth of cut have the most significant effect on reflection coefficient, and the influence of feed is very small contrary to what is in the dry cutting. To examine more about the influence of the machining parameters on the reflection coefficient individually, some data of Figure 7.18 have been re-plotted in linear graphs and are presented in the next paragraphs.

The influence of cutting speed on reflection coefficient in the dry and wet conditions can be seen from Figure 7.19, where the reflection coefficient was increased with increasing cutting speed in dry cutting while the cutting depth and feed were kept constant at *t=2 mm*, *f=0.16 mm/rev*, respectively. These relationships may be explained by the effect of the tool-chip contact length, as discussed in Chapter 6, with increasing cutting speed the tool-chip contact length decreased and thus reducing the tool-chip contact area (see Figure 6.19 and Figure 6.23) that leads to reflect back more ultrasonic energy from the rake face cutting tool. Another possible explanation for these relationships is that as explained in Chapter 6, with increasing cutting speed the cutting forces decreased (see Figure 6.32 and Figure 6.33) and thus low pressure occurs on

the rake face cutting tool which leads to low ultrasonic energy transmission through the interface into the chip (i.e. high reflection coefficient). More detail about the correlation between the contact area, cutting forces and reflection coefficient are given in Chapter 8.

The single most striking observation to emerge from the data comparison was, with applying cutting fluid, the reflection coefficient confirmed to increase with increasing cutting speed. This was in contrast to contact length, contact area and cutting forces findings (discussed in Chapter 6), there was no decrease in reflection coefficient recorded at cutting speeds (*V*<90 *m/min*). More detail will be given in Chapter 8.
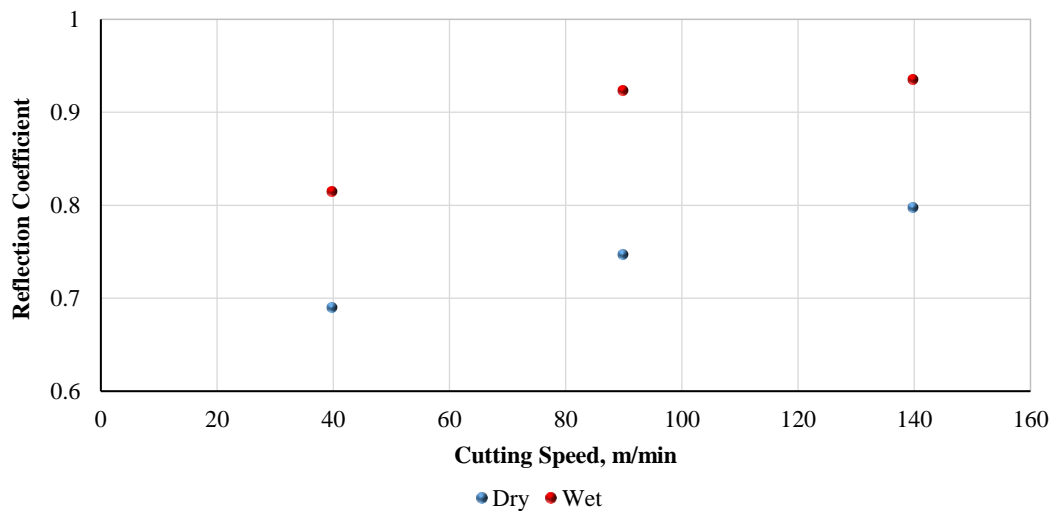
Figure 7.19 Comparison of the reflection coefficient under dry and wet machining of *Al 6082-T6* at different cutting speeds with a constant cutting depth and feed (*t*=2 *mm*, *f*=0.16 *mm/rev*).

To investigate more about the influence of the cutting speed on the reflection coefficient, further experiments were carried out. The machining parameters of these experiments are shown in Table 7.1. Figure 7.20 shows the results of these experiments where it can be seen clearly that the same above results of Figure 7.19 were obtained. These results further support the idea that with increasing cutting speed the tool-chip contact area decreased and pressure decreased and thus the amount of the ultrasonic energy which are reflected back from the rake face of the cutting tool increased.

Table 7.1 Machining parameters

Trials No.	Cutting parameters		
	Cutting Speed (m/min)	**Cutting depth (mm)**	**Feed (mm/rev)**
1	40	2.5	0.12
2	60	2.5	0.12
3	90	2.5	0.12
4	120	2.5	0.12
5	140	2.5	0.12
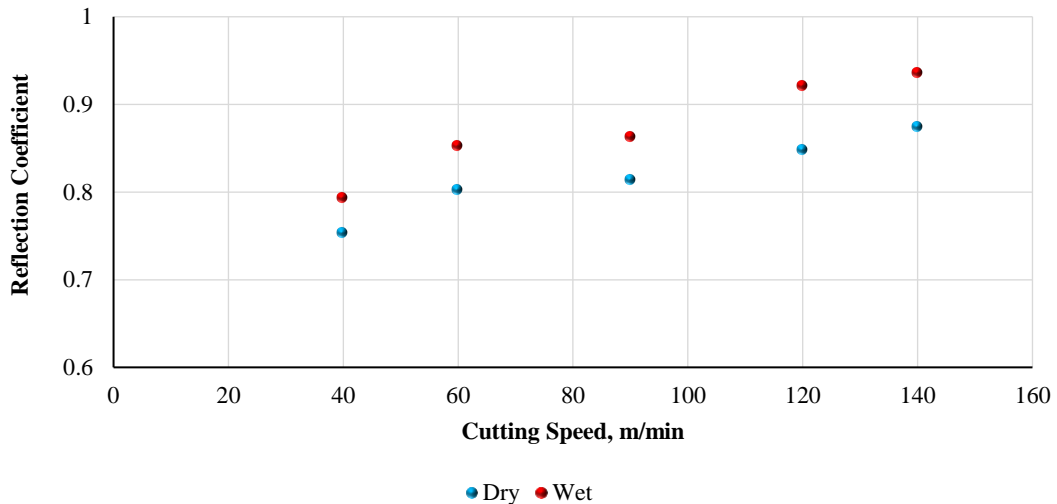
Figure 7.20 Comparison of the reflection coefficient under dry and wet machining of *Al 6082-T6* at different cutting speeds with a constant cutting depth and feed (*t=2.5 mm*, *f=0.12 mm/rev*), respectively.

The results also show that, at dry cutting conditions, the feed has the most significant effect on the reflection coefficient than cutting speed. Where the data reveals that there has been a gradual decrease in the reflection coefficient with increasing feed while the cutting speed and cutting depth were kept constant at *V=90 m/min*, *t=2 mm*, respectively. While at wet conditions, the feed does not have a significant effect. Figure 7.21 shows the influence of feed on the reflection coefficient. The observed decrease in reflection coefficient could be attributed to the increase in tool-chip contact area, where as discussed in Chapter 6, the tool-chip contact length increased with increasing feed, and thus the contact area increased (see Figure 6.20 and Figure 6.22). Increasing the tool-chip contact area leads to transmit more ultrasonic energy through the tool-chip interface and less energy are reflected back. These results confirm the association between the tool-chip contact area and reflection coefficient.

There are, however, other possible explanations for the relation between feed and reflection coefficient, as discussed in Chapter 6, the two orthogonal components of the cutting forces increased with increasing feed (see Figure 6.36 and Figure 6.37). This mean that with increasing feed high pressure are applied on the rake face cutting tool which results in reflecting less ultrasonic energy from the tool-chip interface and transmitting more energy through the interface.
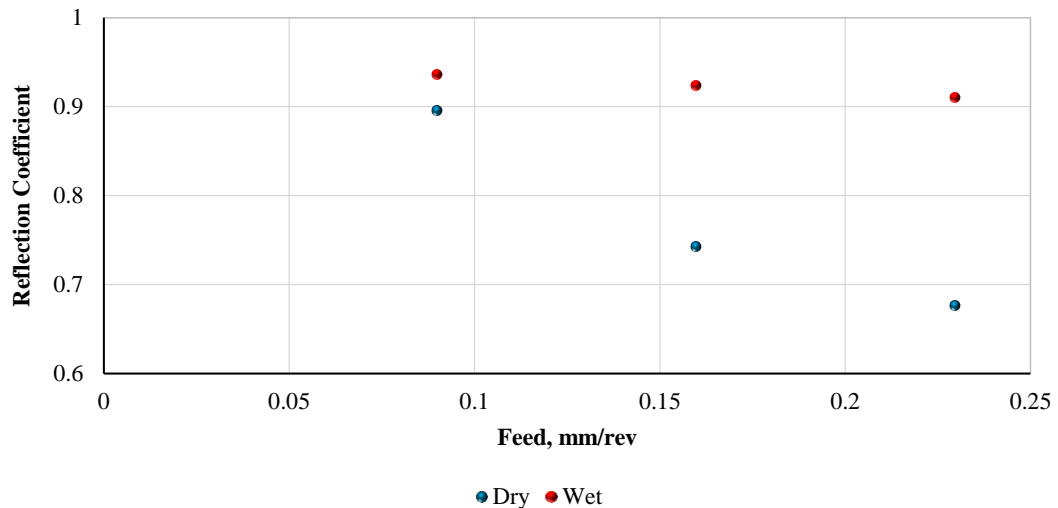
Figure 7.21 Comparison of the reflection coefficient under dry and wet machining of *Al 6082-T6* at different feed with a constant cutting speed and cutting depth (*V=90 m/min*, *t=2 mm*).

The effect of cutting depth on the reflection coefficient in the absence of cutting fluid was very small where it is almost negligible, while with existing cutting fluid the data reveals that the reduction in reflection coefficient with increasing cutting depth is much bigger than in dry cutting (see Figure 7.22). These results confirm the association between the cutting depth and tool-chip contact length; where the effect of the cutting depth on the tool-chip contact length was very small (See Figure 6.21 in Chapter 6). The influence of changes in machining parameters on the reflection coefficient will be presented in detail in Section 7.3.5.
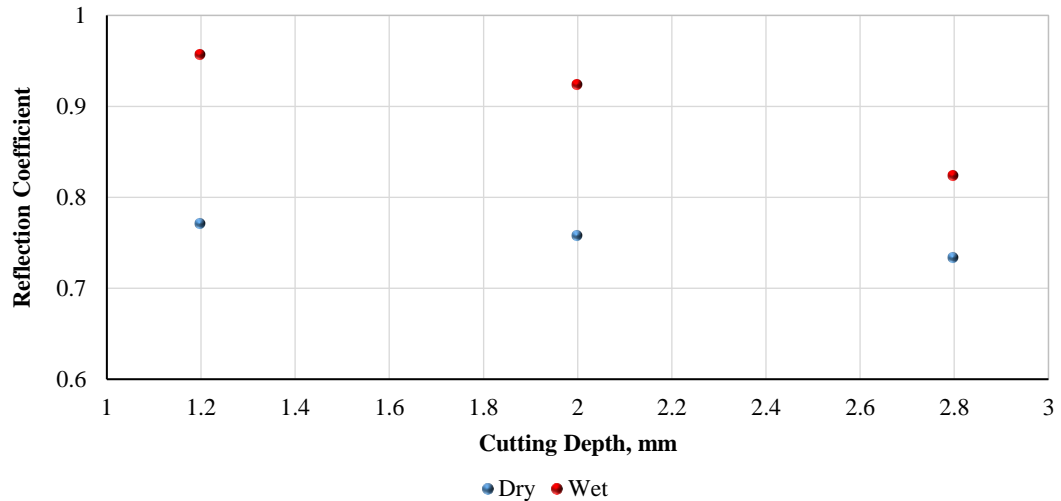
Figure 7.22 Comparison of the reflection coefficient under dry and wet machining of *Al 6082-T6* at different cutting depth with a constant cutting speed and feed (*V=90 m/min*, *f=0.16 mm/rev*).

7.3.4 Analysis of Variance (ANOVA)

As presented in Chapter 5, the ANOVA was conducted on the ultrasonic data to identify the main significant parameters on the reflection coefficient during machining aluminium *Al 6082*, and also to develop the empirical relationships by using the regression analysis. The same procedures have been taken as described in Chapter 6, where the analysis was conducted by using the P-value; if the P-values are less than 0.05 then the obtained models are considered as a statistically significant. The highest influence for the corresponding output parameters has the lowest the P-value. Furthermore, variations of the reflection coefficient with the machining parameters including cutting speed, depth of cut and feed are studied in dry and wet conditions separately. Only the significant parameters are presented here while the complete ANOVA results are presented in Appendix B.

7.3.4.1 Dry Cutting Conditions

The results of the ANOVA of reflection coefficient during dry turning are presented in Table 7.2. This table only shows the significant effect of the machining parameters on the reflection coefficient. It can be seen from Table 7.2 that cutting speed, cutting depth and feed have statistical and physical significance on the reflection coefficient, especially the cutting speed and feed. Moreover, the ANOVA analysis also show that the quadratic value of feed (*feed*feed*) has a significant effect on the reflection coefficient. Table 7.2 also shows the value of the determination coefficient (R^2) which

indicates the goodness of data fit for the model, and the values of adjusted determination coefficient (adj. R^2) and predicted determination coefficient (pred. R^2) are also shown in Table 7.2. The (adj.R^2) denotes a high significant of the model and the (pred. R^2) indicates the agreement with the (adj.R^2). This model can be employed to navigate the design space.

Table 7.2 ANOVA output of the reflection coefficient in dry conditions (Significant)

Source	DF	Adj SS	Adj MS	F-Value	P-Value
Model	4	0.073035	0.018259	135.88	0.000
Linear	3	0.069698	0.023233	172.89	0.000
Speed	1	0.006876	0.006876	51.17	0.000
Depth	1	0.001216	0.001216	9.05	0.009
Feed	1	0.061606	0.061606	458.46	0.000
Square	1	0.003337	0.003337	24.83	0.000
Feed*Feed	1	0.003337	0.003337	24.83	0.000
Error	15	0.002016	0.000134		
Lack-of-Fit	10	0.001826	0.000183	4.80	0.049
Pure Error	5	0.000190	0.000038		
Total	19	0.075051			
R-Squared	0.9731				
R-Squared (adj)	0.9660				
R-Squared (pred)	0.9445				

DF: Degree of freedom Adj SS: Adjusted sum of square Adj MS: Adjusted mean square

Final equation in terms of significant factors for the reflection coefficient model in dry turning is given by Equation 7.2. These models take only the influential factors into account: It is worth to note that the regression equation is in uncoded values (see Table 5.5).

$$R_{Dry} = 1.2304 + 748 * 10^{-6}A - 1887 * 10^{-5}B - 4.695C + 9.43C^2 \qquad 7.2$$

where R: Reflection coefficient, A: cutting speed, B: cutting depth and C: feed.

7.3.4.2   Wet Cutting Conditions

The results of the ANOVA of reflection coefficient during wet turning are presented in Table 7.3. This table only shows the significant effect of the machining parameters on the reflection coefficient. It can be seen from Table 7.3 that the linear model of the machining parameters cutting speed (*A*) and cutting depth (*B*) have a significant influence on the reflection coefficient during wet cutting while feed (*C*) has a less effect on reflection coefficient compared to the other two machining parameters. Furthermore, the ANOVA analysis also showed that the quadratic values of cutting speed (*Speed*Speed*) and cutting depth (*Depth*Depth*) have a significant effect on the

reflection coefficient. Table 7.3 also shows the value of the determination coefficient (R^2) which indicates the goodness of data fit for the model, and the values of adjusted determination coefficient (adj. R^2) and predicted determination coefficient (pred. R^2) are also shown in Table 7.3. It is noticed to mention that the stepwise procedure added the interaction between cutting speed and feed during the procedure in order to maintain a hierarchical model at each step.

Table 7.3 ANOVA output of the reflection coefficient in wet conditions (Significant)

Source	DF	Adj SS	Adj MS	F-Value	P-Value
Model	6	0.026514	0.004419	33.08	0.000
Linear	3	0.015824	0.005275	39.49	0.000
Speed	1	0.010717	0.010717	80.23	0.000
Depth	1	0.003711	0.003711	27.78	0.000
Feed	1	0.001396	0.001396	10.45	0.007
Square	2	0.010360	0.005180	38.78	0.000
Speed*Speed	1	0.004810	0.004810	36.01	0.000
Depth*Depth	1	0.006473	0.006473	48.46	0.000
2-Way Interaction	1	0.000329	0.000329	2.47	0.140
Speed*Feed	1	0.000329	0.000329	2.47	0.140
Error	13	0.001736	0.000134		
Lack-of-Fit	8	0.001681	0.000210	18.93	0.002
Pure Error	5	0.000056	0.000011		
Total	19	0.028250			
R-Squared	93.85%				
R-Squared (adj)	91.02%				
R-Squared (pred)	73.73%				

DF: Degree of freedom Adj SS: Adjusted sum of square Adj MS: Adjusted mean square

Final equation in terms of significant factors for the reflection coefficient model in wet turning is given by Equation 7.3. The equation is in uncoded values (see Table 5.5).

$$R_{Wet} = 0.3686 + 0.005425A + 0.3045B + 0.228C - 2 \times 10^{-5}A^2 \\ - 0.0844B^2 - 0.00535AC \qquad \text{7.3}$$

where *R*: Reflection coefficient, *A*: Cutting speed, *B*: Cutting depth and *C*: Feed.

7.3.4.3 Comparison between the Experimental and Model Results of the Reflection Coefficient

In this section, a comparison has been introduced between the experimental (actual) results shown in Figure 7.18, and the results obtained from the derived Equations (7.2 and 7.3) (predicted results). Where the equations have been used to predict the reflection coefficient and how it is affected by the machining parameters within the

range given in the experimental design. The comparisons between these two values, actual and predicted values, at dry and wet cutting conditions are shown in Figure 7.23 and Figure 7.24, respectively. Very good agreement between the predicted and actual reflection coefficient is shown.
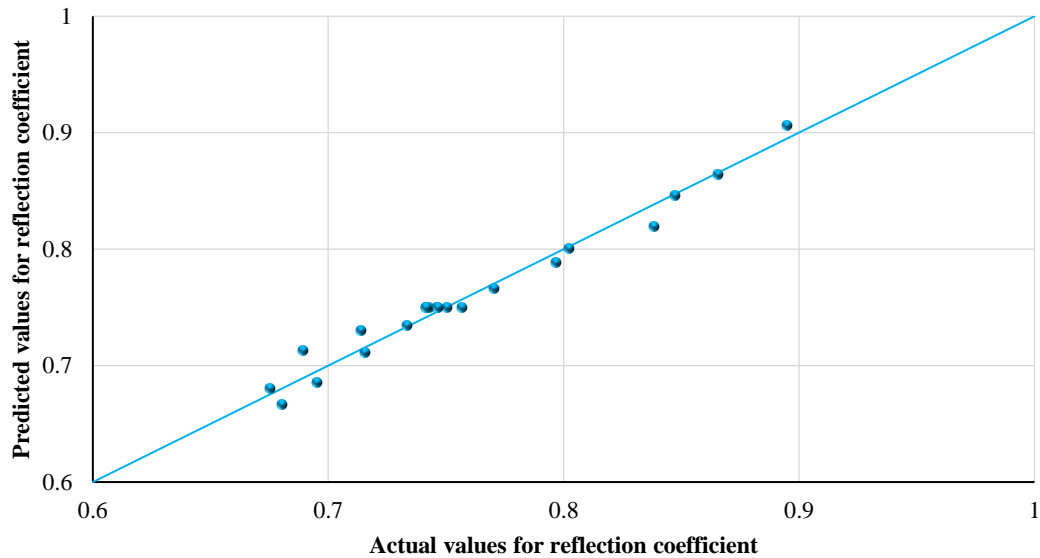
Figure 7.23 Experimental versus predicted values for reflection coefficient in dry condition, solid line indicates exact agreement
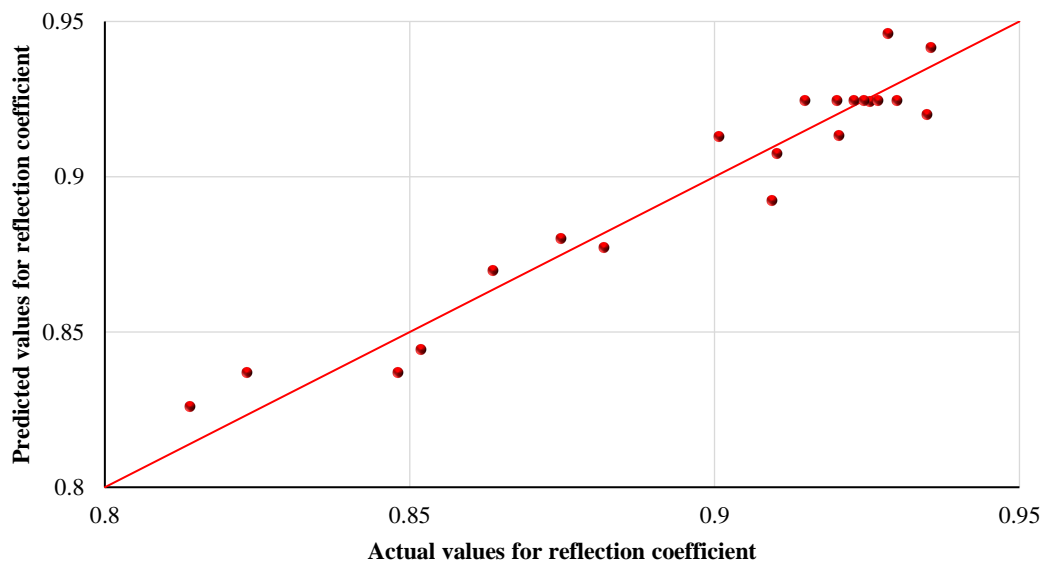
Figure 7.24 Experimental versus predicted values for reflection coefficient in wet condition, solid line indicates exact agreement

A comparison of the experimental results of reflection coefficient, during dry and wet machining of *Al 6082-T6* at different cutting speeds with a constant cutting depth and feed (*t*=2.5 *mm*, *f*=0.12 *mm/rev*), respectively, and the analytically predicted values

using Equations 7.2 and 7.3 are shown by scatter plots with smooth lines in Figure 7.25 and Figure 7.26. It can be seen clearly from the figures that the predicted reflection coefficient magnitudes are agreed well with the corresponding experimental results.
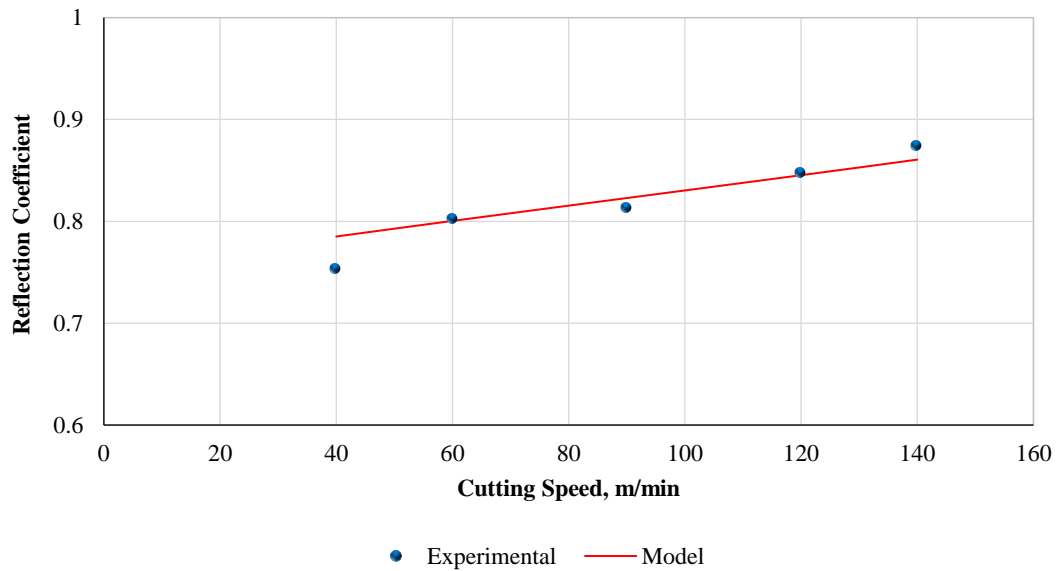
Figure 7.25 Comparison of experimental and predicted reflection coefficient during dry cutting of *Al 6082-T6* at different cutting speeds with a constant cutting depth and feed (*t=2.5 mm*, *f=0.12 mm/rev*).
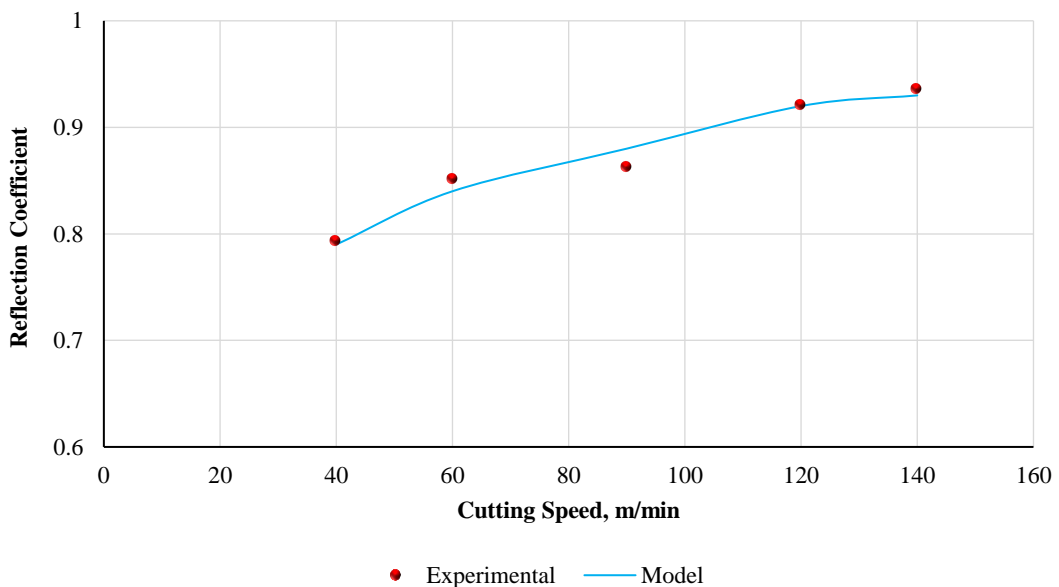
Figure 7.26 Comparison of experimental and predicted reflection coefficient during wet cutting of *Al 6082-T6* at different cutting speeds with a constant cutting depth and feed (*t=2.5 mm*, *f=0.12 mm/rev*).

7.3.4.4   Model Validation Experiments

Further to the experimental runs mentioned in Chapter 5 (Table 5.5) and results presented in a graphical manner in Figure 7.18, another set of orthogonal experiments (validation trials), as described in Chapter 6, have been carried out to validate and confirm the mathematical model, derived equations (7.2 and 7.3). The machining parameters for the validation trials and the results of these experiments are graphically presented in Figure 7.27. The results are also given in Appendix B (Table B.4).

Figure 7.27 shows the comparison between the predicted values from the model developed in the present study (Equations 7.2 and 7.3), with the values obtained experimentally. It can be seen from the results that analytical predicted reflection coefficient values agree well with the corresponding experimental results.
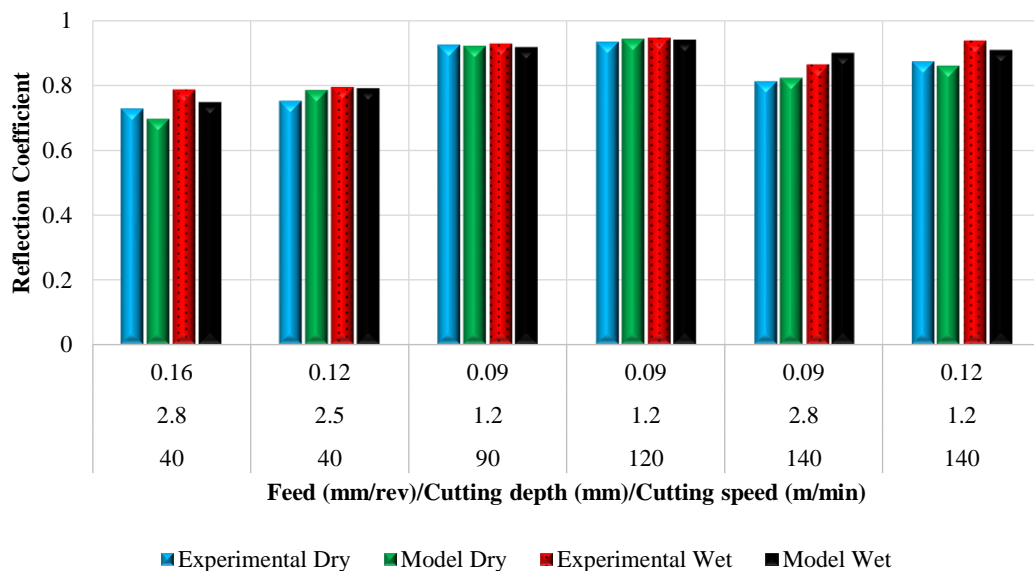
Figure 7.27 Comparison of the validation experiments and predicted results of reflection coefficient for dry and wet cutting conditions

The next section presents the influence of the machining parameters on the reflection coefficient, where from now on, all the results presented are obtained based on the model developed in the present work (Equations 7.27.3).

7.3.5   Reflection Coefficient Versus Cutting Parameters

This section presents the influence of changes in machining parameters including cutting speed, cutting depth and feed on the reflection coefficient. Where one figure

has been chosen for each machining parameter and the other figures are introduced in Appendix B.

7.3.5.1   Cutting Speed and Feed Versus Reflection Coefficient

Figure 7.28 shows the ultrasonic reflection results of the tool-chip interface during dry cutting of *Al 6082*. The figure shows the change in reflection coefficient with the change in cutting speed and feed used when the cutting depth is 2 *mm.* For the other cutting depth values see Appendix B (Figure B.1-Figure B.9). The most surprising correlation is with the tool-chip contact length; where according to the results the transmission of ultrasonic waves and reflection coefficient are directly related to the tool-chip contact length and thus the tool-chip contact area. It seems possible that these results are due to the increased contact length, there is a higher tendency of transmission of ultrasonic waves via the tool-chip interface. This results in a lower reflection coefficient.

On the other hand, the change in speed has an obvious influence on the reflection coefficient. As the speed increases the reflection coefficient increases. The observed increase in reflection coefficient could be attributed to the decrease of the tool-chip contact length with increasing cutting speed. At low speeds, the tool-chip contact area is much bigger than at higher speeds. Therefore, a bigger contact area results in higher reflection coefficient and a reduction in the transmission of ultrasonic waves as shown in Figure 7.28. The correlation between feed and reflection coefficient is interesting because at low feeds (0.09-0.12 *mm/rev*) the change in reflection coefficient is higher than the change at high feeds (0.2-0.23 *mm/rev*) and this is exactly what has been observed in the tool-chip contact length results in Chapter 6.

Figure 7.29 shows the ultrasonic reflection results of the tool-chip interface during wet cutting conditions of *Al 6082*. The figure shows the change in reflection coefficient with the change in cutting speed and feed used when the cutting depth is 2 *mm.* The data reveals that the reflection coefficient increases with increasing cutting speed. This results confirm the penetration of the cutting fluid into the interface at higher cutting speed, where the pressure on the rake face decreases with increasing cutting speed and thus a high reflection coefficient was recorded (wet well)
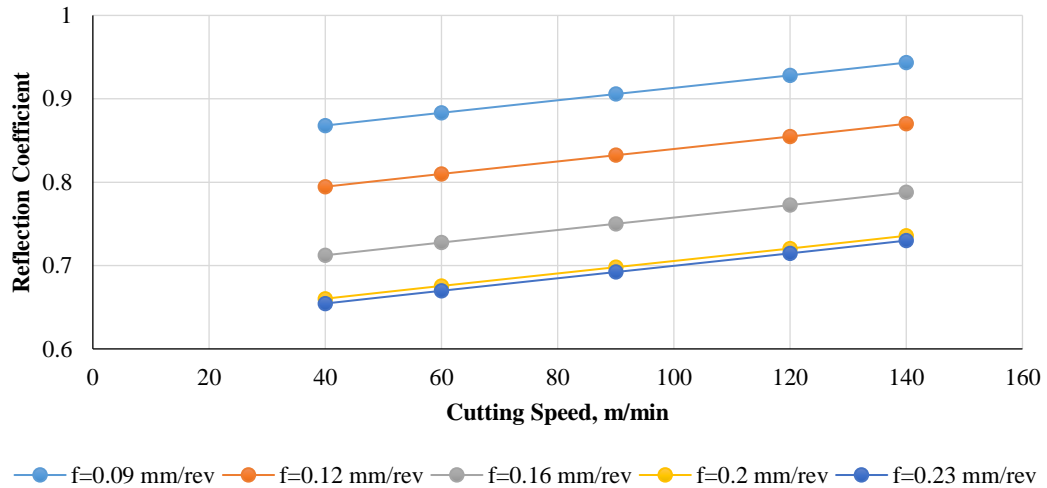
Figure 7.28 Reflection coefficients versus cutting speed at dry condition for different feed at a constant cutting depth of (*t=2 mm*)
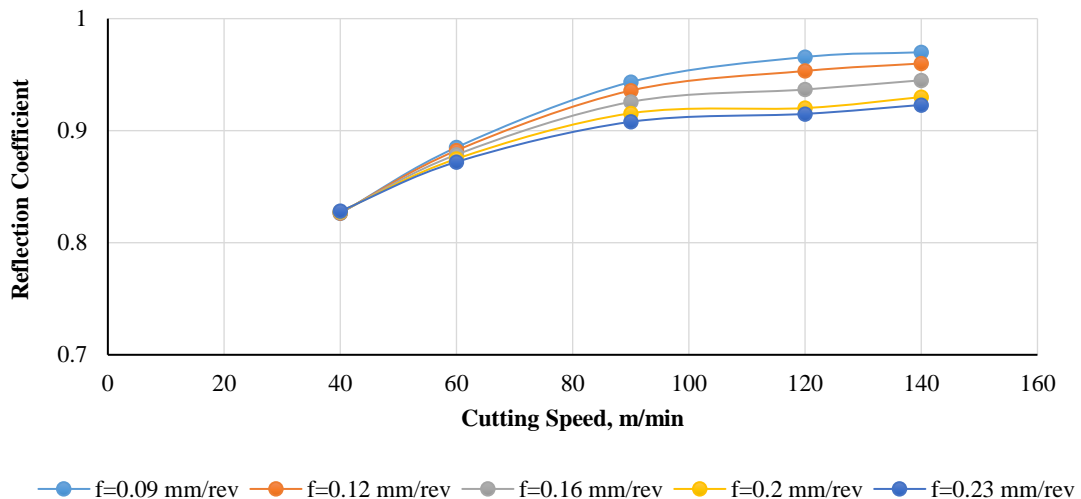
Figure 7.29 Reflection coefficients versus cutting speed at wet condition for different feed at a constant cutting depth of (*t=2 mm*)

7.3.5.2   Cutting Speed and Cutting Depth Versus Reflection Coefficient

Figure 7.30 shows the change in reflection coefficient with the change in cutting speed and cutting depth used at a constant feed of 0.16 *mm/rev*. For the other feed values see Appendix B (Figure B.10-Figure B.18). It can be seen from Figure 7.30, that the minimum value of reflection coefficient is 0.696 when the cutting depth is the maximum (*t=2.8 mm*) and the cutting speed is the minimum (*V=40 m/min*). With a high cutting depth, a low reflection coefficient is recorded. For example, at a speed of 40 *m/min*, the reflection coefficient changes from 0.728 at a cutting depth of 1.2 *mm* to 0.696 at a cutting depth of 2.8 *mm*. This result may be explained by the fact that

increasing cutting depth results in increasing the tool-chip contact area and more transmission of waves through the interface, therefore, lower reflection coefficient is recorded.

The change in cutting depth does not have a significant effect on the reflection coefficient under the conditions used in this study. However, there is a slight change in reflection coefficient on the basis of change in the cutting depth. These results are consistent with data obtained in Chapter 6, where the cutting depth does not have a significant effect on the tool-chip contact length.
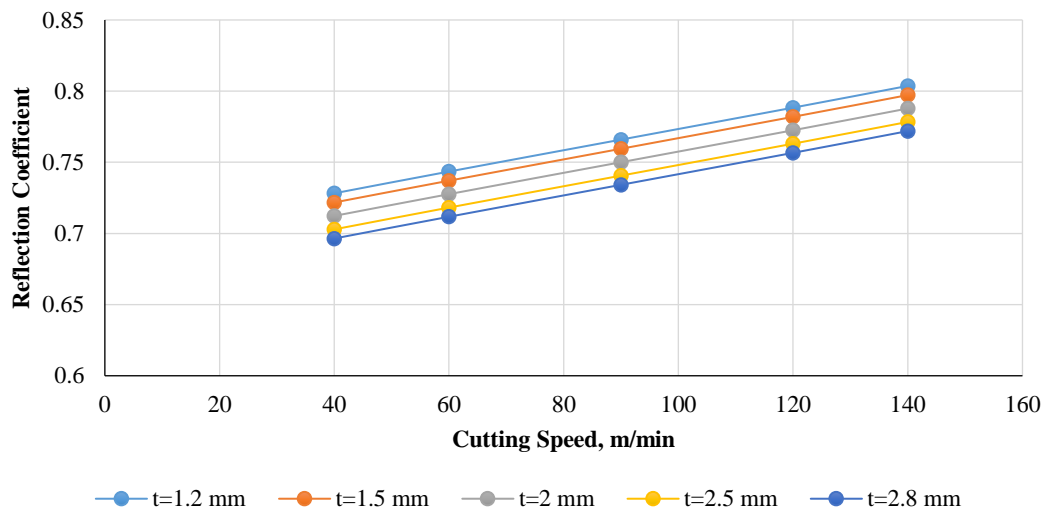
Figure 7.30 Reflection coefficients versus cutting speed at dry condition for different cutting depth at a constant feed of (*f*=0.16 *mm/rev*)

Figure 7.31 shows the ultrasonic reflection results during wet cutting. The figure shows the change in reflection coefficient with the change in cutting speed and depth with a constant feed.
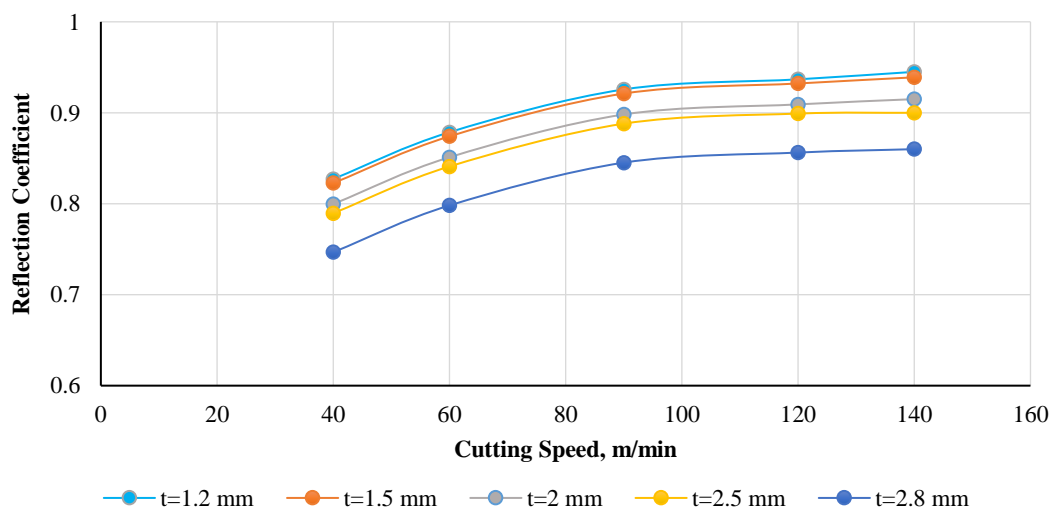
Figure 7.31 Reflection coefficients versus cutting speed at wet condition for different cutting depth at a constant feed of (*f*=0.16 *mm/rev*)

170

7.3.5.3   Cutting Depth and Feed Versus Reflection Coefficient

Figure 7.32 shows the effects of changes in feed and cutting depth on the reflection coefficient, in dry cutting conditions, at a constant cutting speed of 90 *m/min*. For the other feed values of cutting speeds see Appendix B (Figure B.19-Figure B.27). It is apparent from this figure that the minimum value of reflection coefficient is 0.676 when the cutting depth is the maximum (*t*=2.8 *mm*) and the feed is the maximum (*f*=0.23 *mm/rev*). While the maximum value of reflection coefficient is 0.922, this value was observed when was both the cutting depth and feed are minimum (*t*=1.2 *mm*, *f*=0.09 *mm/rev*). The results, as shown in Figure 7.32, indicate that the change in feed significantly influences the reflection coefficient. As the feed increases the reflection coefficient decreases and ranges from 0.922 at a feed of 0.09 *mm/rev* to 0.708 at the feed of 0.23 *mm/rev* at a cutting depth of 1.2 *mm*.

These results also show that the change in cutting depth has little effect on the reflection coefficient under the set of conditions used in this study.
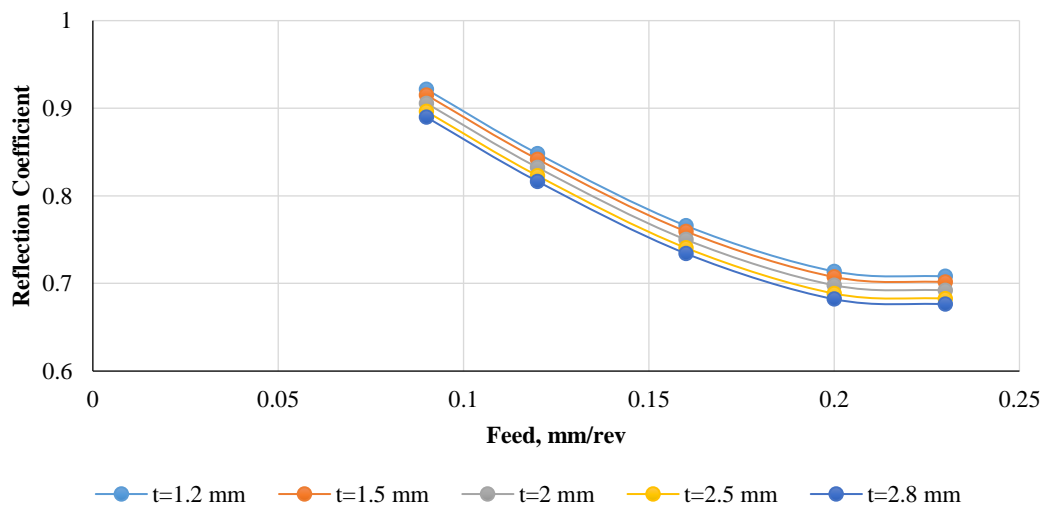
Figure 7.32 Reflection coefficients versus feed at dry condition for different cutting depth at a constant cutting speed of (*V*=90 *m/min*)

Figure 7.33 presents the correlation between reflection coefficient and feed in wet cutting conditions. It can be seen from the figure that the reflection coefficient decreases with increasing feed at a constant cutting speed.
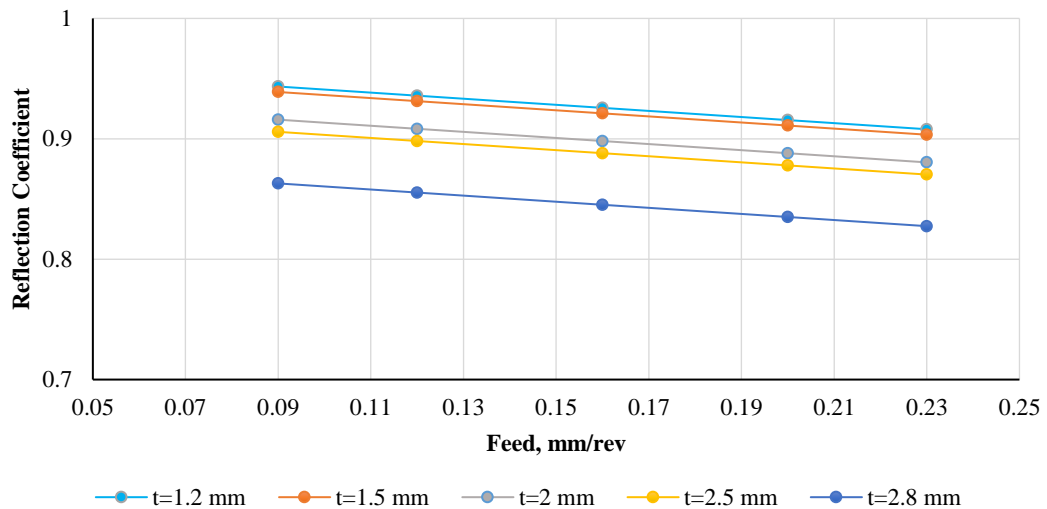
Figure 7.33 Reflection coefficients versus feed at wet condition for different cutting depth at a constant cutting speed of (*V*=90 *m/min*)

7.4 Conclusions

This study set out to monitor the interface between the cutting tool and chip using a novel ultrasonic technique. The ultrasonic transducer was located on the opposite side of the rake face cutting tool so that the sound waves were propagated through the cutting tool insert and the reflections were recorded as the chip passed over the rake face (tool-chip contact area). A set of experiments was conducted at different cutting conditions and the average value of the reflection coefficient was reported. Based on the work conducted in this chapter, the following conclusions can be drawn:

- This study has shown the ability to use the ultrasonic reflection in the metal cutting to investigate and monitor the tool-chip interface in both dry and wet machining.

- The change in the shape of the ultrasonic data stream is related to the chip segmentation and to the irregular movement of the chip on the rake face of the cutting tool and also to the existence of the BUE.

- The dry machining results of this study indicate that feed has the most significant affect on reflection coefficient followed by cutting speed whereas cutting depth has the lowest effect. It is likely that this is due to the tool-chip contact length which is significantly affected by feed while the effect of cutting depth on the contact length was very small. While the wet machining results

indicate that cutting speed and cutting depth have the most significant effect and feed has a lower effect.

- Reflection coefficient increases with increasing cutting speed and decreases with increasing cutting depth and feed. This results may be explained by the fact that tool-chip contact area is decreased with increasing cutting speed and increased with increasing cutting depth and feed. If the contact area is smaller, then more of ultrasonic energy is reflected back from the rake face (high reflection coefficient) and vice versa. Another possible explanation for the increase in reflection coefficient with increasing in cutting speed is due to the chip pressure that applied to the rake face cutting tool, where increasing cutting speed leads to decreasing the pressure/force which results in reflecting back more ultrasonic energy from the rake face. The same reason is true for the reduction in reflection coefficient with increasing cutting depth and feed, where increasing cutting depth and feed lead to increasing the pressure which results in transmitting more ultrasonic energy to the chip through the interface and thus low reflection coefficient.

- The reflection coefficient values are higher when coolant is applied than when dry condition is performed. These results are likely to be related to the pressure on the rake face cutting tool. The pressure is lower in wet cutting than in dry cutting. In wet condition, a low pressure is applied on the rake face which results in transmitting a low energy to the chip through the tool-chip interface and more energy is reflecting back from the cutting tool thus a high reflection coefficient is recorded.

8

Analysis and Discussion of Experimental Results

The aim of this chapter is to examine the results that were presented in Chapter 6 and 7 and discuss the relationships that exist between the reflection coefficient and the machining process. The chapter will focus on key correlations that were observed and physical mechanisms that have been deduced.

8.1 Reflection Coefficient Variation with Contact Area

High tool-chip contact area, or high pressure applied by the chip on the rake face cutting tool result in low reflection coefficient. This section presents the relationship between reflection coefficient and contact area while the next section will introduce the relationship between reflection coefficient and cutting forces.

Figure 8.1 presents the correlation between reflection coefficient and tool-chip contact area in both dry and wet cutting conditions. In dry cutting conditions, there is a clear trend of decreasing reflection coefficient with increasing tool-chip contact area as shown in Figure 8.1. These relationships may be explained by the decrease in the ultrasonic energy which is reflected back from the rake face cutting tool as a result of the increase in contact area, where more of ultrasonic energy was transmitted through the tool-chip interface.
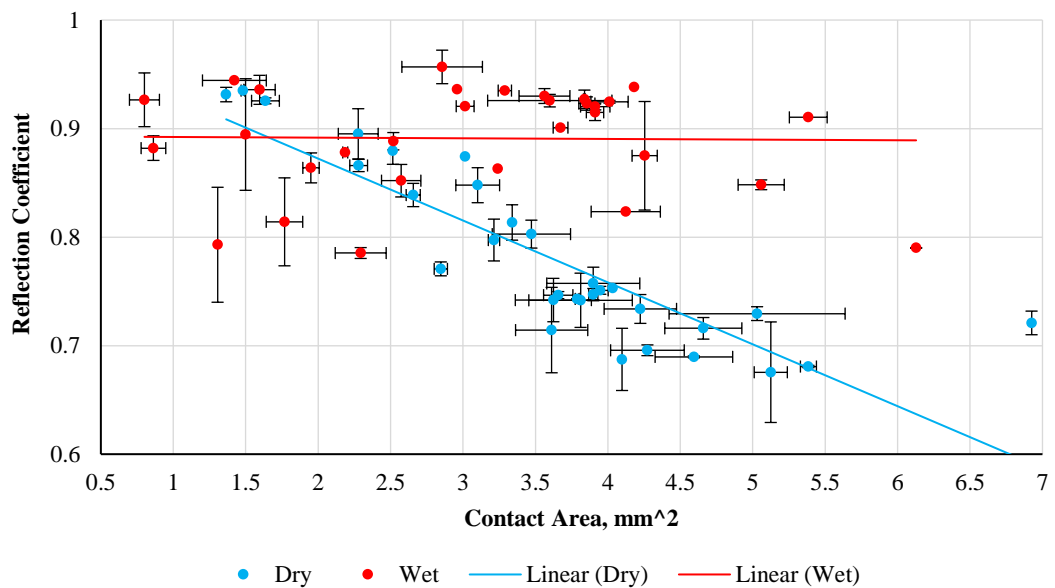
Figure 8.1 Correlation between the reflection coefficient vs contact area at dry and wet cutting

In wet cutting conditions, surprisingly, no decrease in reflection coefficient was detected with increasing in the contact area. Reflection coefficient seems to be not affected by the contact area. One explanation for this might be that cutting fluid caused the chip to lift from the rake face, where the cutting fluid nozzle was directed on the interface between the cutting tool and chip not on the top face of the chip, then only one part of the tool-chip contact length was in contact to the rake face and thus less energy was transmitted to the chip.

175

Another possible explanation for reflection coefficient not affected by contact area in wet conditions is that the cutting fluid may fill the gap outside the cutting tool and chip interface when the contact area is smaller so reflection coefficient does not change much (see Figure 8.2).
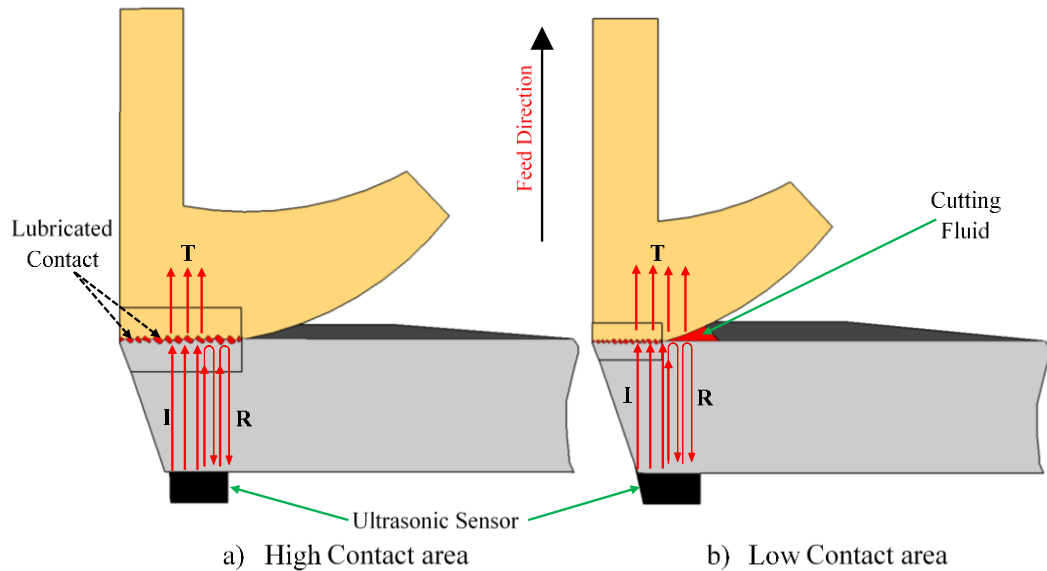
Figure 8.2 Schematic diagram of the reflection signals of the different possible contact area at wet cutting conditions (I: incident wave, T: transmitted wave and R: reflected wave).

Another possible explanation for the wet results is the existence of BUE on the cutting edge, as highlighted in Chapter 6, in wet cutting the results reveal that the BUE existence under all the cutting speeds applied in this study except at a cutting speed of 140 m/min. Where chip was supported by the BUE, it creates a gap between the tool and chip which caused a high reflection coefficient.

Figure 8.3 shows a schematic diagram which illustrates the reflection signals at the BUE during wet conditions. Furthermore, the BUE caused the creation of another interface which is between the BUE and chip. Therefore, some of the ultrasonic energy was reflected from the tool-BUE interface and some was reflected from the BUE-chip interface as shown in Figure 8.4.
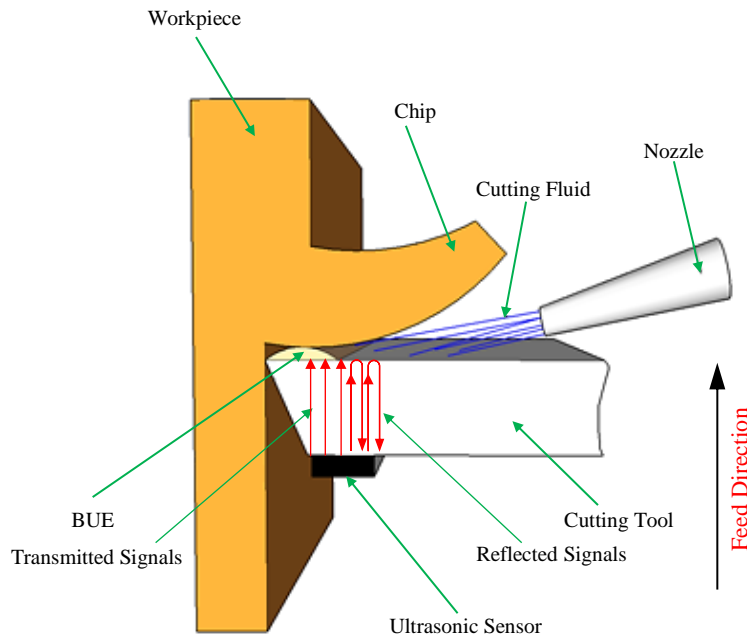
Figure 8.3 Schematic diagram showing the reflection signals with existence a built up edge

a) No BUE   b) BUE
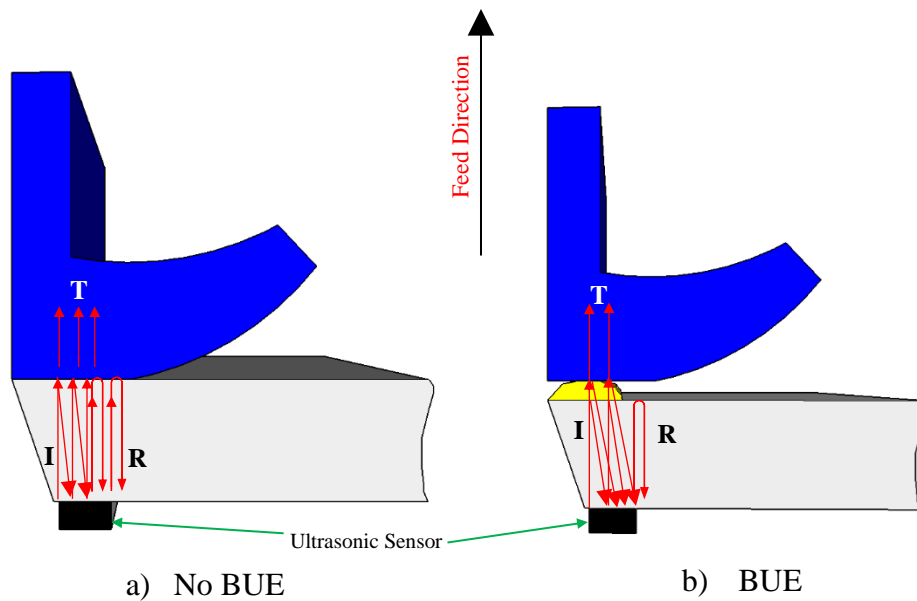
Figure 8.4 Schematic diagram of the reflection signals with and without built up edge (I: incident wave, T: transmitted wave and R: reflected wave)

8.2 Reflection Coefficient Variation with Cutting Forces

As discussed in the previous section, low reflection coefficient means high pressure has been applied on the rake face cutting tool, and vice versa, this section presents the relationship between reflection coefficient and cutting forces. Figure 8.5 and Figure 8.6 show the correlation between reflection coefficient and thrust force F_t and cutting force F_c, respectively, in both dry and wet cutting conditions. In both cutting

conditions, there is a clear trend of decreasing reflection coefficient with increasing cutting forces as shown in Figure 8.5 and Figure 8.6.

The correlation between reflection coefficient and cutting forces are interesting because as the cutting forces increase more pressure is applied on the rake face which results in more ultrasonic energy is transmitted through the interface and low reflection coefficient was recorded and vice versa (i.e. higher reflection coefficient means lower pressure applied on the face) (see Figure 8.7 and Figure 8.8).
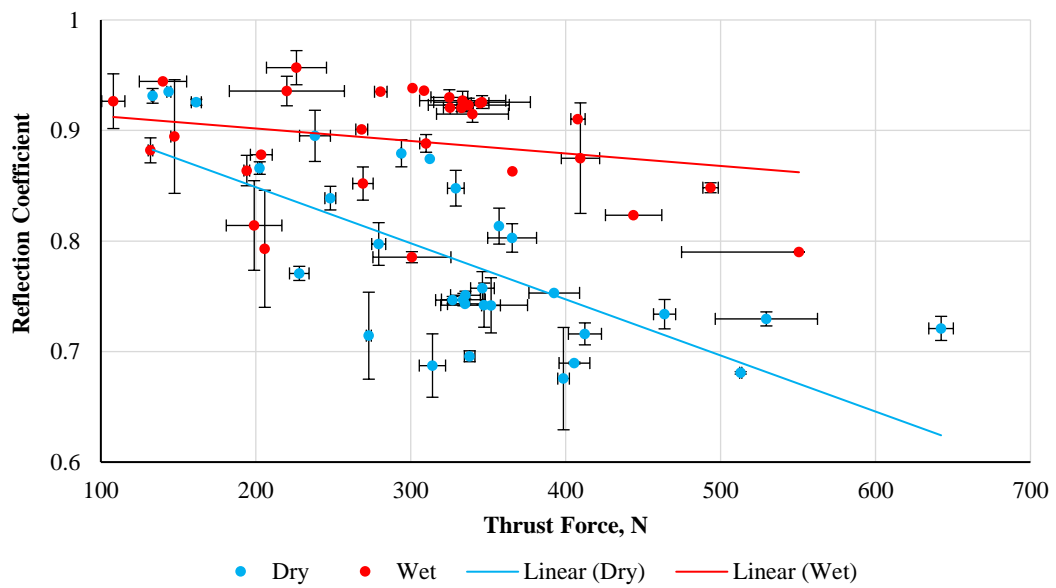
Figure 8.5 Correlation between the reflection coefficient vs thrust force at dry and wet cutting
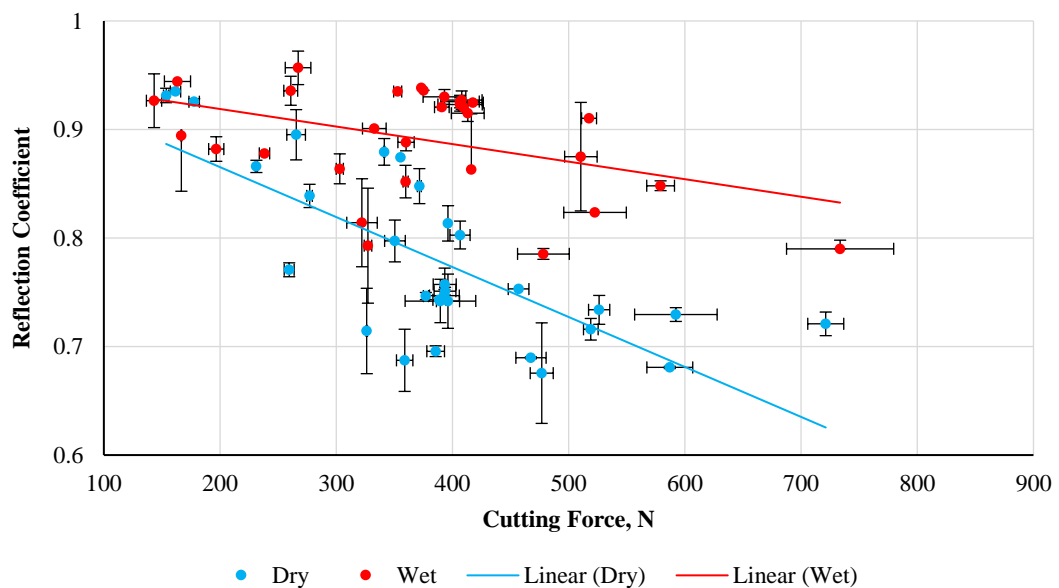
Figure 8.6 Correlation between the reflection coefficient vs cutting force at dry and wet cutting
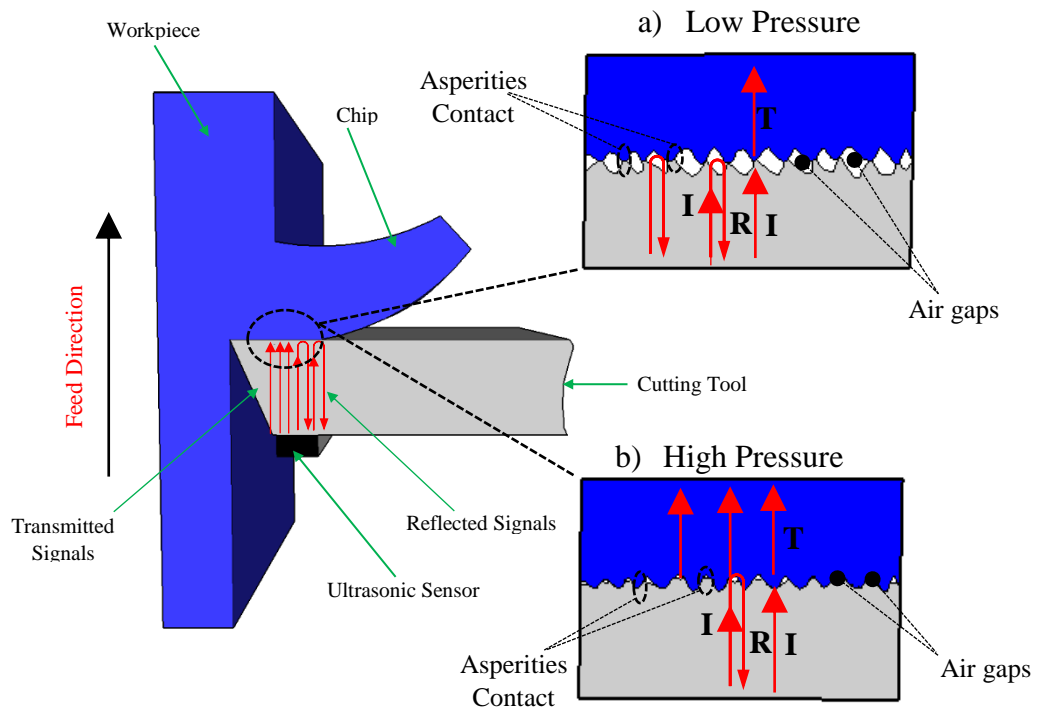
Figure 8.7 Schematic diagram of the reflection signals of the different possible contact conditions at the tool-chip interface at dry cutting conditions (I: incident wave, T: transmitted wave and R: reflected wave).
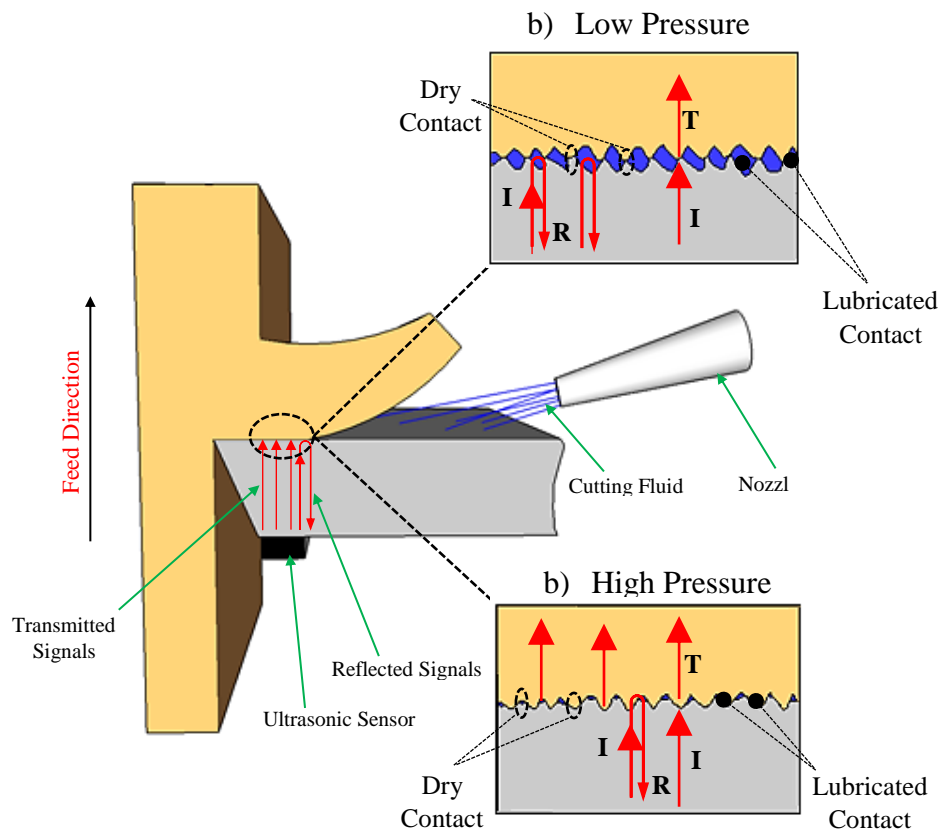
Figure 8.8 Schematic diagram of the reflection signals of the different possible contact conditions at the tool-chip interface at wet cutting conditions (I: incident wave, T: transmitted wave and R: reflected wave).

179

From the data in Figure 8.5 and Figure 8.6, it can be seen clearly that there was a significant difference between the two conditions with respect to the reflection coefficients. Where with applying cutting fluid, the reflection coefficients were higher than when the dry cutting was conducted. As highlighted before, there are several possible explanations for this result. Obviously, a first possibility is that there could be due to the existence of a film layer of cutting fluid that penetrated to the tool-chip interface. In this case, the tool-chip contact was separated by a thin film of cutting fluid, therefore, the incident ultrasonic waves were reflected back from the tool-oil-chip interface and thus a higher reflection coefficients were recorded.

Another possible explanation for the significant difference in reflection coefficients between both dry and wet cutting conditions is due to the type of chip. Where with applying cutting fluid the chips were discontinuous and thus detaching the tool rake face earlier and high reflection coefficients were observed while in dry condition the chips were continuous and therefore stayed more on the tool rake face and thus low reflection coefficients were recorded (see Figure 8.9). Existence of the BUE and the mechanism of cutting fluid are the other reasons for this significant difference (see Figure 8.2 and Figure 8.4).

c) Continuous Chip   c) Discontinuous chip
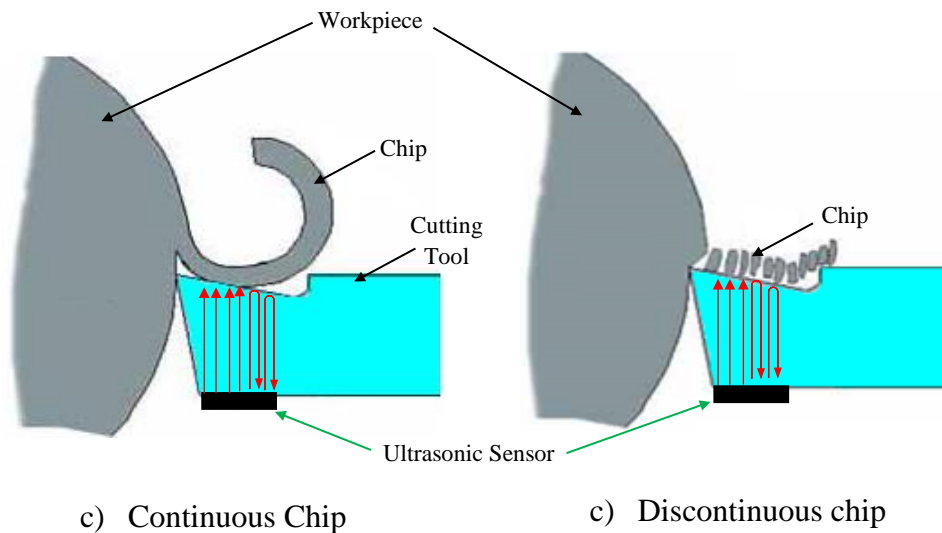
Figure 8.9 Schematic diagram of the reflection signals in different chip types

180

8.3 Reflection Coefficient Variation with Specific Cutting Forces

The specific cutting forces, which represent the energy required to remove a unit area of workpiece material, is calculated by dividing the cutting forces by the undeformed chip cross-section area (i.e. feed times cutting depth).

Figure 8.10 and Figure 8.11 show the correlation between reflection coefficient and specific thrust force K_t and specific cutting force K_c, respectively, in both dry and wet cutting conditions. The most striking result to emerge from the data is the correlation between reflection coefficient and specific cutting forces, where in the both cutting conditions, there is a clear trend of increasing reflection coefficient with increasing specific cutting forces as shown in Figure 8.10 and Figure 8.11. The data also showed that the specific cutting forces were higher in wet cutting conditions. This correlation is interesting because an increase in the specific cutting forces is usually related to the occurrence of a built-up edge (BUE). As highlighted before, using cutting fluid tends to cool the machined material and thus promote BUE compared to dry cutting (see Figure 8.3 and Figure 8.4). That's why reflection was higher in wet cutting whatever the conditions. And then, when Kc increases, this phenomenon is amplified and reflection increases even more.
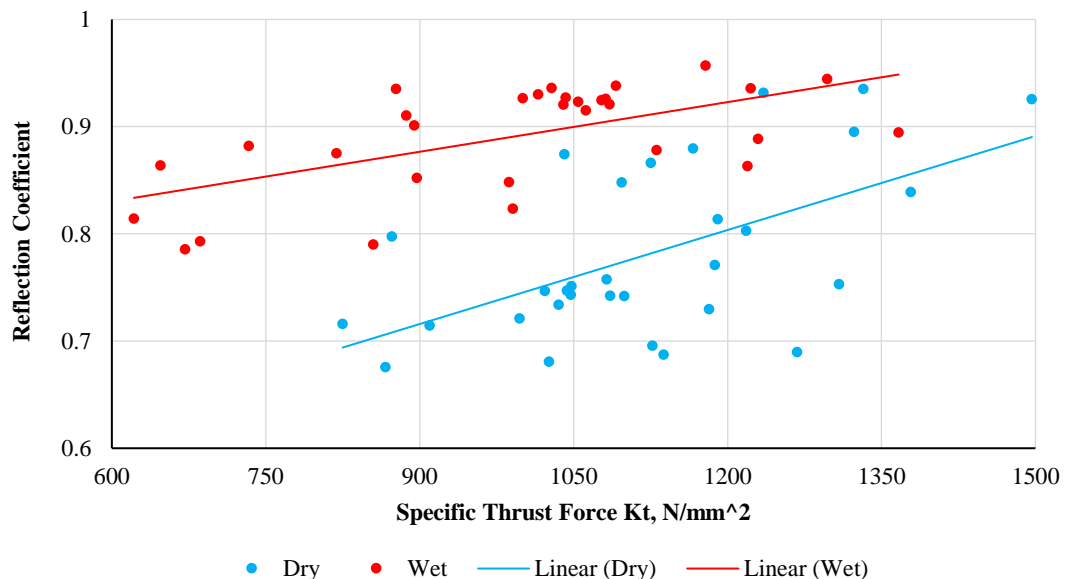
Figure 8.10 Correlation between the reflection coefficient vs specific thrust force at dry and wet cutting conditions
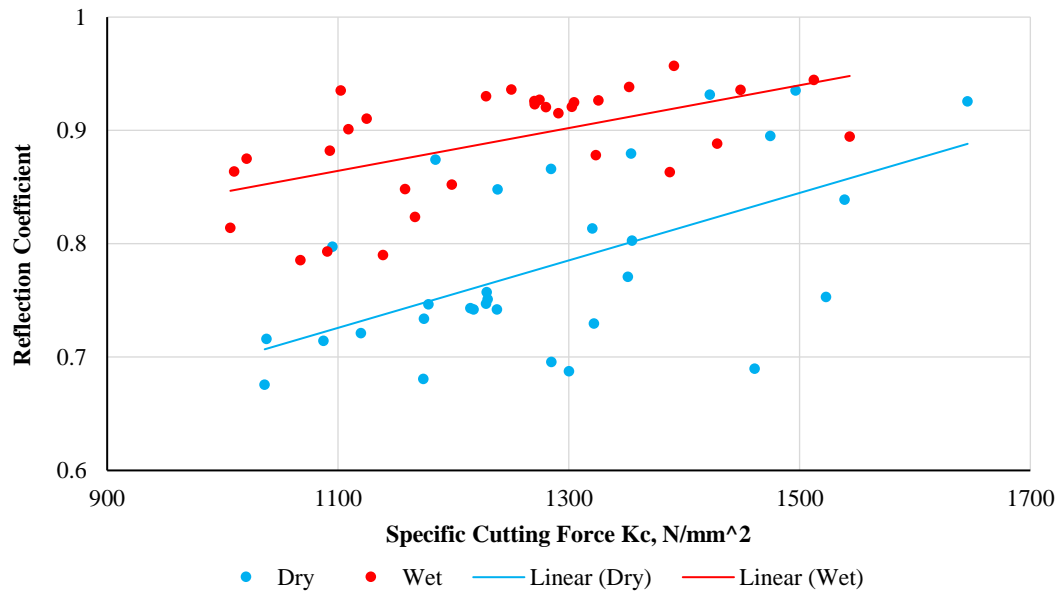
Figure 8.11 Correlation between the reflection coefficient vs specific cutting force at dry and wet cutting conditions

8.4 Conclusions

The present study was designed to determine the ability to use the ultrasonic reflection in the cutting process as a new technique to monitor the tool-chip interface. The aluminium alloy *6082* was selected for this study as the work material. The study of the ability was conducted by correlating the reflection coefficients results with tool-chip contact area and cutting forces results as well as with specific cutting forces. The observed correlation between ultrasonic reflection and machining process can be given as follows:

- The observed correlation between reflection coefficient and tool-chip contact area in dry cutting conditions might be explained by the fact that, with increasing the contact area between cutting tool and chip more ultrasonic energy was transmitted to the chip through the tool-chip interface and thus low reflection coefficient were observed.

- In wet conditions, the contact area made no significant difference to reflection coefficient. The existence of BUE and the mechanism of applying the cutting fluid may explain the correlation between reflection coefficients and tool-chip contact area.

- The second major finding of this study was the relatively good correlation between reflection coefficients and cutting forces. Where the data show that

reflection coefficient decreases with increasing cutting forces in both cutting conditions. The increase in cutting forces led to an increase in the asperity contact between the tool and chip and reduction the air gaps between them and this result in reflecting less ultrasonic energy through the interface.

- Measured specific forces reveal that at wet conditions, specific cutting force is higher than in dry conditions due to existence BUE. Where at dry cutting, specific cutting forces was lower due to thermal softening and material flow softening behavior at higher strain rates. This factor may partially explain the apparent differences between the reflection coefficients in dry and wet cutting conditions.

9

Conclusions and Recommendations

This chapter is divided into two parts; the first part highlights the conclusions drawn from the present study on the cutting forces and chip morphology and the use of a novel ultrasonic technique for monitoring the cutting conditions. The last part of this chapter presents some suggestion for the improvements to the method and possible future work.

9.1 Conclusions

The following conclusions can be drawn from the present study

9.1.1   Chip Morphology

An experimental campaign of orthogonal cutting in turning on aluminium *6082* cylindrical tubes was designed and conducted by considering different machining parameters in order to monitor the tool-chip interface in both dry and wet cutting conditions. A centre composite design (CCD) technique was used to conduct these experiments. For every cutting trial, chips were collected in order to measure the chip cross-section and investigate its morphology. A ball micrometre gauge was used to measure the chip thickness while the width was measured using a Vernier calliper. Both chip thickness and width were measure at six different locations along the chip length and an average was recorded. An SEM was used to examine the existence of BUE on the chip.

The main results of the investigations as follows:

9.1.1.1 Chip Thickness

- For dry cutting conditions, chip thickness reduces with cutting speed and cutting depth; this is a temperature effect. With increasing cutting speed, the temperature at the tool-chip interface increases and leads to softening of the workpiece and hence a reduction in tool-chip interface friction. Both these two factors increase the shear angle and thus decrease the chip thickness.
- Chip thickness increases with increasing feed at dry condition. The results of this study show that feed has the most significant affect on chip thickness followed by cutting speed whereas cutting depth has the lowest effect.
- The experimental results show that whether or not coolant application decreases, chip thickness depends on whether the cutting was at low or high cutting speed. At low speed (*V*<90 *m/min*), coolant application results in an increase in the chip thickness, whereas at high cutting speed (*V*>90 *m/min*) coolant application has a negligible effect on chip thickness.
- At low cutting speed (*V*<90 *m/min*), the chip thickness is affected by cutting fluid where it was thinner than in dry condtions. While at cutting speed higher

than 90 *m/min*, there was no significant effect of cutting fluid on the chip thickness.

- Chip width is larger than the machined ring thickness due to the significant side flow or strain in the direction of the width.

9.1.1.2 Contact Length

- The study has confirmed the findings of Kato et al. (1972) and Toropov & Ko (2003) model which found that the tool-chip contact length is twice the deformed chip thickness.

- This study has found that the tool-chip contact length reduces as cutting speed and cutting depth increase. These relationships may be explained by the effect of temperature, with increasing cutting speed the temperatrure increased and this caused softening the workpiece material and hence the friction between tool and chip decreases. These result in increasing the chip velocity and thus reducing the contact length.

- The result also found that the contact length increases with increasing feed. These results are likely to be related to the size of the primary shear zone. Where the thickness of the primary shear zone increases with increasing feed and the strain rate at the zone decreases.

9.1.1.3 Built-Up Edge (BUE)

- The present study provides additional evidence with respect to the heat flux to the cutting tool where with increasing cutting speed the cutting tool shares heat decreasingly.

- The present work confirms previous findings and contributes additional evidence that suggests the capability of confirming the existence of the BUE on the underside of the chip.

- During the cutting of aluminium *6082*, BUE occurs with or without cutting fluid. However, the application of cutting fluid increases the threshold at which BUE occurs.

- The empirical findings in this study show that the BUE decreases with increasing the cutting speed. This is due to the chip flow rate which is increased with increasing cutting speed and thereby reducing the likelihood of the

breakaway material to adhere to the chip. Another possible explanation for this result is due to the increase in temperature which results in weakening of the BUE structure and eventually breakdown.

9.1.2   Cutting Forces

A dynamometer was used in this study to measure the cutting force F_c and thrust force F_t and below are the main results of the investigation:

- Under dry cutting, thrust force (F_t) and cutting force (F_c) are seen to decrease with increasing cutting speed at a constant cutting depth and feed. This is due to softening of work material resulting from an increase in temperature at the tool-chip interface when the cutting speed is increased. Where the increase in temperature leads to decreasing the shear strength of the workpiece and reducing the cutting forces.

- At cutting speeds <90 *m/min*, F_t and F_c are smaller when coolant is applied than under dry conditions. This is because at low cutting speeds, when the tool temperature is not too high, the coolant act as a lubricant and reduces the friction at the contact areas between the tool and workpiece.

- At cutting speeds >90 *m/min*, the results show that the role of cutting fluid is considered negligible. Where the cutting fluid has a less time to penetrate the asperities contact between the tool-chip; therefore, the cutting fluid will be less effective.

- The feed force is more affected by the coolant than the cutting force. This is due to the decrease in friction between the tool and chip.

- As cutting speed increases, a large amount of the heat generated during the cutting process is carried away by the chip and a small amount goes into the tool and workpiece. Because the temperature measured in this study is that of the tool, where the temperature decreased with increasing cutting speed but the temperature of the interface is still too high and this the reason of the high cutting forces at higher cutting speed.

- In wet conditions, cut chip thickness is much smaller, in the same cases where a force difference was seen.

9.1.3   The Use of Ultrasound for Tool-Chip Interface Monitoring

This is the first study reporting a possibility of using the ultrasonic reflection for monitoring the tool-chip interface in orthogonal cutting. A 10 *MHz* piezoelectric transducer was coupled to the underside of a cutting tool insert so that ultrasonic pulses passed through the insert and reflected from the tool-chip interface and received by the same transducer. Initially (before machining), a signal is reflected from the tool-air contact when there is no chip. This reflected pulse is used as a reference signal. This reference signal was compared to the ultrasonic signal that reflected from the tool-chip interface, during machining process, to measure reflection coefficient. To overcome the problem that the piezo-electric element was temperature sensitive, a thermocouple was positioned close to the ultrasonic transducer. A LabVIEW program was used for processing the temperature compensation.

A set of orthogonal cutting experiments was conducted in order to investigate the effect of the machining parameters on the tool-chip interface, in both dry and wet cutting conditions, using the ultrasonic reflection. A centre composite design (CCD) technique was used in this study to carry out these experiments. It was therefore possible to obtain ultrasonic measurement across a range of cutting parameters during such instances.

The main results of the investigations as follows:

- Observations have been made on the ultrasonic measurements taken during orthogonal cutting of *Al 6082-T6* under different cutting parameters. Different features were highlighted that related to the tribological condition at the tool-chip interface.
- This study has shown the capability of ultrasonic reflectometry in the investigation and monitoring the tool-chip interface in the metal cutting process.
- One interesting finding in this work is the change in the shape of the ultrasonic data stream is related to the irregular movement of the chip on the rake face of the cutting tool. Where the direction of chip flow is changed in second parts, usually advantageously with the spiral pitch being increased, depends upon the cutting condition. Due to the spiral movement of the chip, the flow of the chip

will be unstable on the rake surface. Sometimes the chip is close to the rake surface i.e. contact area is high and low reflection coefficient was recorded or it can be far from the rake surface and hence contact area is reduced and thus high reflection coefficient was recorded.

- The lowest reflection coefficient value was recorded at higher feed (*f*=0.23 *mm/rev*) in dry cutting condition. Where at higher feed the contact area is higher and hence more ultrasonic energy is transmitted to the chip and thus low reflection coefficient was recorded.

- The results of this study indicate that feed has the most significant affect on reflection coefficient followed by cutting speed whereas cutting depth has the lowest effect. It is likely that this is attributed to tool-chip contact length which was significantly affected by feed while the effect of cutting depth on the contact length was very small.

- As the cutting speed increased, more ultrasonic energy was found to reflect from the rake face of the cutting tool. This is due to the decrease in the tool-chip contact area and thus high reflection coefficients were recorded.

- The ultrasonic energy that transmitted through the tool-chip interface was found to increase with increasing feed and cutting depth. This could be attributed to the increase in contact area thus less ultrasonic energy was reflected from the rake face and a low reflection coefficient was recorded.

- This study has also shown that with increasing cutting forces more ultrasonic energy was trasmmitted into the chip through the interface and thus a low reflection coefficient was observed. This result may be explained by the fact that with increasing cutting forces, more pressure is applied on the rake face that leads to reduce the air gaps between the chip and cutting tool and thus more ultrasonic energy is transmitted through the interface and low reflection coefficient is recorded and vice versa.

- The reflection coefficient values are higher when the cutting fluid was applied than when the dry condition was performed. It seems possible that these results are due to the penetration of the cutting fluid to the tool-chip interface. Another possible explanation for this is that the chip detaches the rake face earlier than in dry condition. Where with applying cutting fluid the chip was discontinuous and thus detaching the tool rake face earlier while in dry condition the chip was

continuous (i.e. the chip stayed more on the tool rake face) and low reflection coefficient was recorded.

9.2 Recommendations for Future Work

In this thesis, a novel technique based on the reflection of ultrasound was developed for monitoring the cutting tool-chip interface in both dry and wet cutting conditions. The technique shows significant promise as an effective tool to monitor the interface, non-invasively, in machining process. Possible future work outlined in this section could help to improve and build confidence on the current capability of the system.

9.2.1   Reflection Coefficient Fluctuation with Time

As highlighted before, the oscillation in reflection coefficient that is observed at the tool-chip interface is due to the chip segmentation (see Figure 7.15 and Figure 7.17). It would be worthwhile to investigate the movement of the chip on the rake face cutting tool and the chip segmentation by using a high-speed camera and trying to correlate it to the reflection coefficient. More information on the chip segmentation and chip movement would help establish a greater degree of accuracy on this matter.

9.2.2   Wet Cutting Conditions

Using the test rig developed in this study, further experimental investigations are needed to investigate the role and the effect of cutting fluid on reflection coefficient. To gain further understanding, it would be interesting to assess the effects of using different oil, as a cutting fluid, on the ultrasonic reflection waves. Moreover, future trials should assess the impact of using different method for lubrication namely minimum quantity lubrication (MQL) on the reflection coefficient.

9.2.3   Industrial Relevance of Findings

The findings of this study have a number of important implications for future practice in industries. The benefit of this technique is that it provides in-process evidence about what is happening at the tool-chip interface during machining. Therefore, it could be a new way for monitoring the cutting process including tool wear, contact length and vibration. The finding of this research could also be used for simulation software to predict other parameters. Another important practical implication is that could be used

instead of dynamometer to measure cutting force, where it is much cheaper than a dynamometer. This is could be especially useful for large scale production as a monitor of machining process.

In this study, the ultrasonic sensor was placed underneath the cutting tool insert, so it was not possible to change the cutting tool insert in each experiment; therefore, in order to improve the capability of the technique used in this study and to make it industrial scale and more generic, further investigations are needed to change the location of the sensor and trying to embed the sensor to the machine tool so it will be more generic.

Last but not least, extending the ultrasonic reflection technique to the configuration of metal cutting, oblique cutting, and other form of machining process such as drilling and milling would be very interesting.

References

Ben Abdelali, H. et al., 2012. Experimental Characterization of Friction Coefficient at the Tool-Chip-Workpiece Interface During Dry Cutting of AISI 1045. *Wear*, 286–287, pp.108–115.

Ben Abdelali, H. et al., 2011. Identification of a Friction Model at the Tool-Chip-Workpiece Interface in Dry Machining of a AISI 1045 Steel With a TiN Coated Carbide Tool. *Journal of Tribology*, 133(October), p.42201.

Abhang, L.B. & Hameedullah, M., 2010a. Chip-Tool Interface Temperature Prediction Model for Turning Process. *International Journal of Engineering Science and Technology*, 2(4), pp.382–393.

Abhang, L.B. & Hameedullah, M., 2010b. The Measurement of Chip-Tool Interface Temperature in the Turning of Steel. *International Journal of Computer Communication and Information System (IJCCIS)*, 2(1), pp.1–5.

Abukhshim, N.A., Mativenga, P.T. & Sheikh, M.A., 2004. An Investigation of the Tool-Chip Contact Length and Wear in High-Speed Turning of EN19 Steel. *Proceedings of the Institution of Mechanical Engineers, Part B: Journal of Engineering Manufacture*, 218, pp.889–903.

Abuladze, N., 1962. Character and the Length of Tool–Chip Contact (in Russian). *Machinability of Heat Resistant and Titanium Alloys. Kuibyshev*, pp.68–78.

Ackroyd, B., Chandrasekar, S. & Compton, W.D., 2003. A Model for the Contact Conditions at the Chip-Tool Interface in Machining. *Journal of Tribology*, 125(July), pp.649–660.

Adibi-Sedeh, A.H., Madhavan, V. & Bahr, B., 2003. Extension of Oxley's Analysis of Machining to Use Different Material Models. *Journal of Manufacturing Science and Engineering*, 125(November), pp.656–666.

Andreasen, J.L. & Chiffre, L. De, 1993. Automatic Chip-Breaking Detection in Turning by Frequency Analysis of Cutting Force. *Ann. CIRP*, 42(2), pp.45–48.

Asad, M. et al., 2008. Dry cutting study of an aluminium alloy (A2024-T351): A numerical and experimental approach. *International Journal of Material Forming*, 1, pp.499–502.

Astakhov, V.P., 2006. *Tribology of Metal Cutting* B. J. Briscoe, ed., Tribology and Interface Engineering Series No. 52, Elsevier Ltd.

Atlati, S. et al., 2011. Analysis of a New Segmentation Intensity Ratio SIR to Characterize the Chip Segmentation Process in Machining Ductile Metals. *International Journal of Machine Tools and Manufacture*, 51(9), pp.687–700.

Atlati, S. et al., 2013. Assessment of Chip Segmentation Process in Machining Using Physical Parameters. *Revue de*, 2(6), pp.629–640.

Avan, E.Y., 2013. *Development of a Novel Ultrasonic Method for Non-invasive Measurement of Oil Films in Piston Ring Contacts*. PhD Thesis, University of Sheffield.

Bandyopadhyay, B.P., 1984. Mechanism of Formation of Built-Up Edge. *Precision Engineering*, 6(3), pp.148–151.

Barman, T.K. & Sahoo, P., 2009. Response Surface Modeling of Fractal Dimension in CNC Turning. In *Proceedings of the International Conference on Mechanical Engineering (ICME2009)*. Dhaka, Bangladesh, pp. 26–28.

Barry, J. & Byrne, G., 2002. Chip Formation, Acoustic Emission and Surface White Layers in Hard Machining. *CIRP Annals - Manufacturing Technology*, 51(1), pp.65–70.

Bermingham, M.J. et al., 2011. New Observations on Tool Life, Cutting Forces and Chip Morphology in Cryogenic Machining Ti-6Al-4V. *International Journal of Machine Tools and Manufacture*, 51(6), pp.500–511.

Black, J.T. & Kohser, R.A., 2013. *DeGarmo's Materials and Processes in Manufacturing*, John Wiley & Sons.

Boothroyd, G. & Bailey, J. a, 1966. Effects of Strain Rate and Temperature in Orthogonal Metal Cutting. *Proc IMechE, Part C: Journal of Mechanical*

Engineering Science, 8(3), pp.264–275.

Box, G.E.P. & Hunter, J.S., 1957. Multi-Factor Experimental Designs for Exploring Response Surfaces. *Defense*, 28, pp.195–241.

Carrilero, M.S. et al., 2002. A SEM and EDS Insight into the BUL and BUE Differences in the Turning Processes of AA2024 Al-Cu Alloy. *International Journal of Machine Tools and Manufacture*, 42, pp.215–220.

Carvalho, S.R. et al., 2006. Temperature Determination at the Chip-Tool Interface Using an Inverse Thermal Model Considering the Tool and Tool Holder. *Journal of Materials Processing Technology*, 179, pp.97–104.

Childs, T. et al., 2000. *Metal Machining Theory and Applications*, London: Butterworth-Heinemann.

Childs, T.H.C., 2006. Friction Modelling in Metal Cutting. *Wear*, 260, pp.310–318.

Claudin, C. et al., 2010. Effects of a Straight Oil on Friction at the Tool-Workmaterial Interface in Machining. *International Journal of Machine Tools and Manufacture*, 50(8), pp.681–688.

Courbon, C. et al., 2013. On the Existence of a Thermal Contact Resistance at the Tool-Chip Interface in Dry Cutting of AISI 1045: Formation Mechanisms and Influence on the Cutting Process. *Applied Thermal Engineering*, 50(1), pp.1311–1325.

Dabade, U. a. & Joshi, S.S., 2009. Analysis of Chip Formation Mechanism in Machining of Al/SiCp Metal Matrix Composites. *Journal of Materials Processing Technology*, 209, pp.4704–4710.

Davoodi, B., Payganeh, G.H. & Eslami, M.R., 2012. Cutting Forces in Dry Machining of Aluminum Alloy 5083 with Carbide Tools. *Advanced Materials Research*, 445(September), pp.259–262.

Davoodi, B. & Tazehkandi, A.H., 2014. Experimental Investigation and Optimization of Cutting Parameters in Dry and Wet Machining of Aluminum Alloy 5083 in order to Remove Cutting Fluid. *Journal of Cleaner Production*, 68, pp.234–242.

Devi, K.D., Babu, K.S. & Reddy, K.H., 2015. Mathematical Modeling and Optimization of Turning Process Parameters using Response Surface Methodology. *International Journal of Applied Science and Engineering*, 13(1), pp.55–68.

Dhananchezian, M. & Kumar, M.P., 2010. Experimental Investigation of Cryogenic Cooling by Liquid Nitrogen in the Orthogonal Machining of Aluminium 6061-T6 Alloy. *International Journal of Machining and Machinability of Materials*, 7(5), p.292.

Dogra, M. et al., 2010. Tool Wear, Chip Formation and Workpiece Surface Issues in CBN Hard Turning: a Review. *International Journal of Precision Engineering and Manufacturing*, 11(2), pp.341–358.

Drinkwater, B., Sheffield, S. & Cawley, P., 1997. The Interaction of Ultrasound with a Partially Contacting Solid-Solid Interface in the Low Frequency Regime. *Review of Progress in Quantitative Nondestructive Evaluation*, 16, pp.1229–1236.

Drinkwater, B.W., Dwyer-Joyce, R.S. & Cawley, P., 1996. A Study of the Interaction between Ultrasound and a Partially Contacting Solid--Solid Interface. *Proceedings of the Royal Society A: Mathematical, Physical and Engineering Sciences*, 452(1955), pp.2613–2628.

Dwyer-Joyce, R.S., 2005. The Application of Ultrasonic NDT Techniques in Tribology. *Proceedings of the Institution of Mechanical Engineers, Part J: Journal of Engineering Tribology*, 219(5), pp.347–366.

Dwyer-Joyce, R.S. & Drinkwater, B.W., 2003. In Situ Measurement of Contact Area and Pressure Distribution in Machine Elements. *Tribology Letters*, 14(1), pp.41–52.

Dwyer-Joyce, R.S., Drinkwater, B.W. & Donohoe, C.J., 2003. The Measurement of Lubricant-Film Thickness Using Ultrasound. *Proceedings of the Royal Society of London A: Mathematical, Physical and Engineering Sciences.*, 459(2032), pp.957–976.

Dwyer-Joyce, R.S., Harper, P. & Drinkwater, B.W., 2004A. A Method for the Measurement of Hydrodynamic Oil Films Using Ultrasonic Reflection. *Tribology Letters*, 17(2), pp.337–348.

Dwyer-Joyce, R.S., Reddyhoff, T. & Drinkwater, B.W., 2004B. Operating Limits for Acoustic Measurement of Rolling Bearing Oil Film Thickness. *Tribology Transactions*, 47(3), pp.366–375.

Dwyer-Joyce, R.S., Reddyhoff, T. & Zhu, J., 2011. Ultrasonic Measurement for Film Thickness and Solid Contact in Elastohydrodynamic Lubrication. *Journal of Tribology*, 133(July), pp.1–11.

Fang, N. & Dewhurst, P., 2005. Slip-Line Modeling of Built-Up Edge Formation in Machining. *International Journal of Mechanical Sciences*, 47, pp.1079–1098.

Fang, N., Pai, P.S. & Edwards, N., 2010A. Prediction of Built-Up Edge Formation in Machining with Round Edge and Sharp Tools Using a Neural Network Approach. *International Journal of Computer Integrated Manufacturing*, 23(11), pp.1002–1014.

Fang, N., Pai, P.S. & Mosquea, S., 2010B. The Effect of Built-Up Edge on the Cutting Vibrations in Machining 2024-T351 Aluminum Alloy. *International Journal of Advanced Manufacturing Technology*, 49, pp.63–71.

Fatima, A. & Mativenga, P.T., 2013. A Review of Tool-Chip Contact Length Models in Machining and Future Direction for Improvement. *Proceedings of the Institution of Mechanical Engineers, Part B: Journal of Engineering Manufacture*, 227, pp.345–356.

Friedman, M.Y. & Lenz, E., 1970. Investigation of the Tool-Chip Contact Length in Metal Cutting. *International Journal of Machine Tool Design and Research*, 10, pp.401–416.

Gad, G.S., Armarego, E.J.A. & Smith, A.J.R., 1992. Tool-Chip Contact Length in Orthogonal Machining and Its Importance in Tool Temperature Predictions. *International Journal of Production Research*, 30(3), pp.485–501.

Gekonde, H.O. & Subramanian, S. V, 2002. Tribology of Tool–Chip Interface and Tool Wear Mechanisms. *Surface and Coatings Technology*, 149(2), pp.151–160.

Germain, D., Fromentin, G. & Poulachon, G., 2010. A Force Model for Superfinish Turning of Pure Copper With Rounded Edge Tools At Low Feed Rate. In *: 8th international conference on HSM, 26–28 May, 2010 Luxembourg, ENIM-National School of Engineers of METZ.*

Gokkaya, H., 2010. The Effects of Machining Parameters on Cutting Forces, Surface Roughness, Built-Up Edge (BUE) and Built-Up Layer (BUL) During Machining AA2014 (T4) Alloy. *Strojniski Vestnik/Journal of Mechanical Engineering*, 56, pp.584–593.

Gokkaya, H. & Taskesen, A., 2008. The Effects of Cutting Speed and Feed Rate on Bue-Bul Formation , Cutting Forces and Surface Roughness When Machining Aa6351 (T6) Alloy. *Journal of Mechanical Engineering*, 54, pp.521–530.

Gómez-Parra, A. et al., 2013. Analysis of the Evolution of the Built-Up Edge and Built-Up Layer Formation Mechanisms in the Dry Turning of Aeronautical Aluminium Alloys. *Wear*, 302, pp.1209–1218.

Gonzalez-Valadez, M., Dwyer-Joyce, R.S. & Lewis, R., 2005. Ultrasonic Reflection from Mixed Liquid-Solid Contacts and the Determination of Interface Stiffness. *Tribology and Interface Engineering Series*, 48(5), pp.313–320.

Grabec, I. & Leskovar, P., 1977. Acoustic Emission of a Cutting Process. *Ultrasonics*, 15(1), pp.17–20.

Hahn, S., 1953. The Shear Angle Relationship in Metal Cutting. *Trans. ASME*, 75, pp.273–283.

Hu, J. & Qin, F., 2008. Characteristics of Acoustic Emission Signals in Machining Using Diamond Coated Tools. In *International Manufacturing Science and Engineering Conference (MSEC2008)*. Evanston, Illinois, USA, pp. 1–8.

Huang, L., Chen, J. & Chang, T., 1999. Effect of Tool/Chip Contact Length on Orthogonal Turning Performance. *Journal of Industrial Technology*, 15(2), pp.1–5.

Hwang, J. & Chandrasekar, S., 2011. Contact Conditions at the Chip-Tool Interface in Machining. *International Journal of Precision Engineering and Manufacturing*, 12(2), pp.183–193.

Iqbal, S.A., Mativenga, P.T. & Sheikh, M.A., 2009. A Comparative Study of the Tool-Chip Contact Length in Turning of Two Engineering Alloys for a Wide Range of Cutting Speeds. *International Journal of Advanced Manufacturing Technology*, 42, pp.30–40.

Iqbal, S.A., Mativenga, P.T. & Sheikh, M.A., 2007. Characterization of Machining of AISI 1045 Steel Over a Wide Range of Cutting Speeds. Part 1: Investigation of Contact Phenomena. *Proceedings of the Institution of Mechanical Engineers, Part B: Journal of Engineering Manufacture*, 221, No. 5, pp.909–916.

Iqbal, S.A., Mativenga, P.T. & Sheikh, M.A., 2008. Contact Length Prediction: Mathematical Models and Effect of Friction Schemes on FEM Simulation for Conventional to HSM of AISI 1045 Steel. *International Journal of Machining and Machinability of Materials*, 3, p.18.

J. Blitz, 1963. *Fundamentals of Ultrasonics*, Butterworths, London,.

Jomaa, W., Songmene, V. & Bocher, P., 2014. Surface Finish and Residual Stresses Induced by Orthogonal Dry Machining of AA7075-T651. *Materials*, 7, pp.1603–1624.

Jr, M.C.S., Machado, Á.R. & Mariano, F., 2011. A Study of the Cutting Force and Power in the Machining of 6262-T6 and 7075-T6 Aluminum Alloys. In *21st Brazilian Congress of Mechanical Engineering*.

Juneja, B.L., Sekhon, G.S. & Seth, N., 2003. *Fundamentals of Metal Cutting and Machine Tools*, New Age International.

Kannatey-Asibu, E. & Dornfeld, D. a., 1981. Quantitative Relationships for Acoustic Emission from Orthogonal Metal Cutting. *Journal of Engineering for Industry*, 103(3), pp.330–340.

Kato, S., Yamaguchi, K. & Yamada, M., 1972. Stress Distribution at the Interface Between Tool and Chip in Machining. *Journal of Engineering for Industry*, 94(2), pp.683–689.

Kendall, K. & Tabor, D., 1971. An Ultrasonic Study of the Area of Contact between Stationary and Sliding Surfaces. *Proceedings of the Royal Society A: Mathematical, Physical and Engineering Sciences*, 323, pp.321–340.

Kilic, D.S. & Raman, S., 2007. Observations of the Tool-Chip Boundary Conditions in Turning of Aluminum Alloys. *Wear*, 262, pp.889–904.

Klushin, I.M., 1960. Determination of the Contact Zone between Chip and Rake Face and the Pressure in this Zone. *Stanki i Instrument*, 31, pp.22–23.

Kouam, J. et al., 2013. Dry , Semi-Dry and Wet Machining of 6061-T6 Aluminium Alloy. *INTECH open sciences*, (2013), pp.199–221.

Krautkramer, J. & Krautkramer, H., 1977. *Ultrasonic Testing of Materials*, Springer-Verlag. New York.

Kus, A. et al., 2015. Thermocouple and Infrared Sensor-Based Measurement of Temperature Distribution in Metal Cutting. *Sensors*, 15(1), pp.1274–1291.

Lauro, C.H. et al., 2014. Monitoring and Processing Signal Applied in Machining Processes – A Review. *Measurement*, 58, pp.73–86.

Lee, E.H. & Shaffer, B.W., 1951. The Theory of Plasticity Applied to a Problem of Machining. *Journal of Applied Mechanics*, 18, pp.405–413.

Lewis, R., Marshall, M.B. & Dwyer-Joyce, R.S., 2005. Measurement of Interface Pressure in Interference Fits. *Proceedings of the Institution of Mechanical Engineers, Part C: Journal of Mechanical Engineering Science*, 219(2), pp.127–139.

M'Saoubi, R. & Chandrasekaran, H., 2005. Innovative Methods for the Investigation of Tool-Chip Adhesion and Layer Formation during Machining. *CIRP Annals - Manufacturing Technology*, 54(1), pp.59–62.

Madhavan, V., Chandrasekar, S. & Farris, T.N., 2002. Direct Observations of the Chip-Tool Interface in the Low Speed Cutting of Pure Metals. *Journal of Tribology*, 124, pp.617–626.

Marinov V., 1999. The Tool Chip Contact Length in Metal Cutting. In *In: 5th international conference on advance engineering and technology, AMTECH 99,*. Plovdiv, Bulgaria, pp. 149–155.

Marshall, M., 2005. *An Ultrasonic Investigation of Real Engineering Contacts*. PhD Thesis, The University of Sheffield.

Marshall, M.B. et al., 2004. An Ultrasonic Approach for Contact Stress Mapping in Machine Joints and Concentrated Contacts. *The Journal of Strain Analysis for Engineering Design*, 39(4), pp.339–350.

Marshall, M.B. et al., 2006. Experimental Characterization of Wheel-Rail Contact Patch Evolution. *Journal of Tribology*, 128(3), p.493.

Marshall, M.B., Zainal, I. & Lewis, R., 2010. Influence of the Interfacial Pressure Distribution on Loosening of Bolted Joints. *Strain*, 47(SUPPL. 2), pp.65–78.

Mason, W.P. & Thurston, R.N., 1979. *Physical Acoustics*, Academic Press, New York.

Mathew, P. & Oxley, P.L.B., 1980. Predicting the Cutting Conditions at which Built-Up Edge Disappears when Machining Plain Carbon Steels. *CIRP Annals - Manufacturing Technology*, 29, pp.11–14.

Myers, R.H., Montgomery, D.C. & Anderson-Cook, C.M., 2002. *Response Surface Methodology: Process and Product Optimization Using Designed Experiments*, John Wiley & Sons.

NDT Resource Centre, 2012. Modes of Sound Wave Propagation. Available at: https://www.nde-ed.org/EducationResources/CommunityCollege/Ultrasonics/Physics/modepropagation.htm [Accessed January 1, 2016].

Norouzifard, V. & Hamedi, M., 2014. Experimental Determination of the Tool–Chip Thermal Contact Conductance in Machining Process. *International Journal of Machine Tools and Manufacture*, 84, pp.45–57.

Nouari, M. et al., 2003. Experimental Analysis and Optimisation of Tool Wear in Dry Machining of Aluminium Alloys. *Wear*, 255, pp.1359–1368.

O'Sullivan, D. & Cotterell, M., 2001. Temperature Measurement in Single Point Turning. *Journal of Materials Processing Technology*, 118, pp.301–308.

Ojolo, S.J. & Awe, O., 2011. Investigation into the Effect of Tool-Chip Contact Length on Cutting Stability. *Journal of Emerging Trends in Engineering and Applied Sciences (JETEAS)*, 2(4), pp.626–630.

Ojolo, S.J. & Ohunakin, O.S., 2011. Study of Rake Face Action on Cutting Using Palm-Kernel Oil as Lubricant. *Journal of Emerging Trends in Engineering and Applied Sciences (JETEAS)*, 2(1), pp.30–35.

Olympus NDT, 2010. Olympus Panametrics Ultrasonic Transducers. *Olympus NDT Inc.* Available at: www.olympus-ims.com [Accessed January 1, 2016].

Oraby, S.E.-S., 1989. *Mathematical Modelling and In-Process Monitoring Techniques for Cutting Tools*. PhD Thesis, The University of Sheffield.

Oxley, P.L.B., 1989. Mechanics of Machining: An Analytical Approach to Assessing Machinability. *Journal of Applied Mechanics*, 57(1), p.253.

Ozel, T. & Ulutan, D., 2013. Effects of Machining Parameters and Tool Geometry on Serrated Chip Formation, Specific Forces and Energies in Orthogonal Cutting of Nickel-Based Super Alloy Inconel 100. *Proceedings of the Institution of Mechanical Engineers, Part B: Journal of Engineering Manufacture*, 228(7), pp.673–686.

Pang, L., 2012. *Analytical Modeling and Simulation of Metal Cutting Forces for Engineering*. PhD Thesis, University of Ontario Institute of Technology.

Poletika, M., 1969. Contact Loads on Tool Faces (in Russian). *Machinostrine, Moscow*.

Popov, A. & Dugin, A., 2014. Study of Reasons of Increased Active Force Using Coolant with Uncut Chip Thickness. *The International Journal of Advanced Manufacturing Technology*, 70(9–12), pp.1555–1562.

R.Kesavan, D. & Ramanath, B.V., 2006. *Manufacturing Technology - II*, Firewall Media.

Radhika, N., Subramanian, R. & Sajith, A., 2014. Analysis of Chip Formation in Machining Aluminium Hybrid Composites. *E3 Journal of Scientific Research*, 2(1), pp.9–15.

Raman, S., Longstreet, A. & Guha, D., 2002. A Fractal View of Tool-Chip Interfacial Friction in Machining. *Wear*, 253(11), pp.1111–1120.

Rangwala, S. & Dornfeld, D., 1991. A Study of Acoustic Emission Generated During Orthogonal Metal Cutting-1: Energy Analysis. *International journal of mechanical sciences*, 33(6), pp.471–487.

Reddyhoff, T. et al., 2005. The Phase Shift of an Ultrasonic Pulse at an Oil Layer and Determination of Film Thickness. *Proceedings of the Institution of Mechanical Engineers, Part J: Journal of Engineering Tribology*, 219(6), pp.387–400.

Reddyhoff, T., 2006. *Ultrasonic Measurement Techniques for Lubricant Films*. PhD Thesis, The University of Sheffield.

Reddyhoff, T., Dwyer-Joyce, R. & Harper, P., 2006. Ultrasonic Measurement of Film Thickness in Mechanical Seals. *Sealing Technology*, (7), pp.7–11.

Reddyhoff, T., Dwyer-Joyce, R.S. & Harper, P., 2008. A New Approach for the Measurement of Film Thickness in Liquid Face Seals. *Tribology Transactions*, 51(2), pp.140–149.

Reis, L.L.G., Silva Júnior, W.M. Da & Machado, Á.R., 2007. Effect of Cutting Speed and Cutting Fluid on the BUE Geometry of a SAE 12L14 Free Machining Steel. *Journal of the Brazilian Society of Mechanical Sciences and Engineering*, 29(2), pp.196–201.

Rubenstein, C., 1965. A Simple Theory of Orthogonal Cutting. *International Journal of Machine Tool Design and Research*, 4, pp.123–156.

Sadik, M.I. & Lindström, B., 1995. A Simple Concept to Achieve a Rational Chip Form. *Journal of Materials Processing Technology*, 54, pp.12–16.

Sadik, M.I. & Lindström, B., 1993. The Role of Tool-Chip Contact Length in Metal Cutting. *Journal of Materials Processing Technology*, 37, pp.613–627.

Saglam, H., Yaldiz, S. & Unsacar, F., 2007. The Effect of Tool Geometry and Cutting Speed on Main Cutting Force and Tool Tip Temperature. *Materials and Design*, 28(1), pp.101–111.

Salem, S. Ben & Bayraktar, E., 2012. Effect of Cutting Parameters on Chip Formation in Orthogonal Cutting. *Journal of Achievements in Materials and Manufacturing Engineering*, 50(1), pp.7–17.

Seah, K.H.W. & Li, X., 1997. Influence of Coolant on Cutting Tool Performance. *Journal of Materials Science & Technology*, 13, pp.199–205.

Sharma, V.S., Dogra, M. & Suri, N.M., 2009. Cooling Techniques for Improved Productivity in Turning. *International Journal of Machine Tools and Manufacture*, 49, pp.435–453.

Siddhpura, M. & Paurobally, R., 2012. A Review of Chatter Vibration Research in Turning. *International Journal of Machine Tools and Manufacture*, 61, pp.27–47.

Sreejith, P.S., 2008. Machining of 6061 Aluminium Alloy with MQL, Dry and Flooded Lubricant Conditions. *Materials Letters*, 62(2), pp.276–278.

Stephenson, D.A. & Agapiou, J.S., 2006. *Metal Cutting Theory and Practice*, CRC Press, Taylor & Francis Group, Boca Raton.

Stephenson, D. a., Jen, T.-C. & Lavine, a. S., 1997. Cutting Tool Temperatures in Contour Turning: Transient Analysis and Experimental Verification. *Journal of Manufacturing Science and Engineering*, 119(4A), pp.494–501.

Sun, S., Brandt, M. & Dargusch, M.S., 2009. Characteristics of Cutting Forces and Chip Formation in Machining of Titanium Alloys. *International Journal of Machine Tools and Manufacture*, 49, pp.561–568.

Sutter, G., 2005. Chip Geometries During High-Speed Machining for Orthogonal Cutting Conditions. *International Journal of Machine Tools and Manufacture*, 45(6), pp.719–726.

Takeyama, H. & Ono, T., 1968. Basic Investigation of Built-Up-Edge. *Journal of Engineering for Industry*, May(2), pp.335–342.

Tattersall, H.G., 1973. The Ultrasonic Pulse-Echo Technique as Applied to Adhesion Testing. *Journal of Physics D: Applied Physics*, 6, pp.819–832.

Tay, A.O. et al., 1976. A Numerical Method for Calculating Temperature Distributions in Machining, From Force and Shear Angle Measurements. *International Journal of Machine Tool Design and Research*, 16(4), pp.335–349.

Toropov, A. & Ko, S.L., 2003. Prediction of Tool-Chip Contact Length using a New Slip-Line Solution for Orthogonal Cutting. *International Journal of Machine Tools and Manufacture*, 43(12), pp.1209–1215.

Totten, G.E. & Hong, L., 2004. *Mechanical Tribology : Materials, Characterization, and Applications*, New York: Marcel Dekker.

Trent, E.M., 1977. *Metal Cutting*, London: Butterworths.

Trent, E.M. & Wright, P.K., 2000. *Metal Cutting*, USA: Butterworth–Heinemann.

Vieira, J.M., Machado, a. R. & Ezugwu, E.O., 2001. Performance of Cutting Fluids During Face Milling of Steels. *Journal of Materials Processing Technology*, 116(2), pp.244–251.

Vinogradov, A.A., 1985. Physical Foundations of the Process of Drilling Difficult-to-Cut Materials Using Carbide Drills. *Naukova Dumka, Kiev*.

Wallace, P.W. & Boothroyd, G., 1964. Tool Forces and Tool–Chip Friction in Orthogonal Machining. *Journal Mechanical Engineering Science*, 6(1), pp.74–87.

Wan Ibrahim, M.K., Gasni, D. & Dwyer-Joyce, R.S., 2012. Profiling a Ball Bearing Oil Film with Ultrasonic Reflection. *Tribology Transactions*, 55(4), pp.409–421.

Wang, J. & Zhu, L., 2006. Analysis of the Tool-Chip Contact Length Incorporating the Effects of Shear Strain. In *:Technology and Inovation Conference, 2006. ITIC 2006. International, 6–7 November 2006*. Hangzhou, China, pp. 1331–1334.

Ward, C., 2010. *On-line Determination of Component Quality Using Acoustic Emission*. PhD Thesis, Heriot-Watt University.

White, R.M., 1963. Generation of Elastic Waves by Transient Surface Heating. *Journal of Applied Physics*, 34(12), p.3559.

Williams, J.A. & Tabor, D., 1977. The Role of Lubricants in Machining. *Wear*, 43, pp.275–292.

Woon, K.S. et al., 2008. The Effect of Tool Edge Radius on the Contact Phenomenon of Tool-Based Micromachining. *International Journal of Machine Tools and Manufacture*, 48(12–13), pp.1395–1407.

Wright, P.K., 1981. Frictional interactions in machining: comparrsons between transparent sapphire and steel cutting tools. *Metals Technology*, 8(1), pp.150–160.

Wright, P.K., Horne, J.G. & Tabor, D., 1979. Boundary Conditions at the Chip-Tool Interface in Machining: Comparisons Between Seizure and Sliding Friction. *Wear*, 54(2), pp.371–390.

Xu, D. et al., 2014. Research on Chip Formation Parameters of Aluminum Alloy 6061-T6 Based on High-Speed Orthogonal Cutting Model. *The International Journal of Advanced Manufacturing Technology*, 72(5–8), pp.955–962.

Yazman, S. et al., 2013. The Effect of Build-up Edge Formation on the Machining Characteristics in Austempered Ferritic Ductile Iron. In *Proceedings of the ASME 2013 International Mechanical Engineering Congress and Exposition IMECE2013*. San Diego, California, USA, pp. 1–7.

Zemzemi, F. et al., 2009. Identification of a Friction Model at Tool/Chip/Workpiece Interfaces in Dry Machining of AISI4142 Treated Steels. *Journal of Materials Processing Technology*, 209(2006), pp.3978–3990.

Zhang, H.T., Liu, P.D. & Hu, R.S., 1991. A Three-Zone Model and Solution of Shear Angle in Orthogonal Machining. *Wear*, 143(1), pp.29–43.

Zhang, J., Drinkwater, B.W. & Dwyer-Joyce, R.S., 2005. Calibration of the Ultrasonic Lubricant-Film Thickness Measurement Technique. *Measurement Science and Technology*, 16(9), pp.1784–1791.

Zorev, N., 1966. *Metal Cutting Mechanics* Pergamon P., Oxford.

Appendices

A.

Chip Morphology and Cutting Force Measurements

A.1 Temperature Measurements

Table A.1 shows the machining parameters and the results of the temperature at dry and wet machining conditions.

Table A.1 Cutting parameters and temperature results

	Cutting parameters			Dry	Wet
Run Order	Cutting Speed (m/min)	Depth of Cut (mm)	Feed (mm/rev)	Temperature (°C)	Temperature (°C)
1	90	2	0.16	118.48	56.78
2	90	2	0.16	122.60	49.90
3	90	2	0.16	118.64	56.07
4	40	2	0.16	98.17	34.29
5	60	2.5	0.12	105.11	43.63
6	60	2.5	0.2	130.25	56.92
7	120	1.5	0.12	107.43	51.22
8	140	2	0.16	128.77	40.53
9	90	1.2	0.16	111.26	48.49
10	120	1.5	0.2	132.37	48.67
11	90	2.8	0.16	141.55	47.60
12	120	2.5	0.2	150.01	59.90
13	60	1.5	0.2	109.00	33.98
14	90	2	0.16	119.52	51.40
15	90	2	0.16	122.60	50.32
16	90	2	0.23	147.95	54.71
17	90	2	0.16	119.59	48.53
18	60	1.5	0.12	90.21	31.87
19	120	2.5	0.12	129.93	52.87
20	90	2	0.09	96.54	46.14

A.2 Chip Morphology Analysis

A.2.1 Chip Thickness, Shear Angle and Chip Velocity

Table A.2 shows the experimental results of the chip thickness, shear angle and chip velocity at dry and wet cutting conditions.

Table A.2 Machining parameters and some of the chip morphology results

Run Order	Cutting parameters			Dry			Wet		
	V (*m/min*)	*t* (*mm*)	*f* (*mm/rev*)	*h* (*mm*)	(*φ*)	Chip Velocity (*m/min*)	*h* (*mm*)	(*φ*)	Chip Velocity (*m/min*)
1	90	2	0.16	0.704	12.81	20.47	0.735	12.29	19.60
2	90	2	0.16	0.726	12.43	19.83	0.735	12.29	19.60
3	90	2	0.16	0.720	12.53	20.00	0.733	12.31	19.65
4	40	2	0.16	0.876	10.35	7.31	0.393	22.14	16.28
5	60	2.5	0.12	0.584	11.62	12.34	0.451	14.91	15.98
6	60	2.5	0.2	0.829	13.57	14.48	0.803	13.99	14.95
7	120	1.5	0.12	0.556	12.18	25.90	0.554	12.23	26.02
8	140	2	0.16	0.618	14.51	36.23	0.636	14.12	35.23
9	90	1.2	0.16	0.736	12.27	19.57	0.759	11.91	18.98
10	120	1.5	0.2	0.780	14.38	30.77	0.803	13.99	29.90
11	90	2.8	0.16	0.623	14.40	23.11	0.614	14.60	23.45
12	120	2.5	0.2	0.728	15.36	32.97	0.682	16.34	35.18
13	60	1.5	0.2	0.934	12.09	12.85	0.565	19.49	21.24
14	90	2	0.16	0.694	12.99	20.76	0.680	13.24	21.18
15	90	2	0.16	0.723	12.49	19.93	0.726	12.44	19.85
16	90	2	0.23	0.896	14.40	23.11	0.923	14.00	22.43
17	90	2	0.16	0.738	12.24	19.52	0.735	12.29	19.61
18	60	1.5	0.12	0.644	10.55	11.18	0.268	24.15	26.90
19	120	2.5	0.12	0.520	12.99	27.69	0.513	13.18	28.10
20	90	2	0.09	0.479	10.64	16.90	0.352	14.33	23.00

where *V*: cutting speed, *t*: cutting depth, *f*: feed, *h*: chip thickness, *φ*: shear angle and *Vc*: chip velocity.

A.2.1.1 ANOVA of the Chip Thickness

The results of the ANOVA of chip thickness during dry and wet turning are presented in (Table A.3-Table A.6). It can be seen from Table A.3 that the linear model of the machining parameters cutting speed (*A*), cutting depth (*B*) and feed (*C*) have a stronger effect on the chip thickness during dry cutting. In addition, the quadratic values of cutting depth (B*B) and feed (*C*C) are also significant. As for the quadratic value of cutting speed (*A*A) there is no significant influence on the chip thickness. Regarding to the interaction influence, it can be seen from the ANOVA outputs that there is no significant effect on the chip thickness.

Table A.3 ANOVA output of chip thickness in dry conditions

Source	DF	Adj SS	Adj MS	F-Value	P-Value
Model	9	0.278686	0.030965	81.57	0.000
Linear	3	0.269422	0.089807	236.58	0.000
Speed	1	0.051549	0.051549	135.80	0.000
Depth	1	0.014387	0.014387	37.90	0.000
Feed	1	0.203486	0.203486	536.06	0.000
Square	3	0.006741	0.002247	5.92	0.014
Speed*Speed	1	0.001178	0.001178	3.10	0.109
Depth*Depth	1	0.003194	0.003194	8.42	0.016
Feed*Feed	1	0.002080	0.002080	5.48	0.041
2-Way Interaction	3	0.002522	0.000841	2.21	0.149
Speed*Depth	1	0.000756	0.000756	1.99	0.188
Speed*Feed	1	0.001311	0.001311	3.45	0.093
Depth*Feed	1	0.000454	0.000454	1.20	0.300
Error	10	0.003796	0.000380		
Lack-of-Fit	5	0.002512	0.000502	1.96	0.240
Pure Error	5	0.001284	0.000257		
Total	19	0.282482			

Table A.4 presents only the significant effects, of the ANOVA outputs, of the cutting parameters on the chip thickness. The determination coefficient (R^2) of the model is 98.23% which is indicating the high data fit, the values of adjusted determination coefficient (adj. R^2) and predicted determination coefficient (predR^2) are also shown in Table A.4 (97.19% and 93.67%, respectively). It is noticed to mention that the stepwise procedure added terms during the procedure in order to maintain a hierarchical model at each step.

Table A.4 ANOVA output of chip thickness in dry conditions (Significant)

Source	DF	Adj SS	Adj MS	F-Value	P-Value
Model	7	0.277475	0.039639	95.01	0.000
Linear	3	0.269422	0.089807	215.25	0.000
Speed	1	0.051549	0.051549	123.55	0.000
Depth	1	0.014387	0.014387	34.48	0.000
Feed	1	0.203486	0.203486	487.71	0.000
Square	3	0.006741	0.002247	5.39	0.014
Speed*Speed	1	0.001178	0.001178	2.82	0.119
Depth*Depth	1	0.003194	0.003194	7.66	0.017
Feed*Feed	1	0.002080	0.002080	4.99	0.045
2-Way Interaction	1	0.001311	0.001311	3.14	0.102
Speed*Feed	1	0.001311	0.001311	3.14	0.102
Error	12	0.005007	0.000417		
Lack-of-Fit	7	0.003723	0.000532	2.07	0.220
Pure Error	5	0.001284	0.000257		
Total	19	0.282482			
R-Squared	98.23%				
R-Squared (adj)	97.19%				
R-Squared (pred)	93.67%				

The final equation in terms of significant factors for the chip thickness model in dry turning is given by Equation A.1: It is worth noting that the regression equation is in uncoded values.

$$h_{Dry} = 0.041 - 215 \times 10^{-5}A + 0.1733B + 6.41C + 1 \times 10^{-5}A^2$$
$$- 0.0596B^2 - 7.51C^2 - 0.01067AC$$

A.1

where *h*: chip thickness, *A*: cutting speed, *B*: cutting depth and *C*: feed.

Table A.5 presents the ANOVA outputs of the machining parameters on the chip thickness during applying the cutting fluid. It can be seen from the table that the linear model of the machining parameters cutting speed (*A*) and feed (*C*) have a stronger effect on the chip thickness during wet cutting while the cutting depth has no significant effect. In addition, the quadratic values of cutting speed (*A*A*) and feed (*C*C*) are also significant. As for the quadratic value of cutting depth (*b*b*) there is no significant influence on the chip thickness. Regarding to the interaction influence, it can be seen from the ANOVA outputs that the interaction between cutting speed and cutting depth has the significant effect on the chip thickness while the other two interactions have no significant effect on the chip thickness.

Table A.5 ANOVA output of chip thickness in wet conditions

Source	DF	Adj SS	Adj MS	F-Value	P-Value
Model	9	0.509649	0.056628	18.47	0.000
Linear	3	0.356858	0.118953	38.80	0.000
Speed	1	0.055837	0.055837	18.22	0.002
Depth	1	0.000018	0.000018	0.01	0.941
Feed	1	0.301003	0.301003	98.19	0.000
Square	3	0.103748	0.034583	11.28	0.002
Speed*Speed	1	0.091177	0.091177	29.74	0.000
Depth*Depth	1	0.005075	0.005075	1.66	0.227
Feed*Feed	1	0.018753	0.018753	6.12	0.033
2-Way Interaction	3	0.049043	0.016348	5.33	0.019
Speed*Depth	1	0.042321	0.042321	13.81	0.004
Speed*Feed	1	0.006645	0.006645	2.17	0.172
Depth*Feed	1	0.000077	0.000077	0.03	0.877
Error	10	0.030654	0.003065		
Lack-of-Fit	5	0.028286	0.005657	11.94	0.008
Pure Error	5	0.002368	0.000474		
Total	19	0.540303			

Table A.6 shows only the significant effects, of the ANOVA results, of the machining parameters on the chip thickness during the wet conditions.

Table A.6 ANOVA output of chip thickness in wet conditions (Significant)

Source	DF	Adj SS	Adj MS	F-Value	P-Value
Model	6	0.497852	0.082975	25.41	0.000
Linear	3	0.356858	0.118953	36.43	0.000
Speed	1	0.055837	0.055837	17.10	0.001
Depth	1	0.000018	0.000018	0.01	0.942
Feed	1	0.301003	0.301003	92.18	0.000
Square	2	0.098673	0.049336	15.11	0.000
Speed*Speed	1	0.087821	0.087821	26.89	0.000
Feed*Feed	1	0.017034	0.017034	5.22	0.040
2-Way Interaction	1	0.042321	0.042321	12.96	0.003
Speed*Depth	1	0.042321	0.042321	12.96	0.003
Error	13	0.042451	0.003265		
Lack-of-Fit	8	0.040083	0.005010	10.58	0.009
Pure Error	5	0.002368	0.000474		
Total	19	0.540303			
R-Squared	92.14%				
R-Squared (adj)	88.52%				
R-Squared (pred)	76.98%				

The final equation in terms of significant factors for the chip thickness model in wet turning is given by Equation A.2:

Regression Equation in Uncoded Units

$$h_{Wet} = -2.2 + 0.02736A + 0.439B + 10.55C - 86 \times 10^{-6}A^2 \\ - 21.38C^2 - 485 \times 10^{-5}AB \qquad \text{A.2}$$

where *h*: chip thickness, *A*: cutting speed, *B*: cutting depth and *C*: feed.

A.2.1.2 ANOVA of the Shear Angle

(Table A.7-Table A.10) present the ANOVA outputs of the shear angle in dry and wet cutting conditions. It can be seen from the data in Table A.7 that the linear model of the machining parameters cutting speed (*A*), cutting depth (*B*) and feed (*C*) have a stronger effect on the shear angle during dry cutting. In addition, the quadratic value of cutting depth (B*B) is also significant. As for the quadratic values of cutting speed (*A*A) and feed (*C*C) there is no significant influence on the shear angle. Regarding

to the interaction influence, it can be seen from the ANOVA outputs that there is no significant effect on the shear angle.

Table A.7 ANOVA output of shear angle in dry conditions

Source	DF	Adj SS	Adj MS	F-Value	P-Value
Model	9	35.7436	3.9715	45.48	0.000
Linear	3	34.2632	11.4211	130.80	0.000
Speed	1	14.4983	14.4983	166.04	0.000
Depth	1	4.6067	4.6067	52.76	0.000
Feed	1	15.1582	15.1582	173.59	0.000
Square	3	1.2225	0.4075	4.67	0.027
Speed*Speed	1	0.0208	0.0208	0.24	0.636
Depth*Depth	1	1.1467	1.1467	13.13	0.005
Feed*Feed	1	0.0007	0.0007	0.01	0.930
2-Way Interaction	3	0.2579	0.0860	0.98	0.439
Speed*Depth	1	0.0710	0.0710	0.81	0.389
Speed*Feed	1	0.1458	0.1458	1.67	0.225
Depth*Feed	1	0.0412	0.0412	0.47	0.508
Error	10	0.8732	0.0873		
Lack-of-Fit	5	0.4976	0.0995	1.32	0.383
Pure Error	5	0.3756	0.0751		
Total	19	36.6168			

Table A.8 presents only the significant effects of the cutting parameters on the shear angle in dry conditions.

Table A.8 ANOVA output of shear angle in dry conditions (Significant)

Source	DF	Adj SS	Adj MS	F-Value	P-Value
Model	4	35.4647	8.8662	115.44	0.000
Linear	3	34.2632	11.4211	148.70	0.000
Speed	1	14.4983	14.4983	188.77	0.000
Depth	1	4.6067	4.6067	59.98	0.000
Feed	1	15.1582	15.1582	197.36	0.000
Square	1	1.2015	1.2015	15.64	0.001
Depth*Depth	1	1.2015	1.2015	15.64	0.001
Error	15	1.1521	0.0768		
Lack-of-Fit	10	0.7764	0.0776	1.03	0.519
Pure Error	5	0.3756	0.0751		
Total	19	36.6168			
R-Squared	96.85%				
R-Squared (adj)	96.01%				
R-Squared (pred)	94.53%				

The final equation in terms of significant factors for the shear angle model in dry turning is given by Equation A.3:

Regression equation in uncoded units

$$\varphi_{Dry} = 7.49 + 0.03434A - 3.42B + 26.34C + 1.145B^2 \qquad \text{A.3}$$

where φ: shear angle, A: cutting speed, B: cutting depth and C: feed.

The ANOVA outputs of the experiments data of the shear angle during applying the cutting fluid are shown in Table A.9. It can be seen from the table that the linear model of the machining parameter cutting speed (A) has a stronger effect on the shear angle during wet cutting while the cutting depth and feed have no significant effect on the shear angle. In addition, the quadratic value of cutting speed ($A*A$) is also significant. As for the quadratic values of cutting depth ($B*B$) and feed ($C*C$) have no significant influence on the shear angle. Regarding to the interaction influence, it can be seen from the ANOVA outputs that the interaction between cutting speed and cutting depth and the interaction between cutting speed and feed have the significant effect on the shear angle while the interactions between cutting depth and feed have no significant effect.

Table A.9 ANOVA output of shear angle in wet conditions

Source	DF	Adj SS	Adj MS	F-Value	P-Value
Model	9	199.313	22.1458	11.25	0.000
Linear	3	70.814	23.6046	11.99	0.001
Speed	1	67.212	67.2119	34.13	0.000
Depth	1	3.493	3.4927	1.77	0.212
Feed	1	0.109	0.1094	0.06	0.818
Square	3	70.781	23.5936	11.98	0.001
Speed*Speed	1	66.330	66.3303	33.69	0.000
Depth*Depth	1	2.551	2.5507	1.30	0.282
Feed*Feed	1	7.938	7.9382	4.03	0.072
2-Way Interaction	3	57.718	19.2393	9.77	0.003
Speed*Depth	1	40.633	40.6326	20.64	0.001
Speed*Feed	1	13.782	13.7821	7.00	0.024
Depth*Feed	1	3.303	3.3031	1.68	0.224
Error	10	19.690	1.9690		
Lack-of-Fit	5	18.967	3.7934	26.22	0.001
Pure Error	5	0.723	0.1447		
Total	19	219.003			

Table A.10 presents only the significant effects of the cutting parameters on the shear angle in wet conditions. As explained in Section A.2.1.1, that the stepwise

procedure added terms during the procedure in order to maintain a hierarchical model at each step.

Table A.10 ANOVA output of shear angle in wet conditions (Significant)

Source	DF	Adj SS	Adj MS	F-Value	P-Value
Model	7	193.459	27.6370	12.98	0.000
Linear	3	70.814	23.6046	11.09	0.001
Speed	1	67.212	67.2119	31.57	0.000
Depth	1	3.493	3.4927	1.64	0.224
Feed	1	0.109	0.1094	0.05	0.824
Square	2	68.230	34.1151	16.03	0.000
Speed*Speed	1	64.407	64.4074	30.26	0.000
Feed*Feed	1	7.140	7.1402	3.35	0.092
2-Way Interaction	2	54.415	27.2074	12.78	0.001
Speed*Depth	1	40.633	40.6326	19.09	0.001
Speed*Feed	1	13.782	13.7821	6.47	0.026
Error	12	25.544	2.1287		
Lack-of-Fit	7	24.821	3.5458	24.51	0.001
Pure Error	5	0.723	0.1447		
Total	19	219.003			
R-Squared	88.34%				
R-Squared (adj)	81.53%				
R-Squared (pred)	58.32%				

The final equation in terms of significant factors for the shear angle model in wet turning is given by Equation A.4: Regression equation in uncoded units.

$$\varphi_{Wet} = 94.8 - 0.97A - 14.53B - 240.8C + 2337 \times 10^{-6}A^2 + 438C^2 + 0.1502AB + 1.094AC \tag{A.4}$$

where φ: shear angle, A: cutting speed, B: cutting depth and C: feed.

A.2.1.3 ANOVA of the Chip Velocity

The results of the ANOVA of chip velocity during dry and wet turning are presented in (Table A.11-Table A.14). It can be seen from Table A.11 that the linear model of the machining parameters cutting speed (A), cutting depth (B) and feed (C) have a stronger effect on the chip velocity during dry cutting. In addition, the quadratic values of cutting speed ($A*A$) and feed ($C*C$) are also significant. As for the quadratic value of cutting depth ($B*B$) there is no significant influence on the chip velocity. Regarding

to the interaction influence, it can be seen from the ANOVA outputs that only the interaction between cutting speed and feed is significant while the others not.

Table A.11 ANOVA output of chip velocity in dry conditions

Source	DF	Adj SS	Adj MS	F-Value	P-Value
Model	9	1038.16	115.351	777.13	0.000
Linear	3	1025.78	341.927	2303.58	0.000
Speed	1	970.30	970.301	6536.97	0.000
Depth	1	11.88	11.877	80.01	0.000
Feed	1	43.60	43.602	293.75	0.000
Square	3	7.10	2.368	15.96	0.000
Speed*Speed	1	4.83	4.831	32.55	0.000
Depth*Depth	1	2.65	2.649	17.85	0.002
Feed*Feed	1	0.03	0.028	0.19	0.673
2-Way Interaction	3	5.27	1.758	11.84	0.001
Speed*Depth	1	0.18	0.180	1.21	0.297
Speed*Feed	1	5.00	5.000	33.68	0.000
Depth*Feed	1	0.09	0.095	0.64	0.443
Error	10	1.48	0.148		
Lack-of-Fit	5	0.46	0.092	0.45	0.798
Pure Error	5	1.02	0.204		
Total	19	1039.64			

Table A.12 presents only the significant effects of the machining parameters on the chip velocity. The determination coefficient (R^2) of the model is 99.83% which is indicating the high data fit, the values of adjusted determination coefficient (adj. R^2) and predicted determination coefficient (predR^2) are also shown in Table A.12 (99.75% and 99.59%, respectively).

Table A.12 ANOVA output of chip velocity in dry conditions (Significant)

Source	DF	Adj SS	Adj MS	F-Value	P-Value
Model	6	1037.86	172.976	1258.56	0.000
Linear	3	1025.78	341.927	2487.83	0.000
Speed	1	970.30	970.301	7059.82	0.000
Depth	1	11.88	11.877	86.41	0.000
Feed	1	43.60	43.602	317.25	0.000
Square	2	7.08	3.538	25.75	0.000
Speed*Speed	1	4.95	4.953	36.04	0.000
Depth*Depth	1	2.73	2.730	19.86	0.001
2-Way Interaction	1	5.00	5.000	36.38	0.000
Speed*Feed	1	5.00	5.000	36.38	0.000
Error	13	1.79	0.137		
Lack-of-Fit	8	0.76	0.096	0.47	0.838
Pure Error	5	1.02	0.204		
Total	19	1039.64			
R-Squared	99.83%				
R-Squared (adj)	99.75%				
R-Squared (pred)	99.59%				

The final equation in terms of significant factors for the chip velocity model in dry turning is given by Equation A.5: Regression equation in uncoded units.

$$Vc_{Dry} = 5.55 + 0.0589A - 5.06B - 14.6C + 648 \times 10^{-6}A^2 + 1.732B^2 + 0.659AC$$

A.5

where *Vc*: chip velocity, *A*: cutting speed, *B*: cutting depth and *C*: feed.

Table A.13 and Table A.14 show the ANOVA outputs of the experiments data of the chip velocity during applying the cutting fluid. It can be seen from Table A.13 that the linear model of the machining parameter cutting speed (*A*) has a stronger effect on the chip velocity during wet cutting while the cutting depth and feed have no significant effect on the chip velocity. In addition, the quadratic values of cutting speed (*A*A*) and feed (*C*C*) are also significant. As for the quadratic values of cutting depth (*B*B*) has no significant influence on the chip velocity. Regarding to the interaction influence, it can be seen from the ANOVA outputs that the interaction between cutting speed and cutting depth and the interaction between cutting speed and feed have the significant effect on the chip velocity while the interaction between cutting depth and feed has no significant effect.

Table A.13 ANOVA output of chip velocity in wet conditions

Source	DF	Adj SS	Adj MS	F-Value	P-Value
Model	9	600.871	66.763	20.40	0.000
Linear	3	380.725	126.908	38.78	0.000
Speed	1	379.515	379.515	115.97	0.000
Depth	1	0.396	0.396	0.12	0.735
Feed	1	0.813	0.813	0.25	0.629
Square	3	98.014	32.671	9.98	0.002
Speed*Speed	1	79.615	79.615	24.33	0.001
Depth*Depth	1	8.013	8.013	2.45	0.149
Feed*Feed	1	23.479	23.479	7.17	0.023
2-Way Interaction	3	122.132	40.711	12.44	0.001
Speed*Depth	1	75.460	75.460	23.06	0.001
Speed*Feed	1	38.998	38.998	11.92	0.006
Depth*Feed	1	7.675	7.675	2.35	0.157
Error	10	32.726	3.273		
Lack-of-Fit	5	30.753	6.151	15.59	0.005
Pure Error	5	1.973	0.395		
Total	19	633.597			

Table A.14 presents only the significant effects of the cutting parameters on the chip velocity in wet conditions. As explained earlier in this section that the stepwise procedure added terms during the procedure in order to maintain a hierarchical model at each step.

Table A.14 ANOVA output of chip velocity in wet conditions (Significant)

Source	DF	Adj SS	Adj MS	F-Value	P-Value
Model	7	585.183	83.598	20.72	0.000
Linear	3	380.725	126.908	31.46	0.000
Speed	1	379.515	379.515	94.07	0.000
Depth	1	0.396	0.396	0.10	0.759
Feed	1	0.813	0.813	0.20	0.661
Square	2	90.001	45.000	11.15	0.002
Speed*Speed	1	75.422	75.422	18.69	0.001
Feed*Feed	1	21.041	21.041	5.22	0.041
2-Way Interaction	2	114.457	57.229	14.18	0.001
Speed*Depth	1	75.460	75.460	18.70	0.001
Speed*Feed	1	38.998	38.998	9.67	0.009
Error	12	48.414	4.034		
Lack-of-Fit	7	46.441	6.634	16.81	0.003
Pure Error	5	1.973	0.395		
Total	19	633.597			
R-Squared	92.36%				
R-Squared (adj)	87.90%				
R-Squared (pred)	70.60%				

The final equation in terms of significant factors for the chip velocity model in wet turning is given by Equation A.6: Regression equation in uncoded units.

$$Vc_{Wet} = 107.4 - 0.983A - 18.77B - 400C + 2529 \times 10^{-6}A^2 + 751C^2 \quad \text{A.6}$$
$$+ 0.2047AB + 1.84AC$$

where *Vc*: chip velocity, *A*: cutting speed, *B*: cutting depth and *C*: feed.

A.2.2 Tool-Chip Contact Length Analysis

A.2.2.1 Tool-Chip Contact Length- Pilot Studies

The tool-chip contact length (or simply contact length) was measured experimentally using SEM and compared to theoretical models. As mentioned in the literature review (Chapter 2), the tool-chip contact length L_C was calculated theoretically, in this study, by using the model that concluded by Kato et al. (1972) and Toropov & Ko (2003). The model predicts that the contact length is twice the deformed chip thickness $L_C = 2 * chip\ thickness\ (h)$. Therefore, to verify and use this model (Kato et al. 1972 and Toropov & Ko 2003) in this study, two pilot studies were carried out using a fresh tip in each study. The machining parameters and the results of these two studies are presented in the following sections. The first pilot was carried out by using cutting tool (SCMW 12 04 08 from Sandvick) and without employing experiment design while the other study was conducted using the same cutting tool as the main study and using the design of experiments. The both pilot studies were conducted on a Triumph 2500 lathe using orthogonal cutting of *6082-T6* aluminium tube as a workpiece.

Figure A.1 shows a typical SEM image of the rake face of the cutting tool showing the tool-chip contact length. The carbide material has a higher molecular weight than aluminium therefore the SEM image shows the carbide in lighter in grey shade than the aluminium (see Figure A.2).
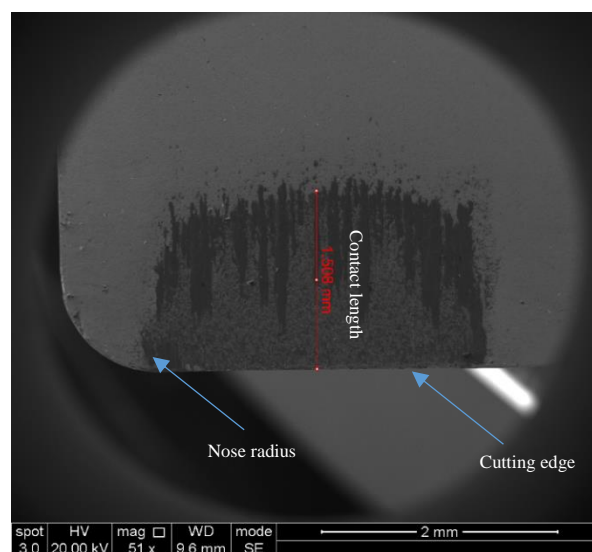
Figure A.1 Backscattered image of the tool-chip contact area

220

As mentioned in Chapter 2, the rake face of the cutting tool was further analysed, as previously reported by Abuladze (1962), the energy dispersive X-ray analysis (EDXA) was used in this study to identify the traces of chip's material on the tool rake face. Figure A.2 and Figure A.3 show a typical result of the EDXA analysis, it can be seen clearly the amount of aluminium transfer from the workpiece to the rake face of the cutting tool. The EDX analysis also shows that as moved away from the cutting edge the tungsten amount increased while the amount of aluminium decreased to zero and this confirms the end of the tool-chip contact length (see Figure A.3).
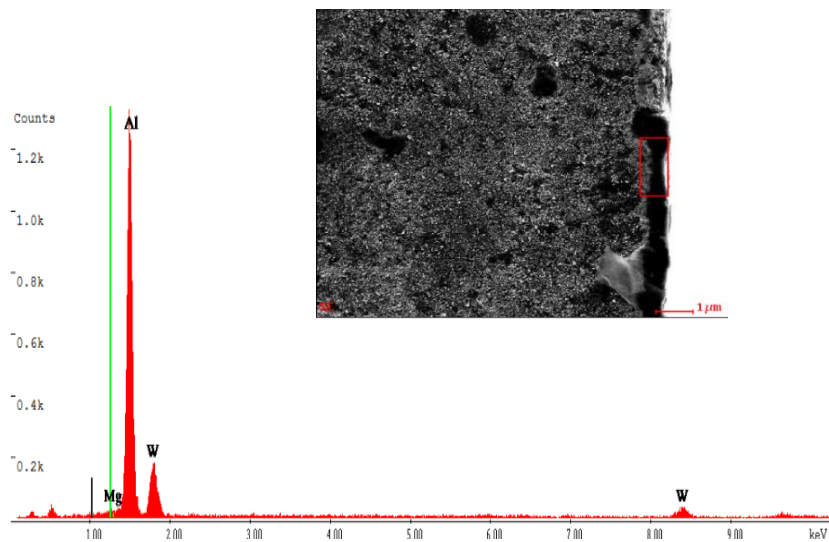
Figure A.2 SEM EDXA aluminium density area along the tool rake face
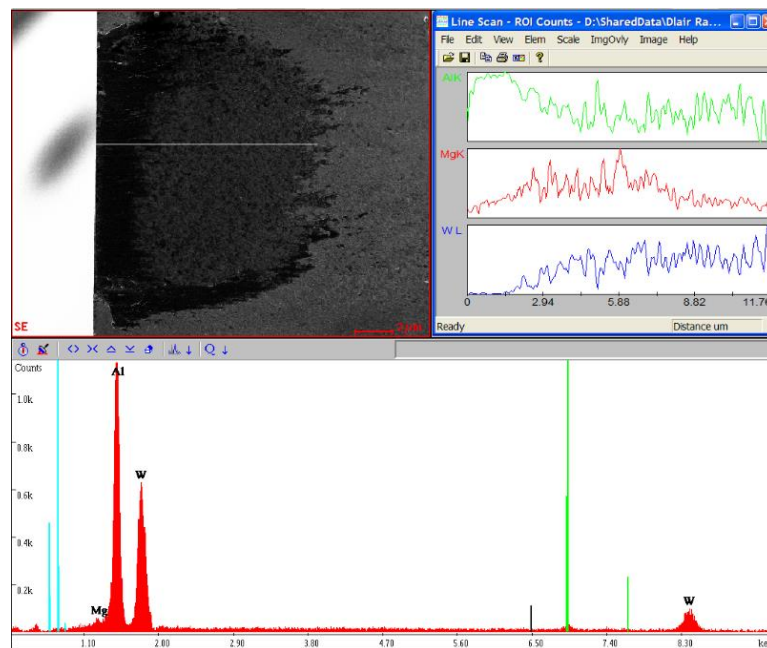
Figure A.3 SEM EDXA aluminium density line along the tool rake face

The results of the tool-chip contact length measurements of the both pilot studies are presented in the next following sections.

A.2.2.1.1   Influence of Cutting Speed

A pilot study aimed at assessing whether Kato et al. (1972) and Toropov & Ko (2003) model could be used in this study to measure the contact length has been carried out. The trials were carried out in dry and wet condition at different cutting speeds with a constant cutting depth and feed *t=2.5 mm*, *f=0.16 mm/rev*, respectively. Table A.15 presents the cutting speeds as well as the experimentally and the analytically results of the contact length. The experimental results obtained from the SEM while the analytical results were gained from the model. The results show that the chip thickness and thus the contact length decreased with increasing cutting speed, this is due to the effect of temperature. As mention in Section 6.1, the temperature of the tool-chip interface increases with increasing cutting speed (see Figure 6.4), and this results in softening the workpiece and hence the friction at the tool-chip interface reduces. As a result of these two factors, the shear angle increases and thus reduce the chip thickness. It can also be seen from the results that the chip thickness is affected by cutting fluid, at low cutting speeds only. A possible explanation for this might be that the cutting fluid may reduce the friction between the tool-chip interface, and thus the shear angle increased leads to decreasing the chip thickness.
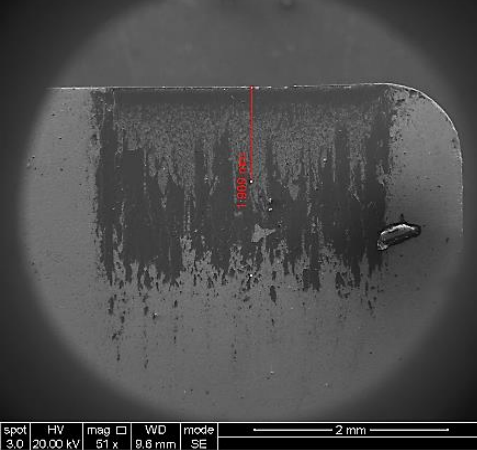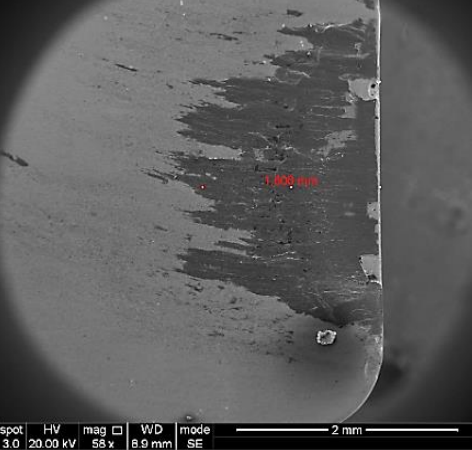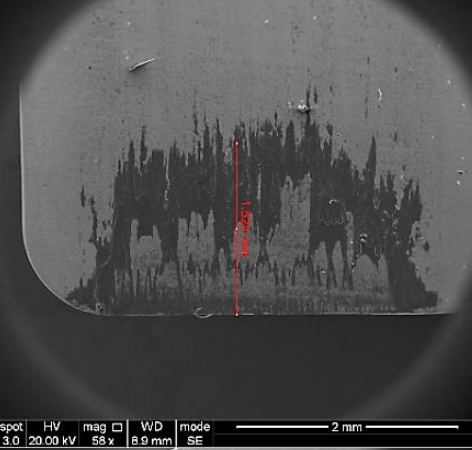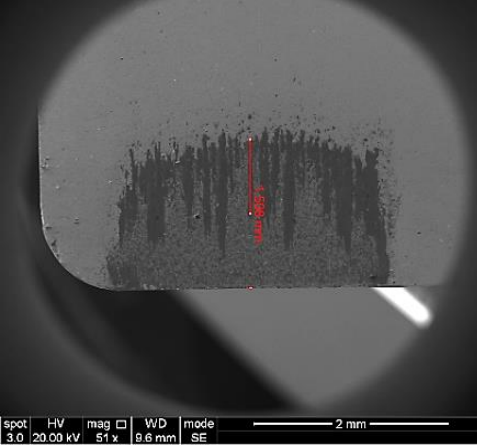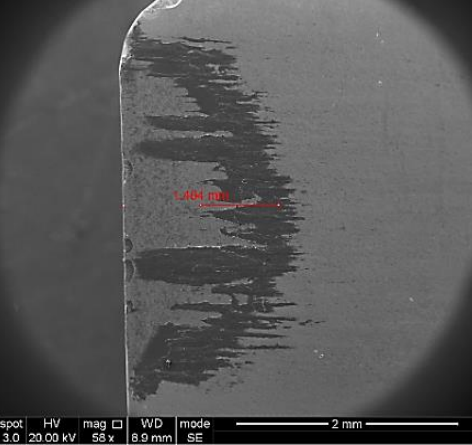
Table A.15 Cutting speeds and the contact length results

Run Order	V (m/min)	Dry			Wet		
		h (mm)	Theoretical L_C (mm)	Experimental L_C (mm)	h (mm)	Theoretical L_C (mm)	Experimental L_C (mm)
1	45	0.9	1.8	1.909	0.76	1.52	1.606
2	65	0.775	1.55	1.718	0.72	1.45	1.524
3	95	0.675	1.35	1.508	0.67	1.35	1.404
4	145	0.57	1.15	1.307	0.6	1.15	1.305
5	215	0.5	1	1.057	0.495	0.99	1.062
6	305	0.42	0.85	0.9039	0.415	0.83	0.9064

where *V* is cutting speed, *h* is chip thickness and *L$_c$* is contact length.

Figure A.4 presents the SEM images of the cutting tools rake faces at different cutting speeds in dry and wet cutting conditions. It is worth noting that the wear appeared in some of the tip in Figure A.4 is due to handling and happened during the preparation

for using them in SEM not from the machining process (see run order 3 and 6 of the Figure A.4 at wet condition).

Trial No.	V (m/min)	Dry	Wet
1	45		
2	65		
3	95		
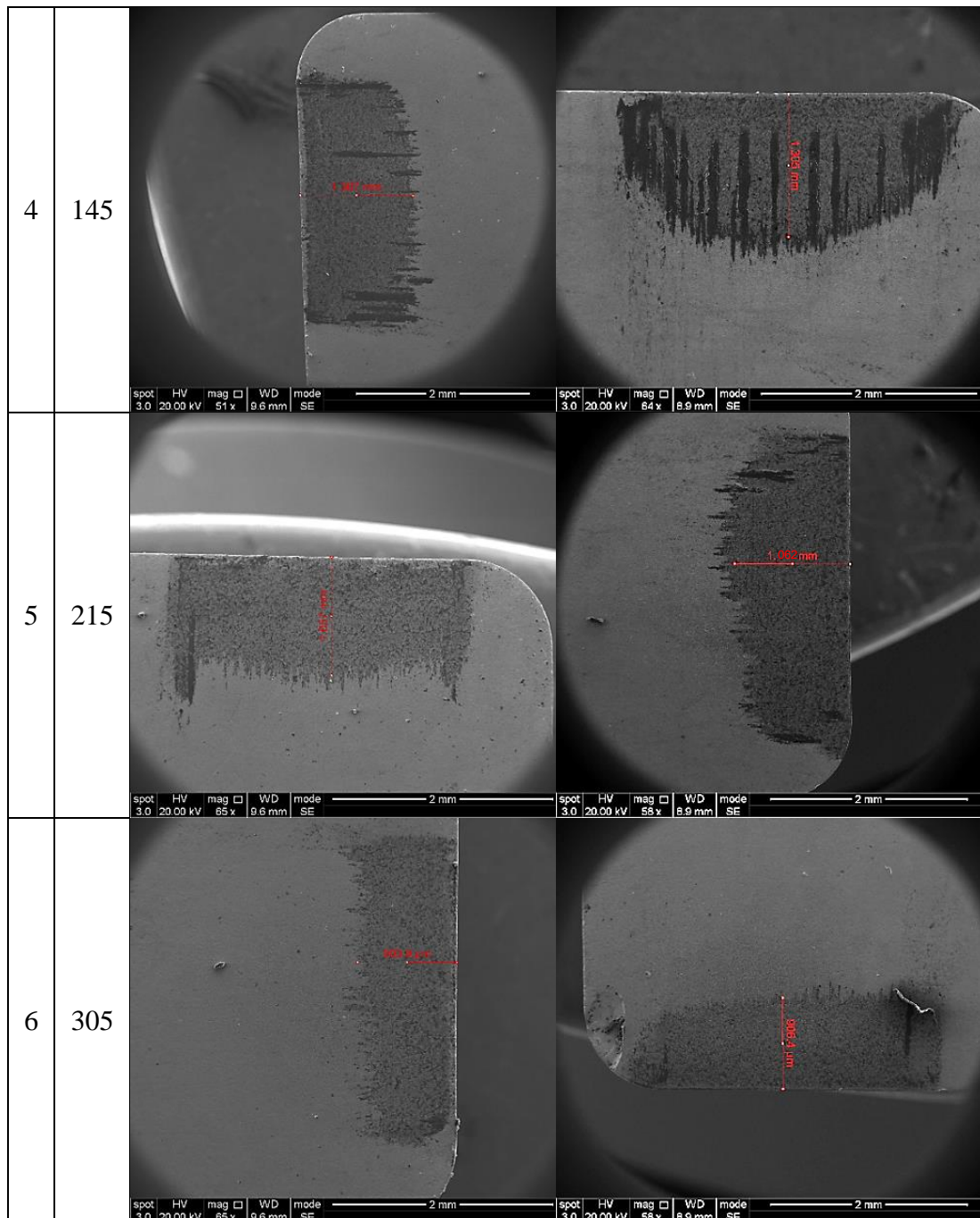
Figure A.4 SEM photographs of the rake face of the cutting tool during dry and wet cutting conditions of *Al 6082* at different cutting speeds and a cutting depth of *t*=2.5 *mm* and feed of *f*=0.16 *mm/rev*

Figure A.5 shows the comparison of the experimental results of the contact length, obtained from the SEM, and the analytical results, gained from Kato et al. (1972) and Toropov & Ko (2003) model, during dry and wet cutting. What is interesting in this data is the good agreement between the both results. As discussed earlier in this section that in both machining conditions (dry and wet) the chip thickness and thus the contact length decreased with increasing the cutting speed. With applying the coolant, the chip

thickness was found smaller than in dry conditions and at low cutting speed (below 90 *m/min*). At cutting speeds higher than 90 *m/min*, there were no significant differences between the contact length in dry and wet cutting conditions.
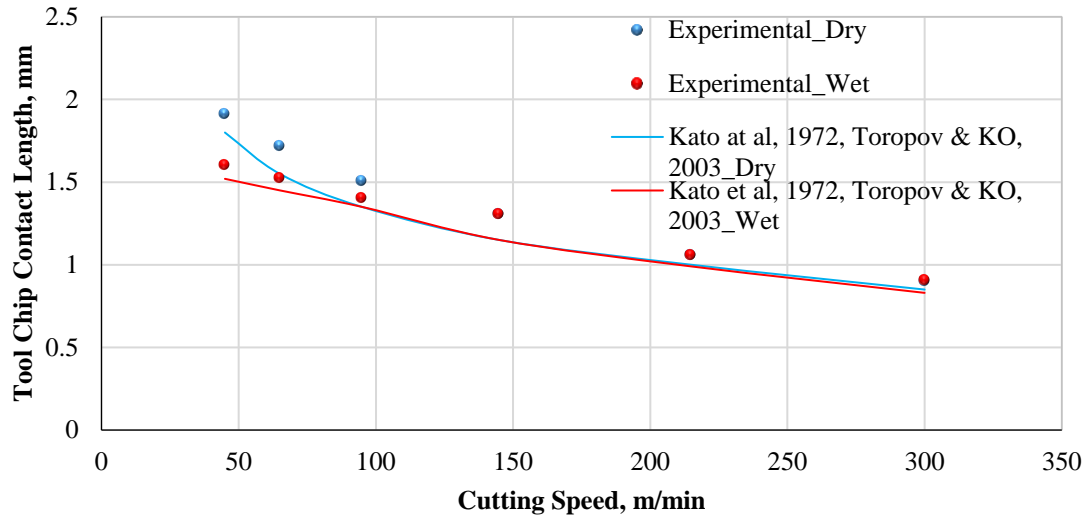
Figure A.5 Comparison of the contact length model with the dry and wet experimental data for different cutting speeds and a cutting depth of 2.5 *mm* and feed of 0.16 *mm/rev* at wet condition

A.2.2.1.2   Influence of Machining Parameters

As mentioned in Chapter 6, that the second pilot study of measuring tool-chip contact length experiment was carried out using a central composite design technique. The reason for conducting these experiments was to measure contact length at the same machining parameters that were used with different sensors including cutting force, ultrasonic, acoustic emission and accelerometer (main study). The experiments were performed, in dry cutting conditions, as per Table A.16. The contact length was measured in the same way as the first pilot study; where the tool-chip contact length was measured experimentally using SEM and compared to theoretical model. Table A.16 shows the contact length results obtained from the SEM and as well as the results gained from the model ($L_C = 2 \times h$) where h is the chip thickness. The Table A.16 also shows the tool-chip contact area which was measured using the SEM.

The SEM photographs of the rake face cutting tool are shown in Figure A.6 and the number under each image represents the run order of the Table A.16.

Table A.16 Cutting parameters and contact length results

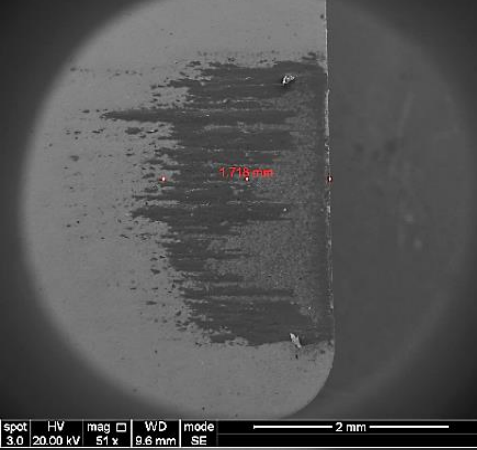| Run Order	Cutting parameters			h (mm)	Theoretical L_C (mm)	SEM Results	Ac (mm²)
	V (m/min)	t (mm)	f (mm/rev)			Experimental L_C (mm)	
1	90	2	0.16	0.800	1.600	1.569	3.800
2	90	2	0.16	0.805	1.610	1.6175	4.097
3	90	2	0.16	0.775	1.549	1.54	3.762
4	40	2	0.16	1.185	2.370	2.304	6.336
5	60	2.5	0.12	0.705	1.410	1.48	4.554
6	60	2.5	0.2	0.978	1.955	1.619	4.807
7	120	1.5	0.12	0.412	0.824	0.804	1.376
8	140	2	0.16	0.612	1.224	1.454	3.354
9	90	1.2	0.16	0.547	1.093	1.15	1.857
10	120	1.5	0.2	0.633	1.265	1.208	2.264
11	90	2.8	0.16	0.719	1.437	1.408	4.722
12	120	2.5	0.2	0.793	1.587	1.35	3.654
13	60	1.5	0.2	0.946	1.892	1.614	3.231
14	90	2	0.16	0.767	1.534	1.533	3.710
15	90	2	0.16	0.664	1.328	1.56	3.855
16	90	2	0.23	0.987	1.974	1.931	5.637
17	90	2	0.16	0.770	1.540	1.604	4.097
18	60	1.5	0.12	0.553	1.107	1.142	2.145
19	120	2.5	0.12	0.571	1.142	0.9308	2.732
20	90	2	0.09	0.510	1.020	1.061	2.490

1)

2)

3)

4)

5)

6)

7)

8)

227

9)

10)

11)

12)

13)

14)

This sample was lost

15)

16)
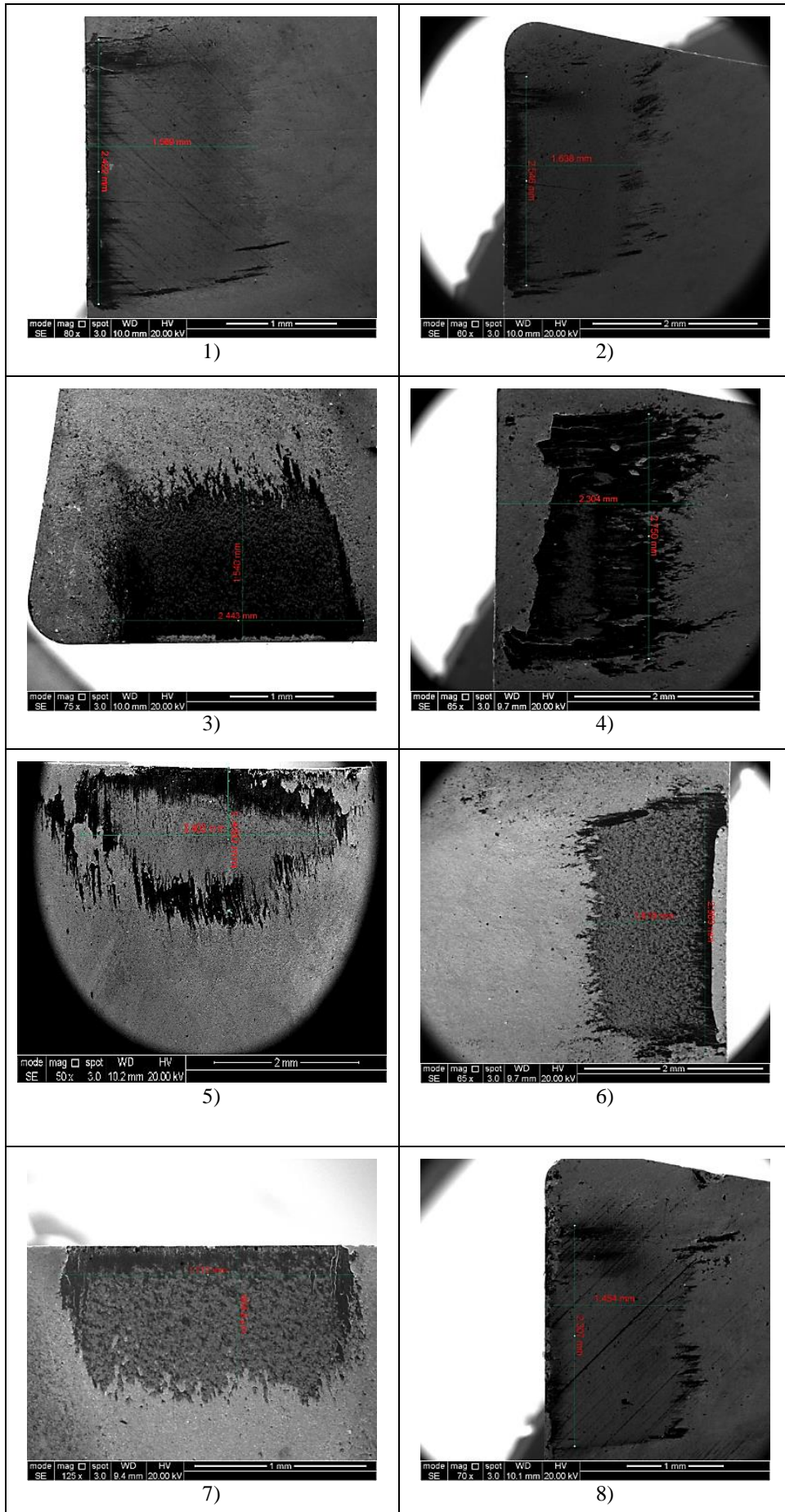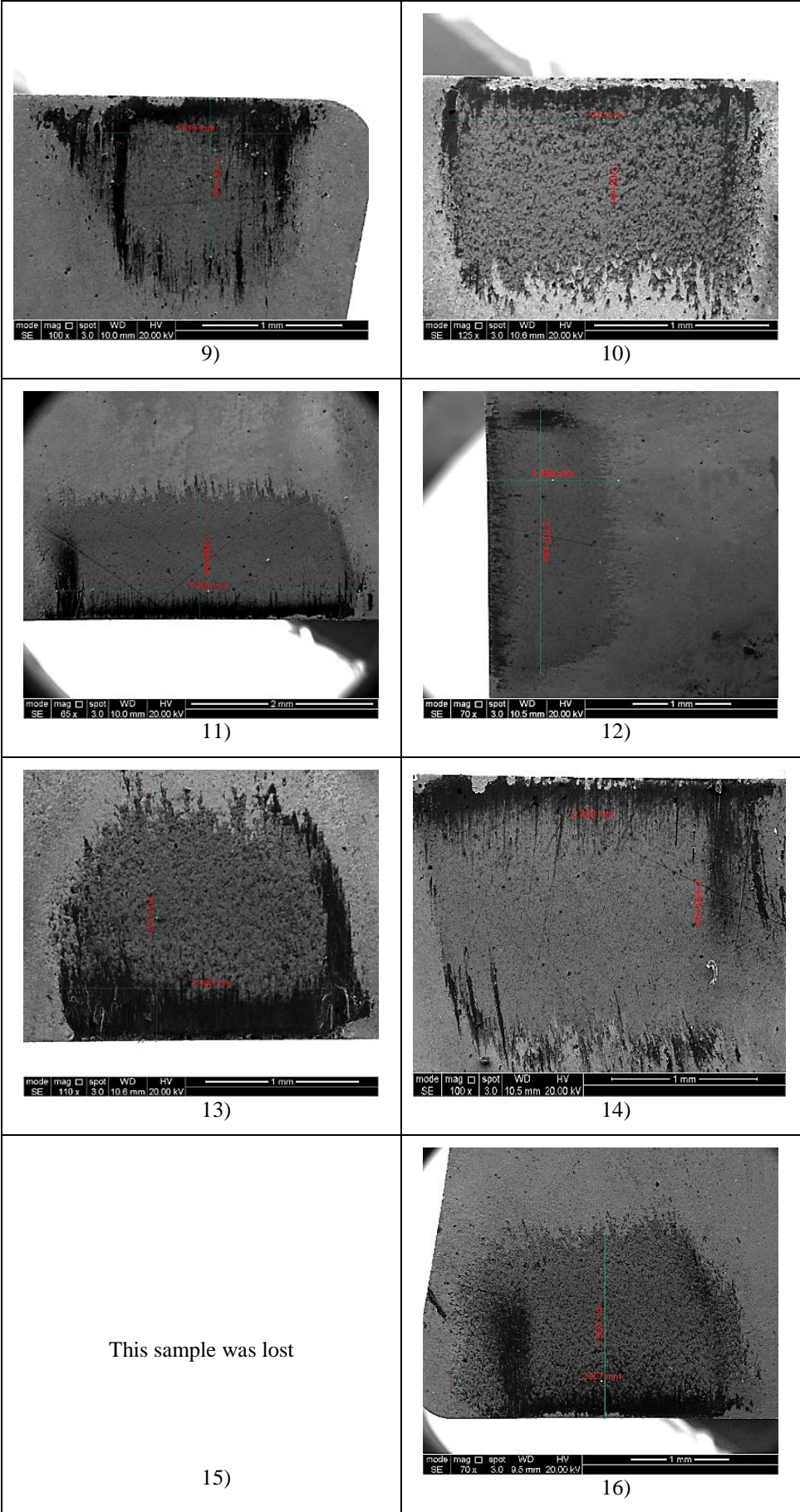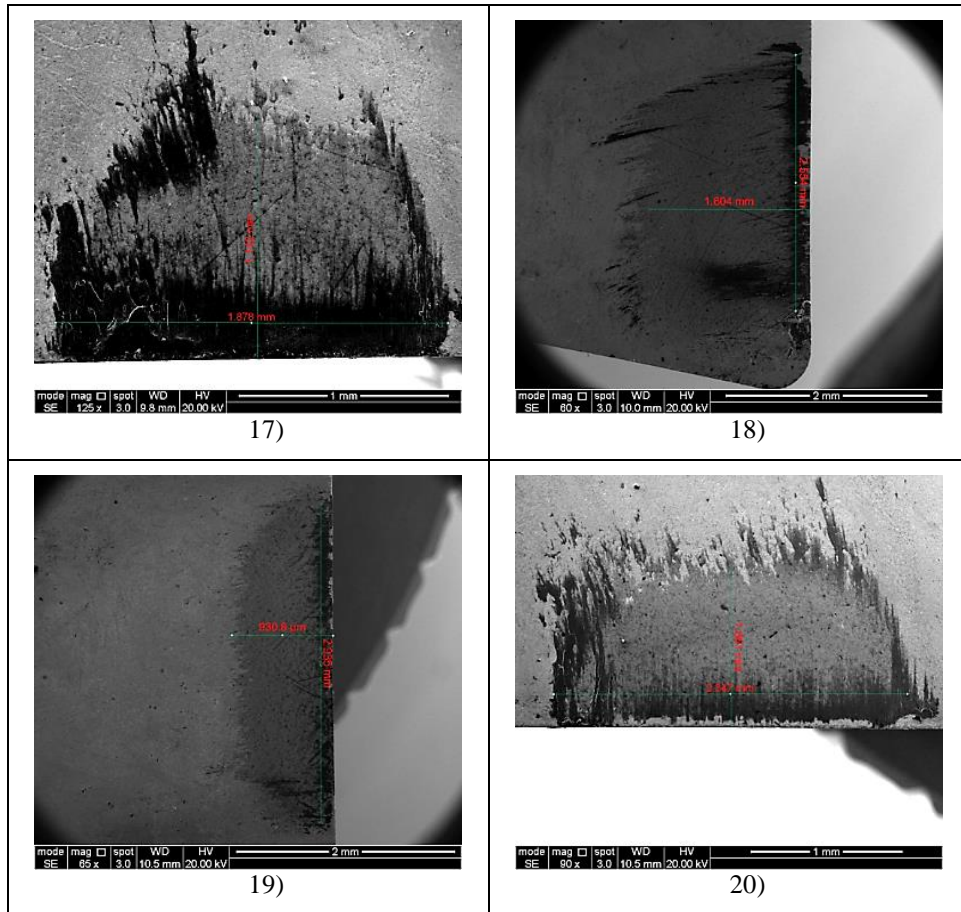
Figure A.6 SEM photographs of the rake face of the cutting tool during dry cutting conditions of *Al 6082* at different cutting speeds, cutting depth and feed

The current results confirm the results of the first pilot study with respect to the relationship between the cutting speed and tool-chip contact length. Figure A.7 shows the comparison of the experimental results of the contact length, obtained from the SEM, and the analytical results, gained from Kato et al. (1972) and Toropov & Ko (2003) model, during dry. What is interesting in this data is the good agreement between the both results.

229
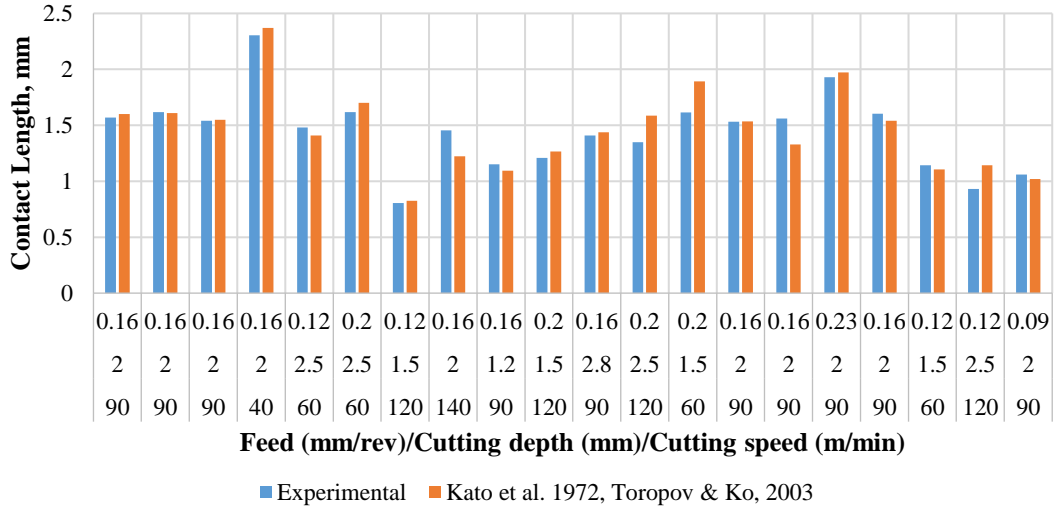
Figure A.7 Benchmarking of contact length model

To study the influence of the machining parameters on the contact length on the temperature, some results of Figure A.7 has been re-presented in linear graphs and presented below.

The influence of cutting speed on the contact length can be seen from the Figure A.8, where the results show that there has been a steady decrease in the contact length with increasing cutting speed while the cutting depth and feed were kept constant at t=2 mm, f=0.16 mm/rev, respectively.
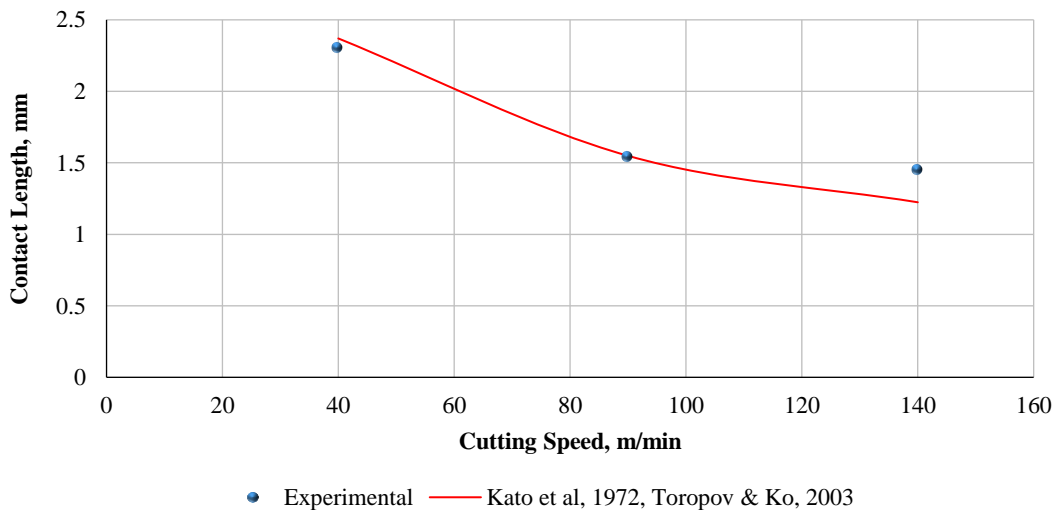
Figure A.8 Comparison of the contact length model with the experimental data for different cutting speeds and a cutting depth of 2 *mm* and feed of 0.16 *mm/rev*

While the relationship between feed and contact length is as follows: the tool-chip contact length increases with the feed. For example, the SEM results show that the

contact length obtained at constant cutting speed of 90 *m/min* and 2 *mm* cutting depth increased from 1.061 *mm* to 1.54 *mm* as the feed increased from 0.09 *mm/rev* to 0.16 *mm/rev*. as the feed increased to 0.23 *mm/rev* and keeping the cutting speed and cutting depth constant the contact length increased from 1.54 *mm* to 1.931 *mm*.
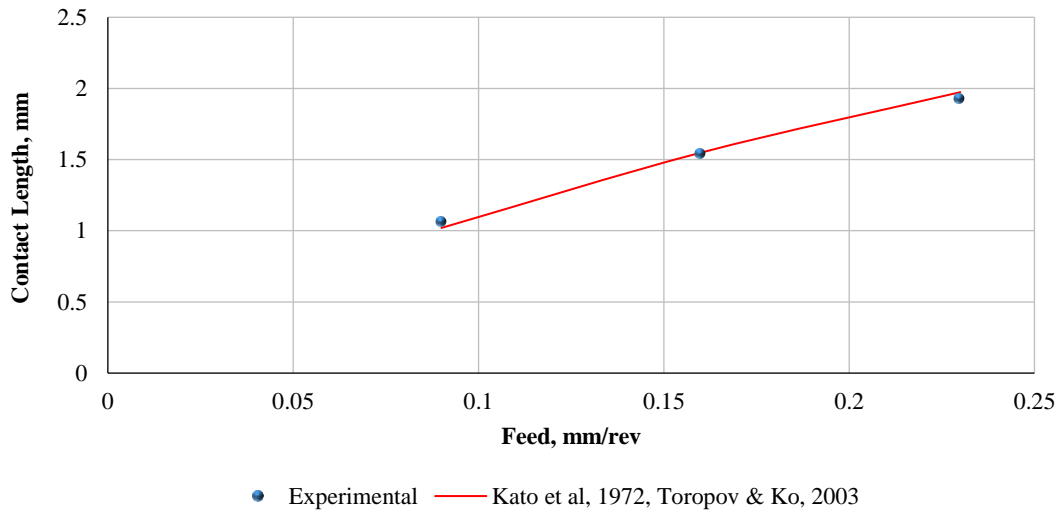
Figure A.9 Comparison of the contact length model with the experimental data for different feed and a cutting speed of 90 *m/min* and cutting depth of 0.16 *mm/rev*

Two different method were used, in this study, to measure the tool-chip contact area. The first method was measuring the tracks area on the rake face cutting tool using the SEM (see Table A.16 and Figure A.6). Multiplying the contact length by the chip width is the other method for measuring the contact area. A good agreement was found between these two results.

A.2.2.2 Contact Length-Main Study

Table A.17 Machining parameters and contact length results (Main study)

Run Order	Cutting parameters			Dry		Wet	
	V (m/min)	t (mm)	f (mm/rev)	L_C (mm)	Ac (mm^2)	L_C (mm)	Ac (mm^2)
1	90	2	0.16	1.41	3.79	1.47	3.86
2	90	2	0.16	1.45	3.95	1.47	3.84
3	90	2	0.16	1.44	3.90	1.47	3.91
4	40	2	0.16	1.75	4.59	0.79	1.77
5	60	2.5	0.12	1.17	3.47	0.90	2.57
6	60	2.5	0.2	1.66	5.38	1.61	5.06
7	120	1.5	0.12	1.11	2.28	1.11	2.19
8	140	2	0.16	1.24	3.21	1.27	3.29
9	90	1.2	0.16	1.47	2.85	1.52	2.86
10	120	1.5	0.2	1.56	3.61	1.61	3.67
11	90	2.8	0.16	1.25	4.22	1.23	4.12
12	120	2.5	0.2	1.46	4.66	1.36	4.25
13	60	1.5	0.2	1.87	4.27	1.13	1.95
14	90	2	0.16	1.39	3.62	1.36	3.56
15	90	2	0.16	1.45	3.81	1.45	3.91
16	90	2	0.23	1.79	5.12	1.85	5.38
17	90	2	0.16	1.48	3.90	1.47	4.01
18	60	1.5	0.12	1.29	2.66	0.54	0.86
19	120	2.5	0.12	1.04	3.10	1.03	3.01
20	90	2	0.09	0.96	2.28	0.70	1.60

where *V*: cutting speed, *t*: cutting depth, *f*: feed, *Lc*: tool-chip contact length and *Ac*: tool-chip contact area.

A.2.2.2.1   ANOVA of the Contact Length

The results of the ANOVA of contact length during dry and wet turning are presented in (Table A.18-Table A.21). It can be seen from Table A.18 that the linear model of the machining parameters cutting speed (*A*), cutting depth (*B*) and feed (*C*) have a stronger effect on the contact length during dry cutting. Furthermore, the quadratic values of cutting depth (B*B*) and feed (*C*C*) are also significant. As for the quadratic value of cutting speed (*A*A*) there is no significant influence on the contact length. Regarding to the interaction influence, it can be seen from the ANOVA outputs that there is no significant effect on the contact length.

Table A.18 ANOVA output of contact length in dry conditions

Source	DF	Adj SS	Adj MS	F-Value	P-Value
Model	9	1.11474	0.123860	81.57	0.000
Linear	3	1.07769	0.359230	236.58	0.000
Speed	1	0.20620	0.206196	135.80	0.000
Depth	1	0.05755	0.057548	37.90	0.000
Feed	1	0.81394	0.813945	536.06	0.000
Square	3	0.02696	0.008988	5.92	0.014
Speed*Speed	1	0.00471	0.004713	3.10	0.109
Depth*Depth	1	0.01278	0.012778	8.42	0.016
Feed*Feed	1	0.00832	0.008320	5.48	0.041
2-Way Interaction	3	0.01009	0.003363	2.21	0.149
Speed*Depth	1	0.00303	0.003026	1.99	0.188
Speed*Feed	1	0.00525	0.005246	3.45	0.093
Depth*Feed	1	0.00182	0.001817	1.20	0.300
Error	10	0.01518	0.001518		
Lack-of-Fit	5	0.01005	0.002010	1.96	0.240
Pure Error	5	0.00514	0.001027		
Total	19	1.12993			

Table A.19 presents only the significant effects of the cutting parameters on the contact length. The determination coefficient (R^2) of the model is 98.23% which is indicating the high data fit, the values of adjusted determination coefficient (adj. R^2) and predicted determination coefficient (predR^2) are also shown in Table A.19 (97.19% and 93.67%, respectively).

Table A.19 ANOVA output of contact length in dry conditions (Significant)

Source	DF	Adj SS	Adj MS	F-Value	P-Value
Model	7	1.10990	0.158557	95.01	0.000
Linear	3	1.07769	0.359230	215.25	0.000
Speed	1	0.20620	0.206196	123.55	0.000
Depth	1	0.05755	0.057548	34.48	0.000
Feed	1	0.81394	0.813945	487.71	0.000
Square	3	0.02696	0.008988	5.39	0.014
Speed*Speed	1	0.00471	0.004713	2.82	0.119
Depth*Depth	1	0.01278	0.012778	7.66	0.017
Feed*Feed	1	0.00832	0.008320	4.99	0.045
2-Way Interaction	1	0.00525	0.005246	3.14	0.102
Speed*Feed	1	0.00525	0.005246	3.14	0.102
Error	12	0.02003	0.001669		
Lack-of-Fit	7	0.01489	0.002127	2.07	0.220
Pure Error	5	0.00514	0.001027		
Total	19	1.12993			
R-Squared	98.23%				
R-Squared (adj)	97.19%				
R-Squared (pred)	93.67%				

The final equation in terms of significant factors for the contact length model in dry turning is given by Equation A.7: Regression equation in uncoded units.

$$Lc_{Dry} = 0.081 - 430 \times 10^{-5}A + 0.347B + 12.83C + 20 \times 10^{-6}A^2$$
$$- 0.1191B^2 - 15.02C^2 - 0.0213AC$$

A.7

where *Lc*: contact length, *A*: cutting speed, *B*: cutting depth and *C*: feed.

Table A.20 and Table A.21present the ANOVA outputs of the contact length during applying the cutting fluid. It can be seen from Table A.20 that the linear model of the machining parameters cutting speed (*A*) and feed (*C*) have a stronger effect on the contact length during wet cutting while the cutting depth has no significant effect on the contact length. In addition, the quadratic values of cutting speed (*A*A*) and feed (*C*C*) are also significant. As for the quadratic values of cutting depth (*B*B*) has no significant influence on the contact length. Regarding to the interaction influence, it can be seen from the ANOVA outputs that the interaction between cutting speed and cutting depth has the significant effect on the contact length while the other interactions have no significant effect on the contact length.

Table A.20 ANOVA output of contact length in wet conditions

Source	DF	Adj SS	Adj MS	F-Value	P-Value
Model	9	2.03860	0.22651	18.47	0.000
Linear	3	1.42743	0.47581	38.80	0.000
Speed	1	0.22335	0.22335	18.22	0.002
Depth	1	0.00007	0.00007	0.01	0.941
Feed	1	1.20401	1.20401	98.19	0.000
Square	3	0.41499	0.13833	11.28	0.002
Speed*Speed	1	0.36471	0.36471	29.74	0.000
Depth*Depth	1	0.02030	0.02030	1.66	0.227
Feed*Feed	1	0.07501	0.07501	6.12	0.033
2-Way Interaction	3	0.19617	0.06539	5.33	0.019
Speed*Depth	1	0.16929	0.16929	13.81	0.004
Speed*Feed	1	0.02658	0.02658	2.17	0.172
Depth*Feed	1	0.00031	0.00031	0.03	0.877
Error	10	0.12262	0.01226		
Lack-of-Fit	5	0.11314	0.02263	11.94	0.008
Pure Error	5	0.00947	0.00189		
Total	19	2.16121			

Table A.21 presents only the significant effects of the cutting parameters on the contact length in wet conditions. As explained in Section A.2.1.1, that in order to maintain a hierarchical model at each step, the stepwise procedure added terms during the procedure.

Table A.21 ANOVA output of contact length in wet conditions (Significant)

Source	DF	Adj SS	Adj MS	F-Value	P-Value
Model	6	1.99141	0.33190	25.41	0.000
Linear	3	1.42743	0.47581	36.43	0.000
Speed	1	0.22335	0.22335	17.10	0.001
Depth	1	0.00007	0.00007	0.01	0.942
Feed	1	1.20401	1.20401	92.18	0.000
Square	2	0.39469	0.19735	15.11	0.000
Speed*Speed	1	0.35128	0.35128	26.89	0.000
Feed*Feed	1	0.06814	0.06814	5.22	0.040
2-Way Interaction	1	0.16929	0.16929	12.96	0.003
Speed*Depth	1	0.16929	0.16929	12.96	0.003
Error	13	0.16980	0.01306		
Lack-of-Fit	8	0.16033	0.02004	10.58	0.009
Pure Error	5	0.00947	0.00189		
Total	19	2.16121			
R-Squared	92.14%				
R-Squared (adj)	88.52%				
R-Squared (pred)	76.98%				

Final equation in terms of significant factors for the contact length model in wet cutting conditions is given by Equation A.8: Regression equation in uncoded units.

$$Lc_{Wet} = -4.401 + 0.05473A + 0.877B + 21.11C - 173 \times 10^{-6}A^2 \\ - 42.8C^2 - 0.0097AB \qquad \text{A.8}$$

where *Lc*: contact length, *A*: cutting speed, *B*: cutting depth and *C*: feed.

A.2.2.2.2 ANOVA of the Contact Area

The results of the ANOVA of contact area during dry and wet cutting are presented in (Table A.22-Table A.25). It can be seen from Table A.22 that the linear model of the machining parameters cutting speed (*A*), cutting depth (*B*) and feed (*C*) have a stronger effect on the contact area during dry cutting. Furthermore, the quadratic value of cutting depth (B*B) is also significant. As for the quadratic value of cutting speed (*A*A) and feed (*C*C) there are no significant influence on the contact area. Regarding

to the interaction influence, it can be seen from the ANOVA outputs that there is no significant effect on the contact area.

Table A.22 ANOVA output of contact area in dry conditions

Source	DF	Adj SS	Adj MS	F-Value	P-Value
Model	9	13.6866	1.52074	95.10	0.000
Linear	3	13.3879	4.46264	279.08	0.000
Speed	1	1.4526	1.45259	90.84	0.000
Depth	1	2.7360	2.73603	171.10	0.000
Feed	1	9.1993	9.19929	575.29	0.000
Square	3	0.2133	0.07110	4.45	0.031
Speed*Speed	1	0.0064	0.00645	0.40	0.540
Depth*Depth	1	0.1715	0.17153	10.73	0.008
Feed*Feed	1	0.0371	0.03710	2.32	0.159
2-Way Interaction	3	0.0854	0.02847	1.78	0.214
Speed*Depth	1	0.0004	0.00043	0.03	0.874
Speed*Feed	1	0.0511	0.05111	3.20	0.104
Depth*Feed	1	0.0339	0.03387	2.12	0.176
Error	10	0.1599	0.01599		
Lack-of-Fit	5	0.0918	0.01835	1.35	0.376
Pure Error	5	0.0681	0.01363		
Total	19	13.8465			

Table A.23 presents only the significant effects of the cutting parameters on the contact area. The determination coefficient (R^2) of the model is 98.80% which is indicating the high data fit, the values of adjusted determination coefficient (adj. R^2) and predicted determination coefficient (predR^2) are also shown in Table A.23 (98.09% and 96.82%, respectively).

Table A.23 ANOVA output of contact area in dry conditions (Significant)

Source	DF	Adj SS	Adj MS	F-Value	P-Value
Model	7	13.6797	1.95425	140.61	0.000
Linear	3	13.3879	4.46264	321.09	0.000
Speed	1	1.4526	1.45259	104.52	0.000
Depth	1	2.7360	2.73603	196.86	0.000
Feed	1	9.1993	9.19929	661.90	0.000
Square	2	0.2068	0.10342	7.44	0.008
Depth*Depth	1	0.1800	0.17997	12.95	0.004
Feed*Feed	1	0.0406	0.04063	2.92	0.113
2-Way Interaction	2	0.0850	0.04249	3.06	0.085
Speed*Feed	1	0.0511	0.05111	3.68	0.079
Depth*Feed	1	0.0339	0.03387	2.44	0.144
Error	12	0.1668	0.01390		
Lack-of-Fit	7	0.0986	0.01409	1.03	0.503
Pure Error	5	0.0681	0.01363		
Total	19	13.8465			
R-Squared	98.80%				
R-Squared (adj)	98.09%				
R-Squared (pred)	96.82%				

Final equation in terms of significant factors for the contact area model in dry turning is given by Equation A.9: Regression equation in uncoded units.

$$Ac_{Dry} = -2.79 - 0.00021A + 2.154B + 30.57C - 0.445B^2 - 33C^2 \\ - 0.0666AC + 3.25BC$$

A.9

where Ac: contact area, A: cutting speed, B: cutting depth and C: feed.

Table A.24 and Table A.25 present the ANOVA outputs of the contact area while applying the cutting fluid. It can be seen from Table A.24 that the linear model of the machining parameters cutting speed (A), cutting depth (B) and feed (C) have a stronger effect on the contact area during wet cutting during wet cutting. In addition, the quadratic value of cutting speed ($A*A$) is also significant. As for the quadratic values of cutting depth ($B*B$) and feed ($C*C$) have no significant influence on the contact area. Regarding to the interaction influence, it can be seen from the ANOVA outputs that the interaction between cutting speed and cutting depth has the significant effect on the contact area while the other interactions have no significant effect on the contact area.

Table A.24 ANOVA output of contact area in wet conditions

Source	DF	Adj SS	Adj MS	F-Value	P-Value
Model	9	24.6145	2.7349	18.01	0.000
Linear	3	18.8774	6.2925	41.43	0.000
Speed	1	2.0119	2.0119	13.25	0.005
Depth	1	5.1139	5.1139	33.67	0.000
Feed	1	11.7516	11.7516	77.37	0.000
Square	3	4.0288	1.3429	8.84	0.004
Speed*Speed	1	3.6758	3.6758	24.20	0.001
Depth*Depth	1	0.3926	0.3926	2.58	0.139
Feed*Feed	1	0.3934	0.3934	2.59	0.139
2-Way Interaction	3	1.7083	0.5694	3.75	0.049
Speed*Depth	1	1.4534	1.4534	9.57	0.011
Speed*Feed	1	0.0897	0.0897	0.59	0.460
Depth*Feed	1	0.1652	0.1652	1.09	0.322
Error	10	1.5190	0.1519		
Lack-of-Fit	5	1.4023	0.2805	12.02	0.008
Pure Error	5	0.1167	0.0233		
Total	19	26.1335			

Table A.25 shows only the significant effects of the cutting parameters on the contact area.

Table A.25 ANOVA output of contact area in wet conditions (Significant)

Source	DF	Adj SS	Adj MS	F-Value	P-Value
Model	5	23.6446	4.7289	26.60	0.000
Linear	3	18.8774	6.2925	35.40	0.000
Speed	1	2.0119	2.0119	11.32	0.005
Depth	1	5.1139	5.1139	28.77	0.000
Feed	1	11.7516	11.7516	66.10	0.000
Square	1	3.3138	3.3138	18.64	0.001
Speed*Speed	1	3.3138	3.3138	18.64	0.001
2-Way Interaction	1	1.4534	1.4534	8.18	0.013
Speed*Depth	1	1.4534	1.4534	8.18	0.013
Error	14	2.4889	0.1778		
Lack-of-Fit	9	2.3722	0.2636	11.29	0.008
Pure Error	5	0.1167	0.0233		
Total	19	26.1335			
R-Squared	90.48%				
R-Squared (adj)	87.07%				
R-Squared (pred)	76.43%				

Final equation in terms of significant factors for the contact area model in wet turning is given by Equation A.10: Regression equation in uncoded units.

$$Ac_{Wet} = -13.09 + 0.1647A + 3.781B + 23.19C - 0.000528A^2 \\ - 0.02842AB \qquad \text{A.10}$$

where *Ac*: contact area, *A*: cutting speed, *B*: cutting depth and *C*: feed.

A.3 Measurement of Cutting Forces

Table A.26 Cutting parameters and cutting forces results

Run Order	Cutting parameters			Dry		Wet	
	Cutting Speed (m/min)	Depth of Cut (mm)	Feed (mm/rev)	Thrust force (N)	Cutting force (N)	Thrust force (N)	Cutting force (N)
1	90	2	0.16	335.1	388.77	337.47	406.57
2	90	2	0.16	335.33	393.57	333.53	407.97
3	90	2	0.16	333.97	393.07	339.87	413.13
4	40	2	0.16	405.67	467.57	198.90	322.17
5	60	2.5	0.12	365.45	406.5	269.15	359.65
6	60	2.5	0.2	513	587.05	493.53	579.13
7	120	1.5	0.12	202.55	231.25	203.57	238.23
8	140	2	0.16	279.33	350.5	280.65	352.85
9	90	1.2	0.16	228.05	259.48	226.27	267.13
10	120	1.5	0.2	272.95	326.3	268.40	332.73
11	90	2.8	0.16	463.85	526.25	443.88	522.70
12	120	2.5	0.2	412.45	519.05	409.57	510.50
13	60	1.5	0.2	338.05	385.55	194.20	303.03
14	90	2	0.16	332.2	371.3	324.93	393.10
15	90	2	0.16	351.8	396.15	332.85	409.70
16	90	2	0.23	398.65	476.8	407.95	517.55
17	90	2	0.16	346.3	393.3	344.75	417.50
18	60	1.5	0.12	248.13	277.03	132.03	196.73
19	120	2.5	0.12	329.1	371.5	325.50	390.85
20	90	2	0.09	238.2	265.47	220.07	260.83

A.2.1 Analysis of Variance (ANOVA)

A.3.1.1 Thrust Forces *Ft*

It can be seen from Table A.27 that cutting speed (*A*), cutting depth (*B*) and feed (*C*), the quadratic value of feed (*C*C*), and the interaction between cutting speed and feed (*A*C*) and the interaction between cutting depth and feed (*B*C*) all have the most significant effect on the thrust force F_t during dry turning; while the quadratic values of cutting speed (*A*A*) and cutting depth (*B*B*) and the interaction between cutting speed and depth of cut (*A*B*) have no significant effect on the thrust force.

Table A.27 ANOVA output of thrust force F_t in dry conditions

Source	DF	Adj SS	Adj MS	F-Value	P-Value	Note
Model	9	116912	12990.2	185.83	0.000	Significant <0.05
Linear	3	114263	38087.5	544.87	0.000	
A	1	15497	15496.8	221.69	0.000	
B	1	66766	66766.3	955.14	0.000	
C	1	31999	31999.4	457.78	0.000	
Square	3	1065	354.9	5.08	0.022	
A*A	1	1	1.2	0.02	0.898	Not Significant >0.05
B*B	1	33	32.8	0.47	0.509	
C*C	1	974	974.2	13.94	0.004	
2-Way Interaction	3	1585	528.3	7.56	0.006	
A*B	1	86	86.0	1.23	0.293	
A*C	1	876	876.2	12.54	0.005	
B*C	1	623	622.6	8.91	0.014	
Error	10	699	69.9			
Lack-of-Fit	5	399	79.9	1.33	0.380	
Pure Error	5	300	59.9			
Total	19	117611				

DF: Degree of freedom Adj SS: Adjusted sum of square Adj MS: Adjusted mean square

The results of the ANOVA of thrust forces during wet turning are presented in Table A.28. It can be seen from the table that the linear model of the machining parameters cutting depth (*B*) and feed (*C*) have a stronger effect effect on the thrust force F_t, while the cutting speed (*A*) has less effect on the output. The ANOVA results also show that the thrust force F_t is strongly affected by the quadratic model of cutting speed (*A*A*). While there is no significant effect of the quadratic value of depth of cut (*B*B*) and feed (C*C) on the thrust force. Regarding to the interaction between the cutting parameters during wet turning, the results show that the thrust force is significantly influenced by (*A*B*) and (*B*C*) more than (*A*C*).

Table A.28 ANOVA output of thrust force F_t in wet conditions

Source	DF	Adj SS	Adj MS	F-Value	P-Value	Note
Model	9	158021	17557.9	35.38	0.000	Significant <0.05
Linear	3	129262	43087.5	86.83	0.000	
A	1	4784	4783.9	9.64	0.011	
B	1	83133	83133.2	167.54	0.000	
C	1	41345	41345.4	83.32	0.000	
Square	3	18518	6172.8	12.44	0.001	
A*A	1	17983	17983.5	36.24	0.000	
B*B	1	38	38.4	0.08	0.786	Not Significant >0.05
C*C	1	1188	1188.1	2.39	0.153	
2-Way Interaction	3	10240	3413.4	6.88	0.009	
A*B	1	3756	3756.3	7.57	0.020	
A*C	1	2368	2368.4	4.77	0.054	
B*C	1	4116	4115.5	8.29	0.016	
Error	10	4962	496.2			
Lack-of-Fit	5	4731	946.2	20.48	0.002	
Pure Error	5	231	46.2			
Total	19	162983				

DF: Degree of freedom Adj SS: Adjusted sum of square Adj MS: Adjusted mean square

A.3.1.2 Cutting Forces *Fc*

The results of the ANOVA of cutting force F_C during dry turning are presented in Table A.29. It can be seen from the table that the linear model of the machining parameters cutting speed (*A*), cutting depth (*B*) and feed (*C*) have a stronger effect on the cutting force F_C. In addition, the quadratic values of cutting speed (*A*A*) and feed (*C*C*) are also significant but, the effect of (*C*C*) is bigger than the cutting speed during dry turning. As for the quadratic value of depth of cut (*B*B*) there is no significant influence on the cutting force. Regarding to the interaction influence, it can be seen from the ANOVA outputs that the interaction between cutting speed and feed (*A*C*) and the interaction between cutting depth and feed (*B*C*) have the significant effect on the cutting force F_C; while the interaction between cutting speed and depth of cut (*A*B*) have no significant effect on the cutting force F_C.

Table A.29 ANOVA output of cutting force F_C in dry conditions

Source	DF	Adj SS	Adj MS	F-Value	P-Value	Note
Model	9	163974	18219.3	398.51	0.000	Significant <0.05
Linear	3	160274	53424.8	1168.55	0.000	
A	1	12005	12004.9	262.58	0.000	
B	1	90647	90647.3	1982.72	0.000	
C	1	57622	57622.0	1260.36	0.000	
Square	3	1491	497.0	10.87	0.002	
A*A	1	399	399.3	8.73	0.014	
B*B	1	3	3.0	0.06	0.804	Not Significant >0.05
C*C	1	954	953.9	20.87	0.001	
2-Way Interaction	3	2209	736.3	16.10	0.000	
A*B	1	1	0.5	0.01	0.918	
A*C	1	270	270.0	5.91	0.035	
B*C	1	1938	1938.3	42.40	0.000	
Error	10	457	45.7			
Lack-of-Fit	5	420	83.9	11.21	0.010	
Pure Error	5	37	7.5			
Total	19	164431				

DF: Degree of freedom Adj SS: Adjusted sum of square Adj MS: Adjusted mean square

Table A.30 shows the ANOVA outputs of the cutting force F_C during wet conditions. It can be seen from the ANOVA that the linear model of the machining parameters cutting depth (*B*) and feed (*C*) have a stronger effect on the cutting force F_C. In addition, the quadratic value of cutting speed (*A*A*) are also significant. The two-way interaction shows that the interaction between (*B*C*) have more significant afect on the cutting force F_C than the other intecations.

Table A.30 ANOVA output of cutting force F_C in wet conditions

Source	DF	Adj SS	Adj MS	F-Value	P-Value	Note
Model	9	191206	21245	66.32	0.000	Significant <0.05
Linear	3	174971	58324	182.08	0.000	
A	1	534	534	1.67	0.226	
B	1	105303	105303	328.74	0.000	
C	1	69134	69134	215.83	0.000	
Square	3	10810	3603	11.25	0.002	
A*A	1	10195	10195	31.83	0.000	
B*B	1	572	572	1.79	0.211	Not Significant >0.05
C*C	1	999	999	3.12	0.108	
2-Way	3	5425	1808	5.65	0.016	
Interaction						
A*B	1	1475	1475	4.61	0.057	
A*C	1	1558	1558	4.86	0.052	
B*C	1	2392	2392	7.47	0.021	
Error	10	3203	320			
Lack-of-Fit	5	2860	572	8.32	0.018	
Pure Error	5	344	69			
Total	19	194409				

DF: Degree of freedom Adj SS: Adjusted sum of square Adj MS: Adjusted mean square

A.3.1.3 Model Validation Experiments

The machining parameters for the validation trials and the results of these experiments are shown in Table A.31.

Table A.31 Machining parameters and cutting forces results of the validation trials

Trials No.	Cutting parameters			Dry		Wet	
	Cutting Speed (m/min)	Cutting depth (mm)	Feed (mm/rev)	Thrust force (N)	Cutting force (N)	Thrust force (N)	Cutting force (N)
1	40	2.8	0.16	529.55	592.25	300.80	478.27
2	40	2.5	0.12	392.65	456.90	205.85	327.30
3	90	1.2	0.09	161.63	177.73	108.05	143.18
4	140	2.8	0.09	326.40	346.00	282.45	337.55
5	140	1.2	0.12	156.40	182.70	166.50	194.30
6	90	2.5	0.12	357.10	396.20	365.80	416.30
7	140	2.5	0.12	312.30	355.40	308.60	375.10

B.

Ultrasonic Reflection from Tool-Chip Interface

B.1 Influence of Machining Parameters

Table B.1 Machining parameters and reflection coefficient results

Run Order	V (m/min)	t (mm)	f (mm/rev)	Dry R	Dry Ac (mm^2)	Wet R	Wet Ac (mm^2)
1	90	2	0.16	0.743	3.79	0.923	3.86
2	90	2	0.16	0.751	3.95	0.927	3.84
3	90	2	0.16	0.747	3.90	0.915	3.91
4	40	2	0.16	0.690	4.59	0.814	1.77
5	60	2.5	0.12	0.803	3.47	0.852	2.57
6	60	2.5	0.2	0.681	5.38	0.848	5.06
7	120	1.5	0.12	0.866	2.28	0.878	2.19
8	140	2	0.16	0.797	3.21	0.935	3.29
9	90	1.2	0.16	0.771	2.85	0.957	2.86
10	120	1.5	0.2	0.714	3.61	0.901	3.67
11	90	2.8	0.16	0.734	4.22	0.823	4.12
12	120	2.5	0.2	0.716	4.66	0.875	4.25
13	60	1.5	0.2	0.696	4.27	0.864	1.95
14	90	2	0.16	0.742	3.62	0.930	3.56
15	90	2	0.16	0.742	3.81	0.920	3.91
16	90	2	0.23	0.676	5.12	0.910	5.38
17	90	2	0.16	0.757	3.90	0.925	4.01
18	60	1.5	0.12	0.839	2.66	0.882	0.86
19	120	2.5	0.12	0.848	3.10	0.921	3.01
20	90	2	0.09	0.895	2.28	0.936	1.60

where: *V*: Cutting speed, *t*: cutting depth, *f*: feed, *R*: Reflection coefficient, *Ac*: Tool-chip contact area,

B.2 Analysis of Variance (ANOVA)

The results of the ANOVA of reflection coefficient during dry and wet cutting are presented in (Table B.2 and Table B.3). It can be seen from Table B.2 that the linear model of the cutting parameters cutting speed (*A*), cutting depth (*B*) and feed (*C*) have a stronger effect on the reflection coefficient during dry cutting. In addition, the quadratic value of feed (*C*C*) is significant. As for the quadratic values of cutting speed (*A*A*) and cutting depth (B*B*) there are no significant influence on the reflection coefficient. Regarding to the interaction influence, it can be seen from the ANOVA outputs that there is no significant effect on the reflection coefficient.

Table B.2 ANOVA output of reflection coefficient in dry conditions

Source	DF	Adj SS	Adj MS	F-Value	P-Value
Model	9	0.073648	0.008183	58.32	0.000
Linear	3	0.069698	0.023233	165.58	0.000
Speed	1	0.006876	0.006876	49.00	0.000
Depth	1	0.001216	0.001216	8.67	0.015
Feed	1	0.061606	0.061606	439.08	0.000
Square	3	0.003546	0.001182	8.42	0.004
Speed*Speed	1	0.000007	0.000007	0.05	0.830
Depth*Depth	1	0.000207	0.000207	1.48	0.252
Feed*Feed	1	0.003456	0.003456	24.63	0.001
2-Way Interaction	3	0.000404	0.000135	0.96	0.449
Speed*Depth	1	0.000141	0.000141	1.01	0.339
Speed*Feed	1	0.000046	0.000046	0.33	0.580
Depth*Feed	1	0.000216	0.000216	1.54	0.243
Error	10	0.001403	0.000140		
Lack-of-Fit	5	0.001213	0.000243	6.38	0.032
Pure Error	5	0.000190	0.000038		
Total	19	0.075051			

Table B.3 presents the ANOVA outputs of the cutting parameters on the reflection coefficient during applying cutting fluid. It can be seen from the table that the linear model of the machining parameters cutting speed (*A*) and cutting depth (*B*) have a stronger effect on the reflection coefficient during wet cutting while feed (*C*) has less effect on the output. In addition, the quadratic values of cutting speed (*A*A*) and cutting depth (*B*B*) are also significant. As for the quadratic value of feed (*C*C*) there is no significant influence on the reflection coefficient. Regarding to the interaction influence, it can be seen from the ANOVA outputs that there is no significant effect on the reflection coefficient.

Table B.3 ANOVA output of reflection coefficient in wet conditions

Source	DF	Adj SS	Adj MS	F-Value	P-Value
Model	9	0.026552	0.002950	17.37	0.000
Linear	3	0.015824	0.005275	31.05	0.000
Speed	1	0.010717	0.010717	63.09	0.000
Depth	1	0.003711	0.003711	21.85	0.001
Feed	1	0.001396	0.001396	8.22	0.017
Square	3	0.010379	0.003460	20.37	0.000
Speed*Speed	1	0.004823	0.004823	28.39	0.000
Depth*Depth	1	0.006479	0.006479	38.14	0.000
Feed*Feed	1	0.000019	0.000019	0.11	0.744
2-Way Interaction	3	0.000348	0.000116	0.68	0.583
Speed*Depth	1	0.000017	0.000017	0.10	0.757
Speed*Feed	1	0.000329	0.000329	1.94	0.194
Depth*Feed	1	0.000002	0.000002	0.01	0.926
Error	10	0.001699	0.000170		
Lack-of-Fit	5	0.001643	0.000329	29.60	0.001
Pure Error	5	0.000056	0.000011		
Total	19	0.028250			

Table B.4 shows the machining parameters of the validation trials and also the reflection coefficient results of these experiments during dry and wet cutting conditions.

Table B.4 Machining parameters and reflection coefficient results of the validation trials

Trials No.	Cutting parameters			Reflection Co. Dry		Reflection Co. Wet	
	V (m/min)	*t (mm)*	*f (mm/rev)*	Experimental	Model	Experimental	Model
1	40	2.8	0.16	0.729	0.696	0.785	0.747
2	40	2.5	0.12	0.753	0.785	0.793	0.789
3	90	1.2	0.09	0.926	0.922	0.927	0.916
4	120	1.2	0.09	0.935	0.944	0.944	0.938
5	90	2.5	0.12	0.814	0.823	0.863	0.898
6	140	2.5	0.12	0.874	0.861	0.936	0.907
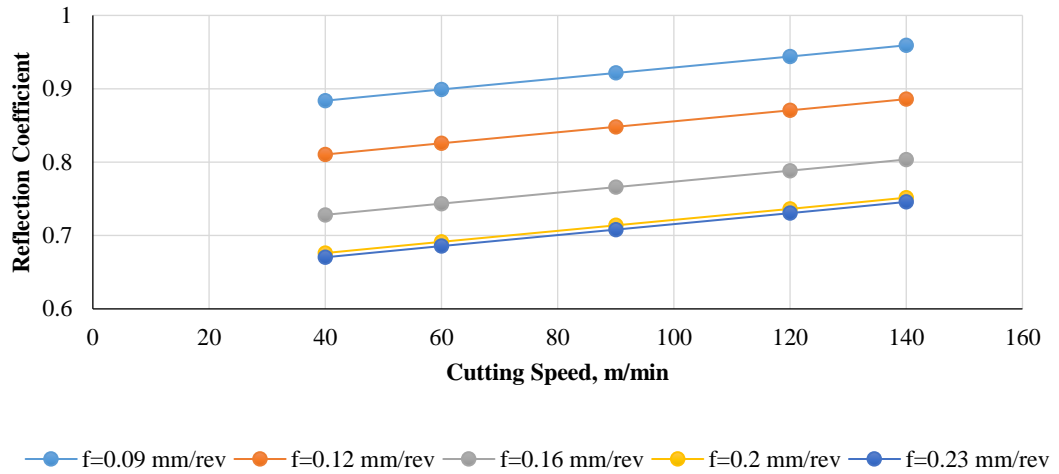
Figure B.1 Reflection coefficients versus cutting speed for different feed at a constant cutting depth of (t=1.2 *mm*)
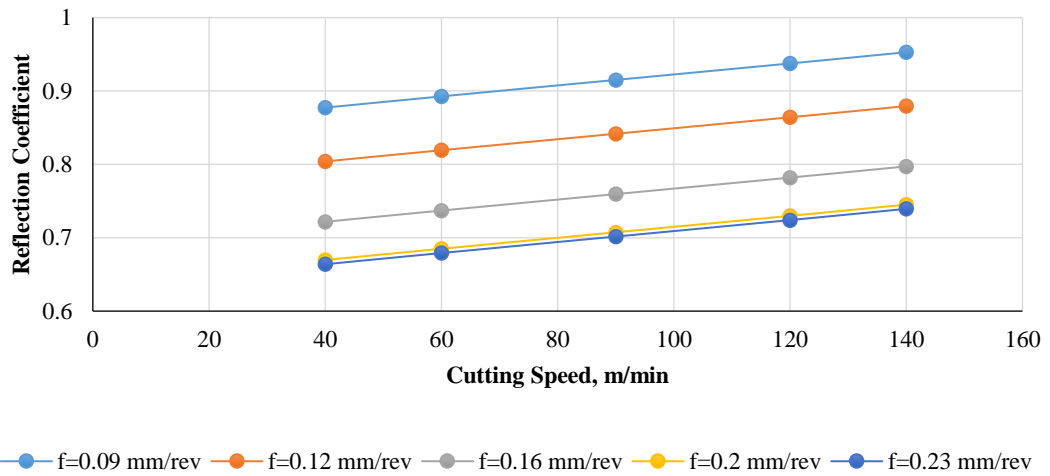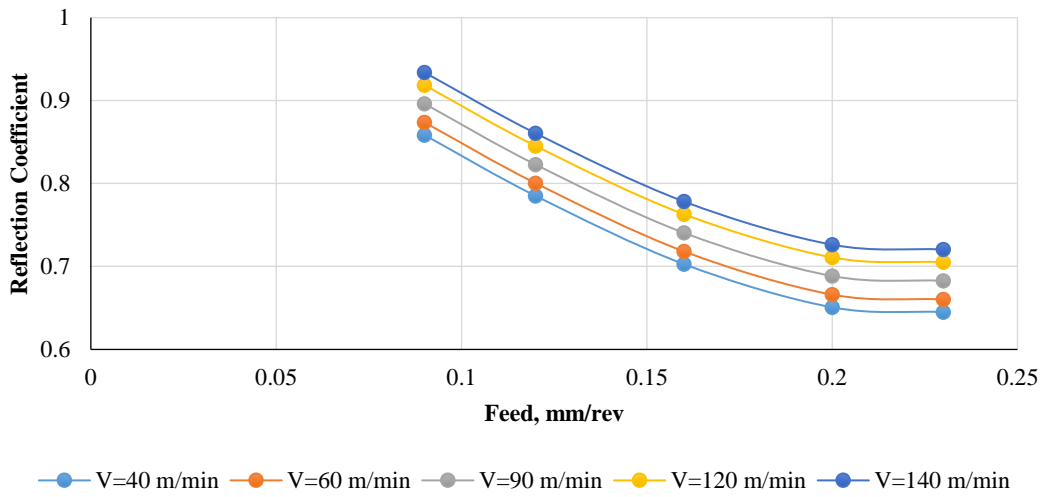

Figure B.2 Reflection coefficients versus cutting speed for different feed at a constant cutting depth of (t=1.5 *mm*)
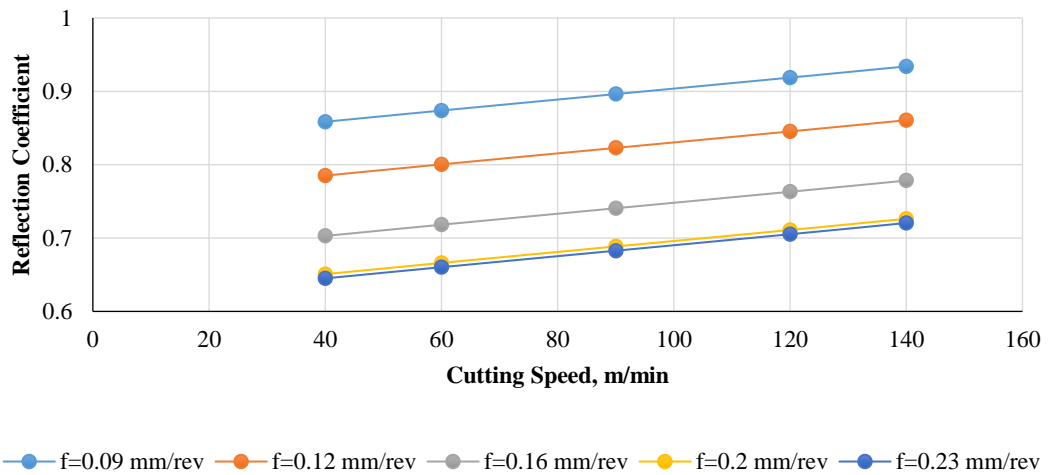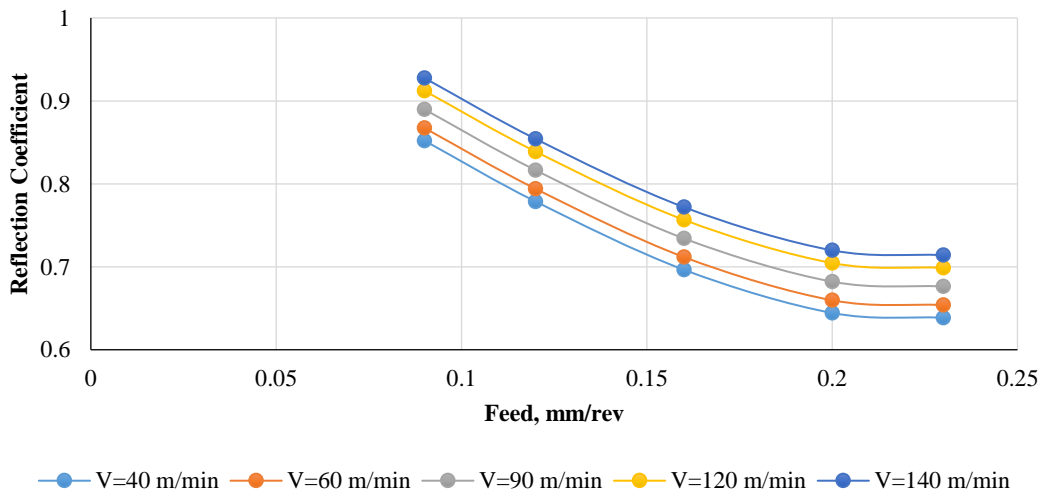

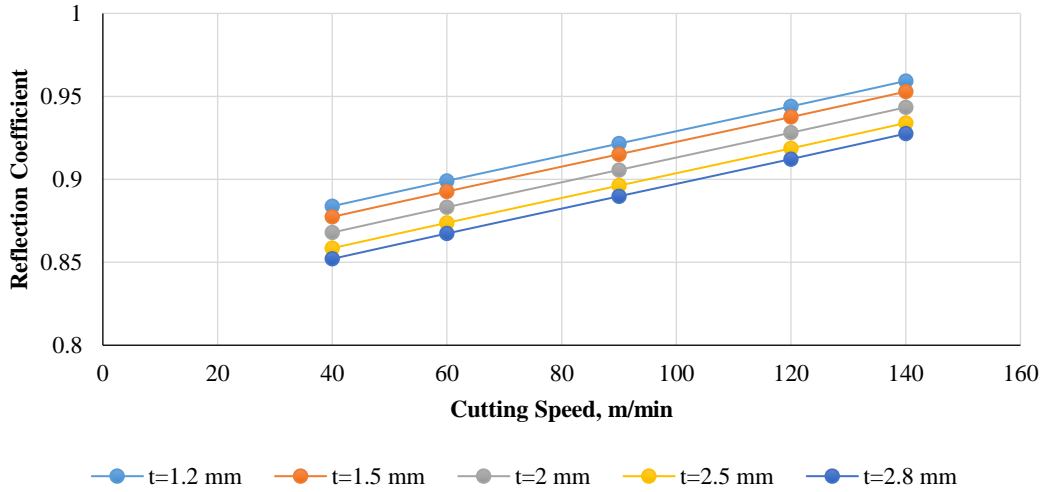**Figure B.3 Reflection coefficients versus cutting speed for different feed at a constant cutting depth of (t=2.5 *mm*)**

248
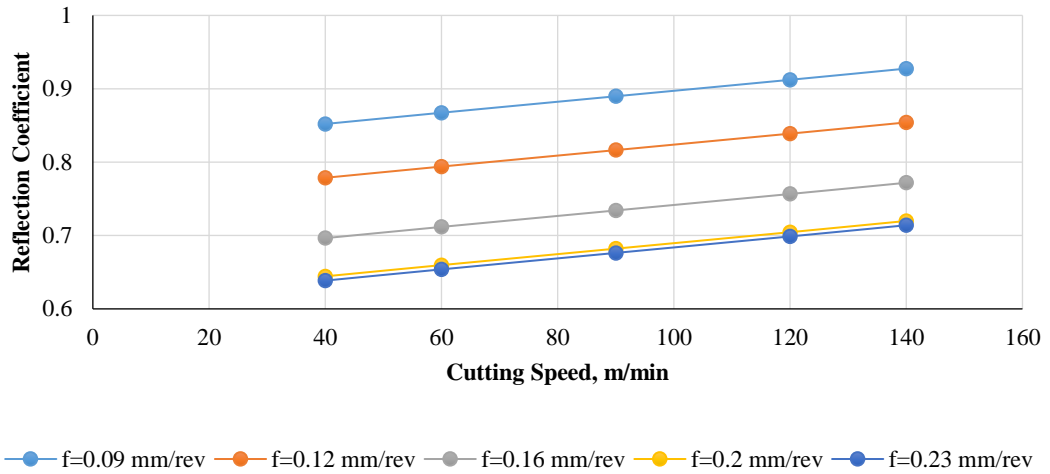
Figure B.4 Reflection coefficients versus cutting speed for different feed at a constant cutting depth of (*t=2.8 mm*)
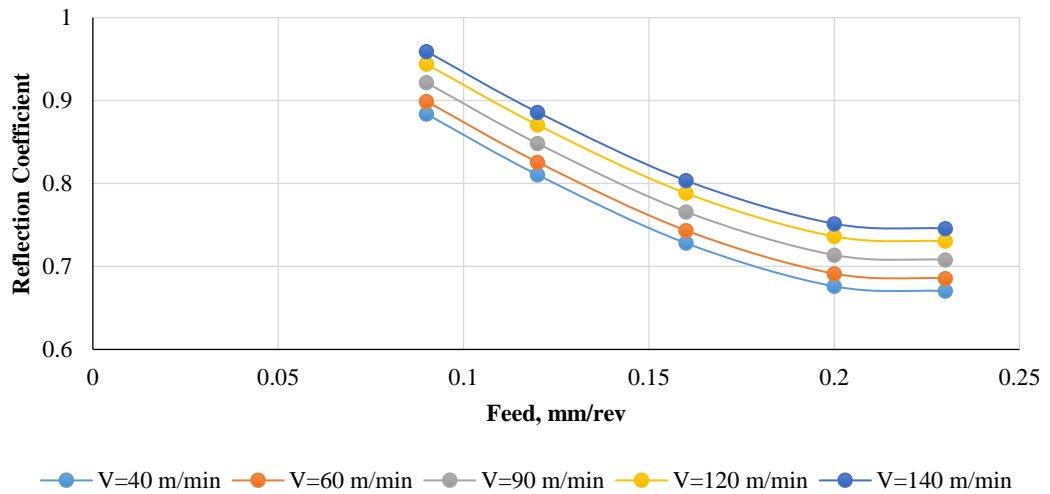
Figure B.5 Reflection coefficients versus feed for different cutting speed at a constant cutting depth of (*t=1.2 mm*)
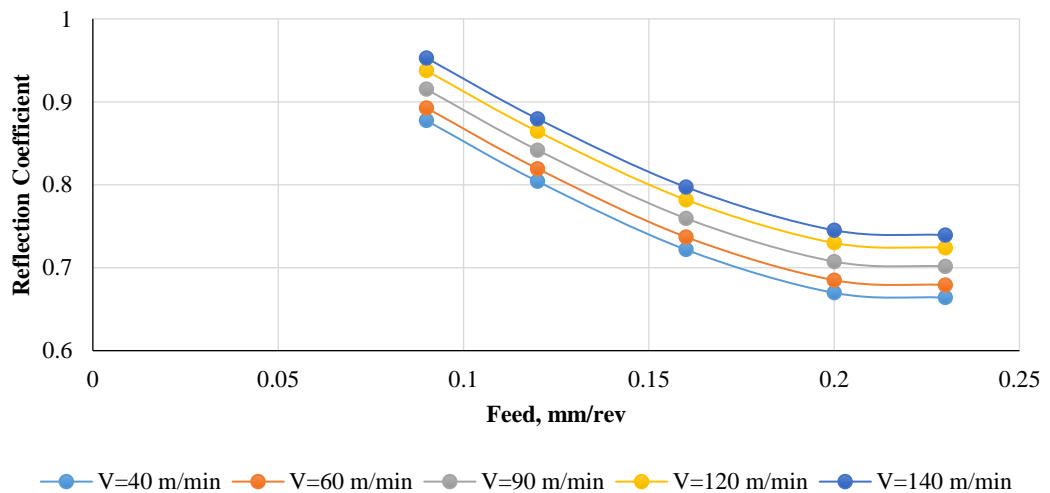
Figure B.6 Reflection coefficients versus feed for different cutting speed at a constant cutting depth of (*t=1.5 mm*)

249
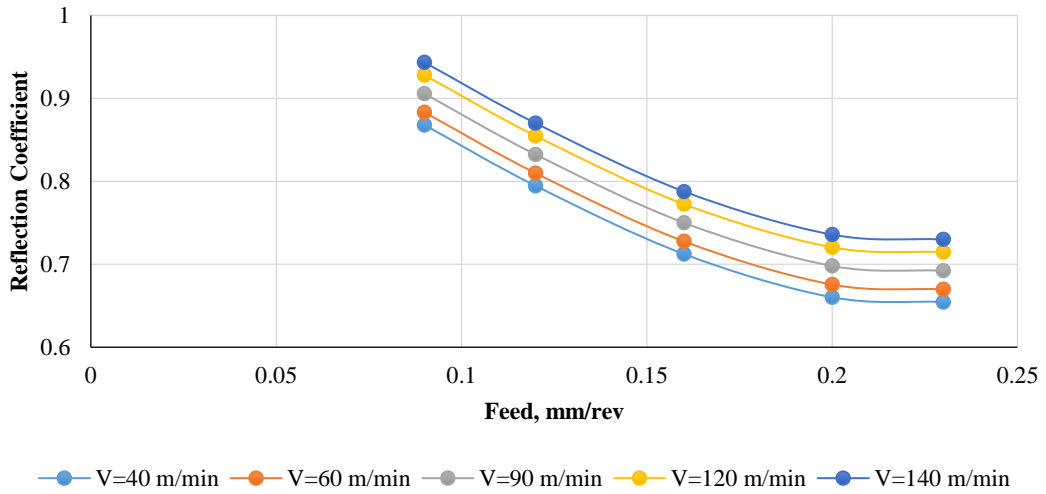
Figure B.7 Reflection coefficients versus feed for different cutting speed at a constant cutting depth of (*t=2 mm*)

Figure B.8 Reflection coefficients versus feed for different cutting speed at a constant cutting depth of (*t=2.5 mm*)

Figure B.9 Reflection coefficients versus feed for different cutting speed at a constant cutting depth of (*t=2.8 mm*)

Figure B.10 Reflection coefficients versus cutting speed for different cutting depth at a constant feed of (*f*=0.09 *mm/rev*)
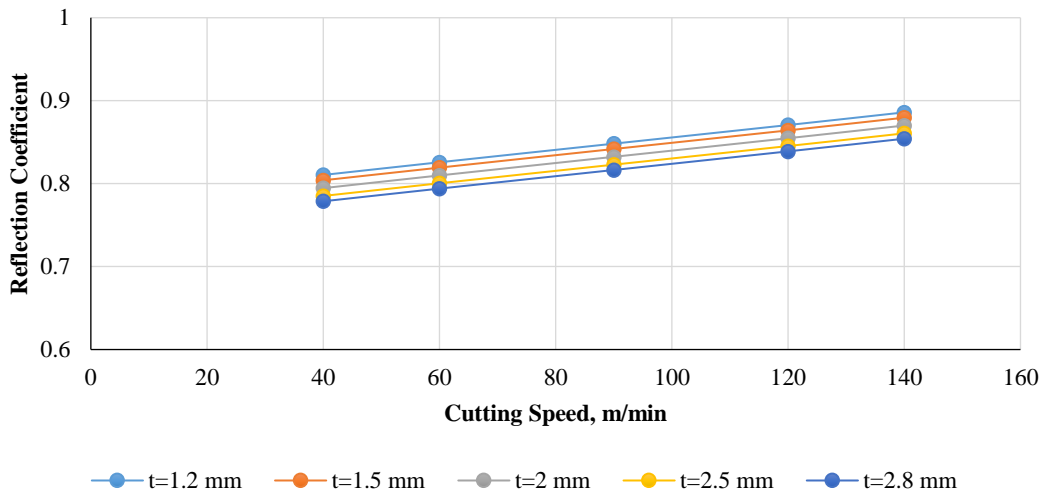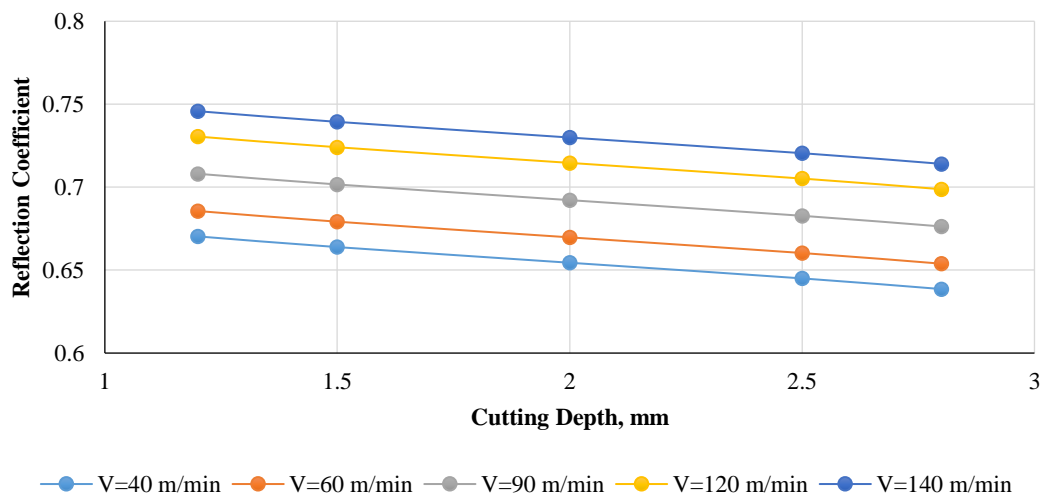

Figure B.11 Reflection coefficients versus cutting speed for different cutting depth at a constant feed of (*f*=0.12 *mm/rev*)
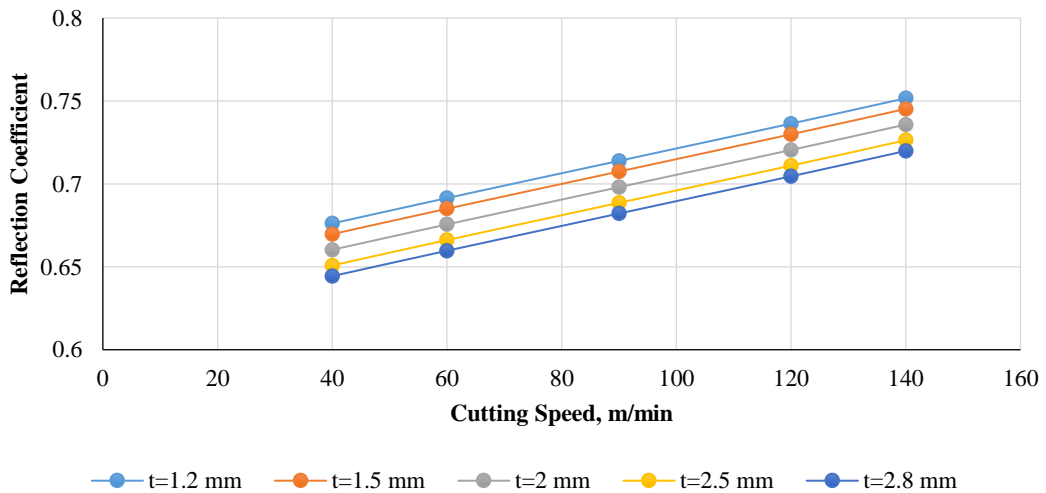
Figure B.12 Reflection coefficients versus cutting speed for different cutting depth at a constant feed of (*f*=0.2 *mm/rev*)
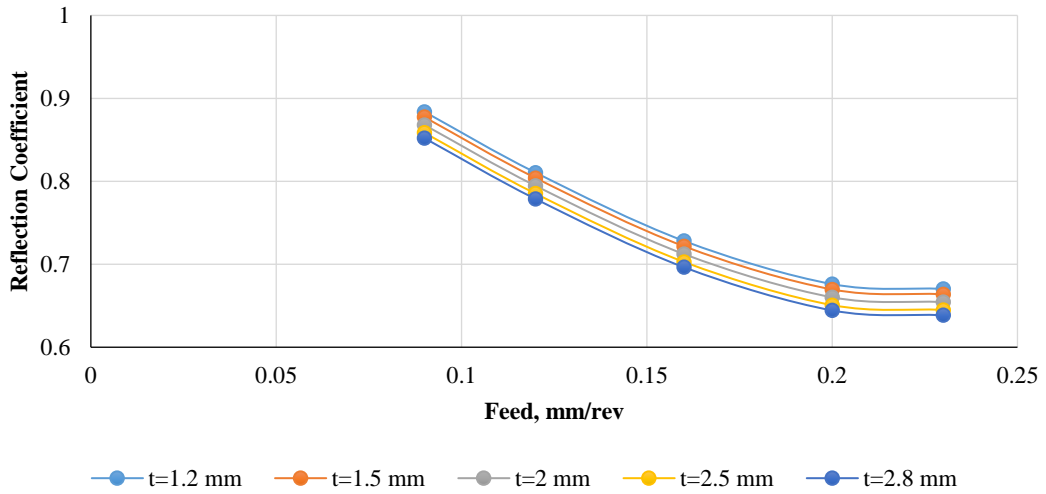
251
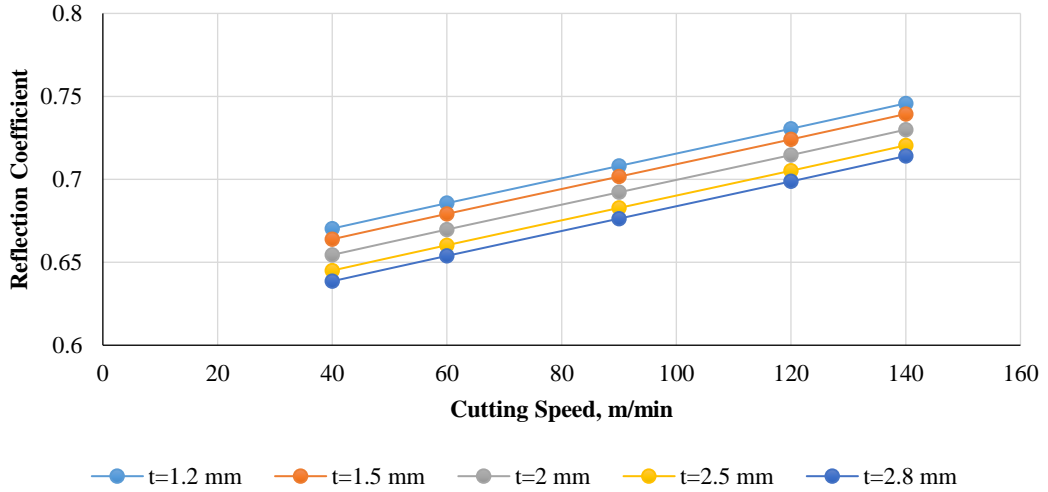
Figure B.13 Reflection coefficients versus cutting speed for different cutting depth at a constant feed of (*f*=0.23 *mm/rev*)
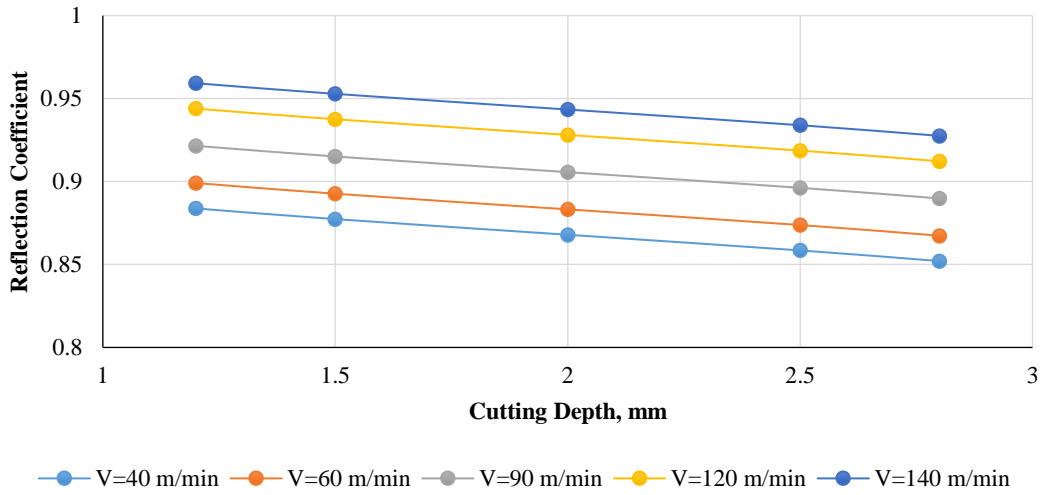
Figure B.14 Reflection coefficients versus cutting depth for different cutting speed at a constant feed of (*f*=0.09 *mm/rev*)
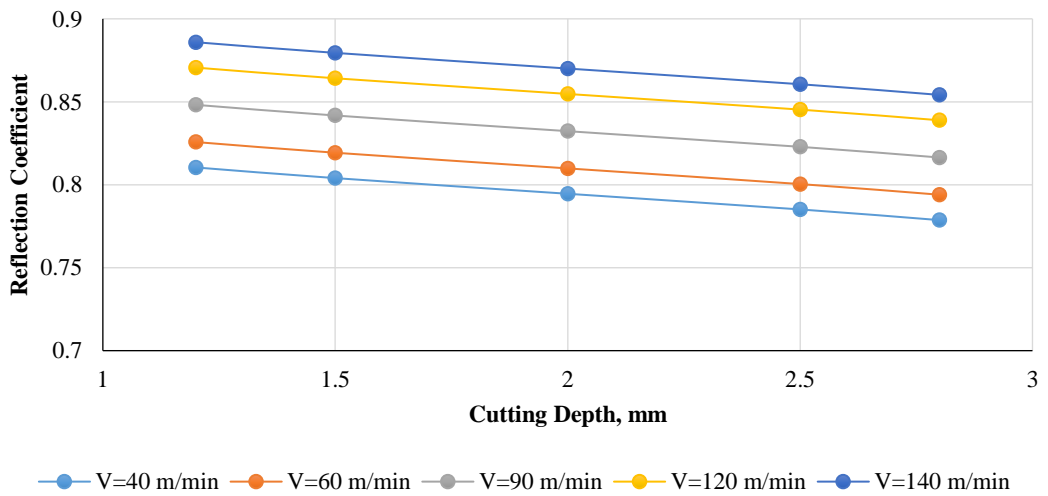
Figure B.15 Reflection coefficients versus cutting depth for different cutting speed at a constant feed of (*f*=0.12 *mm/rev*)
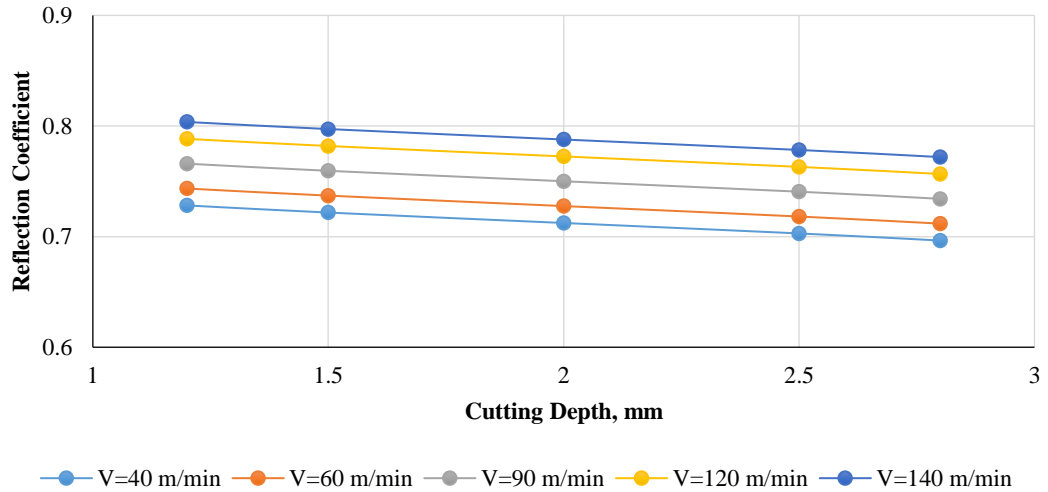
Figure B.16 Reflection coefficients versus cutting depth for different cutting speed at a constant feed of (*f=0.16 mm/rev*)
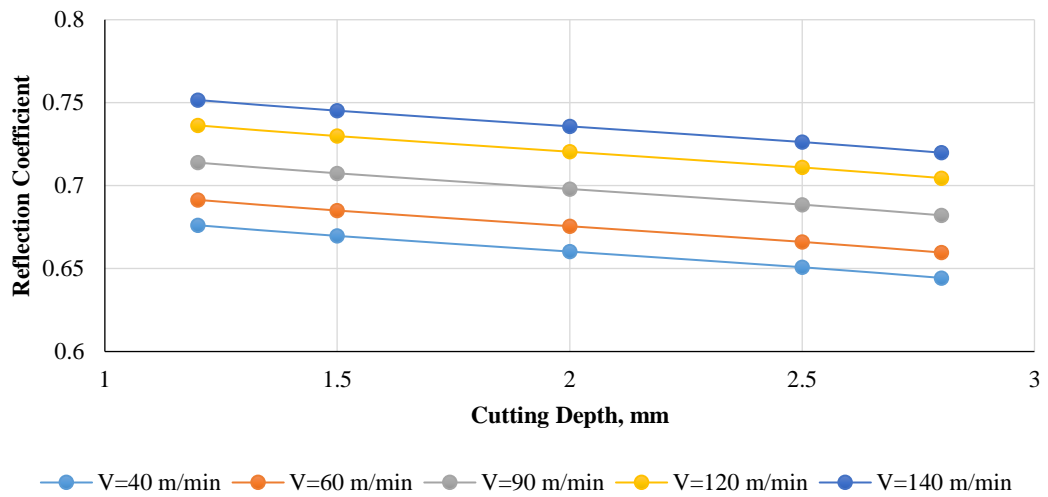
Figure B.17 Reflection coefficients versus cutting depth for different cutting speed at a constant feed of (*f=0.2 mm/rev*)

Figure B.18 Reflection coefficients versus cutting depth for different cutting speed at a constant feed of (*f=0.23 mm/rev*)

Figure B.19 Reflection coefficients versus feed for different cutting depth at a constant cutting speed of (*V=40 m/min*)
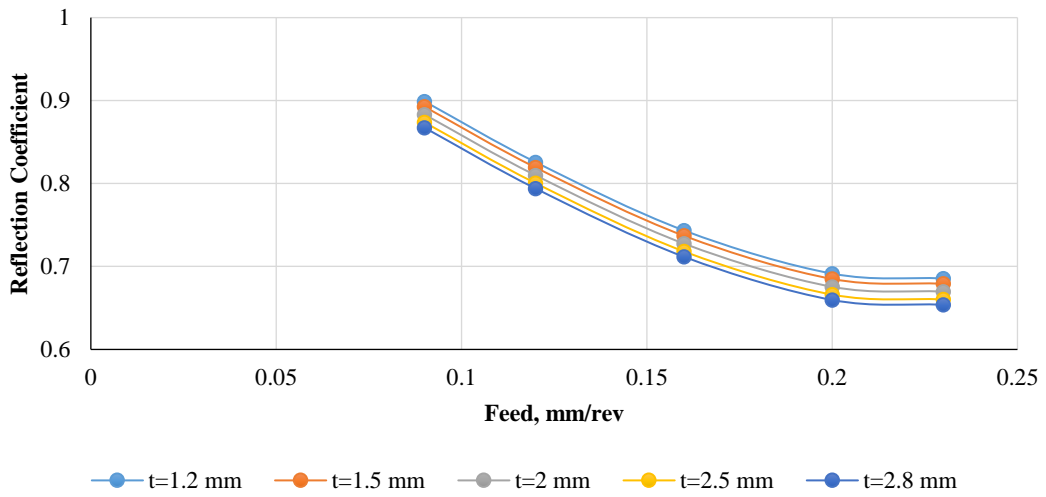
Figure B.20 Reflection coefficients versus feed for different cutting depth at a constant cutting speed of (*V=60 m/min*)
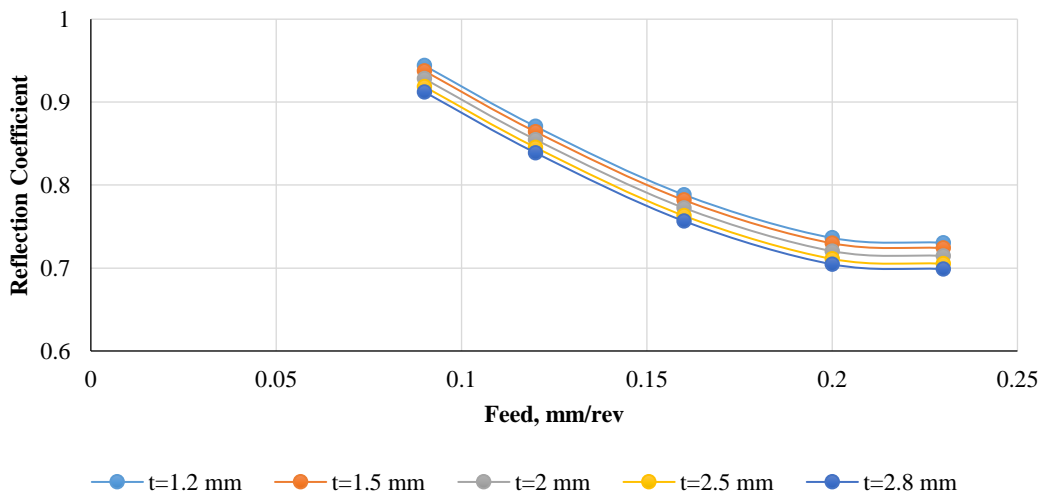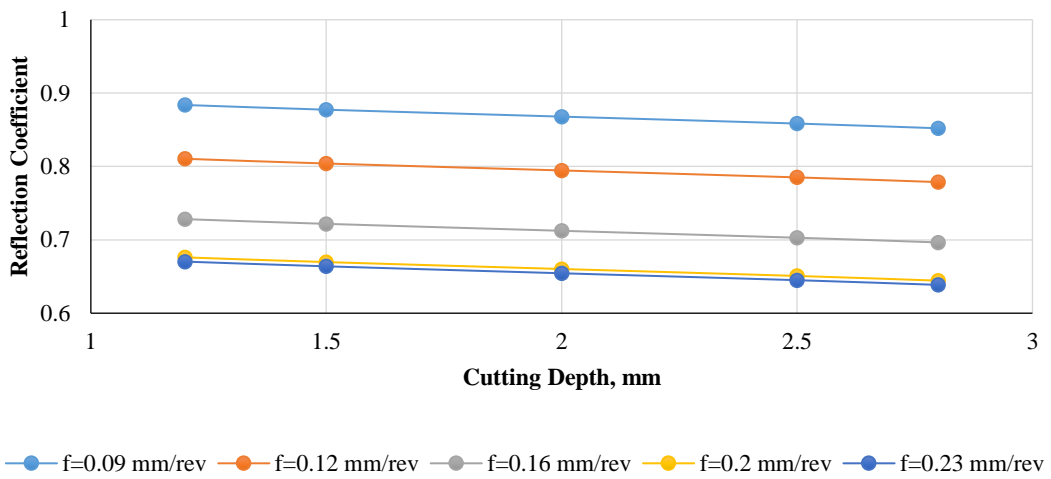

Figure B.21 Reflection coefficients versus feed for different cutting depth at a constant cutting speed of (*V=120 m/min*)
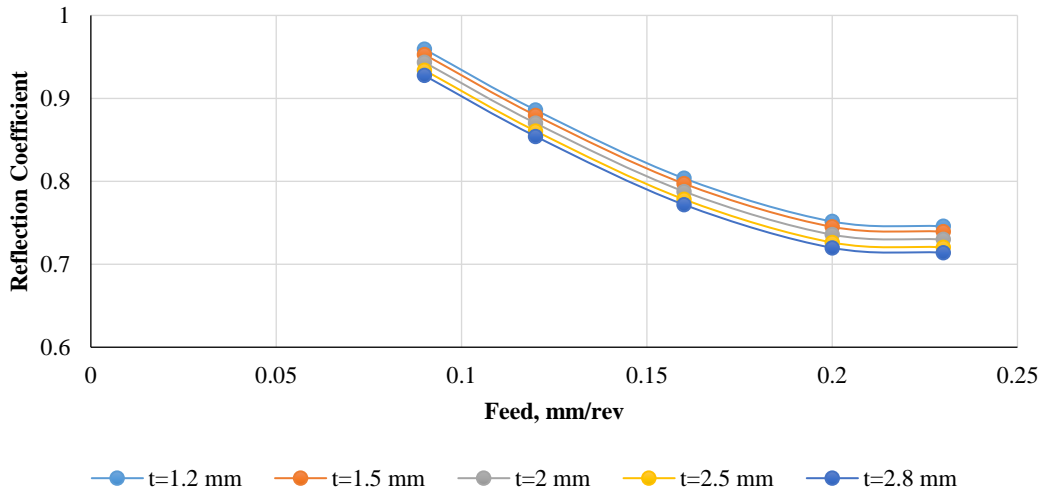
Figure B.22 Reflection coefficients versus feed for different cutting depth at a constant cutting speed of (V=140 m/min)

Figure B.23 Reflection coefficients versus cutting depth for different feed at a constant cutting speed of (V=40 m/min)
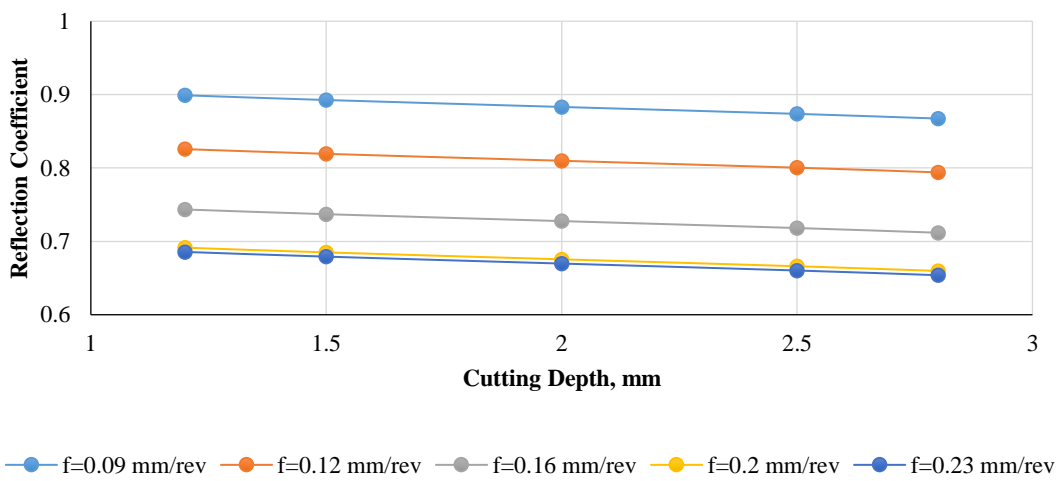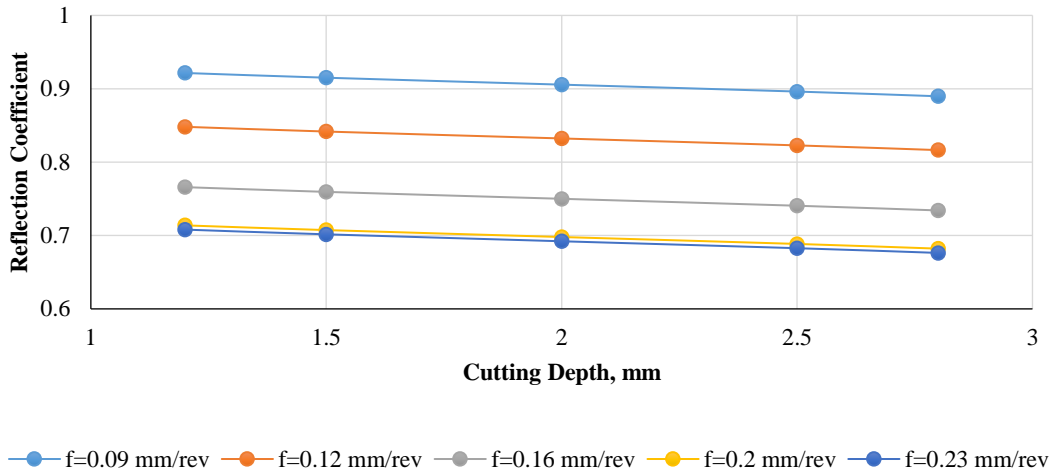

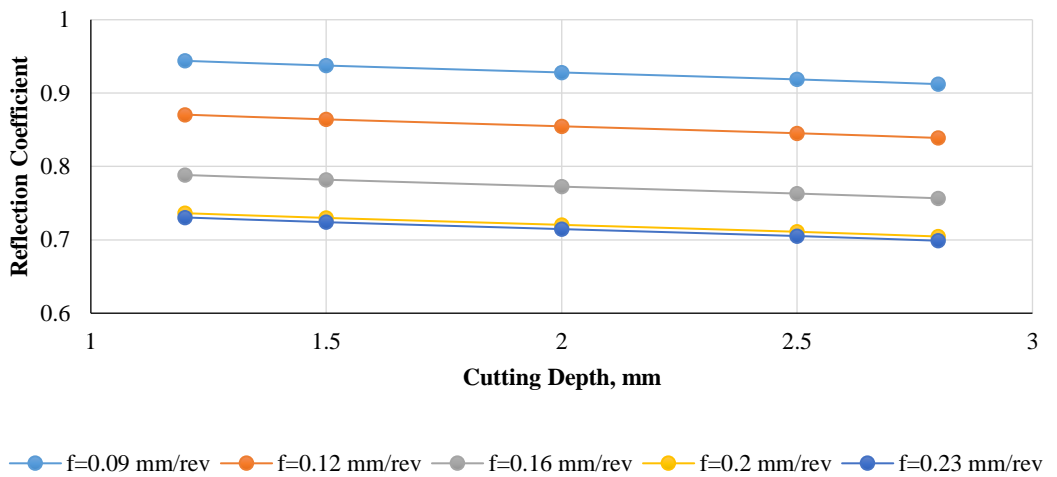**Figure B.24 Reflection coefficients versus cutting depth for different feed at a constant cutting speed of (V=60 m/min)**

Figure B.25 Reflection coefficients versus cutting depth for different feed at a constant cutting speed of (*V=90 m/min*)

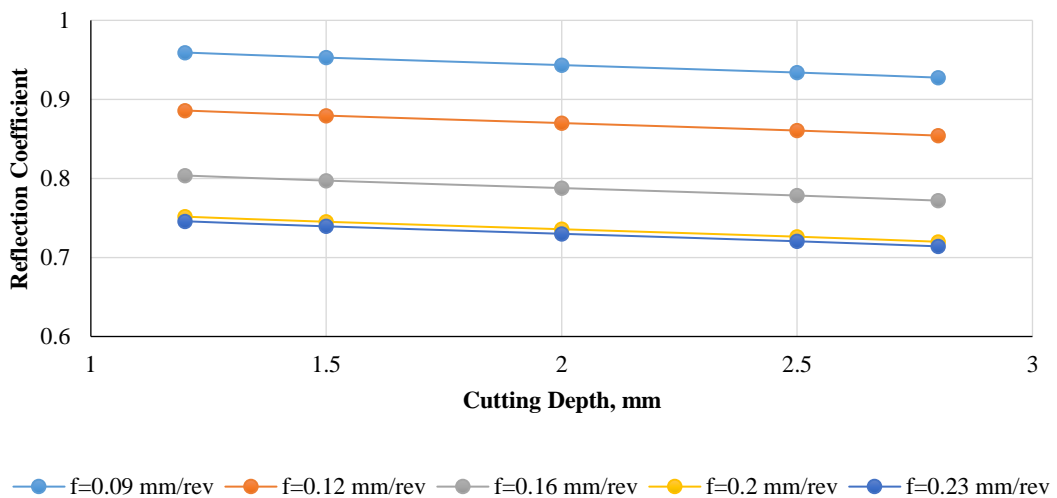**Figure B.26 Reflection coefficients versus cutting depth for different feed at a constant cutting speed of (*V=120 m/min*)**

Figure B.27 Reflection coefficients versus cutting depth for different feed at a constant cutting speed of (*V=140 m/min*